NASA CONTRACTOR REPORT

NASA CR-1768

FLIGHT INSTRUMENT AND TELEMETRY RESPONSE AND ITS INVERSION

by M. R. Weinberger

Prepared by
AVCO CORPORATION, SYSTEMS DIVISION
Wilmington, Mass. 01887
for Langley Research Center

NATIONAL AERONAUTICS AND SPACE ADMINISTRATION • WASHINGTON, D. C. • SEPTEMBER 1971

1. Report No.	2. Government Accession No.	3. Recipient's Catalog No.
NASA CR-1768		

4. Title and Subtitle	5. Report Date
FLIGHT INSTRUMENT AND TELEMETRY RESPONSE AND ITS INVERSION	September 1971
	6. Performing Organization Code

7. Author(s)	8. Performing Organization Report No.
M. R. Weinberger	AVSD-0263-70-CR
	10. Work Unit No.

9. Performing Organization Name and Address	11. Contract or Grant No.
AVCO CORPORATION SYSTEMS DIVISION Wilmington, Massachusetts 01887	NAS 1-8541
	13. Type of Report and Period Covered
12. Sponsoring Agency Name and Address	Contractor Report
National Aeronautics and Space Administration Washington, D.C. 20546	14. Sponsoring Agency Code

15. Supplementary Notes

16. Abstract

Mathematical models of rate gyros, servo accelerometers, pressure transducers and telemetry systems were derived and their parameters were obtained from laboratory tests. Analog computer simulations were used extensively for verification of the validity for fast and large input signals. An optimal inversion method was derived to reconstruct input signals from noisy output signals and a computer program was prepared.

17. Key Words (Suggested by Author(s))	18. Distribution Statement
Instrument response during abnormal events Mathematical models of instruments Dynamic and static testing of instruments Inversion problem	Unclassified - Unlimited

19. Security Classif. (of this report)	20. Security Classif. (of this page)	21. No. of Pages	22. Price*
Unclassified	Unclassified	260	$3.00

*For sale by the National Technical Information Service, Springfield, Virginia 22151

FOREWORD

The work reported here was conducted under the direction of S. J. Ailor and D. M. Foster, Scout Project Office, Langley Research Center. At the Avco Corporation, the laboratory work on the transducers was done under the direction of R. Litte and H. R. Cowan, the experiments on the telemetry under S. A. Dabrowski, the analog simulations by J. O. Brooks and the theoretical modeling and inversion by M. R. Weinberger.

Appendices B and C were written by H. R. Cowan and S. A. Dabrowski, respectively.

CONTENTS

LIST OF SYMBOLS

General Symbols

A, a Linear Accelerations

C Capacitance

E Young's modulus

f Frequency (Hz)

g Gravity Acceleration

G Conductance

I Inertia

K Gain

L Inductance

M, m Mass

P Pressure

R Resistance

s Laplace Operator

t Time

T Time Constant

ζ Damping Factor

ω Angular Rate (Rad/Sec)

Special Symbols

Rate Gyros

B Susceptance

B_g Damping Coefficient

C_M Gain Factor

e Voltage

H_r Wheel Momentum

i Current

j Imaginary Unit

K_g Spring Constant (for Gimbal)

L_1, L_2 Lengths in Gyro Suspension

M_{gw} Mass of Gimbal and Wheel

n_M Transformer-Ratio

T Torques

u, v Voltages

x, y, z Axes of Frames

X Reactances

y_b Bending Deflection

Y Admittances

Z Impedances

Subscript
- c case
- g Gimbal
- m Mounting
- o Inertial Frame
- x Directions Input
- y Output
- z Spin Reference

δ Center of Mass Offset

ζ_{gy} Damping Factor for Gimbal along Output Axis

θ Rotation Angle of Gimbal Along Output Axis

θ_p Rotation Angle of Gimbal along Input Axis

μ_L Mass Per Unit Length

$\varphi(.)$ Spatial Bending Function

φ_s Phase Angle

ϕ_x ϕ_y ϕ_z Euler Angles

ψ_L Magnetic Flux

ω_{br} Resonant Frequency of Bracket

ω_{gy} Resonant Frequency of Gimbal Along Output Axis

$\bar{1}$ Unit Vector

Accelerometers

a, r_c, t, w Dimensions (see Figure 3-1)

k Stiffness Factors for Brackets

L Radius of Gyration of Sensor

S Scale Factor

V Voltage

ζ_n Damping Factor

ψ Scale Factor for Cross-Axis Sensitivities

ω_n Natural Frequency

Pressure Transducers

a, b, h, R	Dimensions (See Figure 4-1)
A	Area Cross-Section Tube
c_o	Unit "Capacitance"
D	Diameter Pipe
f	Friction Coefficient
k	Spring Constant
l_o	Unit "Inertance"
r_o	Unit "Resistance"
$\bar{R}$	Gas Constant
T	Torque
u	Displacement of Tube
U	Energy
v	Poisson's Ratio
V	Volume
Z	Auxiliary Energy Function
α	Sensitivity Coefficient
Δ	Length
ρ	Density
τ	Complex time constant
ζ_{BD}	Damping factor for Bourdon Tube
w_{BD}	Resonant frequency for Bourdon tube
ζ_{oR}	Damping factor for orifice effect

w_{oR} Resonant frequency for orifice effect

ζ_a, ζ_b Damping factors for T-Tubing

w_a, w_b Resonant frequencies for T-Tubing

Telemetry

E, e Voltage

F(.) Transfer-Function

f(.) Impulse Response

G(.) Transfer-Function

i Imaginary Unit

m Deviation Ratio

v Voltage

Subscript E Edge of Filter Band

Inversion

C_q Coefficient in Error Calculation

D(.) Approximate Inversion Operator

E Energy of Signal

G(.) Exact Inversion Operator

h Measure of Error

I(.) Integral in Error Calculation

N Number of Samples

$p = w_n T$

x Input Signal Transducer

y Output Signal Transducer

z Intermediate Signal

Δt	Edge Distance
α, β, γ	Coefficients of Digital Inversion Operator
ζ_n	Damping Factor
μ	Multiplier used for Bandwidth
w_n	Resonant Frequency

FLIGHT INSTRUMENT AND TELEMETRY RESPONSE AND ITS INVERSION

by M. R. Weinberger

Avco Corporation - Systems Division
Wilmington, Massachusetts

SUMMARY

This report presents mathematical models of rate gyros, servo-accelerometers, pressure-transducers and an FM/FM telemetry system used with Scout vehicles. These models permit prediction of instrument response to transient signals, more particularly to signals which are of a duration short compared with normal instrument response time and which reach magnitudes large compared with the nominal range (i. e., imperfect impulses). The models are derived theoretically for all components; and, whenever possible, their relevant parameter values are calculated from data obtained by simple measurements. The instruments were tested in the laboratory and afterwards analog computer simulations were run to find the parameter values giving the best fit to the laboratory results. The theoretical values and those obtained on the simulation were then compared. Generally, a good agreement was found to exist.

A method is derived to reconstruct input signals to the transducers, given the recorded output signals, and taking into account the effect of noise. A digital computer program, based on this method, was prepared and is described here. This inversion scheme is very useful in post-flight analyses to obtain a better idea of the true shape of the input signals to the transducer, since for fast signals the transducers introduce a considerable dynamic lag and distortion. The inversion method developed here is optimum in the minimax sense of minimizing the maximum instantaneous reconstruction error.

1. INTRODUCTION

In the Scout vehicles, and more generally in aircraft and space vehicles, certain events can cause the sensors and transducers in the flight instrument package to receive signals which attain unusually large instantaneous magnitudes and which vary noticeably in a time interval that is short compared with the normal instrument response time. Catastrophic failures in some components, such as the combustion chamber, are likely candidates to generate these signals.

With such signals it becomes important to know the transient response characteristics of the transducers and the telemetry system, in order to evaluate dynamic effects (such as lag, delay, distortion) introduced by them. Therefore, the first part of this report is concerned with the mathematical description of the transient response characteristics of three categories of instruments (rate gyros, servo accelerometers, and pressure transducers) and of an FM/FM telemetry system. In each case, first a theoretical model is constructed, based on whatever is known about the inner structure of the devices. The numerical values of the relevant parameters are then calculated, as far as possible, from simple measurements of dimensions, weights, and data supplied by the manufacturer. Useful information was obtained by opening the instruments (after other laboratory tests were finished) and by inspecting parts and running tests of transient response to disturbances applied at interior points.

Then, the instruments and telemetry components were subjected to tests in the laboratory. A large variety of input signals were used, depending on the equipment employed for particular tests. More particularly, the signals mentioned before were defined (in the contract) as signals with amplitudes up to ten times the nominal full scale range and occurring in time intervals down to two orders of magnitude less than the normal instrument response time. Such signals approach impulses and with the definition just given the equivalent impulse strength (which is the area under the input signal or duration times average magnitude) is sufficiently limited to keep the instrument response in its linear range. Therefore, linear models could be used for most components. Even for a non-linear instrument as the rate gyro, linearized models were generally sufficient. In some cases, such as the phase sensitive demodulators and some accelerometers and pressure transducers, a linear model is applicable, provided some parameter (a damping coefficient) is made dependent upon the type of input signal (polarity or speed, respectively).

Finally, analog computer simulations were made, using the theoretical model to find the parameter values giving the best agreement with the laboratory test results. These values could then be compared with the ones derived from theory earlier. In general the two sets of parameter values were quite compatible.

Once models are constructed, it is relatively easy, using analog or digital computers, to determine the response of the elements studied, given any admissible input signal. However, in many practical applications, such as post mortem analyses of in-flight anomalies, it is rather the reverse problem that matters: one has recorded output signals coming from transducers and telemetry channels and one wants to know what were the true input signals as seen by the transducers. For this reason, the second part of this report develops the theory of this inversion problem for the three kinds of transducers. A digital computer program, based on this theory, prints and plots automatically the reconstructed transducer input, given the output signal. This reconstruction is, in fact, an optimal one in the minimax sense that the method used produces the smallest achievable worst error at any time (this is similar to Chebychev approximation, Reference 1). Since the flight instruments act as signal smoothers, the inversion is fundamentally a differentiation problem in the presence of noise, and the inversion program is some sort of optimum filter.

Most of the references listed in the bibliography deal with problems akin to the ones treated in the present report. For example, the modeling of gyros can be found in many other articles or books than the one quoted in the report (Reference 2). On the other hand, the resonance calculation of the Bourdon tubes, certain parts of the discussion of the band pass filter response, the discussion of interference ripple are, as far as is known, not found elsewhere. A particularity of this study is the systematic comparison of values obtained from the theory and those obtained through simulation.

While the use of a minimax criterion in filtering can be considered classical, the inversion formulation in this report is new. It can, moreover, be generalized to allow inversion of a wide class of linear systems.

For readers who are not interested in the mathematical details of the modeling, Section 7 (Conclusions) gives an expanded verbal description of the most important results.

Note: Time scales on the figures are given in ms/Division. This applies to "major" divisions, corresponding with a distance of 1 cm on the oscilloscope screen.

2. RATE GYROS

The rate gyros in the Langley Scout package belong to one of two types:

for pitch and yaw rates: Honeywell GN 90B1
for roll rates: Honeywell GN 91B1

Both types are close to the Honeywell GG440 GNAT miniature design. Some of their characteristics are specified in the procurement specifications, an extract of which is listed below:

	Pitch and Yaw	Roll
Full Scale Rate (deg/sec)	40	100
Natural Frequency (Hz)	19-26	36-42
Damping Ratio	0.49-1.4	0.49-1.4
Scale Factor V rms/(deg/sec) (with correct load)	0.235 (± 5%)	0.095 (± 7%)

2.1 Theoretical Model

2.1.1 Mechanical Part of the Gyros

The model is based on Newton's angular momentum equation $\frac{d\bar{H}}{dt} = \bar{T}$ (2-1)

where $\bar{H}$ is angular momentum, $\bar{T}$ is torque, and which is valid around either an inertially fixed point or the center of mass (C.M) of the system under consideration. For a moving frame F with instantaneous inertial rotation vector $\bar{\omega}_f$, (2-1) is equivalent with:

$$\left(\frac{\partial \bar{H}}{\partial t}\right)_{\text{in frame F}} + \bar{\omega}_f \times \bar{H} = \bar{T} \qquad (2\text{-}2)$$

The following development parallels closely the one given by J. M. Slater and J. S. Ausman in Reference 2.

The figure below shows the basic configuration.

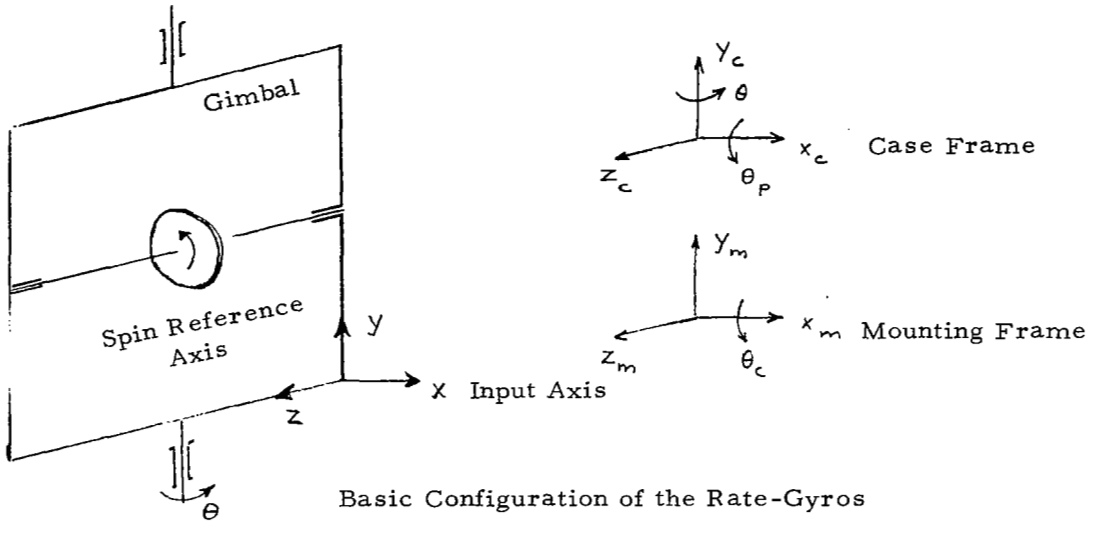

Basic Configuration of the Rate-Gyros

Frames: (x, y, z) is the gimbal frame with x = input axis, y = output axis, z = spin reference axis.

(x_c, y_c, z_c) is the case frame
(x_m, y_m, z_m) is the mounting frame
(x_o, y_o, z_o) is the inertial frame

Rotations: θ is the rotation angle of the gimbal with respect to the case, along the output axis.

θ_p is the rotation angle of the gimbal with respect to the case along the input axis.

θ and θ_p are small angles and hence are commutative.

θ_c is the rotation of the case with respect to the mounting, along the input axis.

ϕ_z, ϕ_y, ϕ_x are the Euler angles, in that order, describing the rotation of the mounting with respect to the inertial frame. (See Figure below).

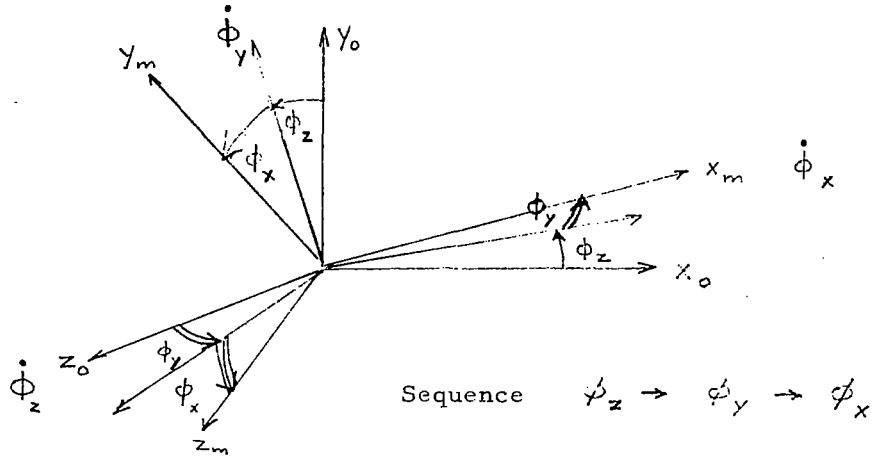

Euler Angles

The general transformation matrix from $(\bar{l}_{xo}, \bar{l}_{yo}, \bar{l}_{zo})$ to $(\bar{l}_{xm}, \bar{l}_{ym}, \bar{l}_{zm})$ is standard (see Reference 2 again) and is listed below.

$$\begin{Bmatrix} \bar{l}_{xm} \\ \bar{l}_{ym} \\ \bar{l}_{zm} \end{Bmatrix} = \begin{bmatrix} \cos\phi_y \cos\phi_z & \cos\phi_y \sin\phi_z & -\sin\phi_y \\ \sin\phi_x \sin\phi_y \cos\phi_z - \cos\phi_x \sin\phi_z & \sin\phi_x \sin\phi_y \sin\phi_z + \cos\phi_x \cos\phi_z & \sin\phi_x \cos\phi_y \\ \cos\phi_x \sin\phi_y \cos\phi_z + \sin\phi_x \sin\phi_z & \cos\phi_x \sin\phi_y \sin\phi_z - \sin\phi_x \cos\phi_z & \cos\phi_x \cos\phi_y \end{bmatrix} \begin{Bmatrix} \bar{l}_{xo} \\ \bar{l}_{yo} \\ \bar{l}_{zo} \end{Bmatrix}$$

The corresponding transformation matrix for small rotation angles is:

$$\begin{Bmatrix} \bar{l}_{xm} \\ \bar{l}_{ym} \\ \bar{l}_{zm} \end{Bmatrix} = \begin{bmatrix} 1 & \phi_z & -\phi_y \\ -\phi_z & 1 & \phi_x \\ \phi_y & -\phi_x & 1 \end{bmatrix} \begin{Bmatrix} \bar{l}_{xo} \\ \bar{l}_{yo} \\ \bar{l}_{zo} \end{Bmatrix}$$

The other transformation matrices are analogous:

$$\begin{Bmatrix} \bar{l}_{x} \\ \bar{l}_{y} \\ \bar{l}_{z} \end{Bmatrix} = \begin{bmatrix} 1 & 0 & -\theta \\ 0 & 1 & \theta_p \\ \theta & -\theta_p & 1 \end{bmatrix} \begin{Bmatrix} \bar{l}_{xc} \\ \bar{l}_{yc} \\ \bar{l}_{zc} \end{Bmatrix}$$

$$\begin{Bmatrix} \bar{l}_{xc} \\ \bar{l}_{yc} \\ \bar{l}_{zc} \end{Bmatrix} = \begin{bmatrix} 1 & 0 & 0 \\ 0 & 1 & \theta_c \\ 0 & -\theta_c & 1 \end{bmatrix} \begin{Bmatrix} \bar{l}_{xm} \\ \bar{l}_{ym} \\ \bar{l}_{zm} \end{Bmatrix}$$

The angles θ, θ_p and θ_c are struaturally constrained to small values. The angles ϕ_x, ϕ_y and ϕ_z are small in the tests described here. Typically, test inputs are pulses of amplitude not exceeding ten times the nominal value, and duration at least one hundredth of the basic time constant of the system. Therefore, for the roll gyro one can expect an angular rotation of not much more than

$$\Delta \phi_x \simeq (1,000\ ^\circ/\text{sec}) \cdot (0.75 \times 10^{-3}\ \text{sec}) = 0.75^\circ$$

which is indeed small enough.

The different instantaneous rotation vectors are calculated next, up to and including second order quantities.

The rotation vector of the mounting with respect to inertial space is $\bar{\omega}_m$

$$\begin{aligned}\bar{\omega}_m = \quad & (\dot{\phi}_x - \phi_y \dot{\phi}_z)\ \bar{1}_{xm} \\ & + (\dot{\phi}_y + \phi_x \dot{\phi}_z)\ \bar{1}_{ym} \\ & + (\dot{\phi}_z - \phi_x \dot{\phi}_y)\ \bar{1}_{zm}\end{aligned}$$

The rotation vector of the case with respect to inertial space is $\bar{\omega}_c$.

$\bar{\omega}_c = \bar{\omega}_m + \dot{\theta}_c\, \bar{1}_{xc}$ (which becomes, with the aid of the matrices above)

$$\begin{aligned} = \ & (\dot{\theta}_c + \dot{\phi}_x - \phi_y \dot{\phi}_z)\ \bar{1}_{xc} \\ & + [\ \dot{\phi}_y + \dot{\phi}_z (\phi_x + \theta_c)]\ \bar{1}_{yc} \\ & + [\ \dot{\phi}_z - \dot{\phi}_y (\phi_x + \theta_c)]\ \bar{1}_{zc}\end{aligned}$$

The rotation vector of the gimbal with respect to inertial space is $\bar{\omega}_g$ (the sequence $\theta_p \rightarrow \theta$ is chosen here, but this choice does not influence the final formulas).

$\bar{\omega}_g = \bar{\omega}_c + \dot{\theta}_p\, \bar{1}_x + \dot{\theta}\, \bar{1}_y + \theta\, \dot{\theta}_p\, \bar{1}_z$ = (use again the transformation matrices)

$$\begin{aligned} = \ & [\ \dot{\theta}_p + \dot{\theta}_c + \dot{\phi}_x - \dot{\phi}_z (\phi_y + \theta)]\ \bar{1}_x \\ & + [\ \dot{\theta} + \dot{\phi}_y + \dot{\phi}_z (\phi_x + \theta_c + \theta_p)]\ \bar{1}_y \\ & + [\ \dot{\phi}_z - \dot{\phi}_y (\theta_p + \theta_c + \phi_x) + \theta (\dot{\theta}_c + \dot{\theta}_p + \dot{\phi}_x)]\ \bar{1}_z\end{aligned}$$

Output axis (or gimbal) equation.

For a gimbal with well-oriented principal axes, carrying a rotor with relative angular momentum H_r, the total angular momentum with respect to the C.M. of this subsystem is given by:

$$\bar{H}_g = I_{gx}\,\omega_{gx}\,\bar{l}_x + I_{gy}\,\omega_{gy}\,\bar{l}_y + (I_{gz}\,\omega_{gz} + H_r)\,\bar{l}_z$$

where I_{gz} is the sum of gimbal z-axis inertia plus wheel-inertia around the spin axis; I_{gz} and I_{gy} are gimbal-plus-wheel inertias along input and output axes.

All inertias are calculated along axes centered on the center-of-mass of gimbal and wheel. If one writes the output axis component of (2-2) and retains only those second order quantities which are multiplied by the large rotor momentum H_r, the following output-equation is obtained.

$$\begin{aligned} I_{gy}\,\ddot{\theta} + B_{gy}\,\dot{\theta} + K_{gy}\,\theta &= H_r\,(\dot{\phi}_x + \dot{\theta}_p + \dot{\theta}_c) \\ &- I_{gy}\,\ddot{\phi}_y - H_r\,\dot{\phi}_z\,(\phi_y + \theta) + T_{gy,\ \text{residual}} \\ &- (g\,M_{gw}\,\delta)\left(\frac{\delta_z}{\delta}\,A_x - \frac{\delta_x}{\delta}\,A_z\right) \end{aligned} \qquad (2\text{-}3)$$

The meaning of the symbols is:

- g: reference acceleration, e.g., g = earth gravity = 32.17 ft/sec^2
- B_{gy}: output-damping coefficient
- K_{gy}: output spring constant
- $T_{gy,\ \text{residual}}$: other (parasitic) torques along output axis, exerted on gimbal (such as gravitational and magnetic torques)
- M_{gw}: combined mass of gimbal plus wheel
- $\delta_z\,\delta_x$: C.M. offsets away from intersection of xyz-axes.
- δ: maximum C.M. offset $\quad(|\delta_x|, |\delta_z| \leq \delta)$
- A_x, A_z: components of inertial linear acceleration of the gimbal and wheel system, expressed in units of "g"

Input Axis Equation

C.M. offsets are neglected here. First, there is the x-axis equation for motion between gimbal and case:

$$\begin{aligned} I_{g\,x}\,\ddot{\theta}_p + B_{gx}\,\dot{\theta}_p + K_{gx}\,\theta_p &= -H_r\,(\dot{\theta} + \dot{\phi}_y) \\ &- I_{gx}\,(\ddot{\theta}_c + \ddot{\phi}_x) - H_r\,\dot{\phi}_z\,(\phi_x + \theta_c + \theta_p) \\ &+ T_{gx,\ \text{residual}} \end{aligned} \qquad (2\text{-}4)$$

where all the notations are analogous to these used in the output-axis equation. Secondly, there is the x-axis equation for motion between case and mounting.

$$I_{cx}\ddot{\theta}_c + B_{cx}\dot{\theta}_c + K_{cx}\theta_c = -I_{cx}\ddot{\phi}_x + B_{gx}\dot{\theta}_p + K_{gx}\theta_p - (\text{part of } T_{gx}, \text{ residual due gimbal-case interaction only}) + T_{\text{mounting on case, x, residual}} \qquad (2\text{-}5)$$

with notations analogous to these used above.

Special cases for Input-Axis Equations:

A) If the case is rigidly attached to the mounting, $K_c \to \infty$ $\theta_c \to 0$ and only (2-4) is left with $\theta_c = 0$, while (2-5) is to be omitted.

B) If the gimbal-case connection is rigid along the input axis, $K_{gx} \to \infty$, $\theta_p \to 0$ and only one equation is left, by addition of (2-4) and (2-5).

$$(I_{cx} + I_{gx})\ddot{\theta}_c + B_{cx}\dot{\theta}_c + K_{cx}\theta_c = -(I_{cx} + I_{gx})\ddot{\phi}_x - H_r(\dot{\theta} + \dot{\phi}_y) - H_r\dot{\phi}_z(\phi_x + \theta_c) + T_{\text{mounting on case, x, residual}} + (\text{part of } T_{yx} \text{ not due to case})$$

C) Finally, if input-axis motions are negligible, (2-4) and (2-5) are both omitted and $\theta_c = \theta_p = 0$ is used in (2-3).

Canonical Form of Equations:

The output axis equation (2-3) can be rewritten as:

$$\frac{\ddot{\theta}}{w_{gy}^2} + 2\zeta_{gy}\frac{\dot{\theta}}{w_{gy}} + \theta = \left(\frac{H_r}{K_{gy}}\right)(\dot{\phi}_x + \dot{\theta}_p + \dot{\theta}_c) - \frac{\ddot{\phi}_y}{w_{gy}^2} - \left(\frac{H_r}{K_{gy}}\right)\dot{\phi}_z(\phi_y + \theta) + \frac{T_{gy,\text{ residual}}}{K_{gy}} - \left(\frac{g M_{gw}\delta}{H_r}\right)\left(\frac{H_r}{K_{gy}}\right)\left(\frac{\delta_z}{\delta}A_x - \frac{\delta_x}{\delta}A_z\right) \qquad (2\text{-}6)$$

with $\omega_{gy}^2 = K_{gy}/I_{gy}$

$$\zeta_{gy} = \frac{B_{gy}}{2\,(I_{gy}\,K_{gy})^{1/2}}$$

The input axis equation (2-4) can similarly be rewritten as:

$$\frac{\ddot{\theta}_p}{\omega_{gx}^2} + 2\zeta_{gx}\frac{\dot{\theta}_p}{\omega_{gx}} + \theta_p = -\left(\frac{H_r}{K_{gx}}\right)(\dot{\theta} + \dot{\phi}_y) - \frac{\ddot{\theta}_c + \ddot{\phi}_x}{\omega_{gx}^2}$$

$$- \frac{H_r}{K_{gx}}\,\dot{\phi}_z\,(\phi_x + \theta_c + \theta_p) + \frac{T_{gx,\ residual}}{K_{gx}} \qquad (2\text{-}7)$$

with

$$\omega_{gx}^2 = K_{gx} / I_{gx}$$

$$\zeta_{gx} = \frac{B_{gx}}{2\,(I_{gx}\,K_{gx})^{1/2}}$$

Stops: There is a mechanical bound on θ:

$$|\theta| \leq \theta_{max} \qquad (2\text{-}8)$$

Note on the Relationship between Input-Axis Stiffness K_{gy} and Output Axis Stiffness K_{gx}

K_{gy} results from the torsional stiffness of a bearing member, while K_{gx} depends on the bending stiffness of the same member. The gimbal is pivoted at one end, which gives a lever-arm amplification for K_{gx} (See Figure below).

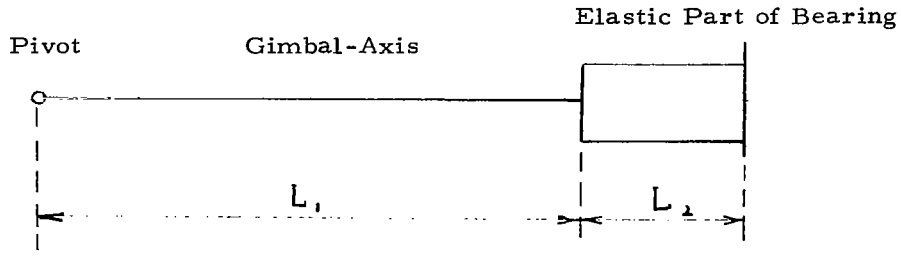

The elastic member is, at least in the main part, a circular cylindrical rod. Thus, one gets, using classical results of strength of materials (see e.g., Reference 3)

$$\frac{K_{gx}}{K_{gy}} = 2 \frac{L_1}{L_2} \cdot \frac{E}{G} \cdot \frac{I_b}{I_p} > 21.3$$

since for most metals the ratio E/G of Young's modulus to torsion modulus equals 2.6, $(L_1/L_2) > 8.2$, $(I_b/I_p) = 1/2$ (bending area moment of inertia divided by polar area moment of inertia for a circular cylinder).

The true value of the ratio K_{gx}/K_{gy} turned out to be much larger than the lower bound derived here.

Some Numerical Results

From manufacturer's data one can estimate

$$\left| \frac{g M_{gw} \delta}{H_r} \right| \leq 5.3 \times 10^{-4} \text{ (rad/sec) per g}$$

further $\theta_{max} = 3^o = 0.052$

Steady state gain $\frac{H_r}{K_{gy}} = 0.0647$ sec (pitch gyro)

$\frac{H_r}{K_{gy}} = 0.0248$ sec (roll gyro)

Nothing is known about T_{gy}, residual and T_{gx}, residual.

One may assume the case-mounting connection to be rigid, i.e., $K_c = \infty$ and $\theta_c \equiv 0$.

2.1.2 Electro-Mechanical Output Device

A Microsyn (variable reluctance) pickoff is used to generate the electrical output signal. This device can be viewed approximately as a transformer with output-axis-dependent (i.e., θ-dependent) transformation ratio n_M.

Therefore, one obtains the circuit diagram of the figure below.

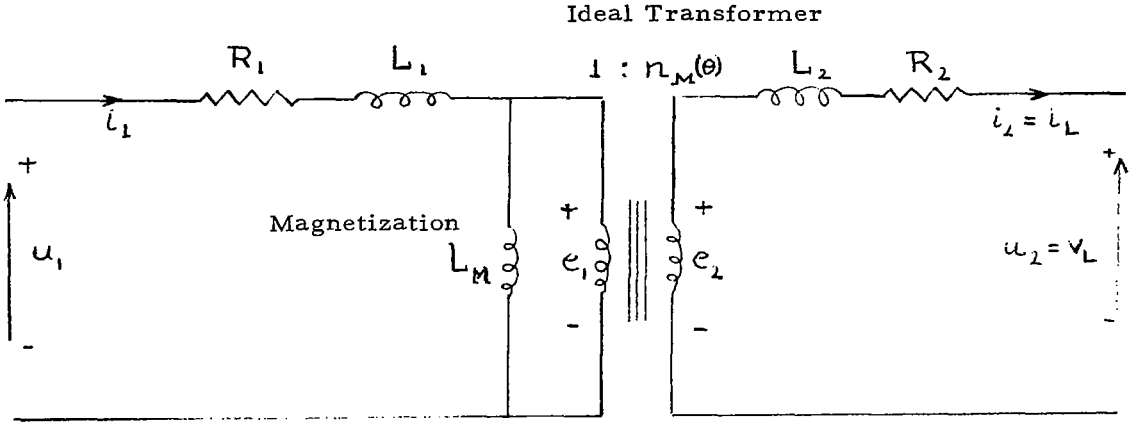

Model for the Microsyn

This model is now somewhat simplified by shifting the magnetization reactance, and the diagram of the figure below is obtained b y adding the load impedance

$$Z_L = \frac{R_L}{1 + R_L C_L s}$$

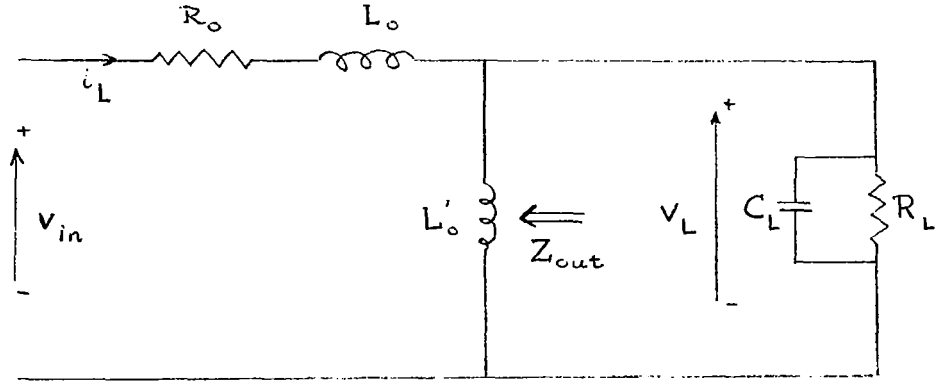

Simplified Model of the Gyro Output Circuit

The elements of Z_{out} on that figure are given by:

$$R_o = R_2 + n_M^2 R_1$$

$$L_o = L_2 + n_M^2 L_1$$

$$L'_o = n_M^2 L_M$$

Strictly speaking, these parameters depend on θ through the ratio n_M. If this dependence is neglected, or an average value for R_o, L_o and L'_o is adopted, the electrical output equations are:

$$u_1(t) = V_s \sqrt{2} \cos (w_s t + \varphi_s) \qquad (2\text{-}9)$$

$$V_{in}(t) = C_M \theta(t) \; u_1(t) \qquad (2\text{-}10)$$

$$V_L = \frac{d\Psi_L}{dt} \qquad (2\text{-}11)$$

$$V_{in} = V_L + R_o i_L + L_o \frac{di_L}{dt} \qquad (2\text{-}12)$$

$$i_L = \frac{\Psi_L}{L'_o} + \frac{v_L}{R_L} + C_L \frac{dv_L}{dt} \qquad (2\text{-}13)$$

Numerical Results for the Electro-Mechanical Output Device

Steady state (i.e., constant input rate) experiments on the pitch and yaw rate gyros show that for

$$\omega_s = 2\pi\, 400 = 2,513 \text{ rad/sec}$$

$$v_s = 6.68 \text{ V rms}$$

$$R_L = 8.06 \times 10^8 \text{ ohm}; \; G_L = \frac{1}{R_L} = 1.241 \times 10^{-4} \text{ mho}$$

$$C_L = 0.28 \times 10^{-6} \text{ F}; \; B_L = \omega_s C_L = 7.04 \times 10^{-4} \text{ mho}$$

v_L and v_{in} are in phase and that the scale factor is:

$$\left(\frac{\partial v_L}{\partial \theta}\right)_{\text{zero phaseshift}} = 0.25 \frac{\text{V rms}}{\text{deg/sec}} = 14.3 \frac{\text{V rms}}{\text{rad/sec}}$$

Moreover, for a purely resistive load ($C_L = 0$), v_L leads v_{in} by 50^o and the scale factor is:

$$\left(\frac{\partial v_L}{\partial \dot{\phi}} \right)_{\text{Resistive Load}} = 0.18 \ \frac{\text{V rms}}{\text{deg/sec}} = 10.3 \ \frac{\text{V rms}}{\text{rad/sec}}$$

Setting $X_o = \omega_s L_o$; $X'_o = \omega_s L'_o$; $B_L = \omega_s C_L$; $G_L = \frac{1}{R_L}$

$$Z_o = R_o + j X_o \quad (j = \sqrt{-1})$$

$$\frac{1}{Z_L} = Y_L = G_L + j \left(B_L - \frac{1}{X'_o}\right)$$

one has

$$\frac{v_L}{v_{in}} = \frac{Z_L}{Z_L + Z_o} = \frac{1}{1 + Z_o Y_L}$$

with

$$Z_o Y_L = R_o G_L + X_o \left(\frac{1}{X'_o} - B_L\right) + j \left[G_L X_o - R_o \left(\frac{1}{X'_o} - B_L\right)\right]$$

The output-impedance is given by

$$Z_{out} = \frac{(R_o + j X_o)\, j X'_o}{R_o + j (X_o + X'_o)} = \frac{R_o X'^2_o + j X'_o \left[R_o^2 + X_o (X_o + X'_o) \right]}{R_o^2 + (X'_o + X_o)^2}$$

According to the manufacturer, $Z_{out} \cong (600 + j\, 1,000)$ ohm. Use of this value of Z_{out}, together with the fact that there is zero phase shift for C_L and R_L as given above leads to

$R_o = 2,260$ ohm

$X_o = 72.8$ ohm; $L_o = 0.029$ henry

$X'_o = 1,413$ ohm; $\frac{1}{X'_o} = 7.08 \times 10^{-4}$ mho; $L'_o = 0.562$ henry

As a verification

$$\measuredangle (Z_o\ Y_L) = 0^o; \quad (Z_o\ Y_L) = 0.281$$

$$Z_{out} = 616 + j\ 1,008$$

For the purely resistive load, V_L leads V_{in} by 50^o, agreeing with the tests. The proportionality factor C_M is now given by

$$C_M = \frac{V_{in}}{\theta\ u_1} = \frac{< \frac{V_{in}}{V_L} >}{< \frac{\theta}{V_L} > < u_1 >}$$

where the symbol $< \cdot >$ is used for steady state amplitude ratios in the zero phase shift case.

Then

$$C_M = \frac{< V_L / \dot{\phi}_x > \frac{\text{volts rms}}{\text{rad/sec}}}{< \frac{V_L}{V_{in}} > V_s \left(\frac{H_r}{K_{gy}} \right)}$$

This gives

$$(C_M)_{\substack{\text{pitch} \\ \text{yaw}}} = 45.9\ \text{rad}^{-1} = 0.80\ \text{deg}^{-1}$$

(see also experimental results later)

Assuming that the same microsyn is used for the roll gyro, one has

$$(C_M)_{\text{roll}} = (C_M)_{\text{pitch, yaw}}$$

As a verification, one obtains the following scale factors for the specified load of $R_L = 10^4$ ohm; $C_L = 0.3 \times 10^{-6}$ farad, nominal conditions.

Scale Factor Pitch-Yaw = $0.244\ \frac{\text{V rms}}{\text{deg/sec}}$

Scale Factor Roll = $0.093\ \frac{\text{V rms}}{\text{deg/sec}}$

The specifications give 0.235 $\frac{\text{volts}}{\text{deg/sec}}$ and 0.095 $\frac{\text{volts}}{\text{deg/sec}}$ ($\pm$ 5%) respectively, showing that the obtained values are within the prescribed tolerances.

The phase shift is found to be 5.2°, less than 10° which is acceptable.

Summarizing, the nominal values for the circuit are:

V_s = 6.3 V (rms)
ω_s = 2π 400 = 2,513 rad/sec
φ_s = arbitrary phase
R_o = 2,260 ohm
L_o = 0.029 henry
L'_o = 0.562 henry
R_L = 10^4 ohm
C_L = 0.3×10^{-6} farad
C_M = 45.9 $(\text{rad})^{-1}$ = 0.80 $(\text{deg})^{-1}$

2.1.3 The Gyro Mounting Bracket

The three rate gyros are assembled on a mounting block as shown in the figure below. The frame (x_m, y_m, and z_m) of section 2.1.1 is attached to this mounting block. The block is then firmly fastened to a mounting bracket of stainless steel which in its turn is fastened to the rocket frame.

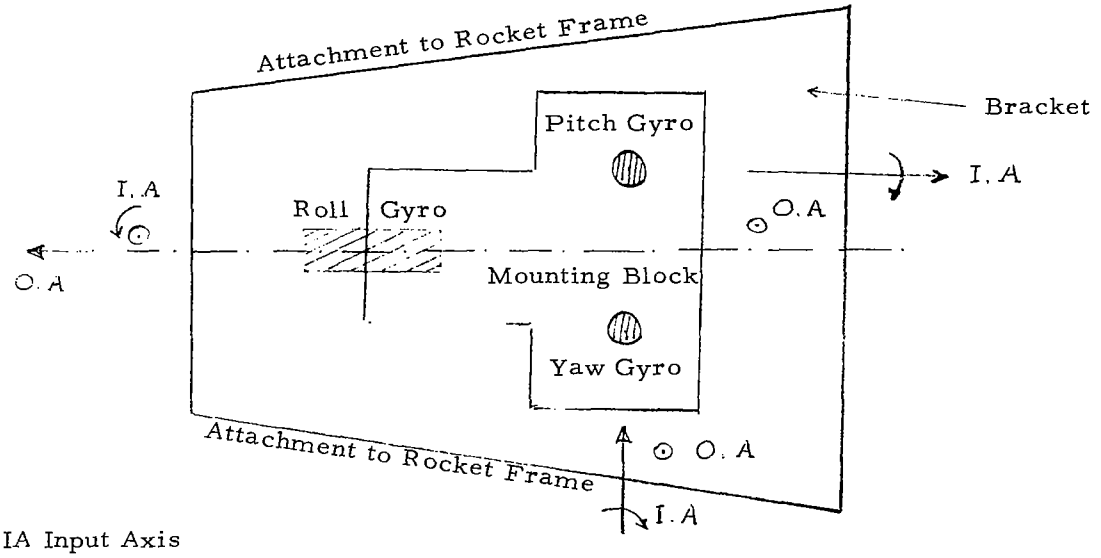

IA Input Axis
OA Output Axis

Gyro Mounting Block and Bracket

Mounting block and rocket frame are to be considered as rigid when compared with the bracket. Therefore, an elastic analysis of the bracket, loaded by mounting block and gyros is in order, to determine the resonances. The rather complicated structure of the bracket is replaced by a simple beam model as indicated on the figure below. The attachments to the rocket frame may be considered to be nearly ideal clamps. The central load of block and gyros is symmetrically located; the bracket itself is replaced by an "equivalent" uniform beam.

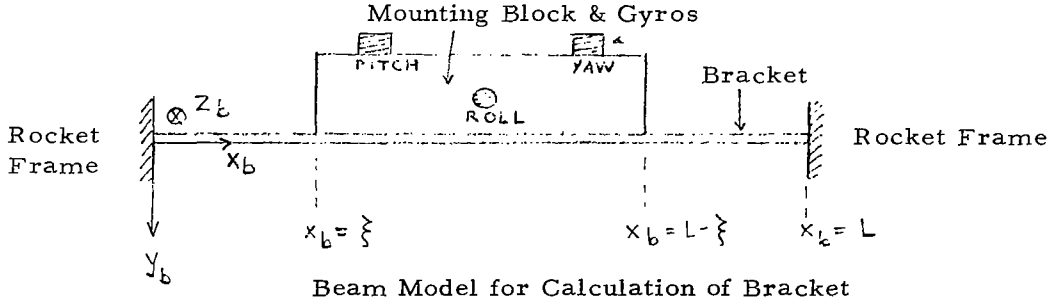

Beam Model for Calculation of Bracket Resonances

The methods explained in Reference 4 produce the partial differential equation for free bending vibrations:

$$E I_b \frac{\partial^4 y_b}{\partial x_b^4} + \mu_L \frac{\partial^2 y_b}{\partial t^2} - \mu_L \omega_{z_b}^2 y_b = 0$$

with

E = Young's modulus
I_b = area moment of inertia (for bending)
μ_L = mass per unit length in x_b direction
w_{zb} = inertial angular velocity along z_b axis
y_b = bending deflection

The different modes are obtained by separating the variables x_b and t. The time dependent part of y_b becomes T (t) with differential equation:

$$\ddot{T}(t) + (w_i^2 - w_{zb}^2(t)) \quad T(t) = 0$$

while the numbers w_i are the characteristic values for the space-dependent part $\varphi_i(x_b)$ with equation:

$$E I_b \frac{d^4 \varphi_i}{d x_b^4} - w_i^2 \mu_L \varphi_i = 0$$

The boundary conditions for symmetric modes are:

$$\varphi_i(0) = 0$$

$$\varphi'_i(0) = 0$$

$$\varphi'_i(\xi) = 0$$

$$\varphi'''_i(\xi) + \frac{M_c w_i^2}{2 E I_b} \varphi_i(\xi) = 0$$

The last two conditions are to be replaced by other ones for antisymmetric modes, viz:

$$\varphi_i(\xi) + \varphi'_i(\xi) \frac{L - 2\xi}{2} = 0$$

and a moment - equation

M_c is the mass of block and gyros, augmented by the mass of the central part of the bracket.

The lowest mode, i = 1, is symmetric and corresponds with linear motions along the roll gyro input axis and along the pitch and yaw gyros output axes.

Integration of the spatial equation and its boundary conditions leads to the following relation for the lowest w_i:

$$w_1 = \left(\frac{\alpha_1}{\xi}\right)^2 \left(\frac{E I_b}{\mu_L}\right)^{1/2}$$

where the dimensionless number α_1 is the smallest positive root of

$$(\sin\alpha \cos h\alpha + \cos\alpha \sin h\ \alpha) + \frac{M_c}{2\mu_L\xi}\alpha(\cos\alpha \cos h\ \alpha - 1) = 0$$

The resonant frequency is w_1 as shown by the time dependent equation for T(t) provided

$$| w_{z\,b}(t) | << w_1$$

The satisfaction of this condition will be verified later. Generally, w_1 is high and, therefore, higher modes (which would affect angular rates) may be neglected in this study, since they are suppressed by the slower gyro-response.

As a result, in conjunction with the various gimbal equations (2-6), one must use for yaw and pitch gyros

$$a_x = A_x,\ a_z = A_z$$

for roll gyro

$$A_x = \frac{a_x}{1+2\zeta_{br}\frac{s}{w_{br}} + \left(\frac{s}{w_{br}}\right)^2},\ A_z = a_z \qquad (2\text{-}14)$$

with $w_{br} = w_1$; ζ_{br} is a dimensionless damping coefficient, the Laplace operator s is d/dt, and a is the inertial linear acceleration of the supporting rocket frame.

Numerical Results for the Gyro Mounting Bracket

For the stainless steel bracket, the following values are used in the equivalent beam model.

$g\rho = 0.282$ lb/in^3
$E = 2.9 \times 10^7$ lb/in^2
$I_b = 0.020$ in^4
$gM_c = 1.70$ lb
$g\mu_L = 0.102$ lb/in
$L = 8.5$ in
$\xi = 2.875$ in

Then

$$\frac{M_c}{2\mu_L \xi} = 2.9$$

$$(E I_b/\mu_L)^{1/2} = 4.7 \times 10^4 \text{ in}^2/\text{sec}$$

smallest root $\alpha_1 = 1.35$

and $\omega_1 \cong 10,400$ rad/sec

Since one can expect $|\omega_{zb}(t)| \leq 7.0$ rad/sec (i.e., ten times the pitch gyro nominal input rate), the condition $|\omega_{zb}| << \omega_1$ is easily satisfied and one has indeed

$$\omega_{br} = \omega_1 = 10,400 \text{ rad/sec}$$

Since ω_1 is already large, higher modes can be neglected in this study.

The value for ω_{br} agrees with a very rough range prediction that can be obtained from the theory of plates.

The damping ζ_{br} is unknown, but may be assumed to be smaller than 1 (no large structural damping).

2.2 Laboratory Tests and Analog Verifications

Several types of tests were performed on the gyroscopes. See Appendix B for a general description.

2.2.1 Opened Instruments

A pitch gyro and a roll gyro were opened, the damping fluid was removed and the gimbals were rotated mechanically and then released. The output waveforms are shown on Figures 2-1, 2-2, clearly indicating the very slightly damped motion of the gimbal.

The experimental results are:

Roll gyro $\omega_{gy} = 280$ rad/sec, $f_{gy} = 44.5$ Hz

Pitch gyro $\omega_{gy} = 158$ rad/sec, $f_{gy} = 25.2$ Hz

2.2.2 Transient Tests on Special Yoke, and Analog Simulation

Figure 2-3 shows one test on the roll gyro. Knowing the total angle of rotation (1^{o}) and the shape of the (upper) accelerometer trace, one can deduce the input waveform to the gyro. Figure 2-4 shows this input and the analog computer simulation response, as well as intermediate signals. The agreement between test (Figure 2-3) and simulation (Figure 2-4) is good (see e.g., the heavy marks on the simulation showing experimental values).

The parameter values used were, for the best fit,

$\omega_{gy} = 264$ rad/sec, $f_{gy} = 42.0$ Hz (roll gyro)

$\zeta_{gy} = 0.84$

$\omega_{gx} = 40\ \omega_{gy}$

$\zeta_{gx} = 0.7$

Microsyn parameter values were listed above.

Figure 2-5 and Figure 2-6 show, respectively, the test results and the simulation for another, more complex, input consisting of four succeeding pulses of alternating sign. The same parameter values were used and the agreement is acceptable between test and simulation.

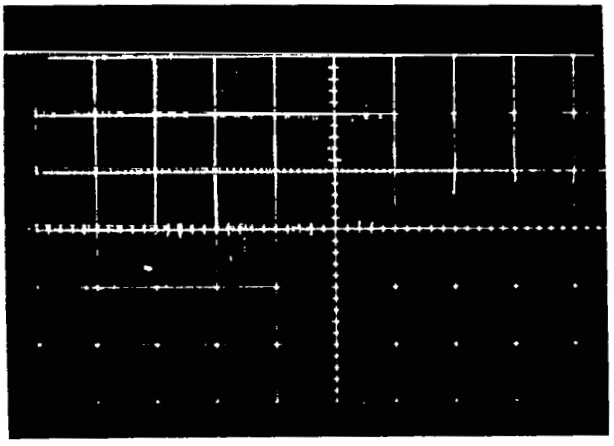

FIGURE 2-1 OPENED ROLL GYRO

TIME SCALE 10 ms/DIVISION

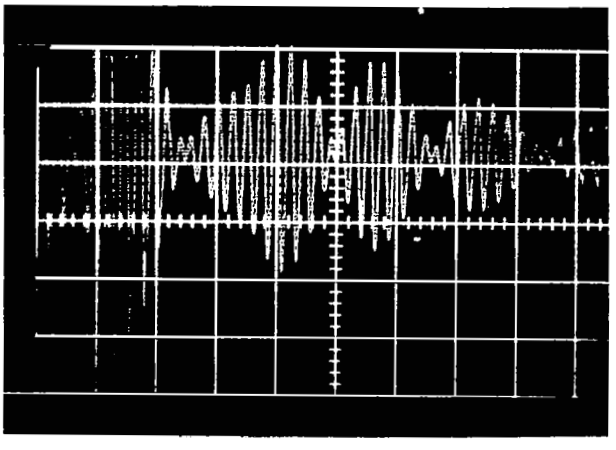

FIGURE 2-2 OPENED PITCH GYRO

TIME SCALE 10 ms/DIVISION

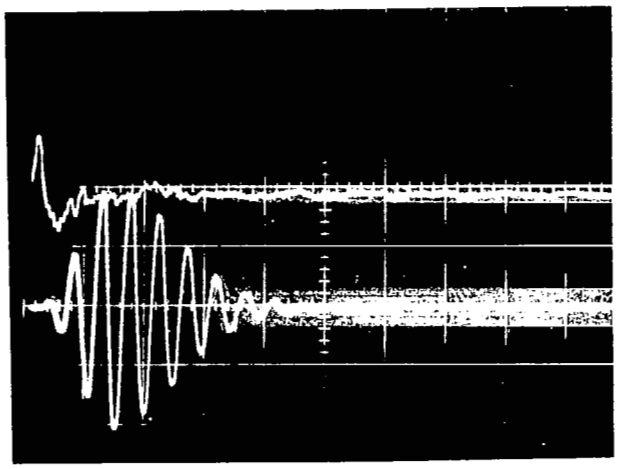

FIGURE 2-3 TRIANGULAR INPUT TO ROLL GYRO
TIME SCALE 5 ms/DIVISION
UPPER TRACE: ACCELEROMETER
LOWER TRACE: ROLL GYRO OUTPUT,
7.5 VOLTS/VERTICAL DIVISION
MAXIMUM ANGULAR ROTATION IS 1°

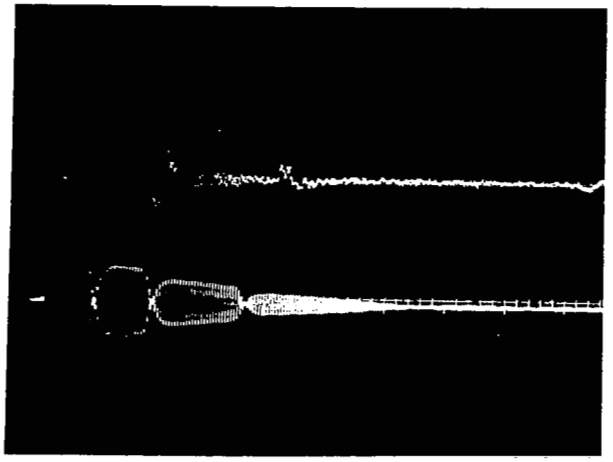

FIGURE 2-5 MULTI-PULSE INPUT TO ROLL GYRO
MAXIMUM ANGULAR ROTATION IS 2.5°
UPPER TRACE: ACCELEROMETER 10 ms/
DIVISION
LOWER TRACE: ROLL GYRO OUTPUT 50 ms/
DIVISION AND 15 VOLTS/VERTICAL DIVISION

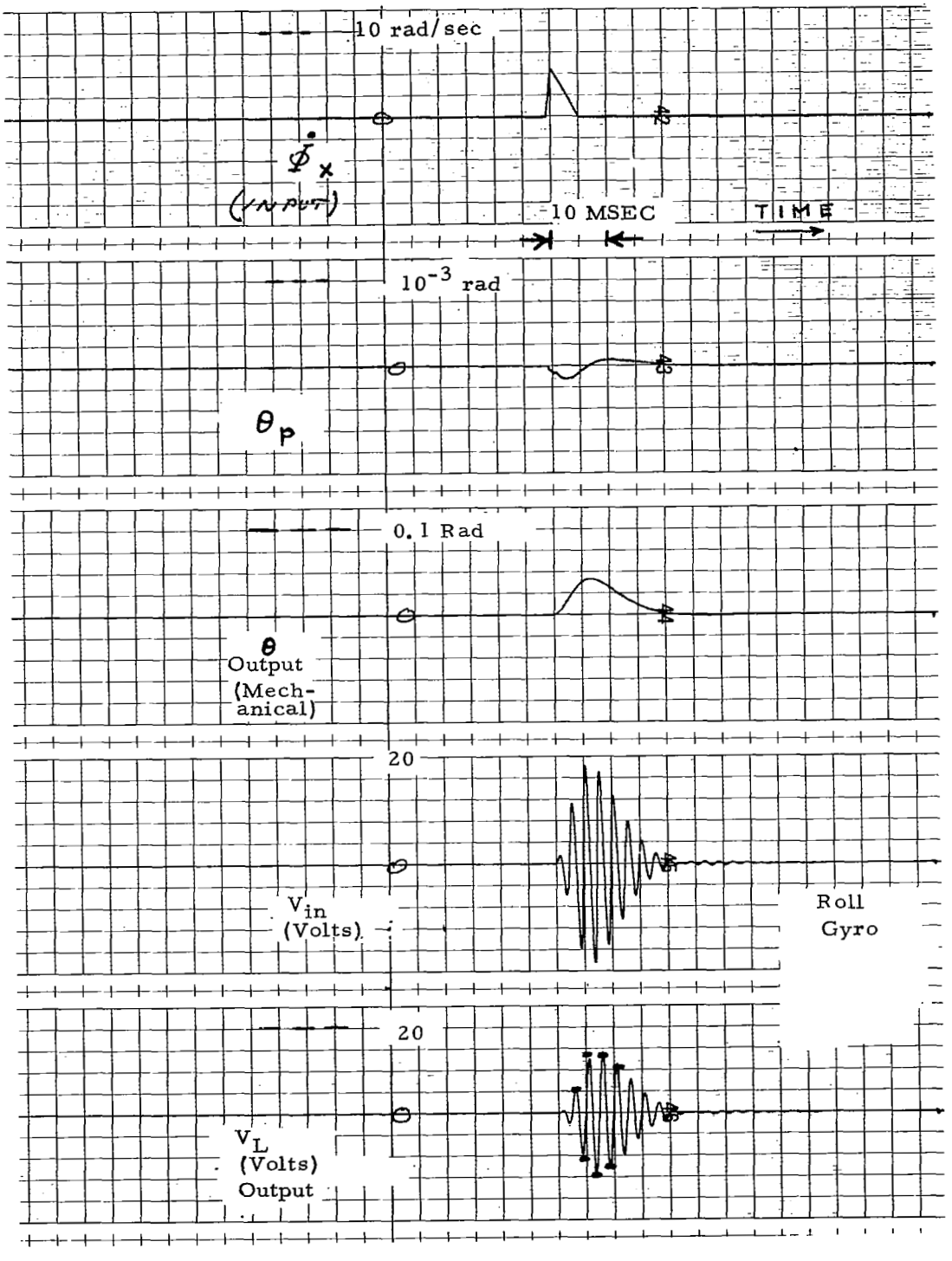

Figure 2-4, Analog Simulation of Figure 2-3

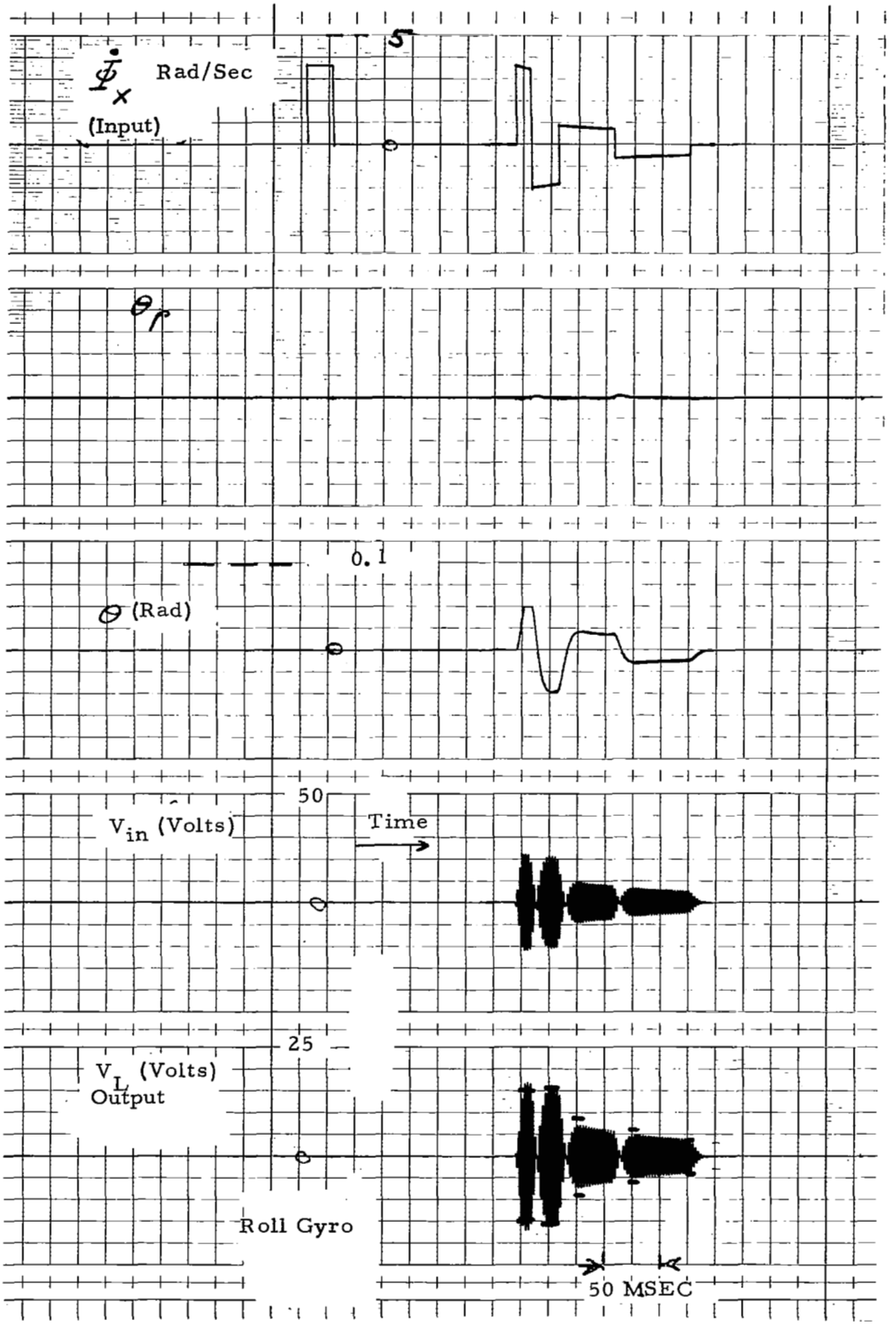

Figure 2-6, Analog Simulation of Figure 2-5

This value for ω_{gy} is consistent with the one found for undamped motion (section 2.2.1), within the accuracy obtainable which is of the order of 5 percent (see also section 7, Conclusions).

2.2.3 Gyro Tests on Flight Table and Analog Simulation

The inner gimbal of a flight table was used to generate particular inputs to the gyros. These inputs consisted of pulses alone or superimposed on sinusoidal inputs. Some pictures of the tests are shown in Figures 2-7 and 2-8 for the roll gyros and 2-9 and 2-10 for the pitch gyros. Upper traces are gyro responses to the inputs shown in the lower traces. The corresponding analog computer simulations are shown in Figures 2-11 and 2-12 (roll gyros) and 2-13 and 2-14 (pitch gyros), respectively. Note that the output modulation was omitted, for clarity; therefore, the simulations give the envelopes of the gyro output waveforms (or in other words, the demodulated output of the gyros). The parameter values for the roll gyro are the same as the ones used in the previous simulations (section 2.2.2); those for the pitch gyro are

$$\omega_{gy} = 164 \text{ rad/sec } (f_{gy} = 26 \text{ Hz})$$

$$\zeta_{gy} = 0.75$$

The agreement between tests and simulation is well within the tolerances and uncertainties.

2.2.4 Summary of Numerical Results for Gyros

	Pitch Gyros (40°/sec)	Roll Gyros (100°/sec)
Output axis	$\omega_{gy} = 164$ rad/sec (26 Hz) $\zeta_{gy} = 0.75$	$\omega_{gy} = 264$ rad/sec (42 Hz) $\zeta_{gy} = 0.84$
Mechanical gain	$\frac{H_r}{K_{gy}} = 0.0647$ sec	$\frac{H_r}{K_{gy}} = 0.0248$ sec
Stop	θ max $= 3^{\circ} = 0.052$ rad	
Full Scale Output	9.75 V rms	9.3 V rms
Input axis	$w_{gx} = 40\ w_{gy}$ $\zeta_{gx} = 0.7$ (note: w_{gx} is sufficiently large to be negligible)	
Output Circuit	See end of Section 2.1.2	
Parasitic Effects	$\lvert g\ M_{gw}\ \delta\ / H_r \rvert \leq 5.3 \times 10^{-4}$ (rad/sec) per g $K_c = \infty$ or $\theta_c \equiv 0$	
Bracket	$w_{br} = 10,400$ rad/sec ($f_{br} = 1,660$ Hz)	

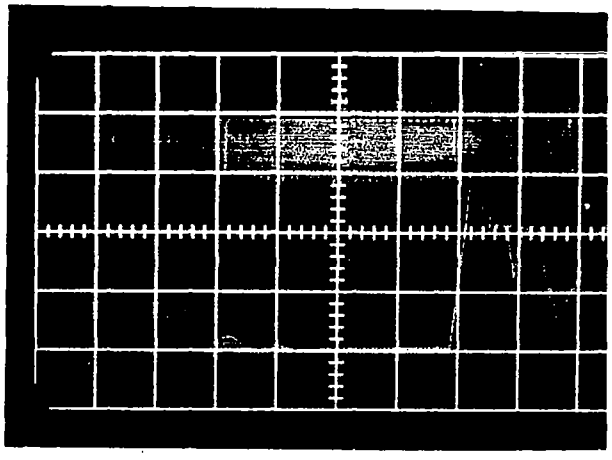

FIGURE 2-7 ROLL GYRO CARCO TABLE TEST:
PULSE INPUT
TIME SCALE: 20 ms/DIVISION
LOWER TRACE: INPUT (RATE)
UPPER TRACE: GYRO RESPONSE
10 VOLT/DIVISION

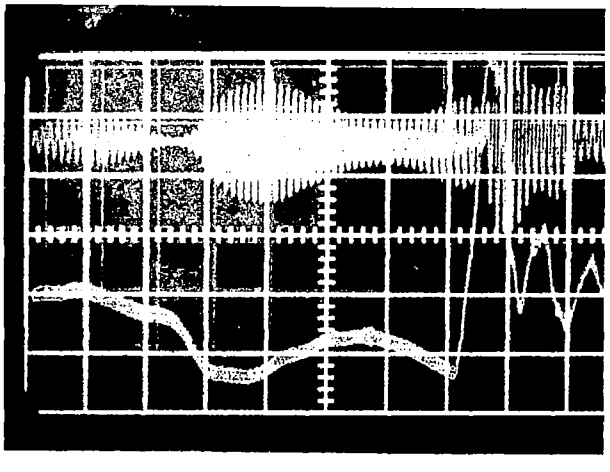

FIGURE 2-8 ROLL GYRO CARCO TABLE TEST:
PULSE PLUS 10 Hz SINUSOIDAL INPUT
TIME SCALE: 20 ms/DIVISION
LOWER TRACE: INPUT (RATE)
UPPER TRACE: GYRO RESPONSE
10 VOLT/DIVISION

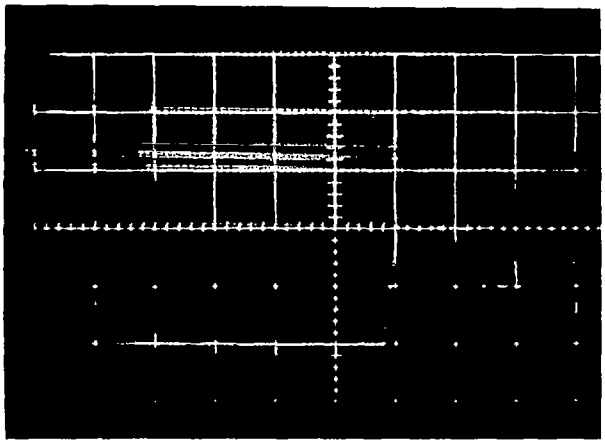

Figure 2-9 PITCH GYRO CARCO TABLE TEST:
PULSE INPUT
TIME SCALE: 20 ms/DIVISION
LOWER TRACE: INPUT (RATE)
UPPER TRACE: GYRO RESPONSE
10 VOLT/DIVISION

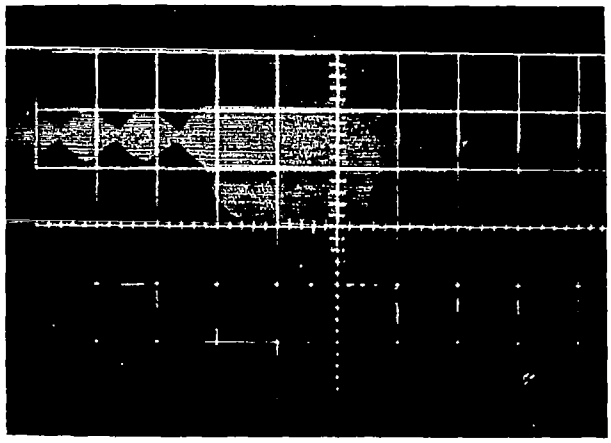

FIGURE 2-10 PITCH GYRO CARCO TABLE TEST:
PULSE PLUS 10 Hz SINUSOIDAL INPUT
TIME SCALE: 50 ms/DIVISION
LOWER TRACE: INPUT (RATE)
UPPER TRACE: GYRO RESPONSE
10 VOLT/DIVISION

Figure 2-11, Pulse-Response of Roll Rate Gyro

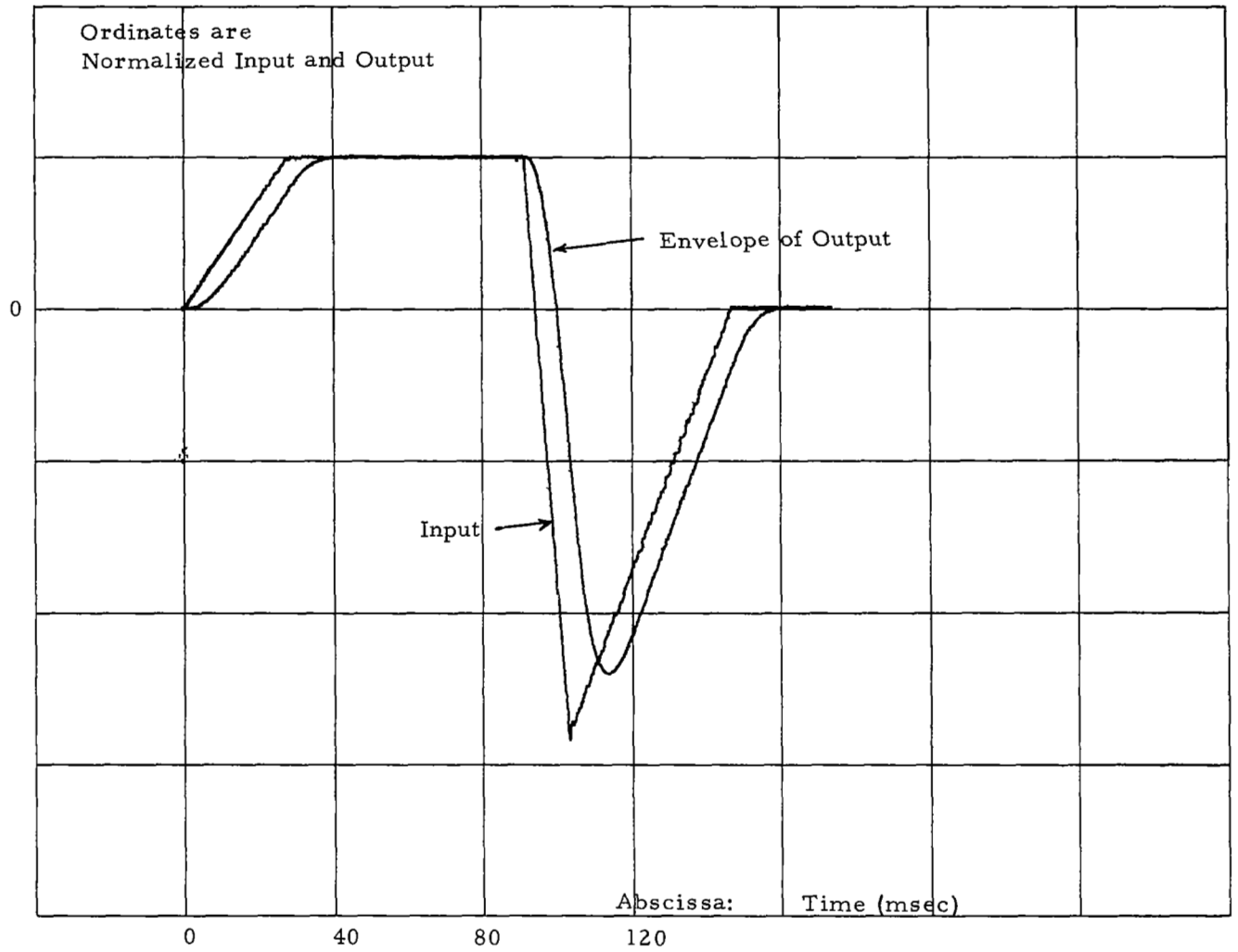

Figure 2-12, Response of Roll Rate Gyro

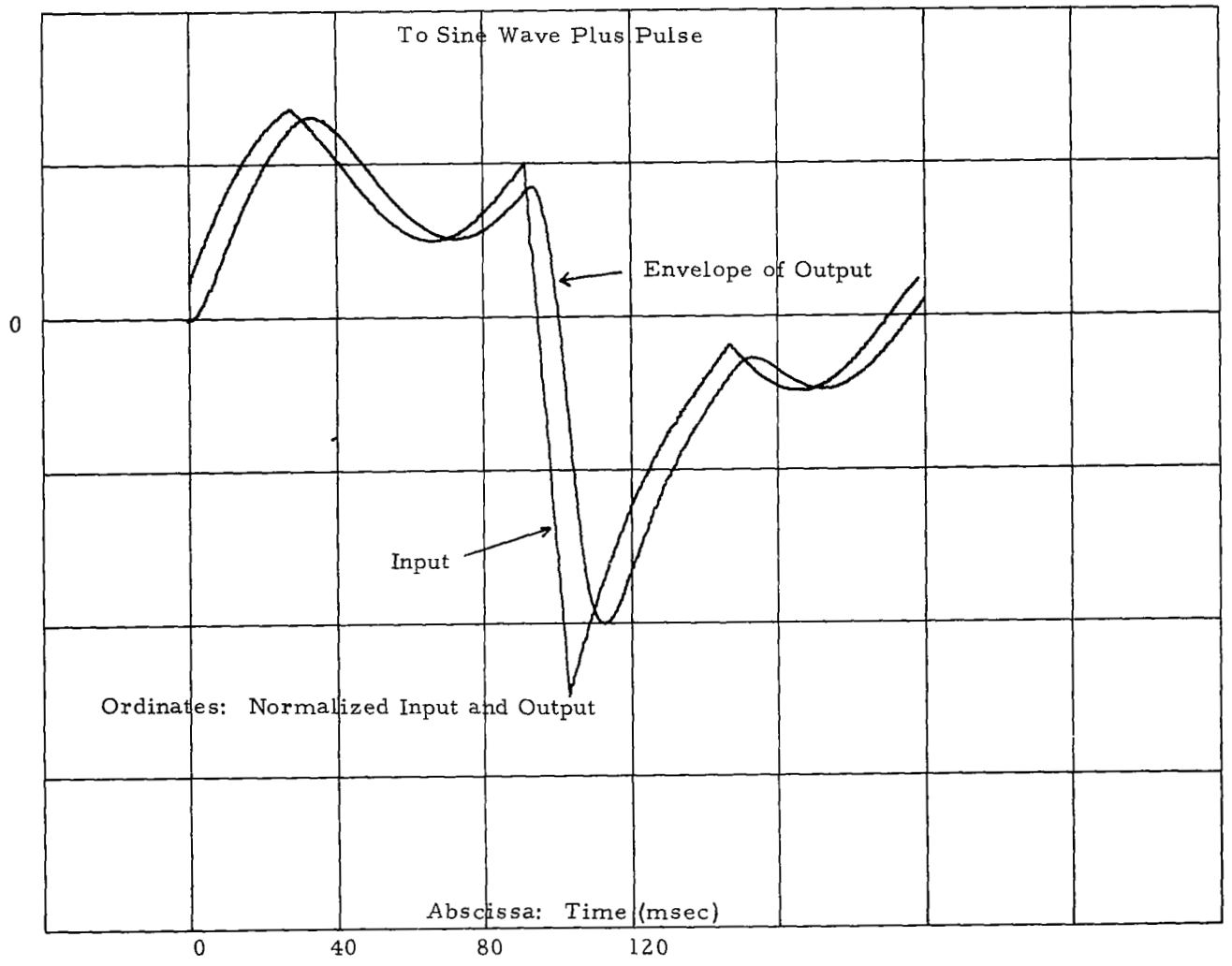

Figure 2-13, Pulse-Response of Pitch Rate Gyro

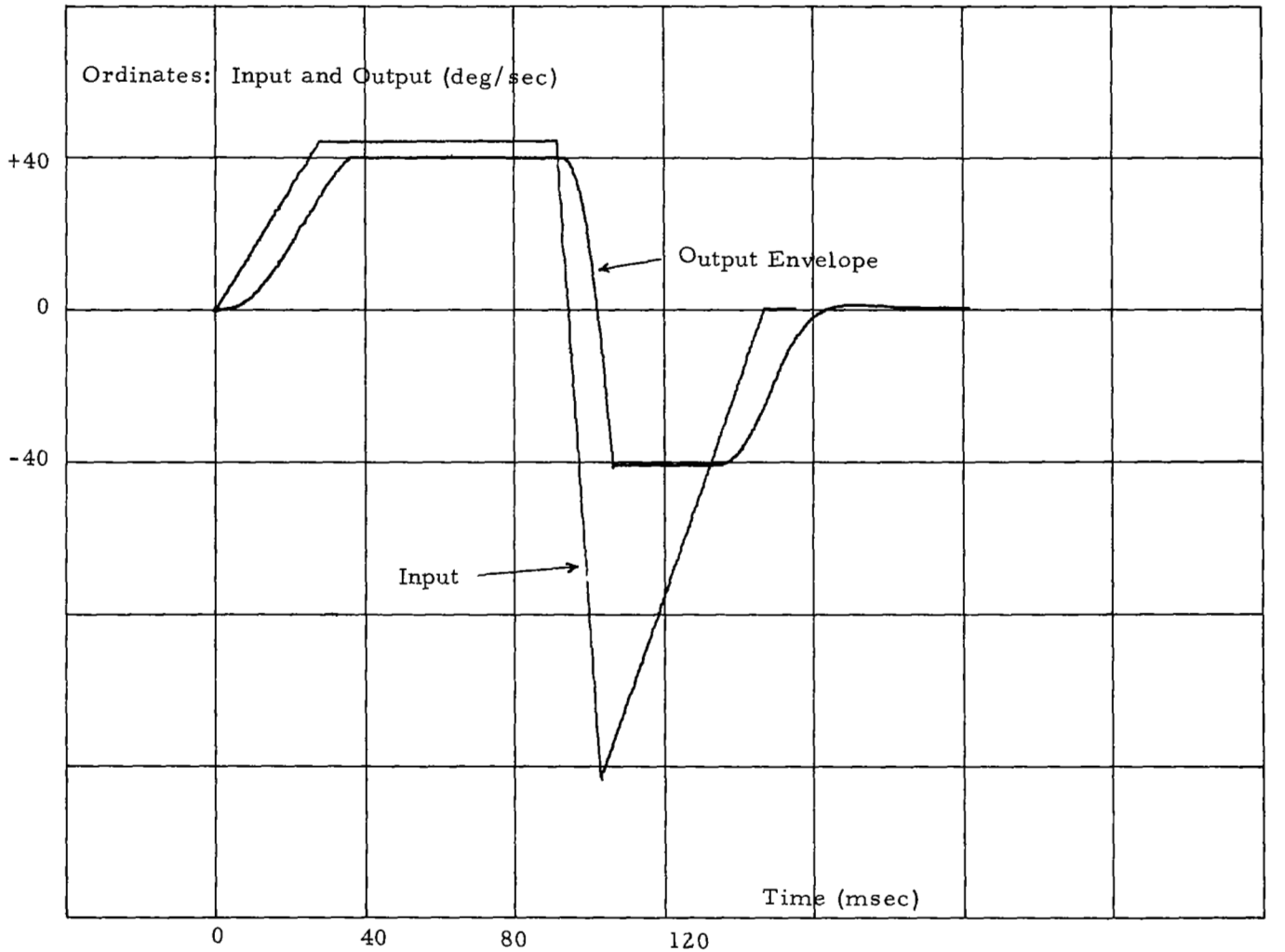

Figure 2-14, Response of Pitch Rate Gyro
to Sine-Plus-Pulse

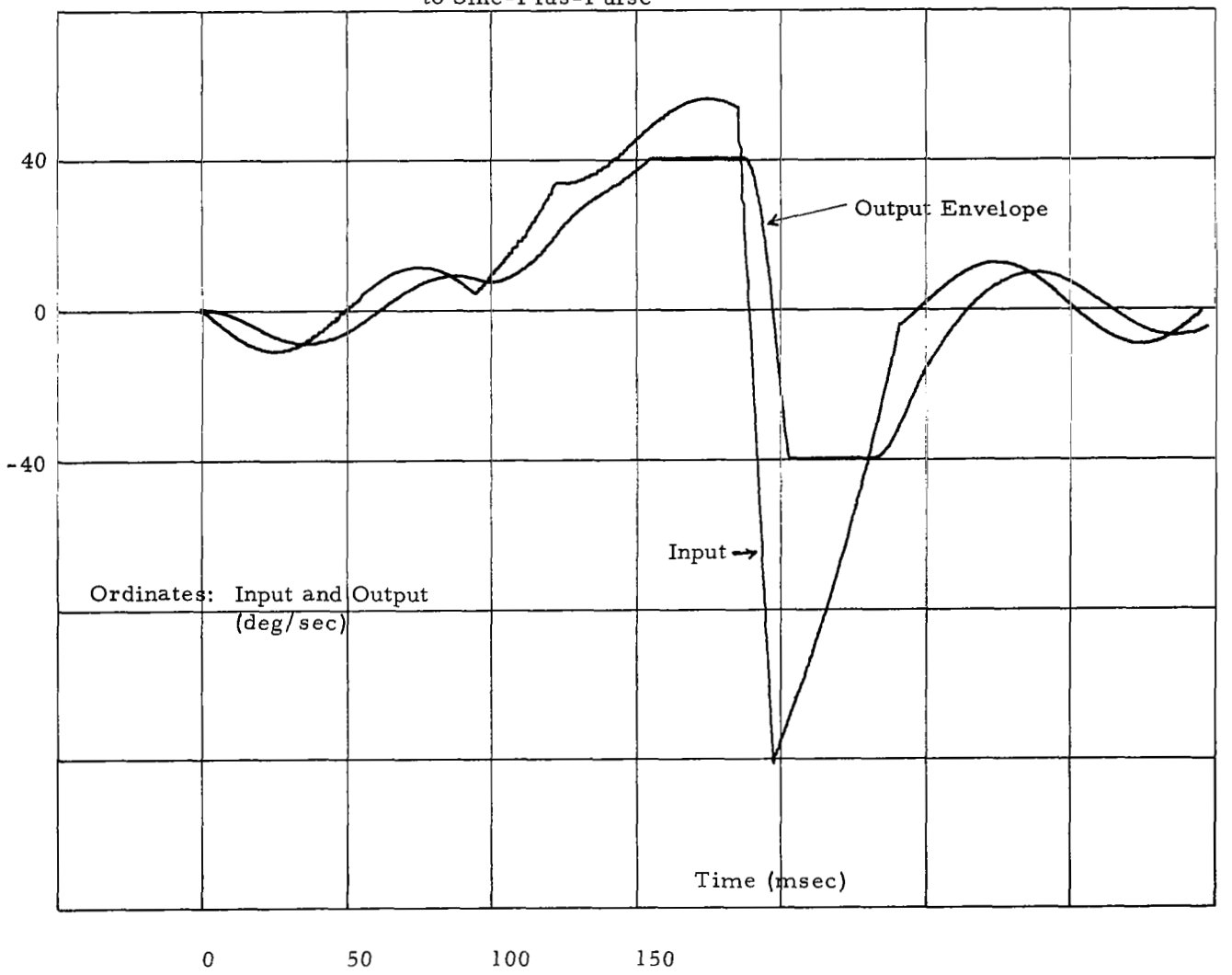

3. ACCELEROMETERS

Two types of single axis accelerometers used on the Scout vehicles are to be modeled here.

Gulton Industries - LA 530250 (±3g)
Gulton Industries - LA 460250 (-1g to +15g)

Both types are servo-accelerometers.

The procurement specifications require:

an output voltage from 0 to +5 VDC into 500 KΩ
a natural frequency of 135 Hz (nominal)
a nominal damping coefficient of 0.6 to 0.8 at 75°F
crosstalk: 0.010 g/g
overload stops: 125% of full range

The manufacturer expects a natural frequency of 90 Hz (-3g, +3g) and 110 Hz (-1g, +15g), with a damping around $\zeta = 0.7$.

3.1 Theoretical Model

3.1.1 Electro-Mechanical Part of Accelerometers

These servo-accelerometers consist of a pendulously supported proofmass, whose motion is detected by an eddy-current pickoff. The pickoff signal, after demodulation, amplification and compensation, actuates a torque generator. Generally, the purpose of the feedback compensation is to obtain a well behaved second order response. However, experiments conducted during a Scout vehicle failure investigation indicate that above the break-frequency of the basic second order system, the system frequency response deviates markedly from ideal order behavior: the attenuation is higher (indicating an apparent increase in damping) while the phase shift corresponds to an apparent decrease in damping. While detailed information on the internal structure (especially damping) and the compensation circuits could not be obtained, an incomplete block diagram, shown below, can still be constructed.

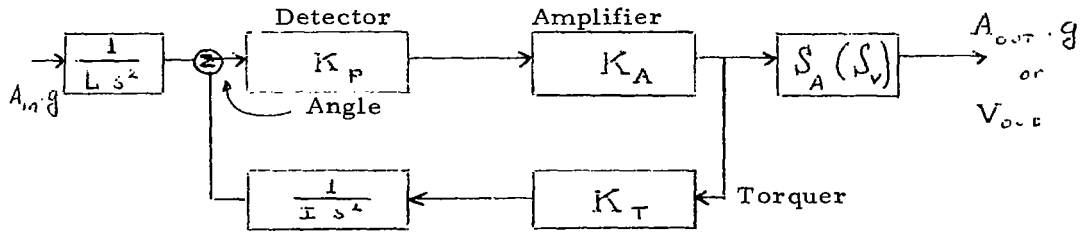

Compensation and Damping Omitted
Block Diagram for Servo-Accelerometers

The notations are:

A_{in}: Input acceleration (g's), (inertial acceleration of case along sensitive axis minus gravitational acceleration on proofmass along same axis)

A_{out}: Output reading converted in g's

V_{out}: Direct output reading in volts

I: Moment of inertia of proofmass with respect to suspension (g cm^2)

L: Radius of gyration of proofmass referred to support (cm)

K_p: Gain of detector or signal generator (V/rad)

K_A: Amplifier gain (A/V)

K_T: Torquer-constant (dyne cm/A)

S_A: Scaling factor to g's ($\frac{cm}{sec^2}$ /A)

S_V: Scaling factor to volts (V/A)

s: Laplace transform operator

The linearized transfer function is then

$$\frac{A_{out}}{A_{in}} = \frac{S_A\, I}{L\, K_T} \quad \frac{1}{1 + s^2 \frac{I}{K_p K_A K_T}}$$

indicating that $S_A = \frac{L\, K_T}{I}$

and that the natural (undamped) frequency is given by

$$w_n^2 = K_p\, K_A\, K_T / I \qquad (3\text{-}1)$$

For a more complete model, damping and cross-coupling must be considered. Due to misalignments and structural constraints, cross-coupling can be expected, i.e., case accelerations A_{cross} perpendicular to the sensitive axis will influence the readings. Lack of knowledge of instrument structure prevents theoretical modeling of the cross-coupling effect. Therefore, the same dynamic behavior is adopted for cross-acceleration, with a scale factor ψ for which an upper bound can be found from manufacturer's data. These considerations lead to the following model:

$$A_{out} = \frac{A_{in}}{1 + 2\zeta \frac{s}{w_n} + \frac{s^2}{w_n^2}} + \psi \frac{A_{cross}}{1 + 2\zeta \frac{s}{w_n} + \frac{s^2}{w_n^2}} \qquad (3\text{-}2)$$

where ψ is bounded $\quad |\psi| \leq \psi_{max} \qquad (3\text{-}3)$

The "angle" ψ_{max} is partly determined by the maximum angular rotation of the proofmass.

Some Numerical Results for the Servo-Accelerometers (see also Appendix B)

A (-1g, +15g) instrument was opened and open loop information was obtained. Measurements of the proofmass and its connecting system led to a calculated value of the inertia

$$I = 0.213 \text{ g cm}^2 \ (\pm 10\%)$$

and a weight of 0.9 gram.

Static experiments on the torquer (using balancing weights added to the proofmass) gave

$$K_T = 0.139 \times 10^6 \text{ dyne cm/A} \ (\pm 5\%)$$

The signal generator (K_p) and amplifier (K_A) were combined in the open loop tests and yielded

$$K_p K_A = 1.22 \text{ A/rad} \ (\pm 10\%)$$

Hence, one finds for the (-1g, +15g) accelerometer

$$w_n = 893 \text{ rad/sec} \ (\pm 15\%)$$

Damping could not be determined after the instrument was opened.

Manufacturer's data show $\psi_{max} = 0.002$

3.1.2 Accelerometer Bracket

The accelerometers are mounted on stainless steel brackets which are then fastened to the rocket frame. The configuration is shown in Figure 3-1. The bracket is very stiff along the sensitive axis and along the perpendicular cross-axis, but less stiff along the lateral cross-axis. The purpose of this section is to calculate the resonant frequency for transmission along the lateral cross-axis.

First one calculates the stiffness k_c of the corners, with definition:

$$k_c = \frac{\text{moment exerted on a corner}}{\text{total additional bending angle of corner (radians)}}$$

Using the theory of bending of curved bars (Reference 4), one finds:

$$k_c = \frac{2}{\pi} E w t r_c \left(1 - \frac{t/r_c}{\ln_e \frac{1 + (t/2 r_c)}{1 - (t/2 r_c)}} \right)$$

where E is Young's modulus and the other symbols are illustrated in the Figure 3-2 (w = width, t = thickness, r_c = rounding radius). $\ln_e$ is the natural logarithm. Next, one calculates the stiffness k_L for the linear displacement deformation of Figure 3-2.

$$k_L = \frac{\text{force along lateral cross-axis through instrument}}{\text{linear displacement (of instrument)}}$$

k_L depends on k_c and the properties of the bending members. Application of beam theory gives after some manipulations

$$\frac{1}{k_L} = \frac{a^2}{2} \left(\frac{1}{k_c} + \frac{2a}{E w t^3} \right)$$

The approximate resonant frequency of the bracket w_{br} is then given by

$$w_{br} = (2 k_L / M_{eff})^{1/2}$$

where M_{eff} = mass of accelerometer plus mass of top plate of bracket.

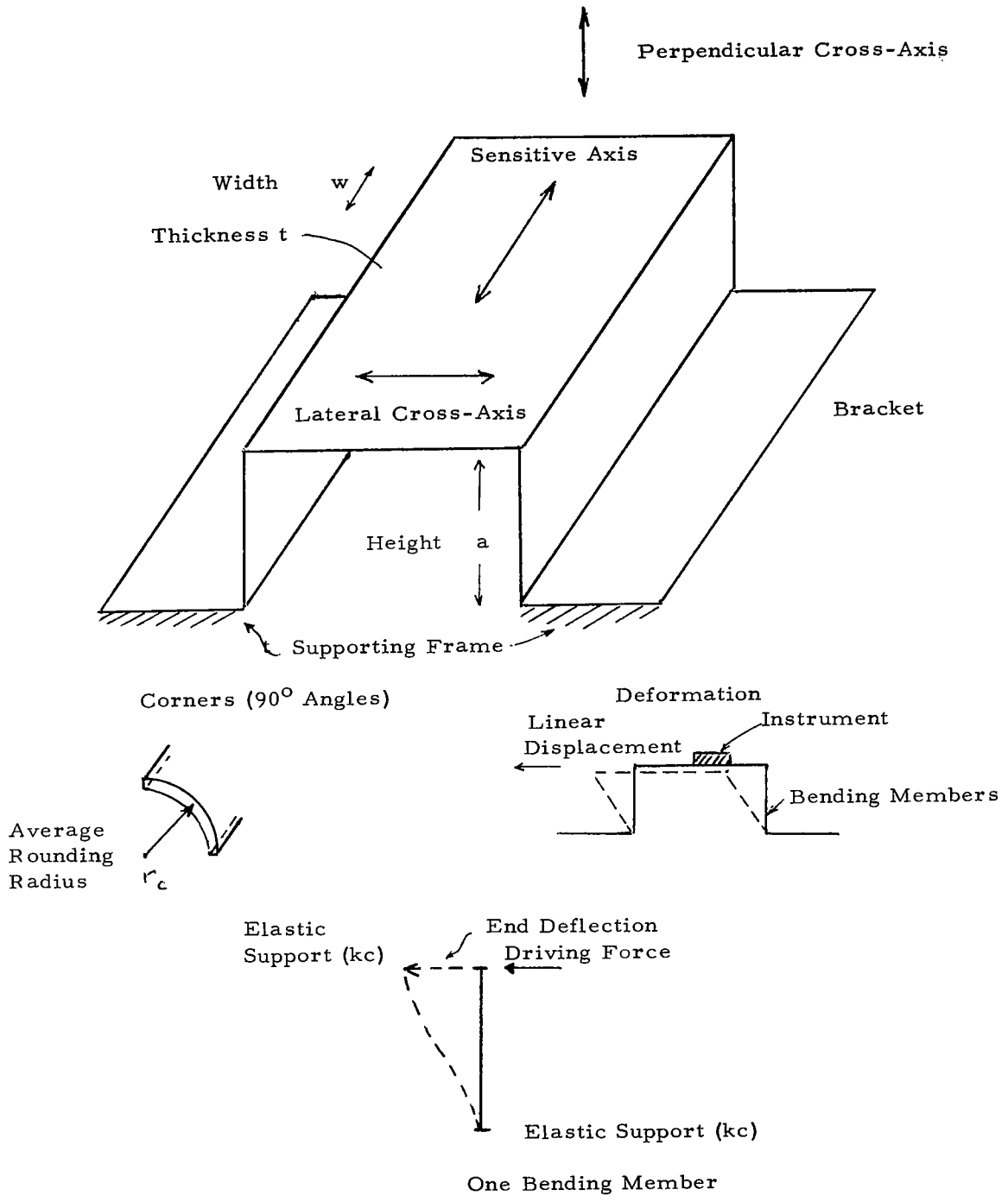

Figure 3-1 Accelerometer Bracket

Then, for accelerations along the lateral cross-axis.

$$A_{\text{lateral, cross}} = a_{\text{lateral, cross}} \frac{1}{1+2\zeta_{br}\frac{s}{w_{br}}+\frac{s^2}{w^2_{br}}} \qquad (3\text{-}4)$$

where $A_{\text{lateral, cross}}$ is a parasitic input to the accelerometer, and $a_{\text{lateral, cross}}$ is the inertial acceleration experienced by the support.

For the other axes, one has:

sensitive axis perpendicular cross-axis	$A = a$

The coefficient ζ_{br} is the dimensionless damping coefficient for the bracket vibrations.

Numerical Results for the Accelerometer Bracket

The same bracket is used for both types of accelerometers.

ζ_{br} is unknown, but may be expected to lie between 0 and a maximum slightly larger than 1.

For the stainless steel bracket with weight density = $(g\rho) = 0.282\ \text{lb/in}^3$

$E = 2.9 \times 10^7\ \text{lb/in}^2$
$w = 3$ in.
$t = 0.047$ in.
$a = 0.625$ in.
length of top plate = 1.375 in.
$r_c = 0.1$ in.

one gets

$$k_c = 0.49 \times 10^4 \ \frac{\text{in. lb.}}{\text{rad}}$$

$$k_L = 1.5 \times 10^4 \ \frac{\text{lb.}}{\text{in.}}$$

The weight of the top plates is 0.055 lb. Then $(g M_{eff}) = 0.274$ lb. finally giving $w_{br} = 6,500$ rad/sec ($f_{br} = 1,040$ Hz) which falls within the frequency range of interest.

3.2 Laboratory Tests and Analog Computer Simulations

As for the gyros, several types of tests were performed on the accelerometers. See general description in Appendix B.

3.2.1 Transient Tests on Special Yoke, and Analog Simulations

Both categories of accelerometers (-3g, +3g) and (-1g, +15g) were subjected to triangular input pulses, shown in Figures 3-2, 3-3, 3-4 and 3-5. The corresponding analog computer simulations are shown for comparison in Figures 3-6, 3-7, 3-8 and 3-9. The agreement is within acceptable tolerances.

The best fit was found for the following parameter values:

	(-3g, +3g)*	(-1g, +15g)
Resonance w_n (rad/sec)	800 (fast input) to 850 (slow input)	750
Damping ζ_n	0.35 (fast input) to 0.55 (slow input)	0.35
Gain	0.85 V per g	0.34 V per g

Nominal output range 0 to 5.1 V

*Note: For another (-3g, +3g) instrument, w_n = 700 rad/sec, ζ_n = 0.3 (fast) to 0.45 (slow) was found to give a best fit. This remark gives an idea of the possible spread among instruments, of the order of 10% to 20%. Such a typical spread immediately yields a bound on the accuracy for which one should strive in obtaining parameter values for a series of instruments in the present study. Of course, for one particular instrument one may try to achieve a higher accuracy in identifying parameter values. One also observes a slight non-linear effect in the decrease of the damping factor ζ_n, when the input gets faster, at least for the (-3g, +3g) type.

3.2.2 Carco Table Tests for Accelerometers and Analog Verification

Pulses, alone or super-imposed on 10 Hz sine values, were used as inputs to the accelerometers. Some experimental results and analog simulations are shown in Figures 3-10, 3-11 3-12, 3-13, respectively. The parameter values used are the same as before (in section 3.2.1). There is some discrepancy, the negative value of the first undershoot in the simulations, but this is probably due to uncertainty caused by ringing in the very first part of the input waveform. Elsewhere, the agreement is acceptable.

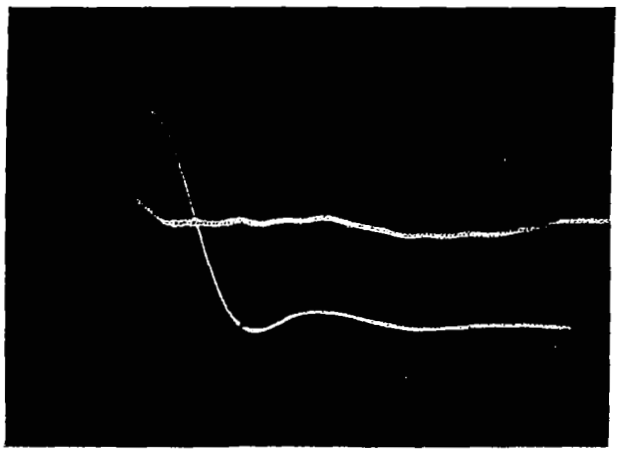

FIGURE 3-2 SLOW TRIANGULAR INPUT TO (-3g, +3g) ACCELEROMETER
TIME SCALE: 2 ms/DIVISION
UPPER TRACE: INPUT (PIEZO-ELECTRIC ACCELEROMETER)
LOWER TRACE: INSTRUMENT RESPONSE 0.5 VOLT/DIVISION

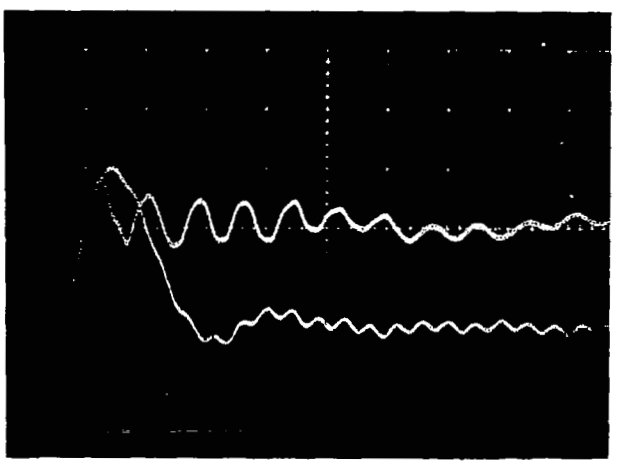

FIGURE 3-3 FAST TRIANGULAR INPUT TO (-3g, +3g) ACCELEROMETER
TIME SCALE: 2 ms/DIVISION
UPPER TRACE: INPUT (PIEZO-ELECTRIC ACCELEROMETER)
LOWER TRACE: INSTRUMENT RESPONSE 0.5 VOLT/DIVISION

Figure 3-6, (-3g, +3g) Accelerometer No. 140

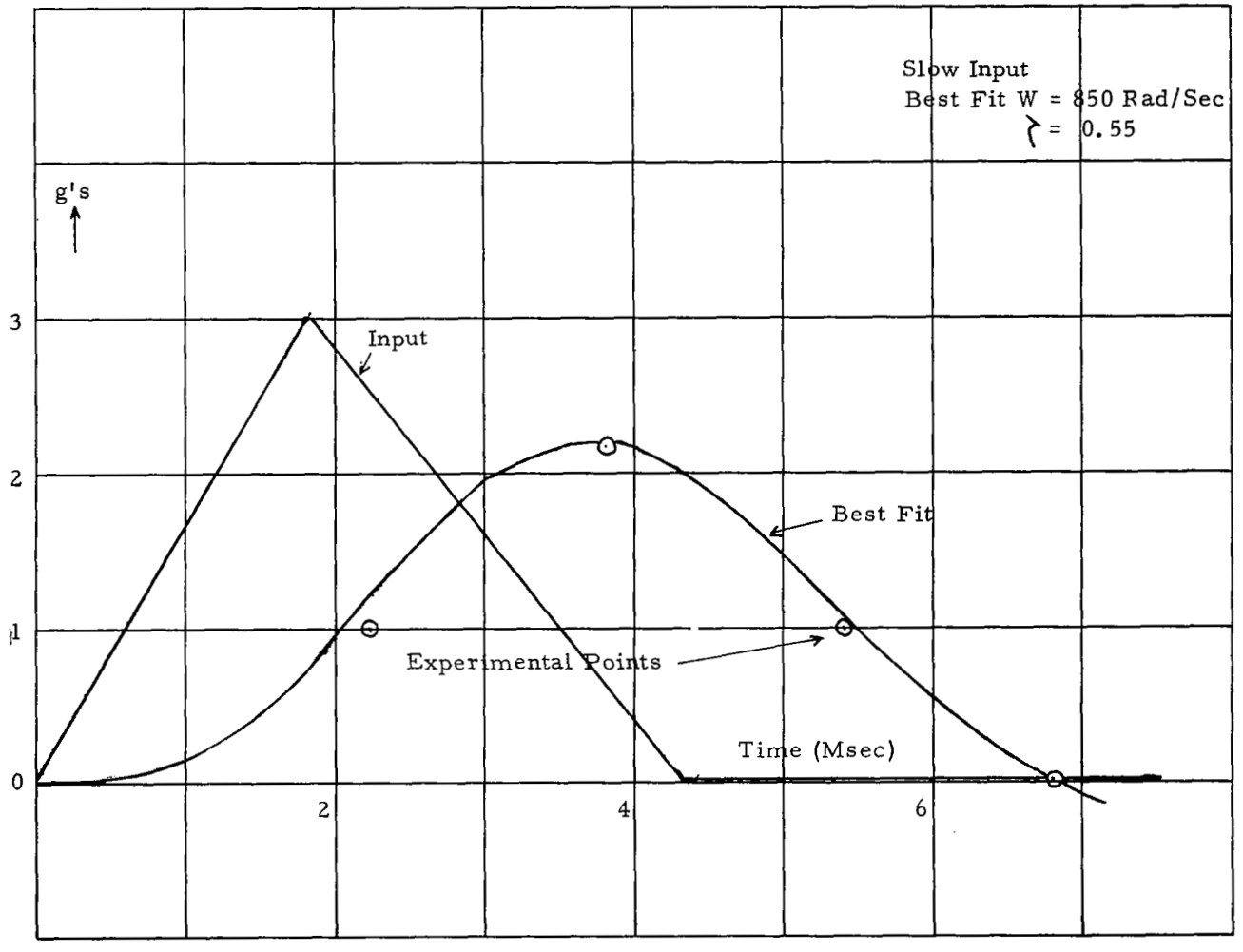

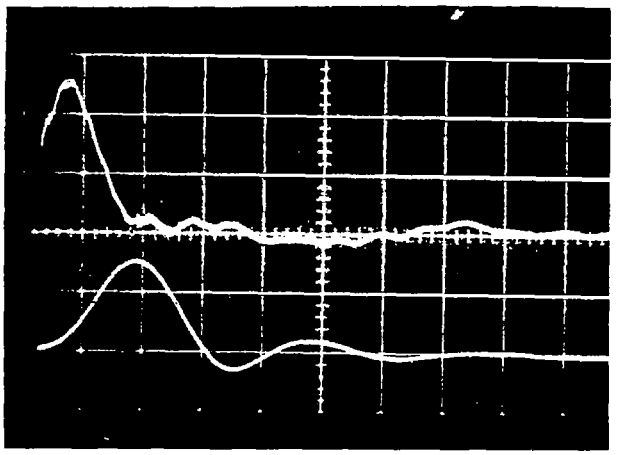

FIGURE 3-4 SLOW TRIANGULAR INPUT TO
(-1g, +15g) ACCELEROMETER
TIME SCALE: 2 ms/DIVISION
UPPER TRACE: INPUT
LOWER TRACE: INSTRUMENT RESPONSE
1 VOLT/DIVISION

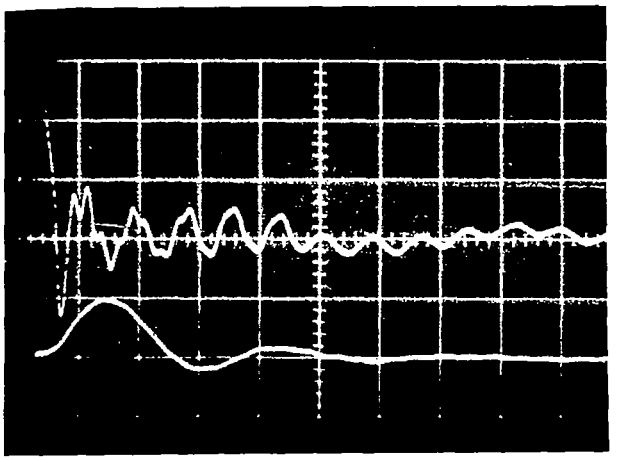

FIGURE 3-5 FAST TRIANGULAR INPUT TO
(-1g, +15g) ACCELEROMETER
TIME SCALE: 2 ms/DIVISION
UPPER TRACE: INPUT
LOWER TRACE: INSTRUMENT RESPONSE
0.5 VOLT/DIVISION

Figure 3-7, (-3g, +3g) Accelerometer No. 140

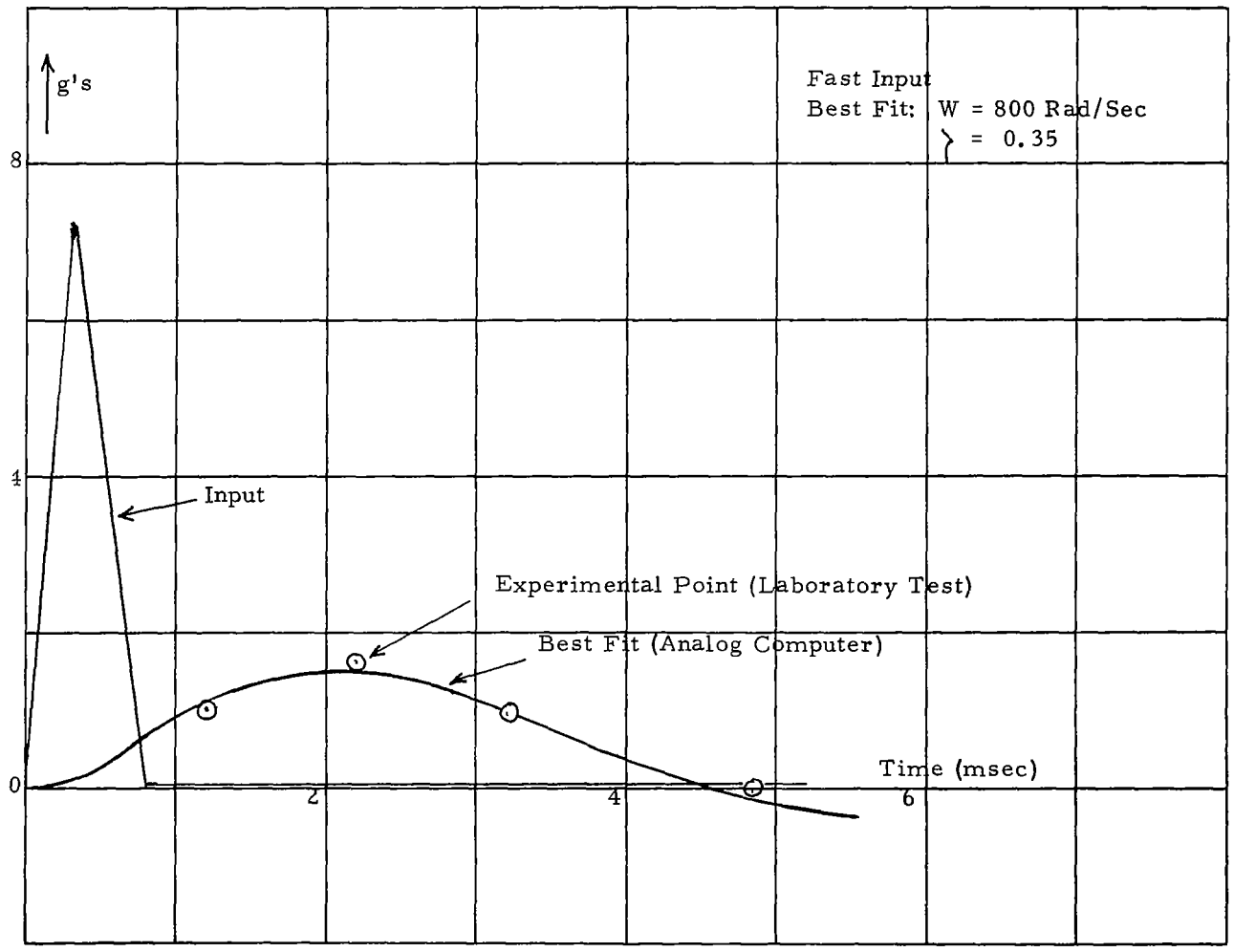

Figure 3-8, (-1g, +15g) Accelerometer No. 119

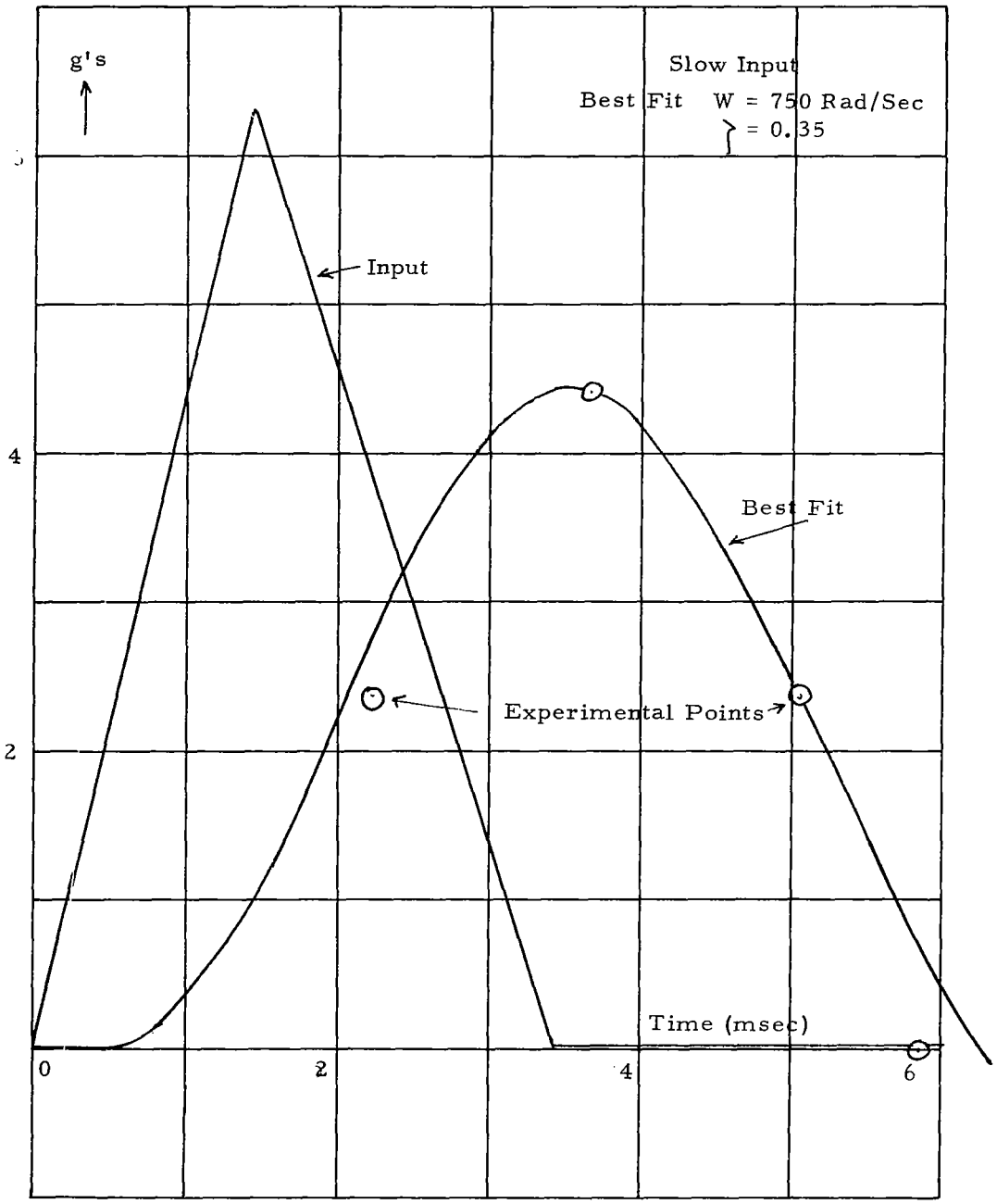

Figure 3-9, (-1g, +15g) Accelerometer No. 119

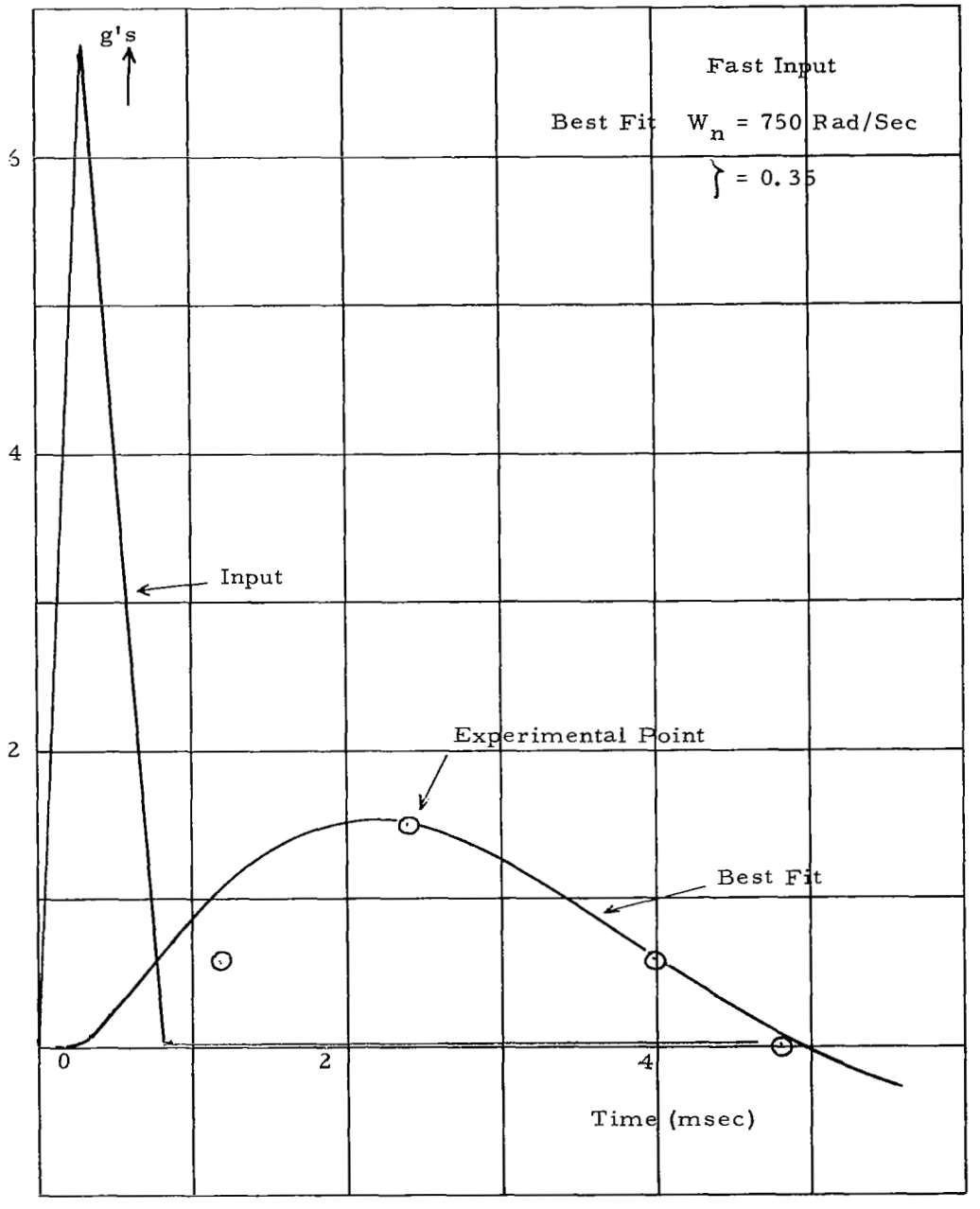

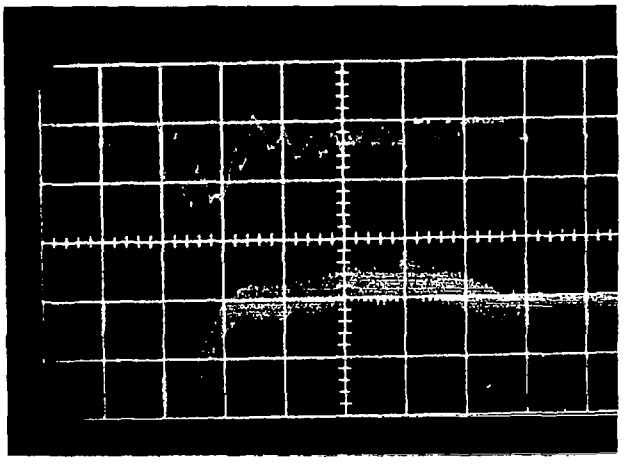

FIGURE 3-10 CARCO TABLE TEST FOR
(-3g, +3g) ACCELEROMETER
TIME SCALE: 20 ms/DIVISION
LOWER TRACE: INTEGRAL OF PULSE INPUT
(A VELOCITY)
UPPER TRACE: INSTRUMENT RESPONSE
1 VOLT/DIVISION

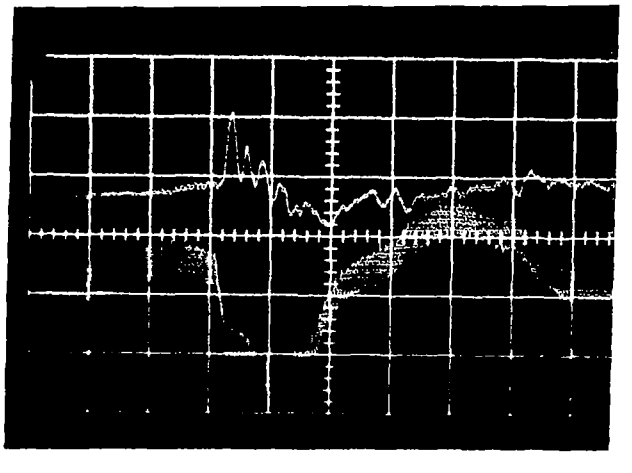

FIGURE 3-11 CARCO TABLE TEST FOR
(-3g, +3g) ACCELEROMETER
TIME SCALE: 20 ms/DIVISION
LOWER TRACE: INTEGRAL OF INPUT
(PULSE PLUS 10 Hz SINE)
UPPER TRACE: INSTRUMENT RESPONSE
2 VOLT/DIVISION

Figure 3-12, Pulse-Response of Accelerometer

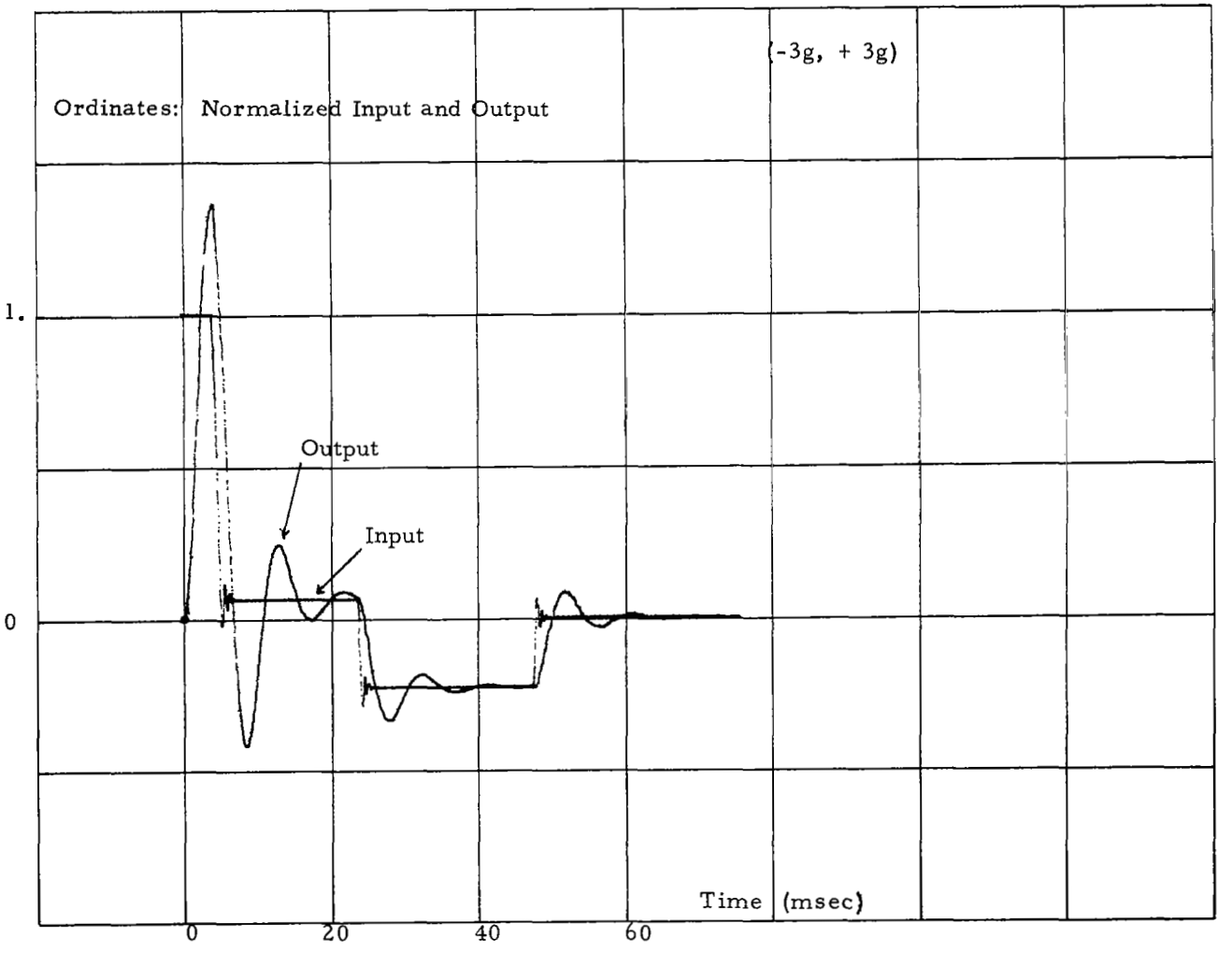

Figure 3-13, Response of (-3g, +3g) Accelerometer to Sine-Plus-Pulse

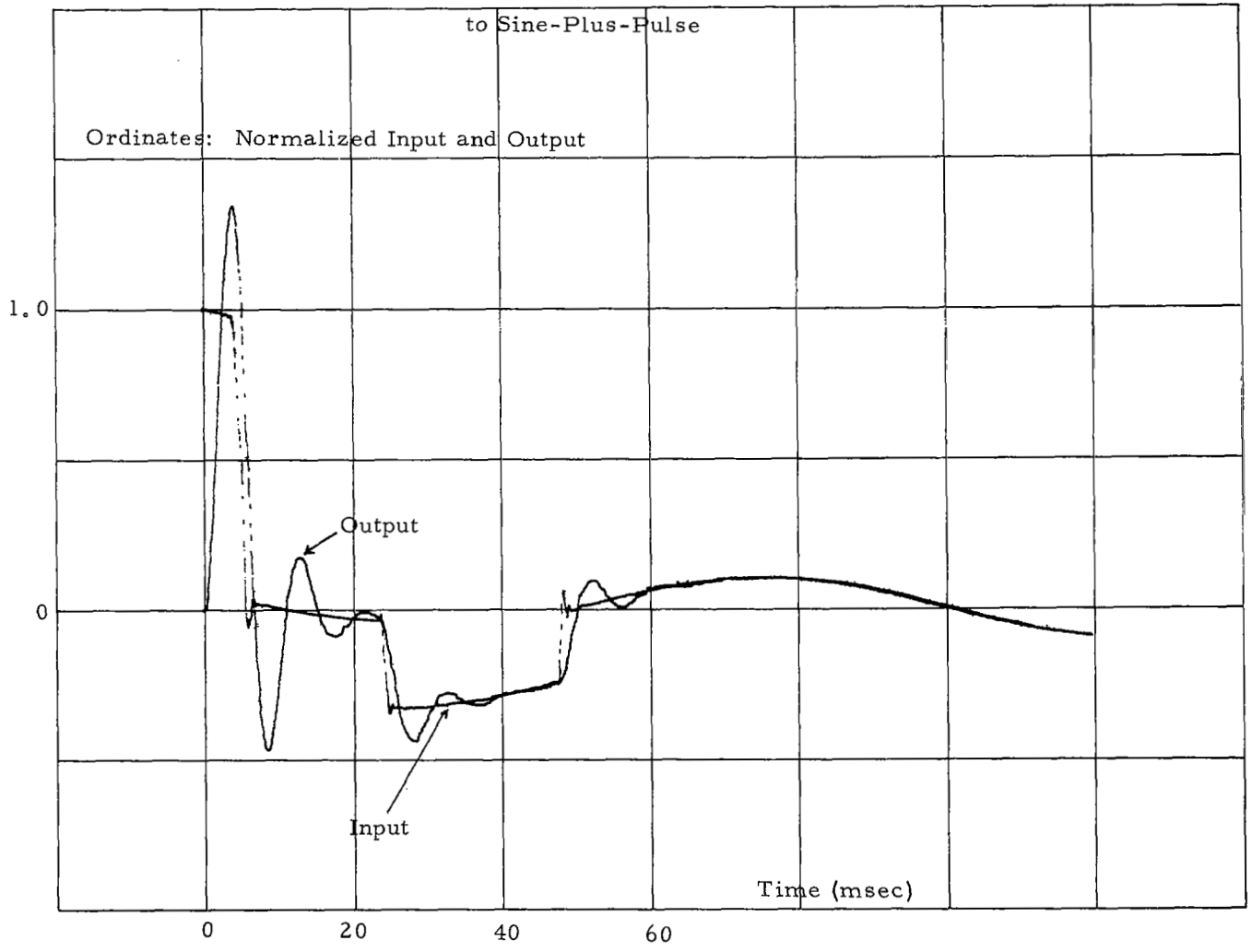

4. PRESSURE TRANSDUCERS

This section deals with two types of pressure transducers used aboard Scout vehicles.

Giannini - 461319BV-2 (0 to 500 psia)

Bourns - 2007253703 (0 to 800 psia)

Both types use a Bourdon - tube as pressure sensing device. The Giannini transducer is connected directly to the pressure source. The Bourns transducer is connected to the pressure source by means of an asymmetric T-tube, whose third arm leads to a switch chamber.

An extract from the procurement specification follows:

- Bourdon tube material Ni-Span-C
- Acceleration sensitivity: $\pm$ 0.05%/g along lateral and transverse axes, $\pm$ 0.004%/g along the longitudinal axis.
- Response time: time for the output to reach 63% of its final value after a step input in pressure shall not exceed 50 milliseconds.

4.1 Theoretical Model

4.1.1 Bourdon - Tube Analysis

Static elastic analysis of Bourdon tubes is quite complicated, and dynamic analysis is even more involved. Therefore, only approximate results can be obtained. Both transducers use flattened sections, shown in Figure 4-1, (see also Reference 5). Giannini employs a helical tube, while Bourns has a spiral tube. Therefore, the treatment of both cases is somewhat different and will be given separately. Basically, the resonant frequencies are obtained here by an application of Rayleigh's principle (see Reference 4). One equates approximate expressions of maximum potential and kinetic energies for the lowest mode of vibration. However, since the trial functions used do not necessarily satisfy all boundary conditions, the resonances found may be smaller as well as larger than the true values.

Giannini (or Helical) Tube

The Giannini tube is a regular helix wound on a circular-cylindrical surface. The radius of curvature R of the axis of the tube is a constant; therefore, the theory of Reference 5 can be applied directly if the helix is replaced by equivalent

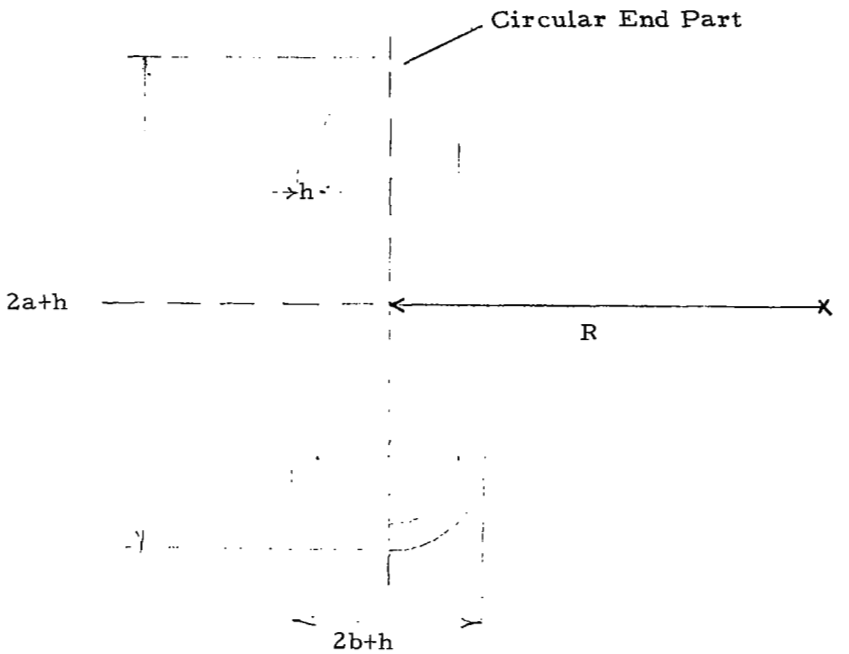

Figure 4-1, Cross-Section of Bourdon Tubes

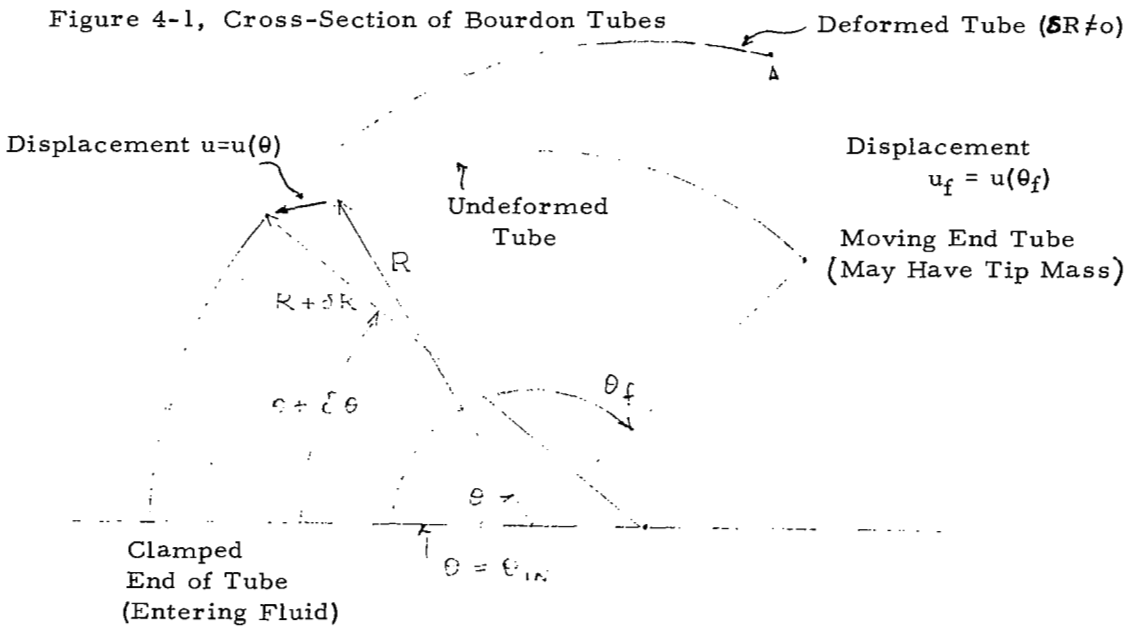

Figure 4-2, Tube Nomenclature

circular rings. Application of pressure results in an increase in radius of curvature δR. Reference 5 gives the following relationship between torque on tube, T, and the angular deflection of the tube, per unit of the angle θ, (see Figure 4-2) $\delta R/R$ (assumed constant over the entire axis of the tube, an assumption equivalent with the hypothesis of constant bending moment).

$$T = k \cdot \frac{\delta R}{R}$$

with

$$k = 4E \frac{\left[hb^2 a \quad 1 + \left(\frac{\pi}{4} - 1\right)\frac{b}{a}\right]\left[1 + \frac{4}{35}(1-\nu^2)\frac{a^4}{R^2h^2}F_1\right]}{R \qquad \left[1 + \frac{8}{21}(1-\nu^2)\frac{a^4}{R^2h^2}F_2\right]}$$

E = Young's modulus
ν = Poisson's ratio
a, b, h, R: See Figure 4-1, geometric quantities describing the tube cross-section.
F_1, F_2: dimensionless coefficients, tabulated in Reference 5.

The corresponding maximum potential energy of deformation is then given by:

$$U_{pot} = \frac{1}{2} k \theta_f \left(\frac{\delta R}{R}\right)^2$$

In a helix with constant length of the tube axis, the displacement u (see Figure 4-2) is given by

$$u^2 = (\delta R)^2 \left[2 (1 - \cos \theta) + \theta^2 - 2 \theta \sin \theta\right]$$

In harmonic motion with angular frequency w_B, the corresponding maximum kinetic energy is (for m_f = tip mass)

$$U_{kin} = \frac{1}{2} w_B^2 Z_{kin}$$

where

$$Z_{kin} = \rho A R^3 \left(\frac{\delta R}{R}\right)^2 \left(\frac{\theta_f^3}{3} + 2 \theta_f - 4 \sin \theta_f + 2 \theta_f \cos \theta_f\right) + m_f u_f^2$$

ρ = mass density of tube (metal plus pressurized fluid)
A = cross-sectional area given by

$$A = 4h a \left[1 + \left(\frac{\pi}{2} - 1\right) \frac{b}{a}\right]$$

Therefore, the approximate resonant frequency of the undamped tube is

$$w_B^2 = 2 U_{pot} / Z_{kin}$$

The mass of the pressurized fluid should be added as a correction to ρ. Generally, this is a very small effect.

When the tube is immersed in a damping fluid, some of this damping fluid will oscillate with the metal tube. This phenomenon can be interpreted as an additional apparent mass which has to be added to ρ as the correction:

$$\rho_{eff} = \rho + \rho_{apparent}$$

This value of ρ_{eff} should be inserted in the formulas above for greater accuracy, yielding a value $Z_{kin,\ eff}$. Again, this is normally a small correction.

Then, the resonant frequency with damping fluid, w_{BD}, is given by:

$$w_{BD}^2 = \frac{2 U_{pot}}{Z_{kin,\ eff}}$$

The transfer-function for the Bourdon tube with damping fluid now takes the form, if the damping is included, and with proper scaling (i. e., zero steady state error).

$$\frac{P_{out}}{P_{in}} = \frac{1}{1 + 2 \zeta_{BD} \frac{s}{w_{BD}} + \left(\frac{s}{w_{BD}}\right)^2} \qquad (4\text{-}1)$$

However, the tube is also sensitive to accelerations. The lowest mode for accelerations will be close to the lowest mode for pressure-input. Therefore, the following transfer-characteristic can be written down:

$$p_{out} = \frac{p_{in}}{1+2 \zeta_{BD} \frac{s}{w_{BD}} + \left(\frac{s}{w_{BD}}\right)^2} + \sum_{i=1}^{3} \alpha_i p_{FS} \frac{A_i}{1+2 \zeta_{BD} \frac{s}{w_{BD}} + \left(\frac{s}{w_{BD}}\right)^2} \qquad (4\text{-}2)$$

where

A_i = acceleration (expressed in units of "g") of the transducer along one of three perpendicular axes (i = 1, 2, 3)

P_{FS} = full scale, or nominal, pressure

α_i = sensitivity coefficients (dimensionless numbers) indicating fractions of full scale per g along the three perpendicular axes (i = 1, 2, 3). Because of the directional properties of the Bourdon tube, the α_i-coefficients are different for each direction; they also depend on the properties of any balancing masses that may be used. Their bounds can be deduced from manufacturer's data and from the specifications.

Numerical Results for the Giannini Transducer

The tube material is always Ni-Span-C

with $E = 2.6 \times 10^7$ lb/in^2

$(g\rho) = 0.293$ lb/in^3

$g = 386$ in/sec^2

$v = 0.3$

From manufacturer's data, confirmed by opening of an instrument, one finds:

$a = 0.080$ in.
$b = 0.021$ in.
$h = 0.008$ in.
$R = 0.225$ in.
$\theta_f = 11\pi$ (i.e., 5 1/2 turns)
$P_{FS} = 500$ lb/in^2 (absolute)

Reference 5 gives $F_1 = 1.058$, $F_2 = 1.451$

One calculates immediately

$k = 40.3$ in. lb.
$A = 2.94 \times 10^{-3}$ in^2

At full pressure and a temperature of 535°R (or 75°F), using nitrogen as the medium, one has

$$\frac{\text{mass tube}}{\text{mass compressed gas}} = 125$$

and hence the mass correction due to the compressed gas is entirely negligible. The damping fluid correction is also negligible.

Finally, one has

$$w_{BD}\ (\text{rad/sec}) = \frac{1,990}{\left(1 + m^*_f\right)^{1/2}}$$

m^*_f being the tip mass, expressed in grams.

Opening an instrument showed that the total tip mass is not more than 1.4 gram. The effective tip mass, taking into account mass distribution and support is smaller. Hence, one has: $1,260 < w_{BD} < 1,990$ (rad/sec).

A probable value for effective tip mass is about 1 gram, yielding

$$w_{BD} = 1,380 \text{ rad/sec.}$$

The manufacturer's estimate was $w_{BD} = 1,250$ rad/sec. Manufacturer-supplied data indicate a bound for the acceleration sensitivity coefficients.

$$|\alpha_i| \leq 2 \times 10^{-4} \text{ for all axes in fractions of full scale per g.}$$

These values for $|\alpha_i|$ agree with (i.e., are smaller than) a theoretical upper limit found by assuming no balancing is available.

Opening of Giannini Transducer (See Also Appendix B)

One transducer was opened and the damping fluid removed. An impulsive mechanical displacement was then applied to the Bourdon tube and the response is exhibited in Figure 4-3. One deduces from it that $w_{BD} = 1,250$ rad/sec, which is compatible with the results above. Shock inputs to the damped tube also roughly indicated a damping factor ζ_{BD} of the order of 0.2, i.e., a rather lightly damped system.

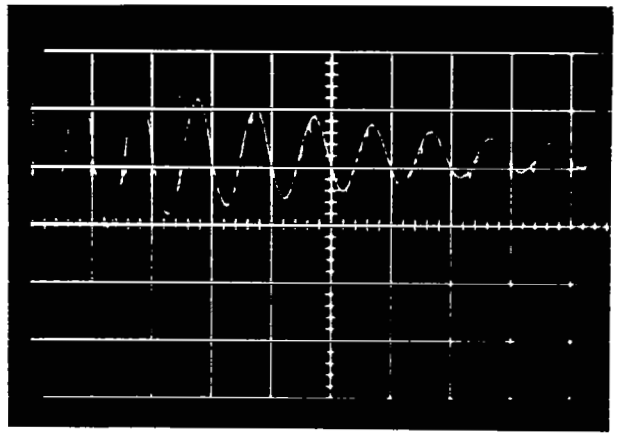

FIGURE 4-3 RESPONSE OF UNDAMPED GIANNINI BOURDON TUBE (OPENED INSTRUMENT)

TIME SCALE: 5 ms/DIVISION

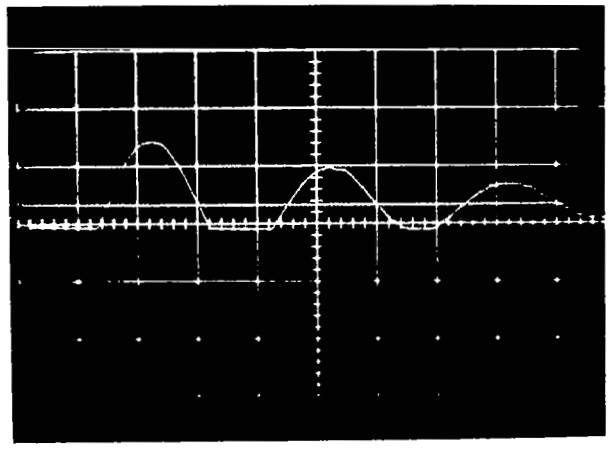

FIGURE 4-4 RESPONSE OF UNDAMPED BOURNS BOURDON TUBE (OPENED INSTRUMENT)

TIME SCALE: 2 ms/DIVISION

Bourns (or Spiral) Tube

For the spiral tube R varies with θ and the theory of Reference 5 is not directly applicable. The method used here is the well-known quasi-steady approximation, i.e., R is taken constant over short lengths of the tubing axis. The manufacturer's drawings show that the Bourdon tube is made up of consecutive half circles with increasing radius. This real shape is replaced by an equivalent spiral of Archimedes with polar equation:

$$r = q_s \theta$$

taken between two limits:

The lower limit: $\theta = \theta_{in}$ (fixed end, where fluid enters)
and
The upper limit: $\theta = \theta_f$ (free, moving end of tube)

The coefficient q_s is the appropriate average value: $q_s = \dfrac{r_f - r_{in}}{\theta_f - \theta_{in}}$

giving $\theta_{in} = r_{in}/q_s$.

For θ not too small (i.e., $\theta_{in} \gg 1$) polar radius r and radius of curvature R are nearly equal for the spiral of Archimedes as they must be for the successive half circles.

$$R \cong r = q_s \theta$$

The bending theory of curved beams (Reference 4) shows that for a constant bending moment, one has $\delta R/R^2$ (the angular deflection of the gage per unit of its length) nearly constant. Therefore, one can write

$$T = (k R)_{av} \frac{\delta R}{R^2}$$

where

$$(kR)_{ave} = 4 E h b^2 a \left[1 + \left(\frac{\pi}{4} - 1\right) \frac{b}{a}\right] \left(\frac{1 + \frac{4}{35} (1-\nu^2) \frac{a^4}{R^2 h^2} F_1}{1 + \frac{8}{21} (1-\nu^2) \frac{a^4}{R^2 h^2} F_2} \right)_{av}$$

The maximum potential energy of deformation now is given by

$$U_{pot} = \frac{1}{2} (kR)_{av} \frac{\delta R_f^2}{R_f^2} \quad \frac{1 - (R_{in}/R_f)^2}{2 q_s}$$

Again for θ **not** too small, the displacement u is given approximately by

$$|u| \approx (\theta - \theta_{in}) \; |\delta R|$$

since, approximately,

$$\pm |u| = R \, \delta \theta \approx - (\theta - \theta_{in}) \, \delta R$$

Therefore, the maximum kinetic energy for oscillations with angular frequency w_B becomes

$$U_{kin} \approx \frac{1}{2} w^2_B \; Z_{kin}$$

with

$$Z_{kin} = A \rho \int_{\text{tube + tip mass}} u^2 \, R \, d\theta$$

$$= A \rho \frac{\delta R^2_f}{8 q^3_s} R^4_f \left[1 - \frac{16}{7} \frac{R_{in}}{R_f} + \frac{8}{6} \left(\frac{R_{in}}{R_f}\right)^2 - \frac{1}{21} \left(\frac{R_{in}}{R_f}\right)^8 \right]$$

$$+ m_f \frac{R^2_f}{q^2_s} \delta R^2_f \left(1 - \frac{R_{in}}{R_f}\right)^2$$

The expression for the tube area A is given above in the discussion for the helical tube. The remainder of the discussion for the spiral tube is exactly the same as for the helical tube and leads to identical forms for the final transfer functions.

Numerical Results for the Bourns Transducer

The tube is made of Ni-Span-C (see Giannini data). According to data from the manufacturer, confirmed by opening an instrument (except for tip mass)

$a = 0.148$ in.
$b = 0.046$ in.
$R_{in} = 0.28$ in.
$R_f = 0.61$ in.
$h = 0.014$ in.

$\Delta\theta = \theta_f - \theta_{in} = 6.14\,\pi$ (or 3 complete turns plus an additional 25°)

$P_{FS} = 800$ lb/in^2 (absolute)

Total tip mass between 2 and 4 grams (this is doubtful as indicated below)

Hence, one finds

$q_s = 0.0172$ in/rad
$\theta_{in} = 16.4 = 5.2\,\pi$
$\theta_f = 35.8 = 11.4\,\pi$

From Reference 5, one obtains $F_1 = 1.053$, $F_2 = 1.506$

Also: $A = 0.976 \times 10^{-2}$ in^2

The mass correction due to the presence of pressurized gas is again negligible, since for nitrogen at 800 lb/in^2 and 535°R

$$\frac{\text{mass tube}}{\text{mass compressed gas}} = 62$$

The damping fluid correction is also negligible. One finds $(k\,R)_{in} = 109$ in^2 lb and $(k\,R)_f = 166$ in^2 lb; an average value $(k\,R)_{av} = 138$ in^2 lb is taken.

Finally one finds

$$w_{BD}\ (\text{rad/sec}) = \frac{1,170}{(1 + 0.358\ m^*_f)^{1/2}}$$

with m^*_f expressed in grams

For $m^*_f = 0.6$, an approximate value found by opening an instrument, one has $w_{BD} = 1,060$ rad/sec.

Also, according to the manufacturer, one finds bounds for the acceleration sensitivities $|\alpha_1|, |\alpha_2| \leq 5 \times 10^{-4}$ (most sensitive axes)

$$|\alpha_3| \leq 4 \times 10^{-5}$$ (least sensitive axis, perpendicular to the plane of the spiral)

expressed as fractions of full scale per g.

Opening of Bourns Transducer (See Also Appendix B)

The procedure here is exactly the same as was already explained for the Giannini transducer. Figure 4-4 shows the results, from which one deduces $w_{BD} = 1,050$ rad/sec, in very good agreement with the numbers arrived at above. A shock test of the damped (unopened) tube roughly pointed to a ζ_{BD} of the order of 0.2.

4.1.2 Electrical Output Devices

The displacement of the free end of the Bourdon tube is converted into a (direct) output voltage across a resistor by means of a moving wiper. Because of lack of detailed information on the output device, its dynamics are neglected. However, this does not affect the instrument model much, since the output device responds much faster than the mechanical part.

4.1.3 Connecting Pipes (Bourns-Transducer)

The Bourns transducer is connected with the pressure source by means of an asymmetric T, shown in Figure 4-5.

The model for the pipes is the transmission line with longitudinal losses, shown in Figure 4-6. The transfer relations for it are derived in Reference 6, and the end results are listed below.

$$\begin{Bmatrix} P_G \\ Q_G \end{Bmatrix} = \begin{bmatrix} \cosh(\tau s) & Z_o \sinh(\tau s) \\ \frac{1}{Z_o} \sinh(\tau s) & \cosh(\tau s) \end{bmatrix} \begin{Bmatrix} P_L \\ Q_L \end{Bmatrix}$$

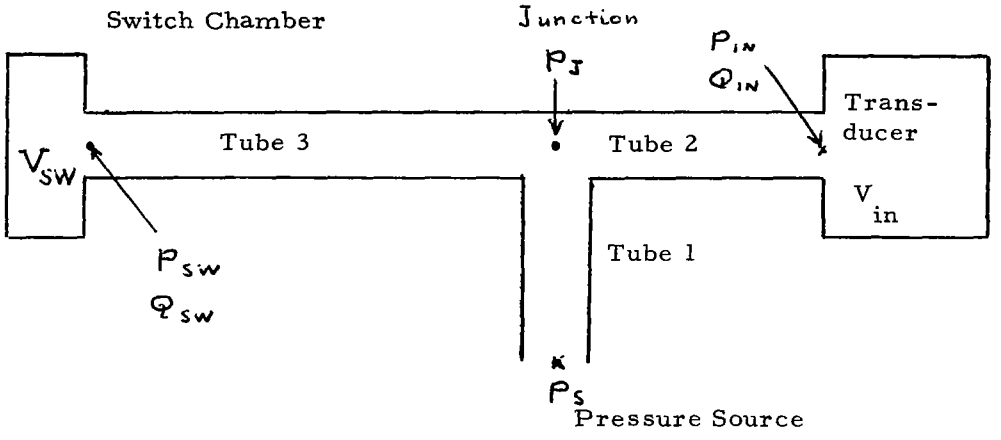

Length of Tube 1 = Δ_1, Volume = V_1
Length of Tube 2 = Δ_2, Volume = V_2
Length of Tube 3 = Δ_3, Volume = V_3

Figure 4-5, Connecting T-Pipe

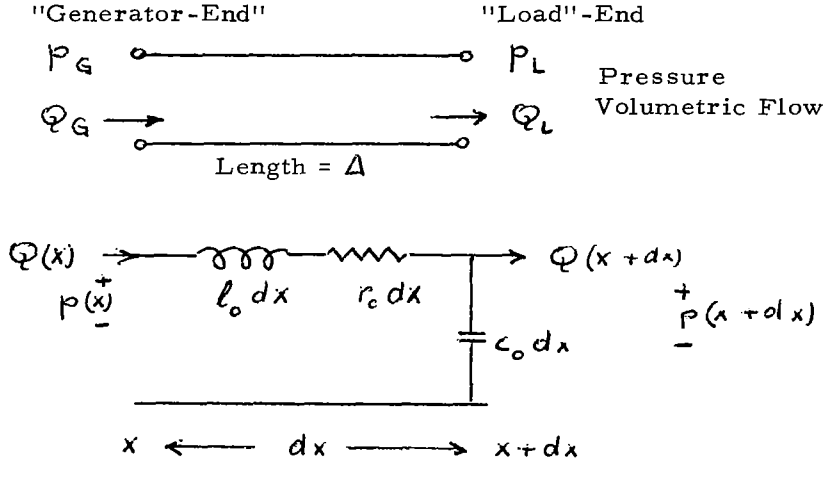

Figure 4-6, Lossy Transmission Line Model

with p = pressure (say lb/in^2), Q = volumetric flow (say in^3/sec), Z_o is the characteristic impedance

$$Z_o = \left(\frac{1_o + \frac{r_o}{s}}{c_o} \right)^{1/2}$$

and τ is the "time constant"

$$\tau = \Delta \left(c_o \left(1_o + \frac{r_o}{s} \right) \right)^{1/2}$$

Δ is the length of the pipe, c_o is the "capacitance" per unit length (say $\frac{in^4}{lb}$, 1_o is the "inertance" per unit length (say $lb\ sec^2/in^6$), r_o is the "resistance" per unit length (say $lb\ sec/in^6$), and s is the operator $\frac{d}{dt}$. For a compressible, ideal gas one has the pressure-density relation.

$$p = \rho \bar{R} T$$

The flow is to be taken as isothermal in this case:

$$T = \text{constant} = T_o$$

Then one finds

$$c_o 1_o = (\bar{R} T_o)^{-1} \quad (\text{say, } sec^2/in^2)$$

$$c_o r_o = 2 f (D \sqrt{\bar{R} T_o})^{-1} \quad (\text{say, } sec/in^2)$$

where f is the usual dimensionless friction coefficient (defined as ratio of pressure drop per quarter inner diameter length to dynamic pressure) and D is the inner diameter of the pipe.

The transducer can be considered as a constant volume device, i.e., as a capacitance C_{in} with

$$\frac{C_{in}}{C_2} = \frac{C_{in}}{C_o \Delta_2} = \frac{V_{in}}{V_2}$$

The switch has two positions, corresponding with two chamber volumes. At the pressure of 50 lb/in^2 the chamber goes from a smaller volume (0.07 in^3) to a larger volume (0.14 in^3) and stays there. Since 50 lb/in^2 is rather small compared with the nominal pressure (800 lb/in^2), one can take V_{sw} = constant (and equal to the larger volume) for the present approximate analysis.

Then the switch acts as a capacitance C_{sw} with

$$\frac{C_{sw}}{C_3} = \frac{C_{sw}}{C_o \Delta_3} = \frac{V_{sw}}{V_3}$$

(Capacitance being proportional to volumes)

One finds the impedance ratios:

$$\frac{Z_o}{Z_{sw}} = Z_o C_{sw} s = \frac{Z_o C_{sw}}{\tau_3} \tau_3 s = \frac{C_{sw}}{C_3} \tau_3 s$$

$$\frac{Z_o}{Z_{in}} = Z_o C_{in} s = \frac{C_{in}}{C_2} \tau_2 s$$

Repeated application of the basic transmission line formula and of the relations

$$p_{in} = \frac{Q_{in}}{C_{in} s}, \quad p_{sw} = \frac{Q_{sw}}{C_{sw} s}$$

leads to the transfer-relation:

$$\left(\frac{p_{in}}{p_s}\right)^{-1} = (\cos h(\tau_2 s) + Z_o C_{in} s \sin h(\tau_2 s)) \left\{\cos h(\tau_1 s) + \sin h(\tau_1 s) \left[\frac{\sin h(\tau_3 s) + Z_o C_{sw} s \cos h(\tau_3 s)}{\cos h(\tau_3 s) + Z_o C_{sw} s \sin h(\tau_3 s)} + \frac{\sin h(\tau_2 s) + Z_o C_{in} s \cos(\tau_2 s)}{\cos h(\tau_2 s) + Z_o C_{in} s \sin h(\tau_2 s)}\right]\right\}$$

(4-3)

This complicated transcendental transfer function is now replaced by the low order rational approximation.

$$\frac{P_{in}}{P_s} = \frac{1 + 2\zeta_a \frac{s}{w_a} + \frac{s^2}{w^2_a}}{1 + 2\zeta_b \frac{s}{w_b} + \frac{s^2}{w^2_b}} \qquad (4\text{-}4)$$

Best values of w_a and w_b are found by a product-development of the transcendental numerator and denominator of p_{in}/p_s.

The zeros of p_{in}/p_s (or the poles of p_s/p_{in}) are given by the equation

$$\cos h\,(\tau_3 s) + Z_o\, C_{sw}\, s \sin h\,(\tau_3 s) = 0$$

If one sets $\tau_3 s = (-1)^{1/2} v$, v is real for the roots of the preceding equation. In fact, the zeros v_n are given by

$$(\tan v_n)_{\text{zeros}} = v_3/v_{sw}$$

The smallest positive root $(v_1)_{zero}$ yields w_a

$$w_a = \frac{(v_1)_{zero}}{\Delta_3 (\ell_o C_o)^{1/2}}$$

The damping is given by: $\zeta_a = \frac{r_o}{2 \ell_o w_a}$

The poles of p_{in}/p_s (zeros of p_s/p_{in}), including w_b, are given by the (real) roots of the equation in v:

$$\cos\left(\frac{\Delta_1}{\Delta_3} v\right)\left[\cos\left(\frac{\Delta_2}{\Delta_3} v\right) - \frac{v_{in}}{v_3} v \sin\left(\frac{\Delta_2}{\Delta_3} v\right)\right]\left[\cos v - \frac{v_{sw}}{v_3} v \sin v\right]$$

$$- \sin\left(\frac{\Delta_1}{\Delta_3} v\right)\left[\sin\left(\frac{\Delta_2+\Delta_3}{\Delta_3} v\right)\left(1 - \frac{v_{sw} v_{in}}{v^2_3} v^2\right) + \cos\left(\frac{\Delta_2+\Delta_3}{\Delta_3} v\right)\frac{v_{in}+v_{sw}}{v_3} v\right] = 0$$

The smallest positive root $(v_1)_{pole}$ yields w_b

$$w_b = \frac{(v_1)_{pole}}{\Delta_3 (\rho_o C_o)^{1/2}}$$

with damping $\zeta_b = \frac{r_o}{2 \rho_o w_b}$

In order for the model to be acceptable, one should have

$$(w_b/w_a)^2 \ll 1 \qquad (4\text{-}5)$$

because then the initial response to a step-input is small.

(Theoretically, this initial response is zero). Otherwise, one must take more zeros and poles in the product development. This point is discussed further for the numerical evaluations. Note that for the ideal gases ζ_a, ζ_b and $\frac{w_a}{w_b}$ are independent of the kind of gas, provided f has the same value.

Numerical Values for the T-Tubes

One has for the pipes

the volumes $v_1 = 0.17$ in^3
$v_2 = 0.26$ in^3
$v_3 = 1.13$ in^3

the lengths $\Delta_1 = 5.38$ in
$\Delta_2 = 8.27$ in
$\Delta_3 = 36.0$ in

and inner diameter D = 0.20 in.

The switch has a volume $v_{sw} = 0.14$ in^3

The Bourdon tube has a volume $v_{in} = 0.17$ in^3

One takes (for the laboratory experiments)

$T_o = 535^oR$ (75^oF)

Obviously, for real Scout-data, the appropriate (possibly) different temperature must be taken.

The gas constants are

for nitrogen $\bar{R}_{N_2} = 2.56 \times 10^5 \quad \frac{in^2}{sec^2\ R}$

for helium $\bar{R}_{He} = 1.79 \times 10^6 \quad \frac{in^2}{sec^2\ R}$

Damping estimates are found to be unreliable; they give only an order of magnitude estimate. It is best to rely on experimental evidence to find ζ_a, ζ_b. Since helium was used in the laboratory experiments, the constants were calculated for this gas.

One finds successively

$$c_o \frac{1}{\rho_o} = 1.04 \times 10^{-9}\ sec^2/in^2 \quad , \frac{1}{(\frac{1}{\rho_o} c_o)^{1/2}} = 3.1 \times 10^4\ in/sec$$

$(v_1)_{zero}$ = 1.45 (corresponding with 82.9°)

$(v_1)_{pole}$ = 1.25 (corresponding with 71.6°)

w_a = 1,250 rad/sec

w_b = 1,080 rad/sec

One sees that w_b is only a little smaller than w_a. Theoretically, as discussed before, one should then take more zeros and poles in the tube-model. However, the need for additional terms in the tube-model is obviated by the effect of orifices, to be discussed in the description of the experiments later on (Section 4.2.3).

4.2 Laboratory Tests and Analog Computer Simulation (See also Appendix B for Description)

4.2.1 Giannini Transducers

Figures 4-7 A&B, 4-8 A&B, 4-9 A&B, show inputs and outputs for tests performed on one Giannini instrument. There is a connecting orifice between the transducer and the pressure source, and this connecting orifice accounts for a second quadratic term besides the basic Bourdon transfer-function derived in Section 4.1.1. The total transfer-function is now to be taken as

$$\frac{P_{out}}{P_{in}} = \frac{1}{\left(1+2\zeta_{or}\frac{s}{w_{or}}+\frac{s^2}{w_{or}^2}\right)\left(1+2\zeta_{BD}\frac{s}{w_{BD}}+\frac{s^2}{w_{BD}^2}\right)} \qquad (4\text{-}6)$$

Full scale gives 4.94v out.

Figures 4-10, 4-11 and 4-12 show, respectively, the best fits obtained on the analog computer for the preceding inputs. These fits are quite good for the range of inputs considered.

Summarizing, one finds for the

Bourdon tube $w_{BD} = 1,300$ rad/sec ($f_{BD} = 207$ Hz)

$\zeta_{BD} = 0.2$

agreeing well with the theoretical values derived in Section 4.1.1.

For the connecting orifice, one gets

$w_{or} = 1,300$ rad/sec to $1,600$ rad/sec

$\zeta_{or} = 0.3$ (slow input) to 0.7 (fast input)

again showing some non-linear effect in the gas flow, with damping increasing as the input gets faster. The spread among instruments of the same category reaches at least 10 percent.

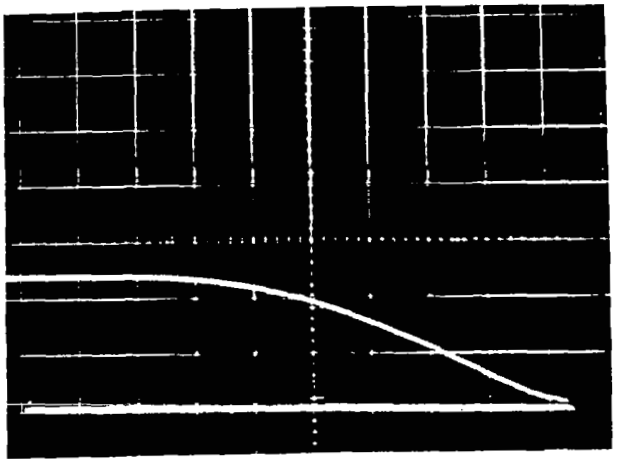

FIGURE 4-7 A INPUT TO GIANNINI, 195 PSI FINAL
TIME SCALE: 1 ms/DIVISION
(POSITIVE LEFTWARD)

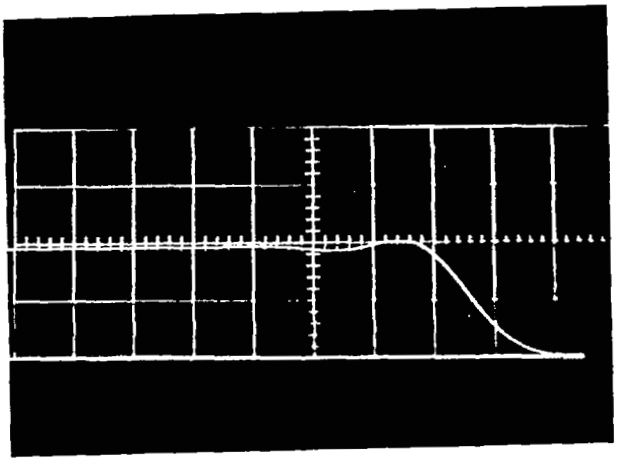

FIGURE 4-7 B GIANNINI RESPONSE
TIME SCALE: 2 ms/DIVISION
SMALL FIXTURE WITH 0.150" ORIFICE

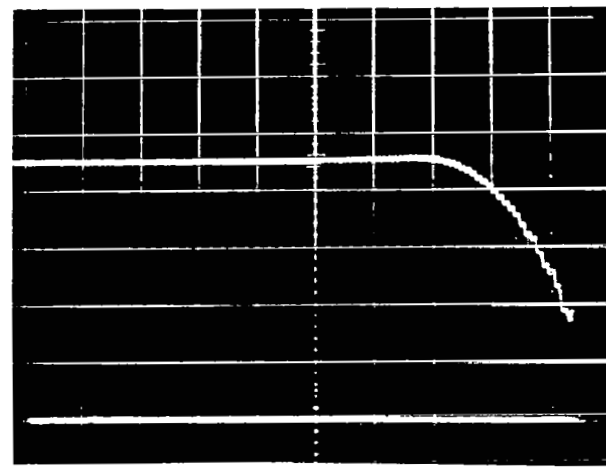

FIGURE 4-8 A INPUT TO GIANNINI, 150 PSI FINAL
TIME SCALE: 1 ms/DIVISION
(POSITIVE LEFTWARD)

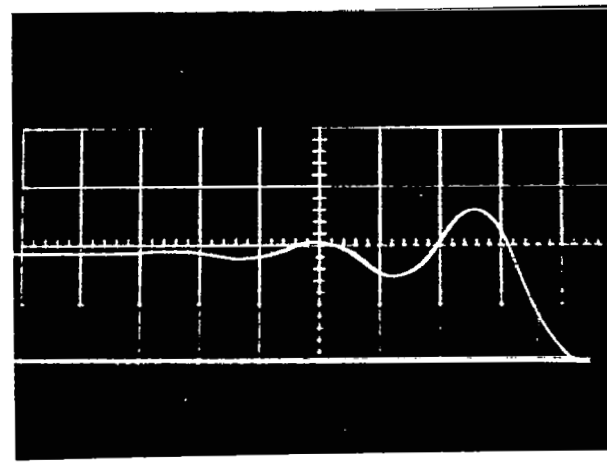

FIGURE 4-8 B GIANNINI RESPONSE
TIME SCALE: 2 ms/DIVISION
SMALL FIXTURE WITHOUT ORIFICE

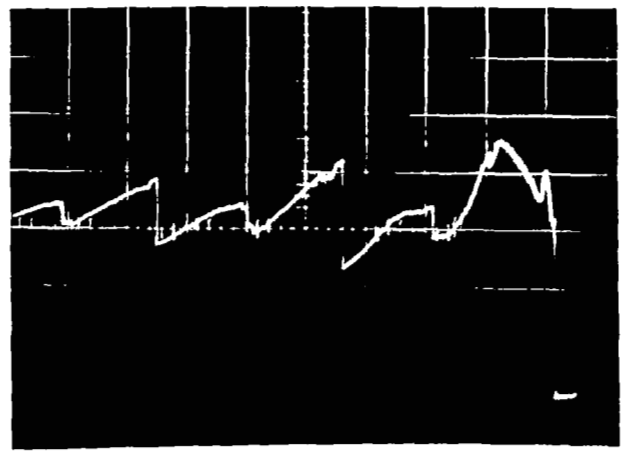

FIGURE 4-9 A INPUT TO GIANNINI, 200 PSI MAXIMUM
TIME SCALE: 5 ms/DIVISION
(POSITIVE LEFTWARD)

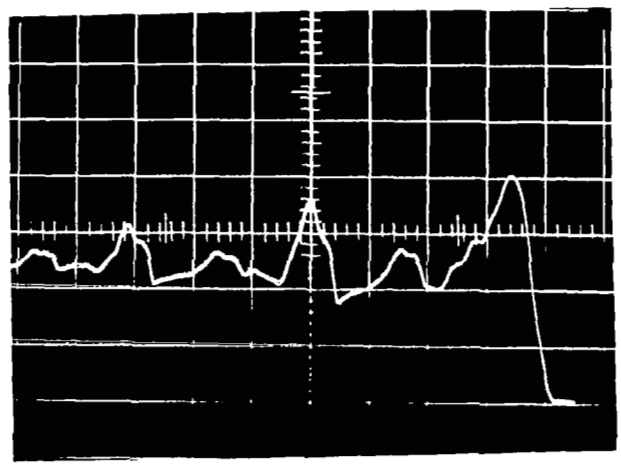

FIGURE 4-9 B GIANNINI RESPONSE, 235 PSI PEAK
TIME SCALE: 5 ms/*DIVISION*
SHOCK TUBE WITH FAST RISE

Figure 4-10, Giannini 500 lb/in^2 (No. 465-1)

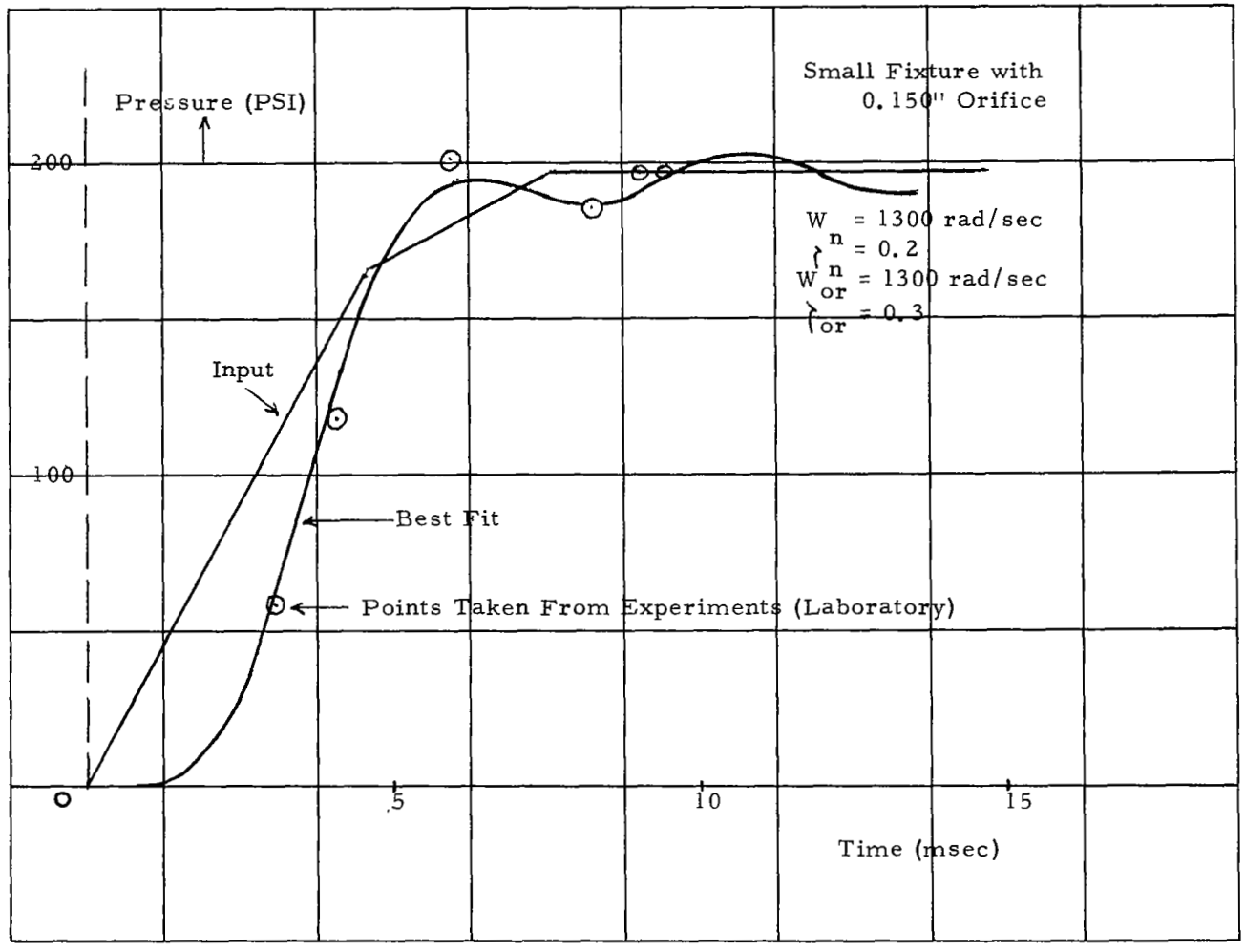

Figure 4-11, Giannini 500 lb/in^2 (No. 465-1)

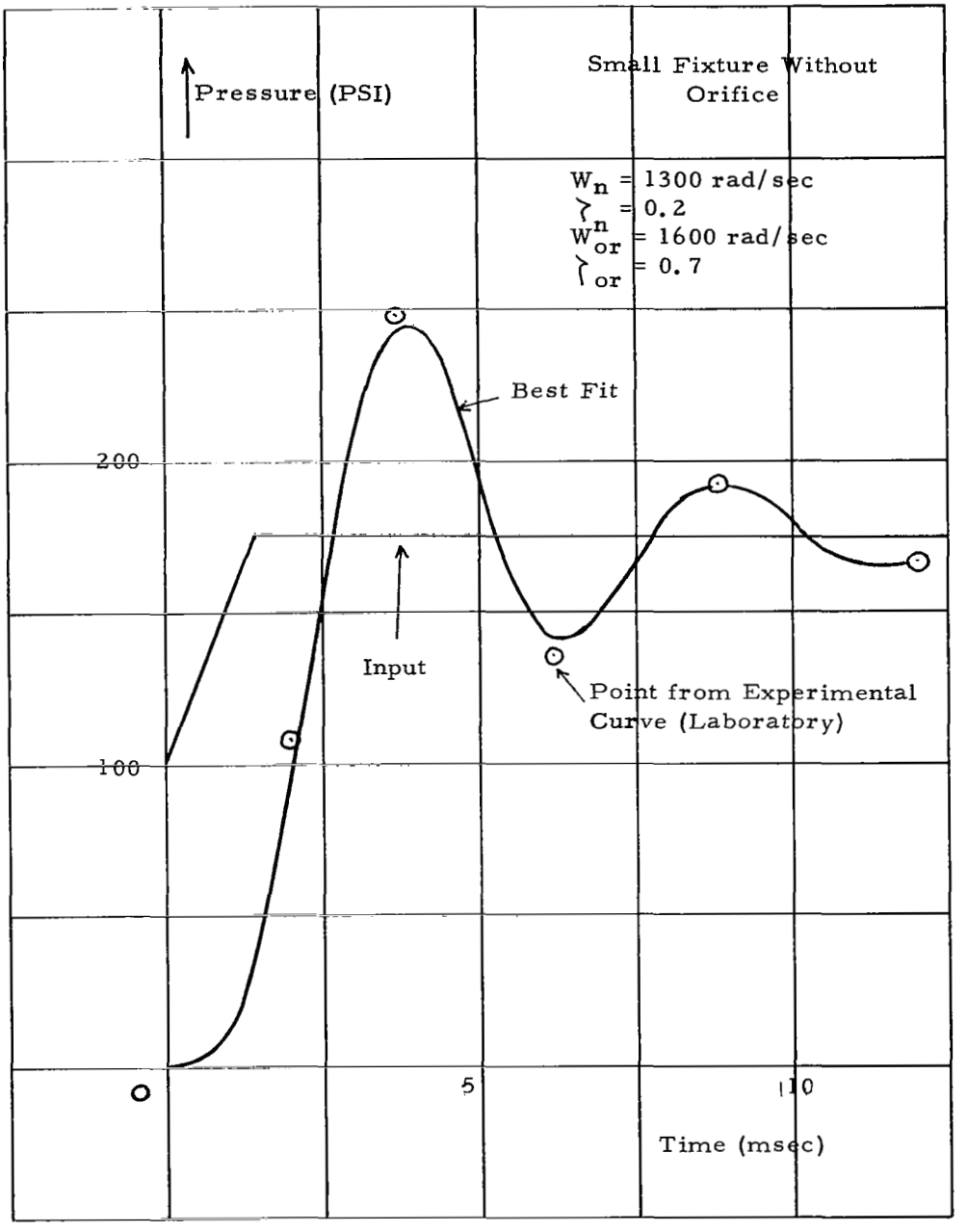

Figure 4-12, Giannini 500 lb/in^2 (No. 465-1)

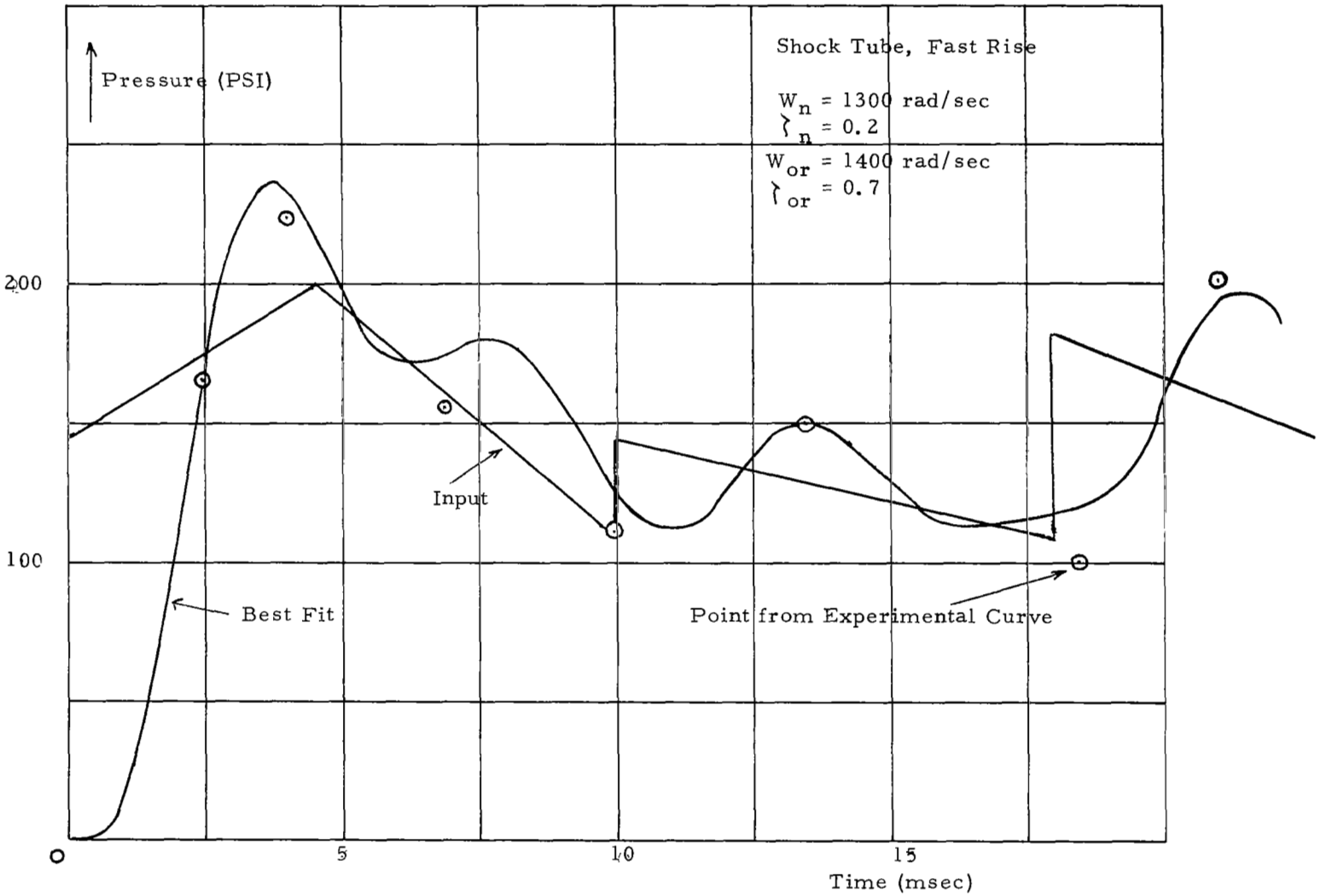

4.2.2 Bourns Transducers without T-Tubing

In order to test the value of the theoretical calculations of Section 4.1.1, the Bourns transducer was subjected to tests without T-tubing (in order to avoid masking the Bourdon tube response by other components).

One such test is shown in Figure 4-13 A&B, and the corresponding best analog computer fit is on Figure 4-14. As in the case of the Giannini tests of the preceding Section 4.2.1, there is a connecting orifice. The best fit parameter values are

for the Bourdon tube: $w_{BD} = 1,000$ rad/sec (160 Hz)

$\zeta_{BD} = 0.2$

and for the orifice effect: $w_{or} = 1,000$ rad/sec

$\zeta_{or} = 3.0$

Full scale corresponds with $4.94\ v_{out}$.

The Bourdon resonance value from this test agrees very well with the theoretical prediction of Section 4.1.1.

4.2.3 Bourns Transducers with T-Tubing

Figure 4-15 shows the response of the T-tubing and Bourns transducer for what was essentially a step input in pressure (using helium as a pressure medium) and Figure 4-16 exhibits the best fit obtained on the analog computer. The response at the T-tube end is also shown. The entire numerical transfer function (best fit) can be written as

$$\frac{1 + 2 \times 0.8 \left(\frac{s}{1,000}\right) + \left(\frac{s}{1,000}\right)^2}{1 + 2 \times 0.8 \left(\frac{s}{200}\right) + \left(\frac{s}{200}\right)^2} \quad \frac{1}{1 + 2 \times 0.3 \left(\frac{s}{400}\right) + \left(\frac{s}{400}\right)^2} \qquad (4\text{-}7)$$

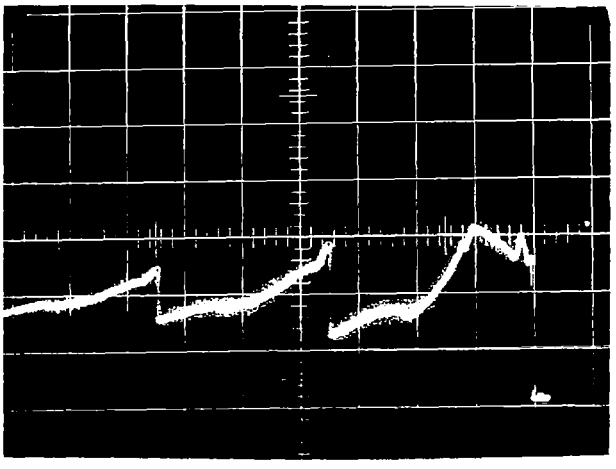

FIGURE 4-13 A INPUT TO BOURNS TRANSDUCER
TIME SCALE: 5 ms/DIVISION
(POSITIVE LEFTWARDS)
700 PSI PEAK

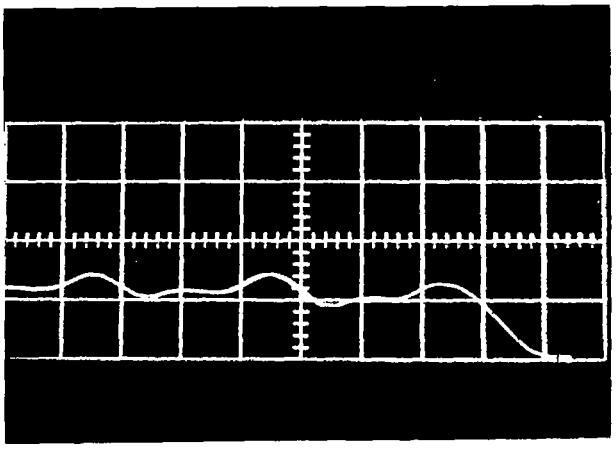

FIGURE 4-13 B BOURNS RESPONSE (NO T-TUBING)
TIME SCALE: 5 ms/DIVISION
SHOCK TUBE WITH FAST RISE
520 PSI PEAK

Figure 4-14, Bourns 800 lb/in^2 (No. 44-203)

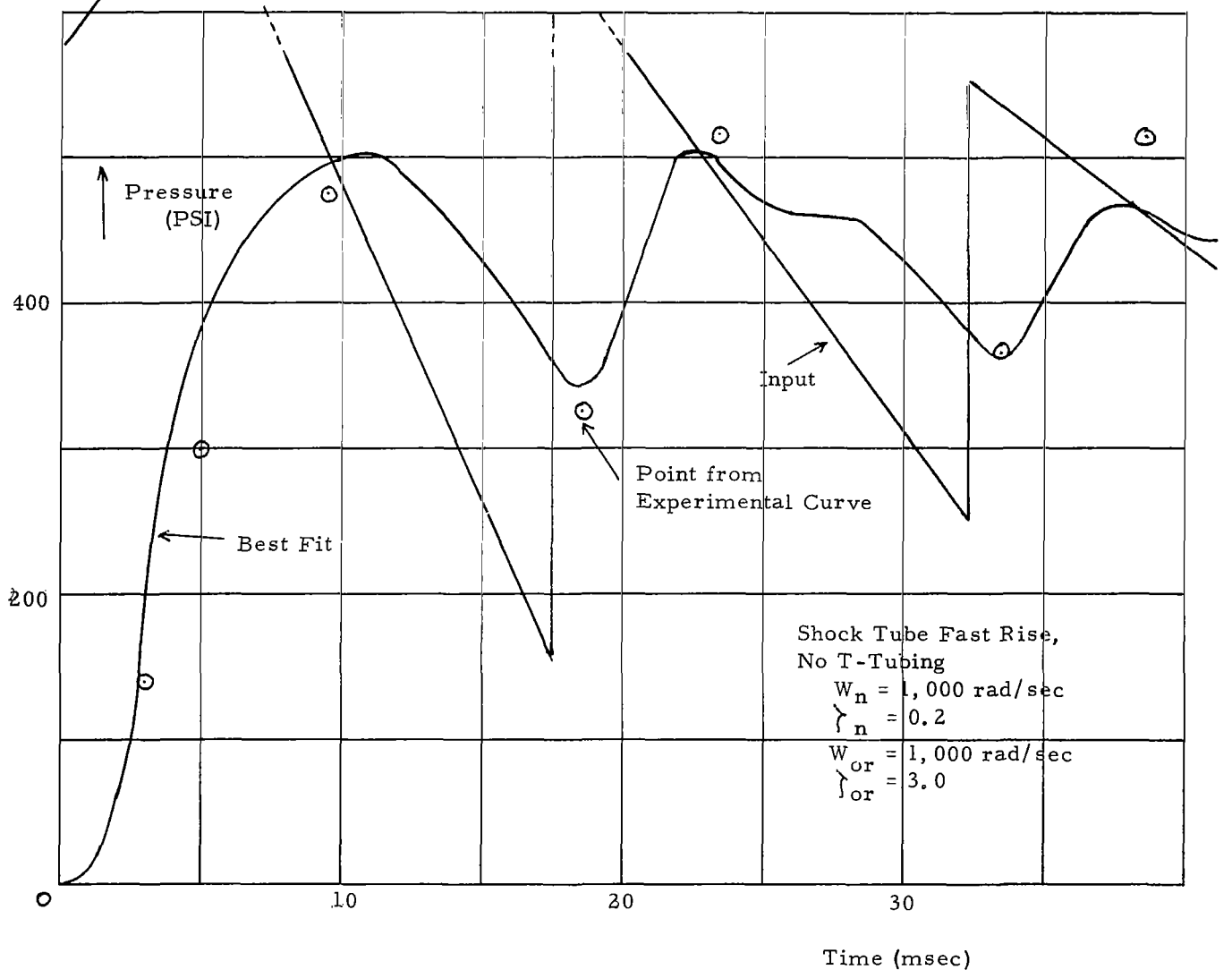

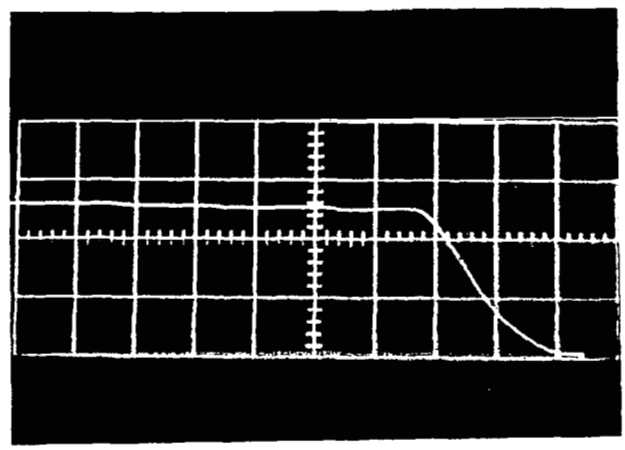

FIGURE 4-15 STEPRESPONSE OF T-TUBE AND BOURNS-TRANSDUCER
TIME SCALE: 5 ms/DIVISION (POSITIVE LEFTWARDS)

Figure 4-16, Bourns 800 lb/in^2 (No. 44-203)

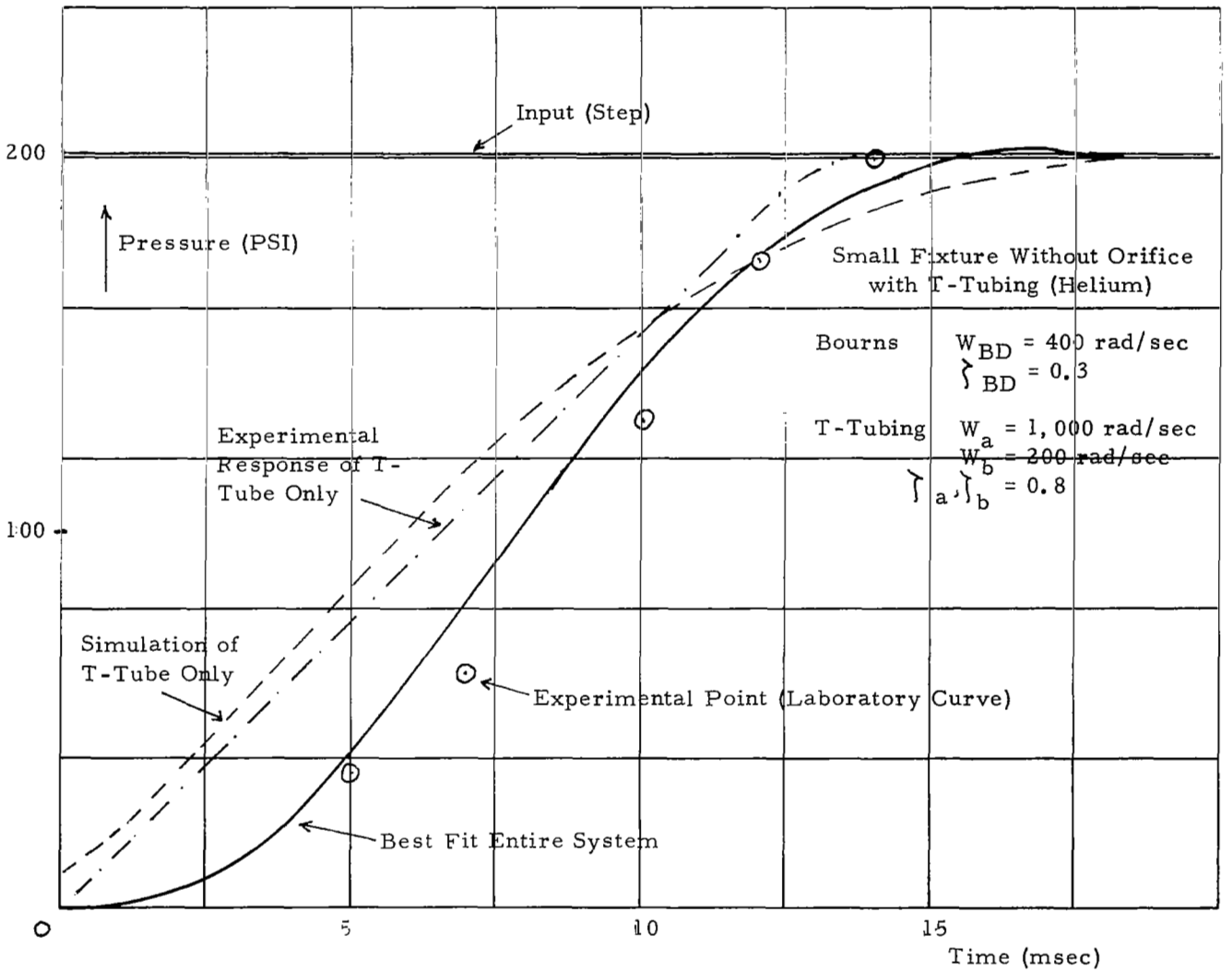

While this expression has the theoretical form of Sections 4.1.1 and 4.1.3, Equations 4-1 and 4-4, some remarks are in order. The numerical numerator above agrees with the theoretical w_a calculated in Section 4.1.3 (1,250 rad/sec) within the expected accuracy. The denominator factors, however, are numerically widely different from w_b and w_{BD} calculated before. This discrepancy is probably due to relatively slow orifice effects between pressure source and T-tube on the one hand and between T-tube and Bourdon tube on the other hand, whose effect is to mask the faster response connected with w_b and w_{BD}. The Bourdon resonance w_{BD} was indeed experimentally verified as valid in the results of Section 4.2.2. The comparison of the results of 4.2.2 and 4.2.3, moreover, points out that the numerical transfer functions obtained must be considered as global (overall) descriptions of individual systems and that it is dangerous to try and split these expressions in an effort to identify individual components. Such a conclusion is expected because of the interaction of successive components in a fluid flow system. A good example of this interaction is afforded by the discussion of Section 4.1.3, which clearly shows that p_{in}/p_s for the T-tube depends on the type of termination (here defined by the "admittance" C_{in} s).

5. TELEMETRY STUDY

5.1 General Description

The airborne, NASA-supplied equipment which is discussed in this report consists of:

a) An S-band Telemetry Transmitter CTM-UHF-305 (Conic Corp., San Diego, California)

b) A Lightweight Telemetry Package TDD 1799A (Tele-Dynamics, Philadelphia, Pennsylvania)

The principal Avco ground-equipment used in conjunction with the NASA material is an EMR Model 229 Tunable Discriminator made by Electro-Mechanical Research, Inc., Sarasota, Florida. Some other equipment was also employed and its name is given where applicable.

For the purposes of this study, the following block diagram of the T/M chain is applicable:

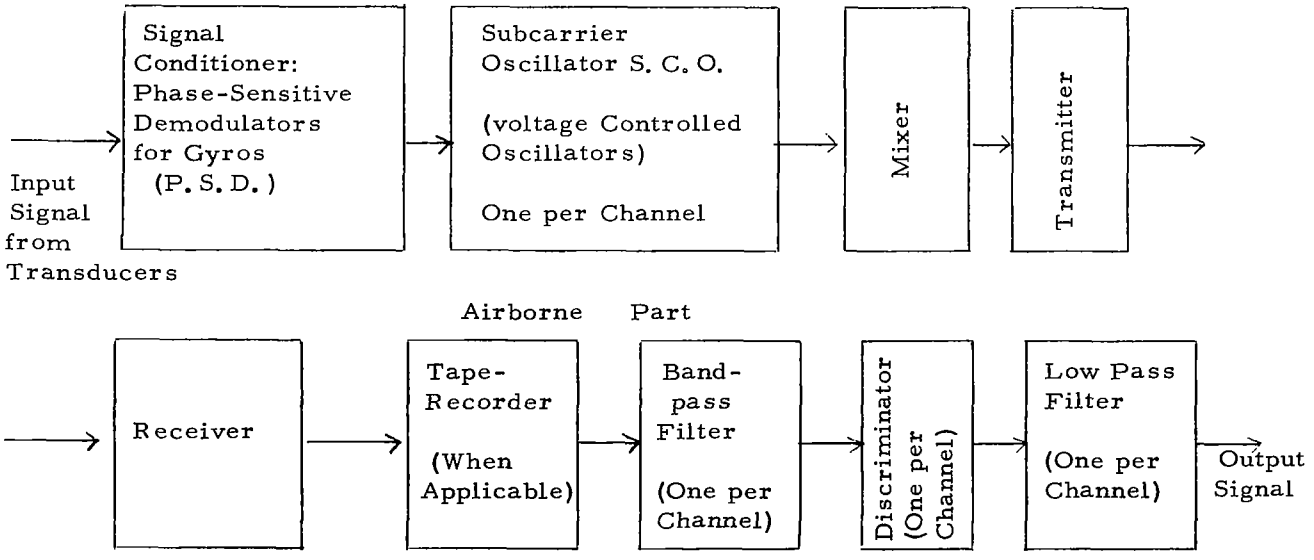

Ground Equipment

The various components will be discussed in the logical order they occupy in the block diagram.

The various instruments transmit data over a number of standard channels of the IRIG Telemetry Standards for FM/FM (see Reference 7). The relevant channels are listed in the table 5-1 below.

TABLE 5-1

IRIG CHANNELS

Maximum deviation is ± 7.5% of center frequency of each channel.

Band Number	Center Frequency (kHz) Fc	Lower Limit (kHz)	Upper Limit (kHz)	Frequency Response (Hz)	Instrument and Appendages with Lowest Proper Frequency in Hz
5*	1.3	1.202	1.399	20	-----
6	1.7	1.572	1.828	25	Yaw-rate gyro (26)
7	2.3	2.127	2.473	35	Roll-rate gyro (42)
8	3.0	2.775	3.225	45	Pitch rate gyro (26)
10	5.4	4.995	5.805	81	Bourns pressure transducer (32) (2nd stage headcap pressure)
11	7.35	6.799	7.901	110	Bourns pressure transducer (32) (1st stage headcap pressure) Also: Giannini pressure transducer (3rd stage headcap pressure) (207)
12	10.5	9.712	11.288	160	Transverse accelerometer (-3g, +3g) (110 to 135)
13	14.5	13.412	15.588	220	Normal accelerometer (-3g, +3g) (110 to 135)
14	22.0	20.350	23.650	330	Longitudinal accelerometer (-1g, +15g) (119)
15	30.0	27.750	32.250	450	

*NOTE: Channels 5 and 15 are not used by the transducers in this study, but their characteristics are given for the study of interference or of filter selection.

Channel 15 is not used by any of the basic instruments studied in earlier reports; however, the study of its behavior for different combinations of filters was desired by NASA.

The frequency response in the table is based upon maximum deviation and a deviation ratio of 5; it is not necessarily compatible with the actual bandwidth of the corresponding transducers. In fact, for the yaw rate gyro (channel 6) roll rate gyro (channel 7) and for the Giannini pressure transducer (channel 11) the transducer bandwidth is certainly larger than the tabulated frequency response.

Some nomenclature is recalled here: an ideal FM subcarrier oscillator has as input signal a variable voltage $v_{in}(t) = S^{-1} w_{in}$ starting at time $t = 0$, S^{-1} being a scale factor (volts X sec/rad) and as output signal a voltage (or current)

$$v_{out}(t) = A \cos \left(w_o t + \int_o^t w_{in}(t^1)\, dt^1\right)$$

where A = constant amplitude

$w_o/(2\pi) = f_o$ = center frequency of the S. C. O.

$2\pi f(t) = w(t) = w_o + w_{in}(t)$ = instantaneous pulsation of the output signal

$(w-w_o)/(2\pi) = f - f_o$ = instantaneous deviation of output frequency

Now $v_{in}(t)$ can be decomposed in its sine-cosine components by Fourier-series or Fourier-integral.

One such component may be:

$$v_{in,\Omega}(t) = \varepsilon \Delta w \cos \Omega t; \quad 0 \leq |\varepsilon| \leq 1$$

with $\varepsilon \Delta w$ = a fixed amplitude

Ω : pulsation within the transmission band of the transducer

Combination of the two preceding equations yields:

$$v_{out,\Omega}(t) = A \cos \left(w_o t + \frac{\varepsilon \Delta w}{\Omega} \sin \Omega t\right)$$

Hence, one has the maximum instantaneous frequency - deviation

$$(f - f_o)_{max} = |\Delta w| / (2\pi)$$

The deviation ratio is defined as

$$m = |\Delta w| / \Omega_{max}$$

(and the modulation index is sometimes defined as $|\varepsilon \Delta w| / \Omega$) and m determines the side bands in the classical Bessel-function expansion. For the table above, m = 5 is used conventionally; however, the actual transducers can in some cases possess a Ω_{max} larger than that implied by m = 5 and $|\Delta w|$ imposed by IRIG - Standards.

The components to be discussed are, in order

- phase-sensitive demodulators
- subcarrier oscillators
- mixer
- transmitter-receiver
- tape recorders
- bandpass filters
- discriminators
- lowpass filters

followed by a discussion of the entire chain viewed as a single block. The experimental test setup is described, with diagrams, in Appendix C.

5.2 Phase-Sensitive Demodulators (P. S. D.)

The output of the rate gyro output circuit is an AM-signal. A phase-sensitive demodulator is required to recover the envelope with correct algebraic sign. Its output is constrained to vary between 0 and 5 V in order to be compatible with the S. C. O. that follows.

The type used here is a ring demodulator as shown in the figure below.

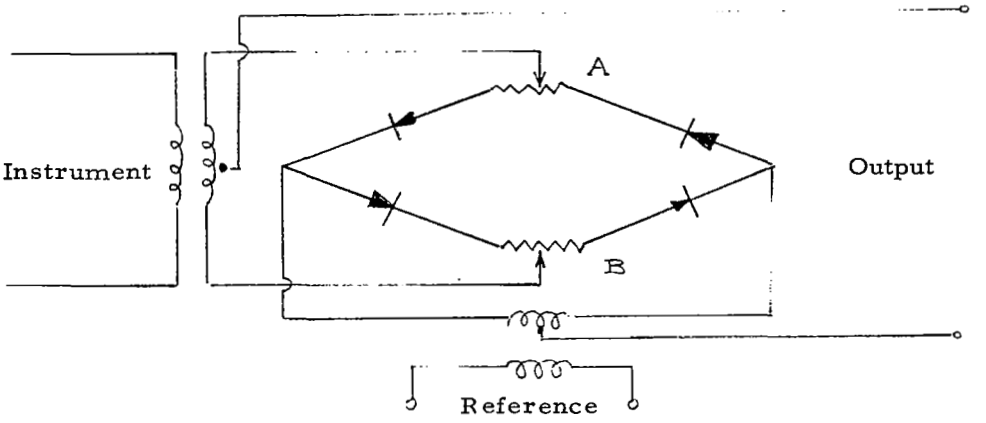

Phase-Sensitive Demodulator

The static input-output relation for P. S. D. was found to be very linear within the normal range. Beyond the normal range there is first saturation and ultimately the output dips. Experimental data are shown in Figure 5-1. These characteristics provide a bound on over-ranging in channels 6, 7 and 8 and thereby help reduce channel interference.

According to specifications, the P. S. D. sensitivity is bounded by

maximum sensitivity: 5V out (D. C.) for 20m V rms input
minimum sensitivity: 5V out (D. C.) for 200m V rms input

Experimental data on sensitivities are shown in the table below.

TABLE
Steady State Gains for P. S. D.

Number of P. S. D.	E_{in} (mV) r. m. s.	E_{out} (V. D. C.)	E_{in} (mV) r. m. s. for 5V output	$\frac{\Delta \text{ Volts out} = K}{\text{Volts in (r. m. s.)}}$
1	40	4.377	53.3	47.0
2	38	4.280	53.4	46.8
3	38	4.350	51.4	48.6
4	41.5	3.173	153.0	16.3
5	38	4.351	51.3	48.7
6	40	3.107	165.0	15.1

Figure 5-1
Phase-Sensitive Demodulator #1

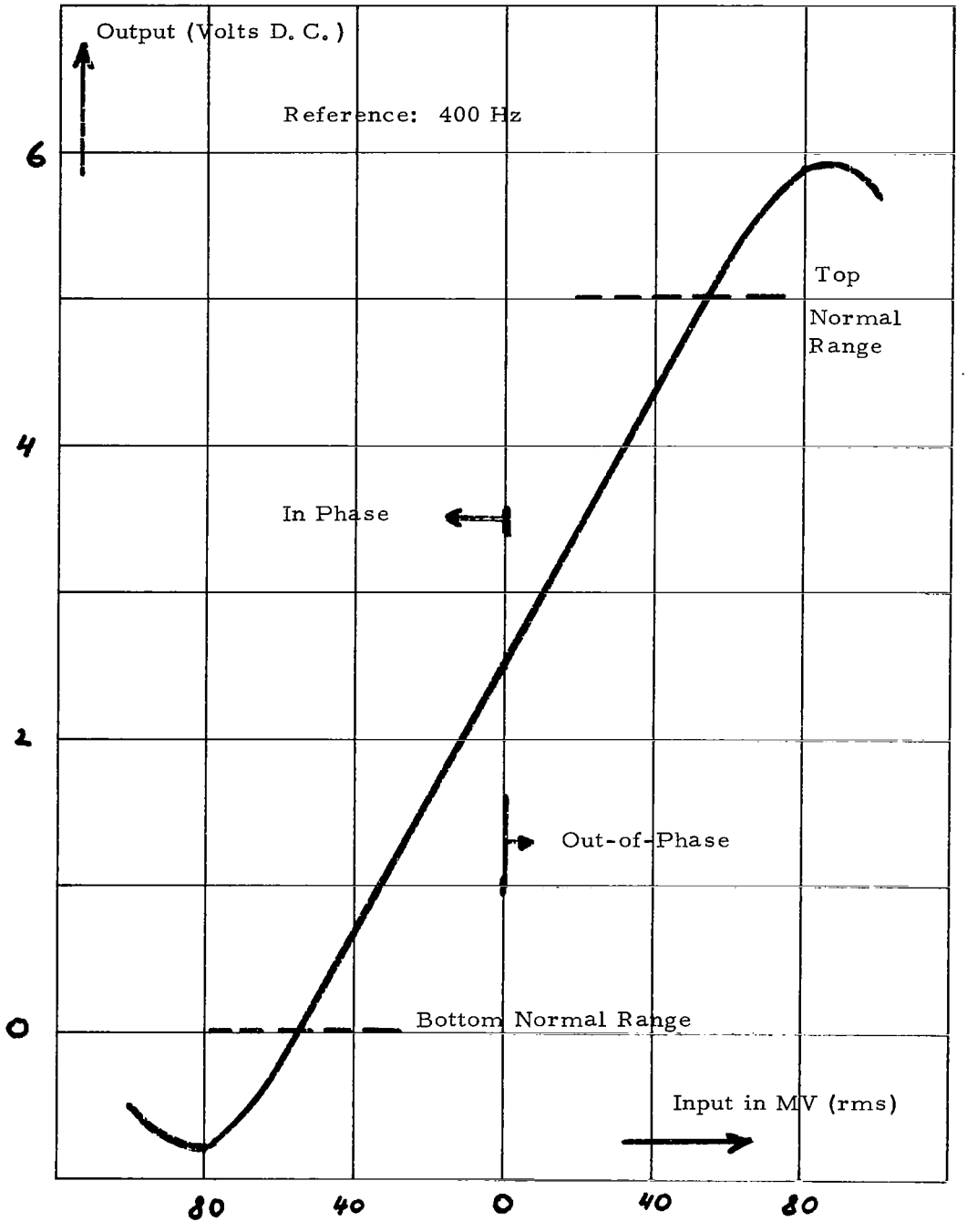

The P. S. D. #4, 6 have low sensitivity, the others have high sensitivity (high gain).

The transient response, here particularly the step response, turned out to be sensitive to direction of voltage swing at the output.

While all these responses can be described with sufficient accuracy by a second-order transfer-function (including the ripple-filter)

$$\frac{\Delta V_{out}}{V_{in}\ (\text{algebraic envelope})} = \frac{K}{1+2\zeta\frac{s}{w_n}+\frac{s^2}{w^2_n}} \qquad (5\text{-}1)$$

(remembering the bias of 2. 5 volts at output)

responses where the output voltage increases show some overshoot (with individual variations) while the responses where the output voltage decreases do not show any measurable overshoot (and this is so whether the input is in-phase or out-of-phase).

Some experimental results are shown in Figures 5-2 and 5-3. Analog simulations are given in Figure 5-4 for the best fit (for which the agreement is quite good).

The results of best fitting of experimental data are given in the table below.

TABLE
Dynamic Parameters of P. S. D.

Number of P. S. D.	Output up		Output down	
	ζ	w_n (rad/sec) (f_n)(Hz)	ζ	w_n (rad/sec) (f_n)(Hz)
1	0.62	195 (35)	1.0	200 (31.8)
6	0.82	185 (29.4)	1.0	185 (29.4)

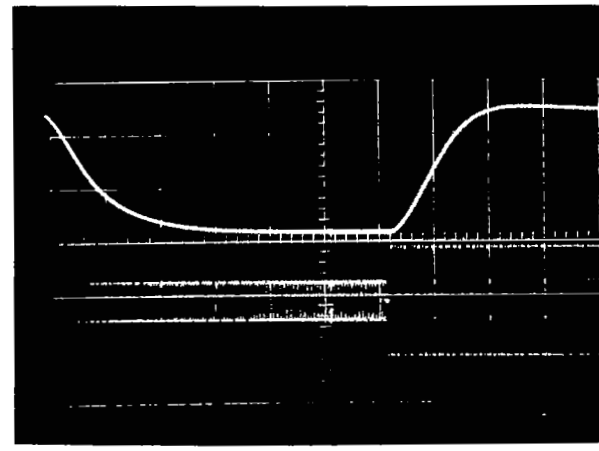

FIGURE 5-2 STEPRESPONSES OF PHASE - SENSITIVE
DEMODULATOR #1 (UPPER TRACE)
TIME SCALE 10 ms/DIVISION
INPUT ON LOWER TRACE

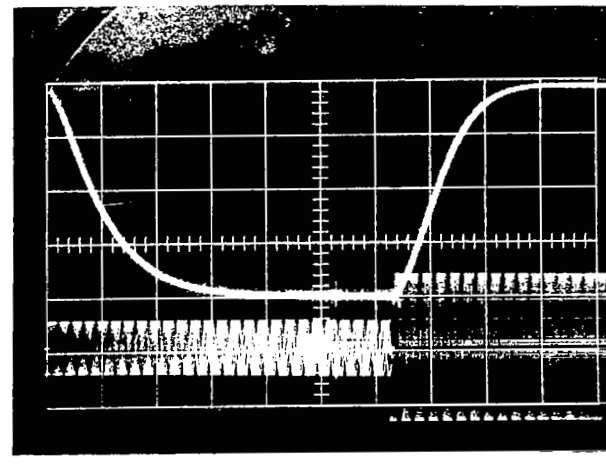

FIGURE 5-3 STEPRESPONSES OF PHASE - SENSITIVE
DEMODULATOR #6 (UPPER TRACE)
TIME SCALE 10 ms/DIVISION
INPUT ON LOWER TRACE

Figure 5-4, Step Responses of P. S. D.

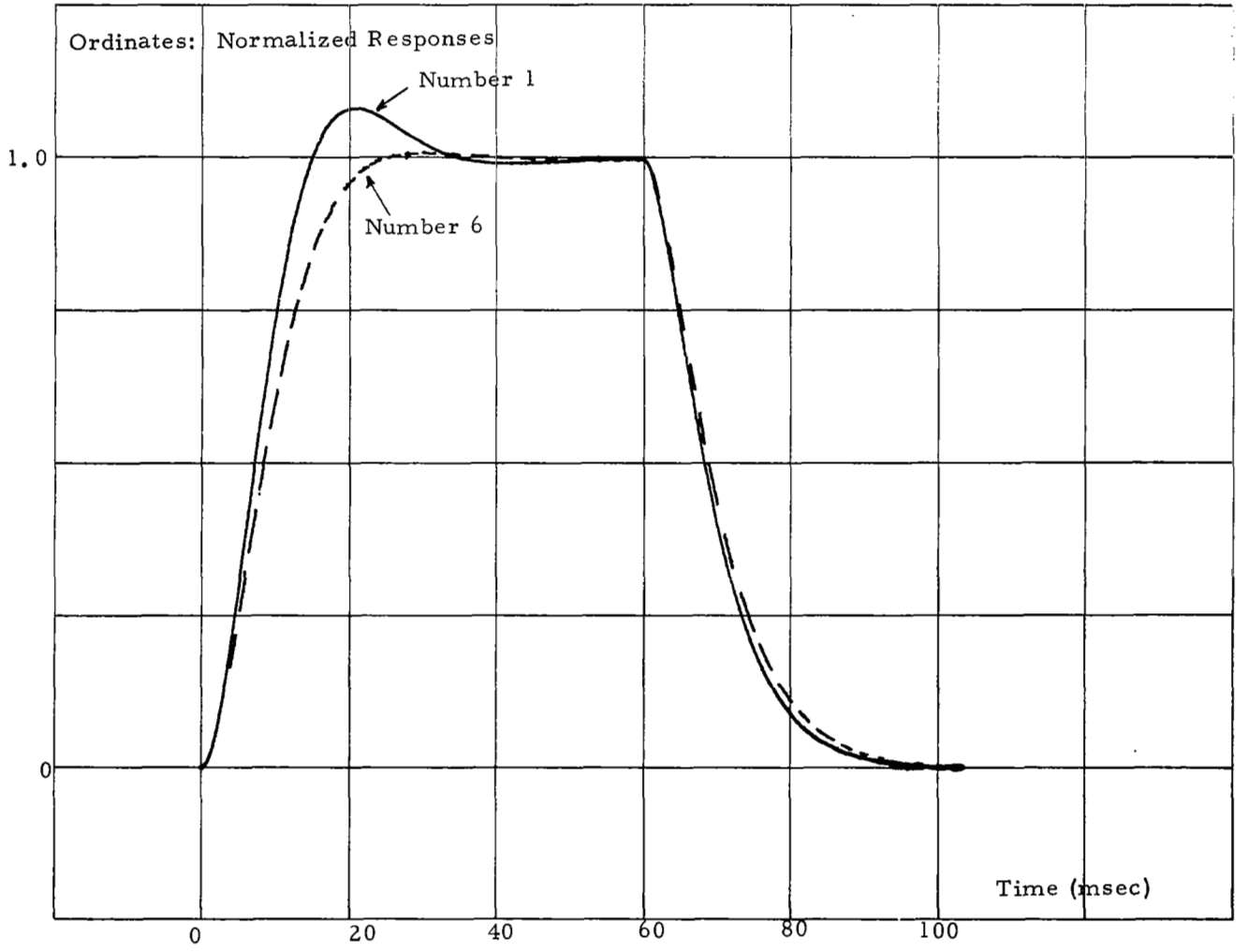

Therefore, the lag associated with the P. S. D. is comparable to that of the rate gyros proper. One also observes some spread between individual P. S. D. 's (compare ζ for #1 and 6, output up).

The parameters for underdamped response (output up) were obtained from values of overshoot and time of overshoot. Other points of the response were then compared with the theoretical values and found to agree within the accuracy of experimental data.

E. g., time of first full-scale passage { experiment 15 msec
P. S. D. #1 { theoretical 14. 7 msec

Similar agreement was obtained for the (over) critically damped responses (output down). The fact that ζ depends on direction of output swing while w_n varies very little can be explained by the observation that a resistance shift (in points A, B of the circuit diagram above) is used for the P. S. D. to obtain the bias of 2. 5V out. Therefore, the resistance in the up-and-down current paths is different, leading to different damping coefficients.

NOTE 1: No detailed circuit-schematics were available for the P. S. D., and therefore the present second order model is mainly based on experimental evidence.

NOTE 2: Full scale output voltage from the gyro output circuit is approximately 9. 5V r. m. s. On the other hand, maximum normal input to the P. S. D. 's varies between 0. 0513 V rms and 0. 165 V rms as shown in the table for steady state gains. Therefore, some signal reduction between gyros and P. S. D. 's is very likely. The amount of this reduction, however, is unknown since no complete schematics for this part were available.

5. 3 Sub-Carrier Oscillators

The S. C. O. 's are voltage controlled oscillators whose output has an instantaneous frequency deviation proportional to the input voltage, except for transient effects. (see Section 5. 1 for the ideal case).

Steady State Characteristics ("Static Gains")

The experimental data on static input-output relationships are shown in Figures 5-5 through 5-10 as output-frequency (Hz) versus input volts D. C. It is clear that these are very linear relationships, which moreover extend considerably beyond the nominal input range (0 to 5 V. D. C.) without any sign of saturation. The edges (0V and 5V) also correspond accurately with the specified IRIG-values.

Figure 5-5, Static Gain of S. C. O. 6 (1.7 kHz)

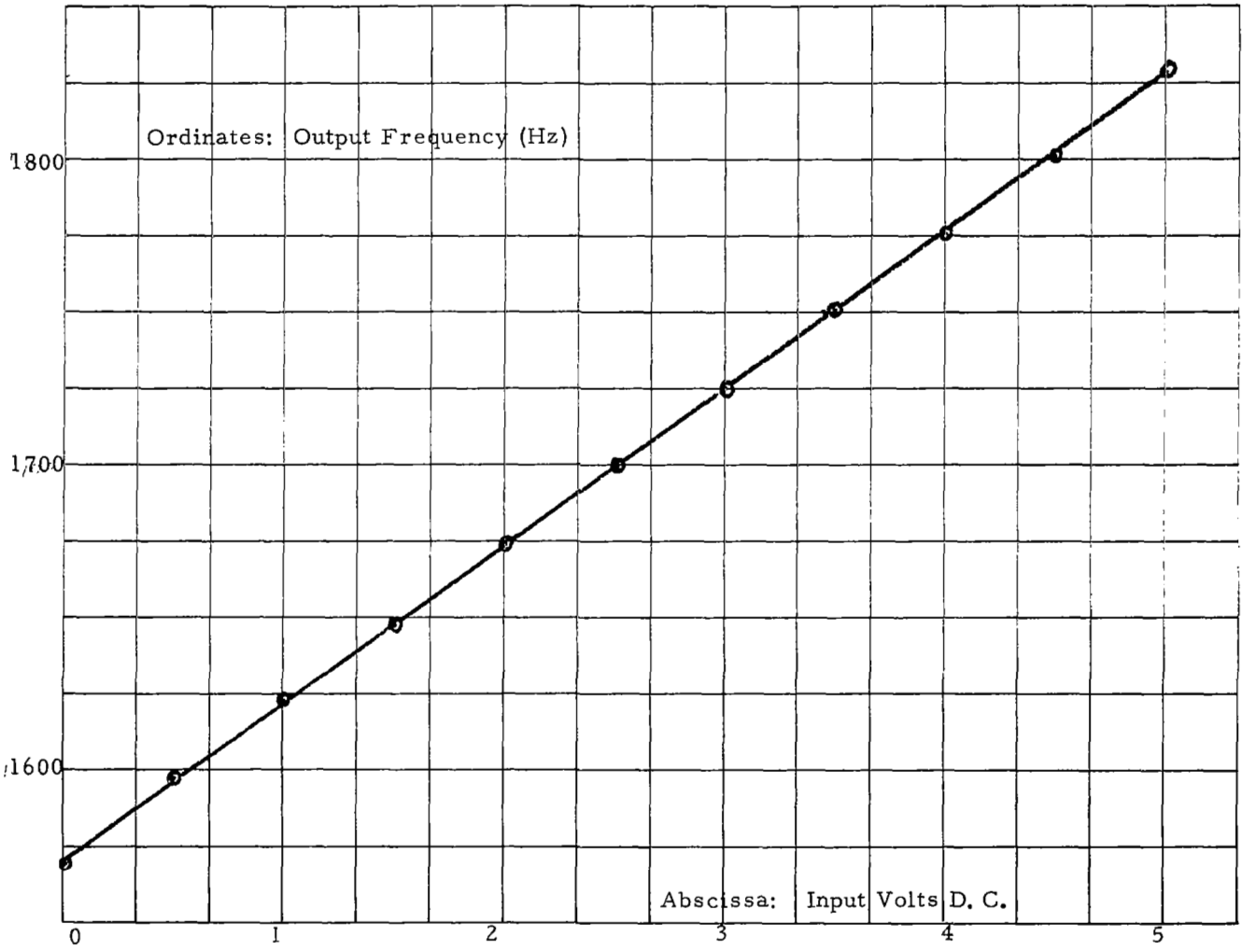

Figure 5-6, Static Gain of S. C. O. 7(2.3 kHz)

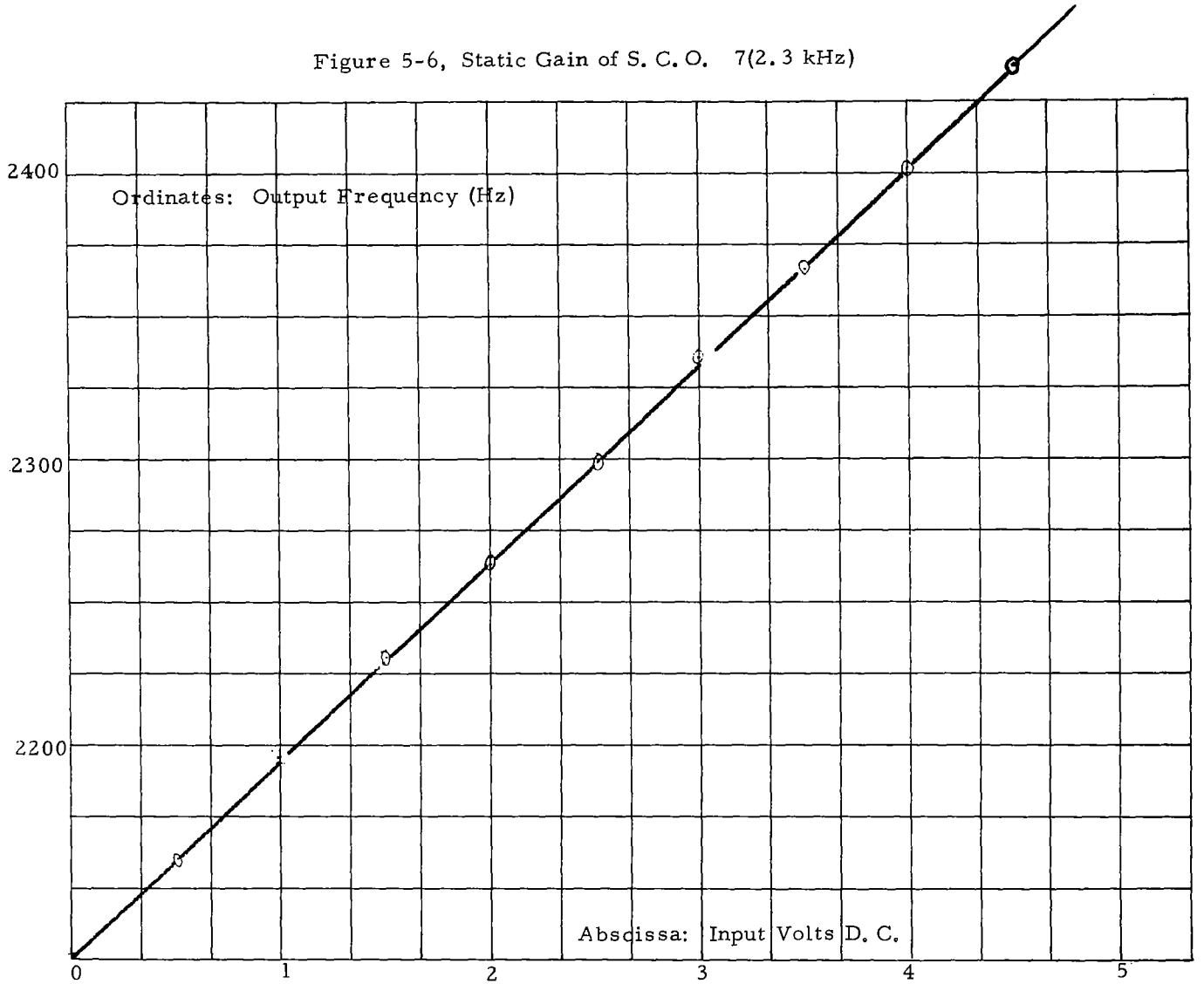

Figure 5-7

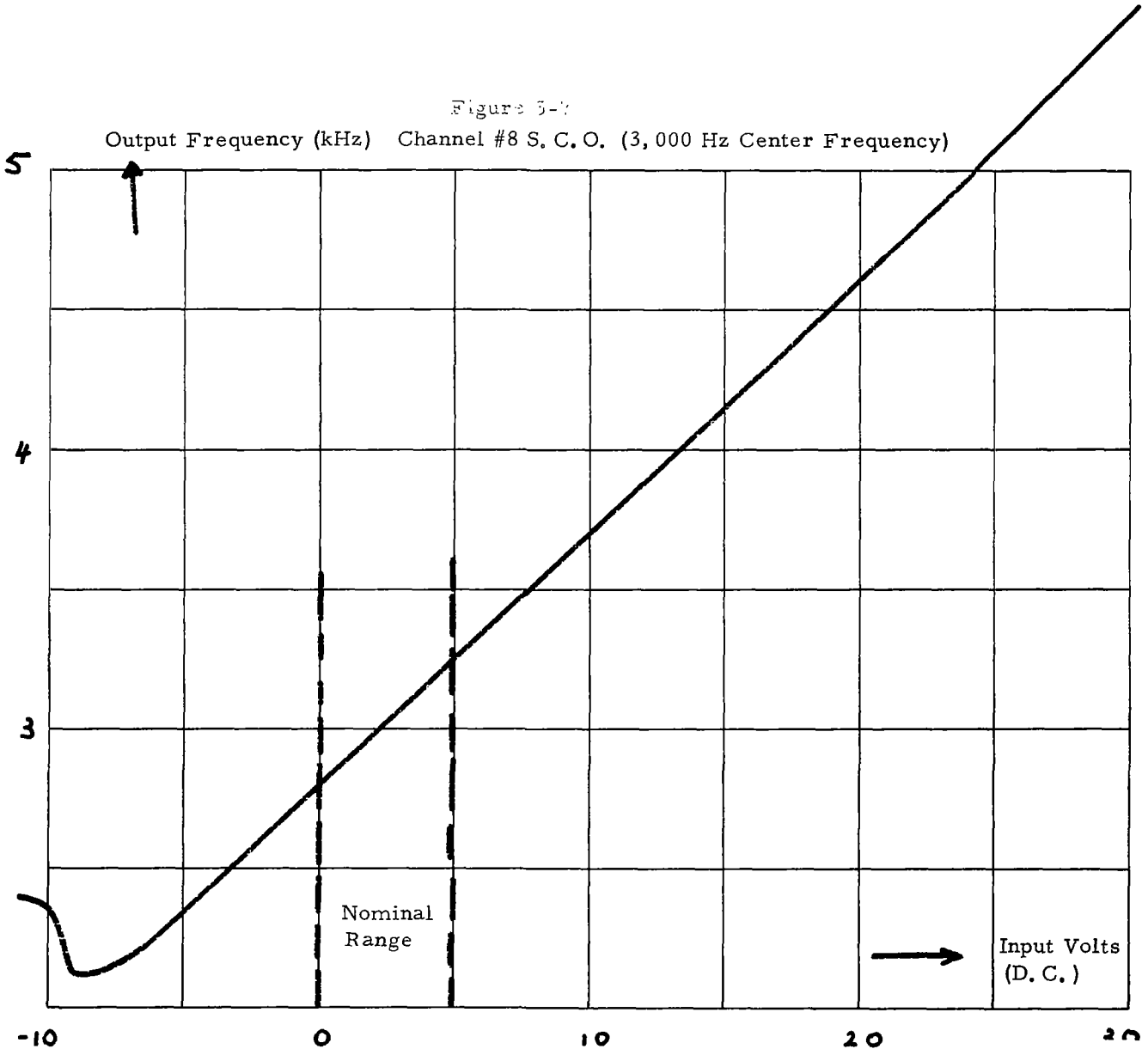
Output Frequency (kHz) Channel #8 S. C. O. (3, 000 Hz Center Frequency)
5
4
3
Nominal Range
Input Volts (D. C.)
-10
0
10
20

Figure 5-8, Static Gain of S. C. O. 10 (5. 4 kHz)

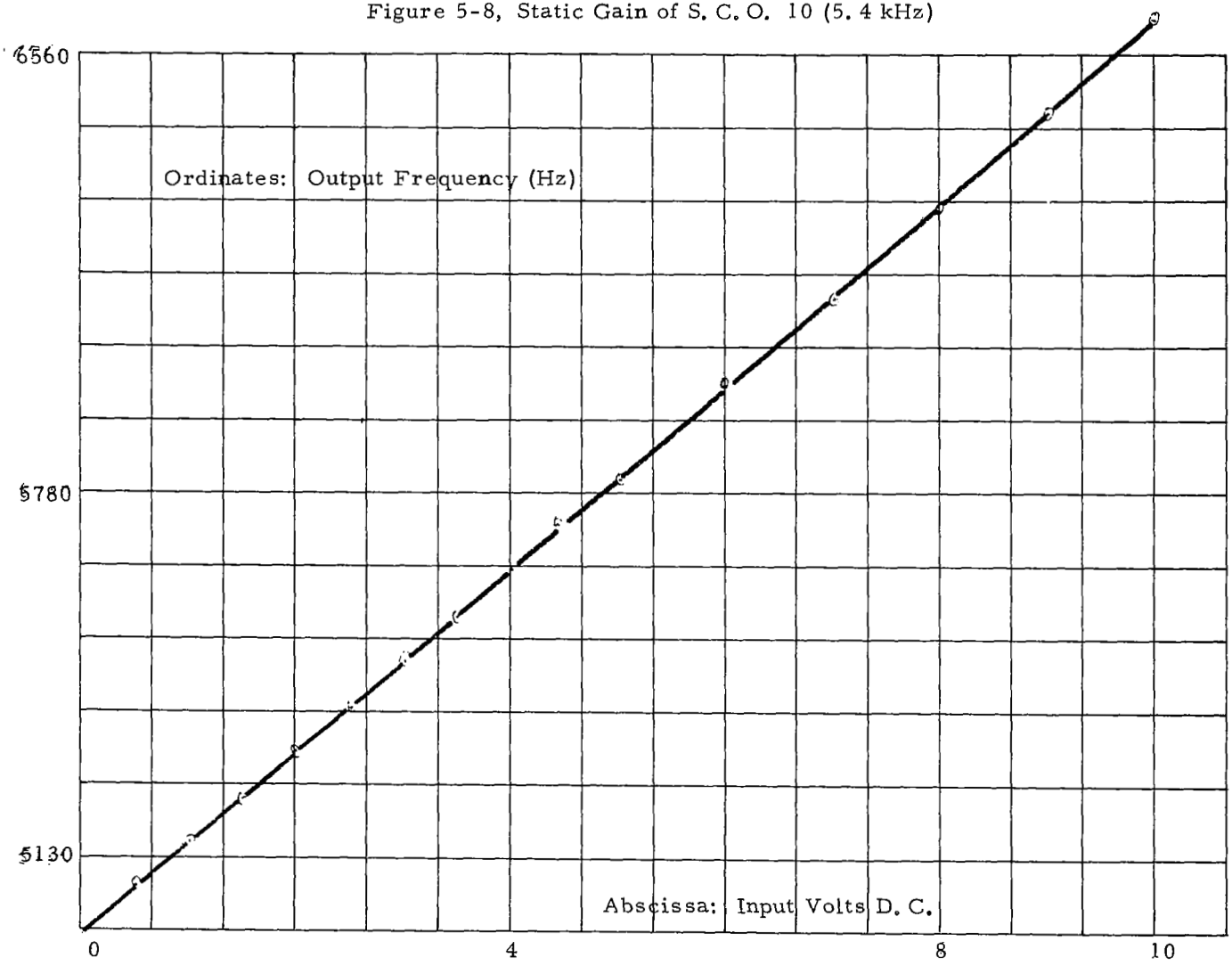

Figure 5-9, Static Gain S. C. O. 11 (7.35 kHz)

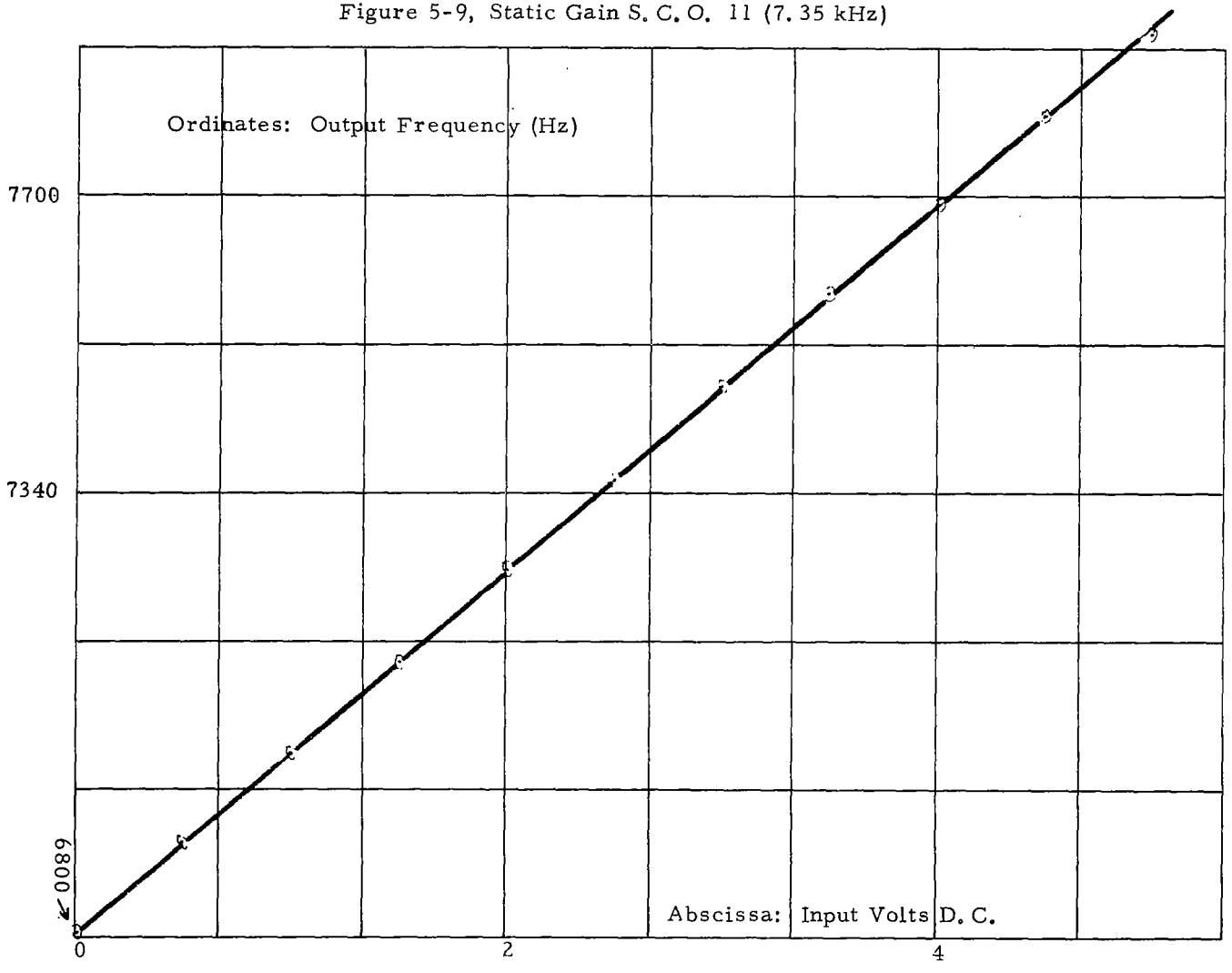

Figure 5-10, Static Gain of S. C. O. 12 (10.5 kHz)

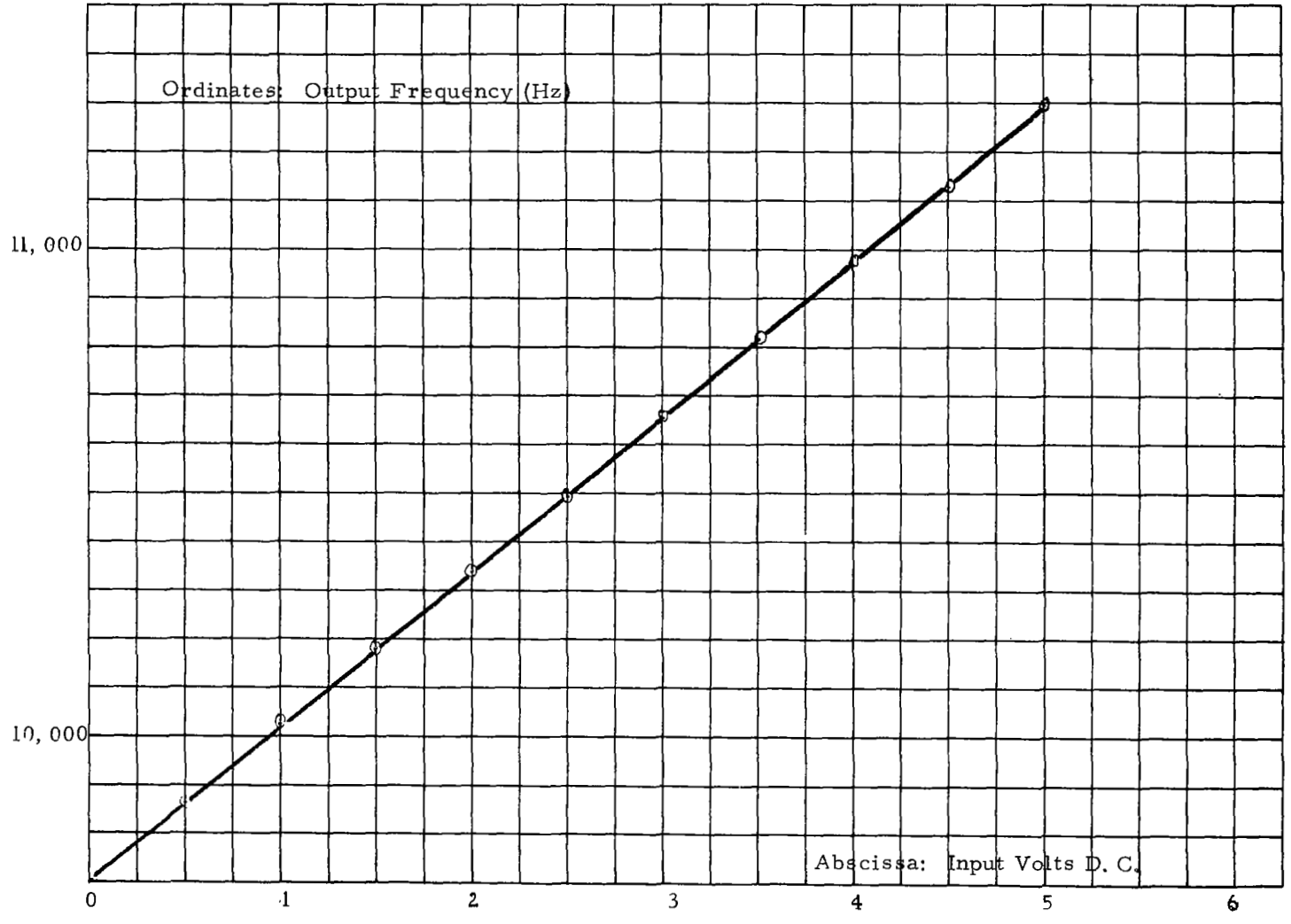

The very wide range of linearity is most clearly exhibited on Figure 5-7, the S. C. O. of channel #8, especially on the side of the positive input voltages. This figure also gives an idea of the variations in output frequency with voltage in. This means that adjacent channels could possibly interfere with each other, unless a limitation occurs earlier. For the gyros, the P. S. D. exhibits saturation as was explained in the preceding Section 5. 2. The pressure transducers have a maximum supply voltage of 5 volts, imposing a bound. The accelerometers are also limited around their normal range. Therefore, no interference is expected in normal operation with standard filters (see also further discussion of interference in Section 5. 11).

The differential static gains are listed in the table below.

TABLE S. C. O. Static gains $K_w \frac{\Delta \text{ (rad/sec) out}}{(\Delta \text{ Volts) in}}$; $K_f \frac{\Delta \text{ (Hz) out}}{\Delta \text{ (Volts) in}}$

Channel Number	K_w	K_f
6	322.	51.2
7	435.	69.2
8	565.	90.0
10	1020.	162.0
11	1380.	220.4
12	1980.	315.2
13	3740.	435.2
14	4150.	660.0
15	5650.	900.0

One has obviously $K_w = 2\,\pi\, K_f$; comparing with the expression in Section 5. 1 one has also

$$(K_w)_{ideal} = S$$

Generally, $K_f = 0.03\,(F_c)$ (Hz)

where F_c is the center-frequency of the pertinent channel.

Transient Response (Step Response)

A more realistic description than that of Section 5.1 for the S. C. O. response to an input signal $V_{in}(t)$, starting at t = 0, is given by

$$V_{out}(t) = A \cos \left(w_o t + K_w \int_o^t \int_o^{t'} V_{in}(t'') \, g(t'-t'') \, dt'' \, dt'\right)$$

This relation assumes a linear, time-invariant dynamic response for the output frequency characterized by the normalized input response g(t) (with $\int_o^\infty g(t)\, dt = 1$) or by the normalized transfer-function $G(s) = \int_o^\infty g(t) \exp(-st)\, dt$, with G(o) = 1 (the Laplace transform of g(t)). The idealized model assumed that $G(s) \equiv 1$ for all s. The present model assumes no changes in the output voltage envelope A; unless A is made to depend upon $V_{in}(t)$. However, the only dynamics of interest here are described by G(s), as a transfer function.

$$\frac{\Delta w_{out}(s)}{V_{in}(s)} = K_w G(s) \qquad (5\text{-}2)$$

Experimentally, $V_{in}(t)$ can be realized easily as a step (or as a rectangular wave with sufficiently low repetition rate to allow settling of the output). The output-frequency $w_{out}(t)$, however, is not directly measurable. A complicated way of obtaining $w_{out}(t)$, could be based on a correlation study of $V_{out}(t)$. On the other hand, the delay or lag associated with the S. C. O. is experimentally found to be quite small compared to other components in the T/M chain, especially the low-pass filter. Therefore, a simple approximation to $w_{out}(t)$ is sufficient, and this is obtained by measuring time-intervals between successive zero-crossings of $V_{out}(t)$ after the step-change in $V_{in}(t)$. The results appear as shown in the figure below (exaggerated for clarity).

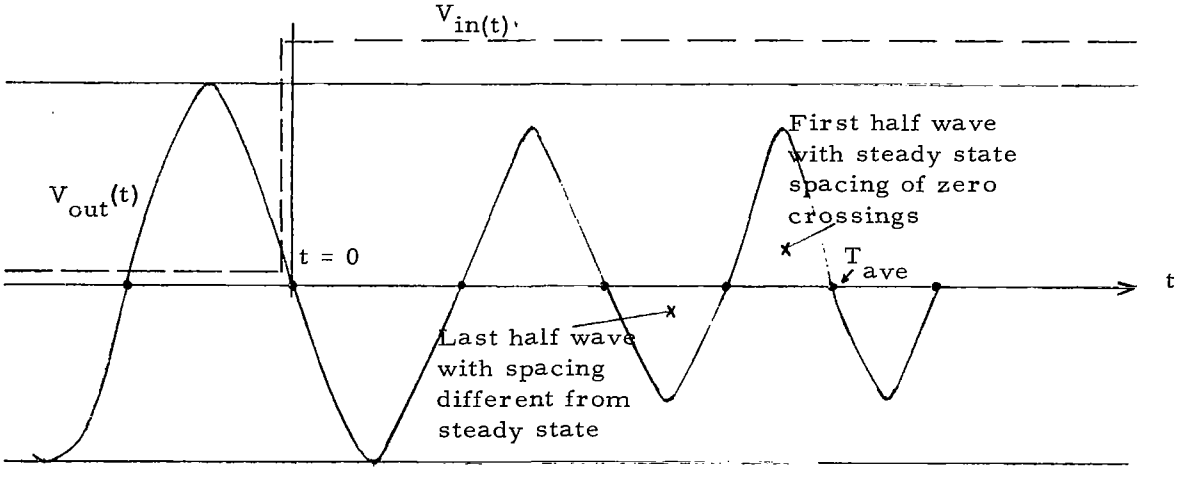

S. C. O. Step Response

The meaning of T_{ave} is also explained in this figure. Typical experimental results are shown in Figures 5-11 a, b, c for channel #8. An average value at T_{ave} has been used for rise and fall in $V_{in}(t)$. Numerical results are shown in the table below, together with the experimental uncertainties.

TABLE
Settling Times for S. C. O. 's

Channel Number and F_c (kHz)	T_{ave} (msec) Experimental	Uncertainty $\lvert \Delta T_{ave} \rvert$ (msec)	$[1.75/F_c$ (kHz)] (msec) Average Fit
6 1.7	1.3	0.15	1.03
7 2.3	0.65	0.11	0.76
8 3.0	0.66	0.08	0.58
10 5.4	0.32	0.046	0.32
11 7.35	0.25	0.034	0.24
12 10.5	0.166	0.024	0.166
13 14.5	0.112	0.026	0.120
14 22.0	0.091	0.011	0.080
15 30.0	0.067	0.008	0.058

In fact $\lvert \Delta T_{ave} \rvert = \frac{0.25}{F_c}$

These results are also shown on Figure 5-12, indicating for the present equipment, channel #7 has unusually fast S. C. O. response (but well within the uncertainties and permitted tolerances). Figure 5-12 also indicates a good approximate average fit.

$$T_{ave} = \frac{1.75}{F_c}$$

also shown in the table above

Inspection of the transient behavior shows that one can take for G(s) a second order expression

$$G(s) = \frac{1}{1 + 2\zeta \frac{s}{w_n} + \frac{s^2}{w^2_n}} \qquad (5\text{-}3)$$

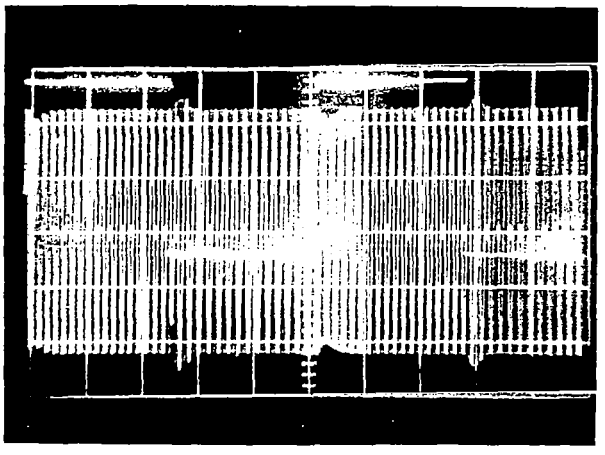

FIGURE 5-11A

STEPRESPONSE OF S. CO. #8 (3 KHz). TIME SCALE 2 ms/DIVISION. INPUT IS 0 - 5 VDC SQUARE WAVE

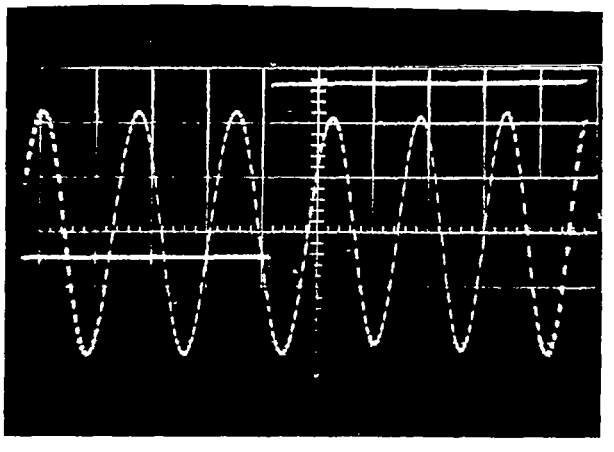

FIGURE 5-11B

DETAIL OF FIGURE 5-11A
(RISE OF INPUT)
TIME SCALE 0.2 ms/DIVISION

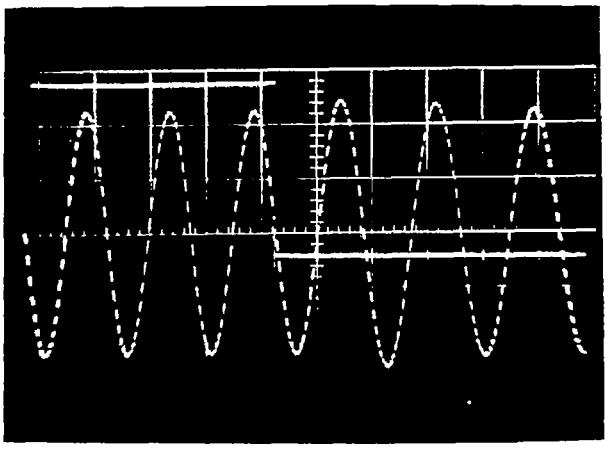

FIGURE 5-11C

DETAIL OF FIGURE 5-11A
(FALL OF INPUT)
TIME SCALE 0.2 ms/DIVISION

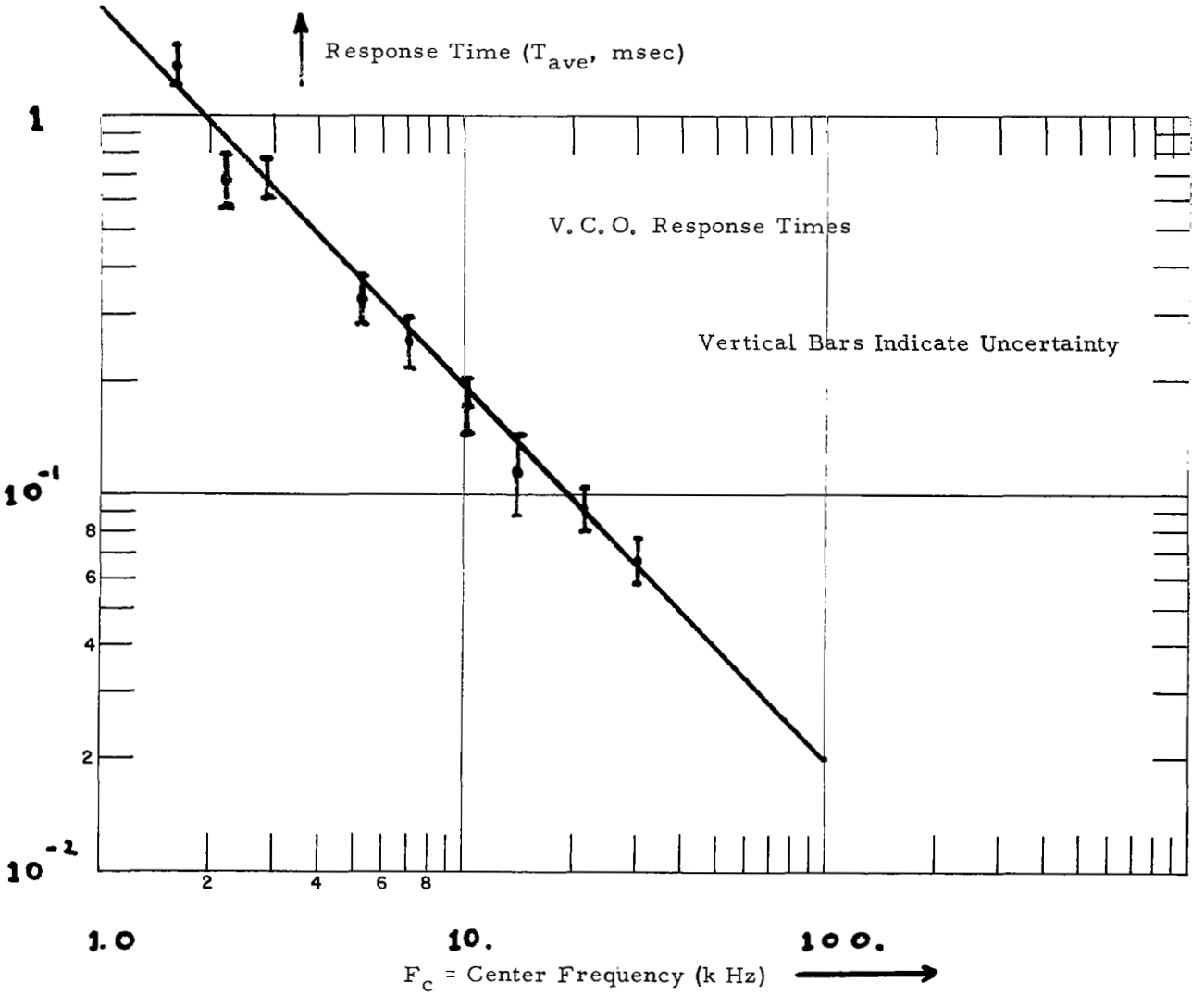

Figure 5-12, S. C. O. Response Time

with little or no discernible overshoot (with an accuracy not better than 5% of full scale). Since overshoot for $\zeta = 0.7$ is 4.5%, a sufficiently accurate model is

$$\zeta = 0.7 \text{ for all channels}$$

and then $$w_n = \frac{3.3}{T_{ave}}$$

(this is the point where the output first reaches full scale)

So, if the average fit is used, one gets

$$w_n \text{ (rad/sec)} = 1.9\ F_c^{(Hz)} = 1,900\ F_c^{(kHz)}$$

$$f_n^{(Hz)} = 0.30\ F_c^{(Hz)} = 300\ F_c^{(kHz)}$$

These results are listed in the table below

TABLE
Frequencies of Transfer Functions for
S. C. O.

Channel No.	w_n(rad/sec) Experimental	w_n(rad/sec) Average Fit	f_n(Hz) Average Fit
6	2,540	3,230	510
7	5,100	4,360	690
8	5,000	5,700	900
10	10,300	10,250	1,620
11	13,200	14,000	2,205
12	19,900	20,000	3,150
13	29,500	27,600	4,350
14	36,300	41,800	6,600
15	49,200	57,000	9,000

It is obvious from the last two tables that the dynamic lag due to the S. C. O. is indeed quite a small fraction of the lag due to the basic transducers.

5.4 The Mixer

The mixer takes the different signals from the S. C. O. 's of each channel and adds them to form a single composite output signal.

$$V_{(\text{output mixer})} = \sum_{\text{all channels}} V_{(\text{output signals of S. C. O.})}$$

Figures 5-13 and 5-14 show that the mixer has a nearly perfectly flat gain over the frequency band of interest and for normal input voltage amplitudes (steady state results). As for the dynamic behavior, excitation with a triangular wave of variable repetition frequency showed no lag, delay or distortion at the output within the frequency-band of interest (certainly between 0. 5 kHz and 100 kHz). Only at very low rates of 100 Hz (quite below the channel 6 frequency of 1, 700 Hz) did some distortion appear.

Therefore, the mixer can be represented by a constant gain K (of 1. 0), same for all channels 6 through 15, without any dynamical distortion effects.

5. 5 Transmitter and Receiver

The transmitter proper and the receiver proper are very wideband and have a very linear output-input characteristic; they are considered to have perfect, instantaneous response (compared with the delays and lags of the other components) and, for this study, their transfer-function is taken to be unity. The radio link in vacuum and atmosphere depends, of course, on a series of widely variable and often uncontrollable factors, such as distance and altitude, atmospheric conditions, and its study was not a part of the present effort.

5.6 Tape Recorders

For the channels studied in this program with center frequencies between 1, 700 Hz and 30, 000 Hz, experiments showed that recording on tape and reading off tape introduced no discernible distortion, differential lag or delay in the signals from the various channels. The setup used to study this problem is shown in Figure 5-15. Conventional equipment was used. The counter was employed to determine accurately whether any differential change in the Δt (see Figure 5-15) could be observed, when the tape-machines were used, compared with the Δt without tape-machines. Since no such effect was observed, the tape recorder can be viewed as an ideal component with transmission equal to unity.

Figure 5-13, Mixer Gain Versus Frequency

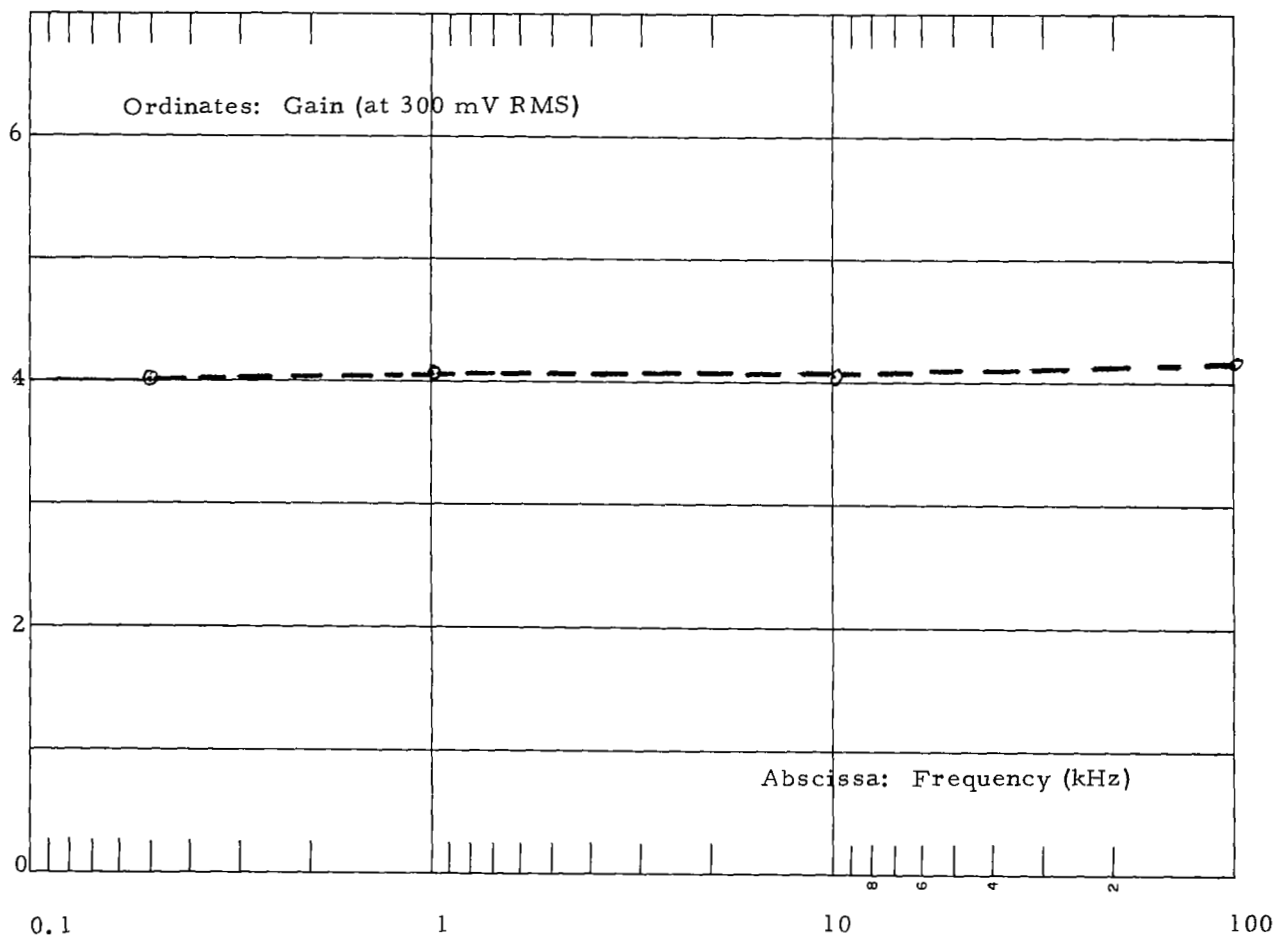

Figure 5-14, Mixer Gain Versus Input Volts

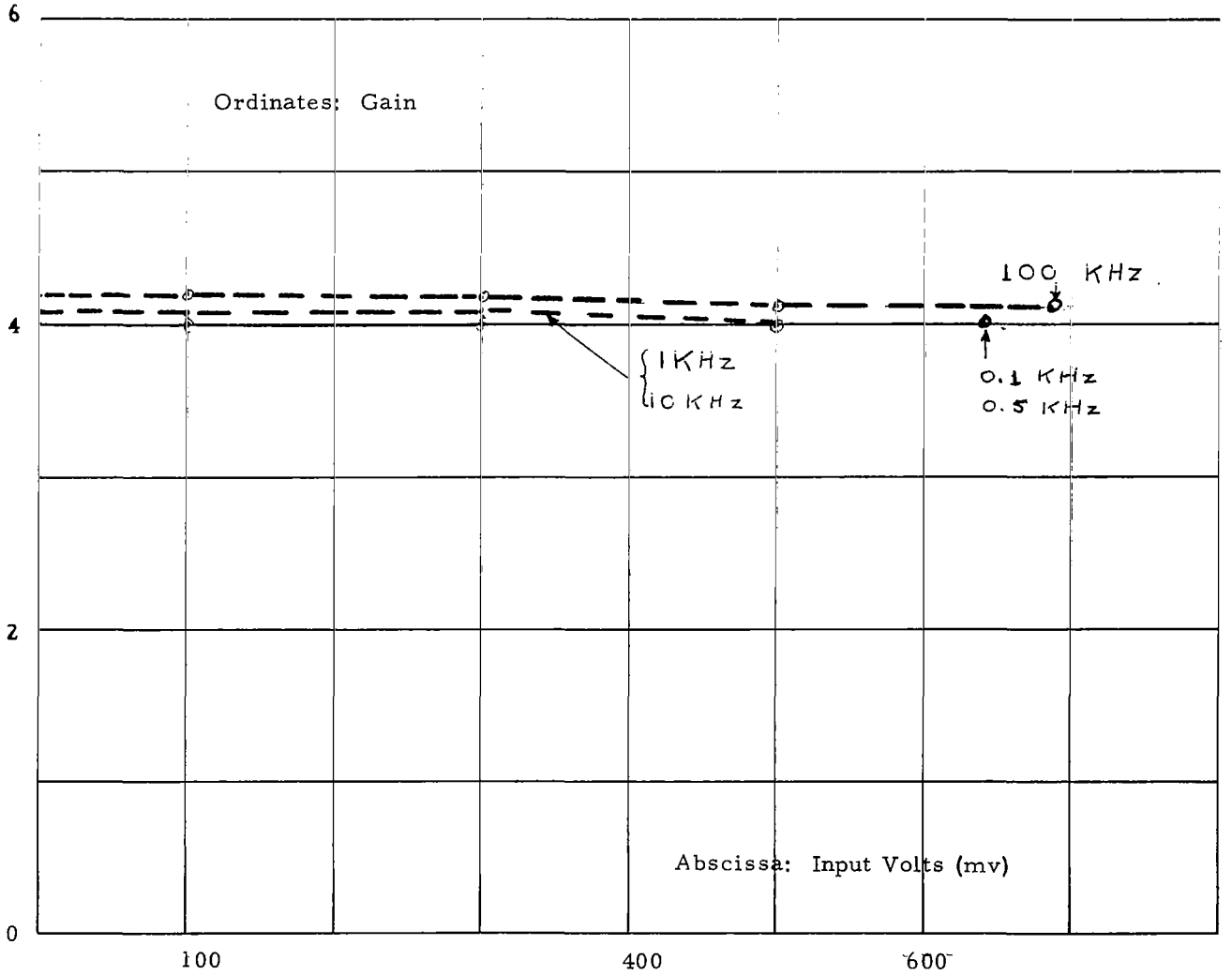

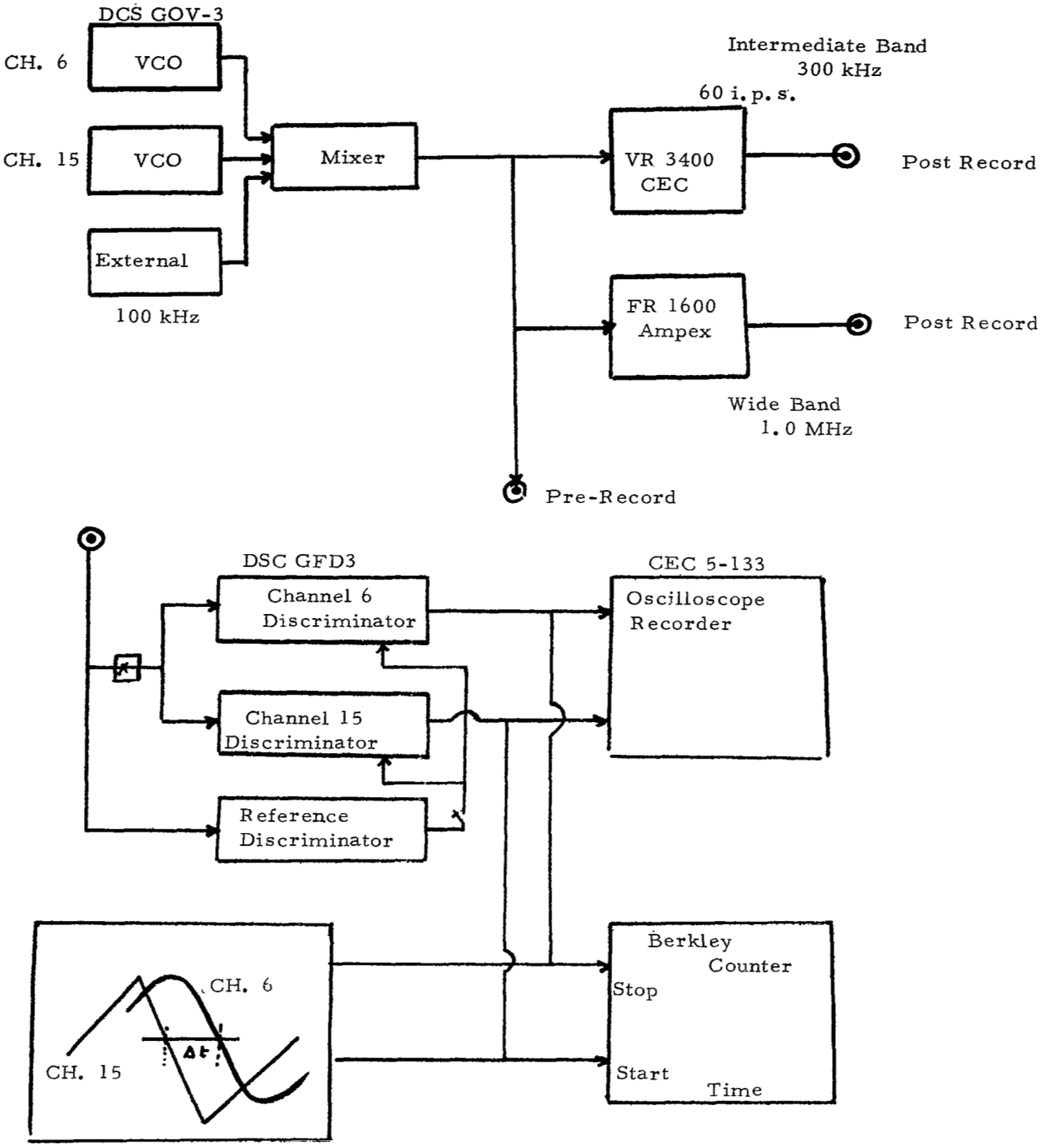

Figure 5-15, Tape Recording

5.7 Bandpass Filters (B. P.)

For the EMR Model 229 Tunable discriminator, the B. P. filters are active two-stage filters. Each stage consists of a feedback amplifier with band-reject bridged-T feedback network.

The conventional transfer-function of a bandpass-filter is defined by

$$F_{BP}(s) = \frac{E_{out}(s)}{E_{in}(s)} \tag{5-4}$$

with $E_{out}(s)$ and $E_{in}(s)$ being the Laplace-transforms of BP output signal $e_{out}(t)$ and BP input signal $e_{in}(t)$. However, in telemetry $e_{in}(t)$ is essentially a sum of output signals from S. C. O. 's (see Section 5. 3).

$$e_{in}(t) = \sum_k A_k \cos\left(w_{o,k}t + K_{w,k}\int_o^t dt'\int_o^{t'} v_{in,k}(t'')g_k(t'-t'')dt''\right)$$

$$= \sum_k A_k \cos\left(w_{o,k}t + \int_o^t \Delta\, w_{in,k}(t')dt'\right)$$

with index k indicating the various IRIG-channels.

Theoretically, each BP filter lets pass through only the correct k-component for the particular channel, and $e_{out}(t)$ has the form, for channel k.

$$e_{out}(t) = A_{out,k}\cos\left(w_{o,k}\,t + \int_o^t \Delta\, w_{out,k}(t')\,dt'\right)$$

The desired transfer-function in this study is not $F_{BP}(s)$ but the frequency-transfer function defined as

$$\hat{F}_{BP,k}(s) = \frac{\Delta w_{out,k}(s)}{\Delta\, w_{in,k}(s)} \tag{5-5}$$

for each channel k.

$\hat{F}_{BP,k}(s)$ is hard to measure directly (and would require extensive data processing, like correlation studies, etc.), but fortunately two properties permit its indirect identification.

First Property: Bandpass to Low Pass Transformation

If a BP filter with (conventional) TF-function $F_{BP}(s)$ can be regarded as a displaced low pass (DLP) filter with TF-function $F_{DLP}(s)$, such that, for $s = iw$ $(i = \sqrt{-1})$

$$F_{BP}(i\,w) = e^{-i\varphi} F_{DLP}(i\,(w-w_o)) + e^{i\varphi} F_{DLP}(i\,(w+w_o))$$

then the impulse-responses are connected by

$$f_{BP}(t) = 2\, f_{DLP}(t) \cos(w_o t - \varphi)$$

Therefore, the envelope of the response of BP to an amplitude-modulated signal (with centered carrier-frequency $\frac{w_o}{2\pi}$: $m(t) \cos(w_o t - \psi)$ is the response of the DLP to the envelope $m(t)$, both being given by

$$\int_o^t f_{DLP}(t - t')\, m(t')\, dt'$$

provided the BP filter is relatively narrow (i.e., its pass band is relatively small compared to its center frequency $\frac{w_o}{2\pi}$ or, equivalently, the time-constant of $f_{DLP}(t)$ is large compared to $\frac{2\pi}{w_o}$). This property is discussed in Chapter 7 of Reference 8.

Second Property: Relationship Between Conventional and Frequency Transfer Functions of a BP-Filter

Generalizing a result found by H. Salinger and reported in Appendix 13 of Reference 9, one can show that for a BP filter having the first property, the following simple result is valid.

$$\hat{F}_{BP}(s) \cong \frac{F_{DLP}(s)}{F_{DLP}(o)}$$

provided the maximum average frequency deviation in the input is very small relative to the bandwidth of the bandpass filter. Appendix A of this report derives this result and the conditions of its applicability.

Conclusion

To determine $\hat{F}_{BP}(s)$ it is sufficient to measure (experimentally) the envelope of the transient response of the BP filter to an amplitude-modulated signal with centered carrier (say, with a step-change in amplitude).

Each stage of the BP has the configuration shown below. The transfer function for such a stage is easily found to be

$$\frac{E_o(s)}{E_i(s)} = - \frac{(R_2C_1)s}{(1+(R_1C_1)s)} \frac{(1 + R_3C_2\, s)\,(1 + R_4C_3\, s)}{(1 + R_3C_2\, s + R_3C_2\, R_4C_3\, s^2)}$$

$$= - \frac{R_2\, C_1\, s}{1 + R_1C_1\, s} \left(1 + \frac{R_4\, C_3\, s}{1 + R_3C_2\, s + R_3C_2R_4C_3s^2} \right)$$

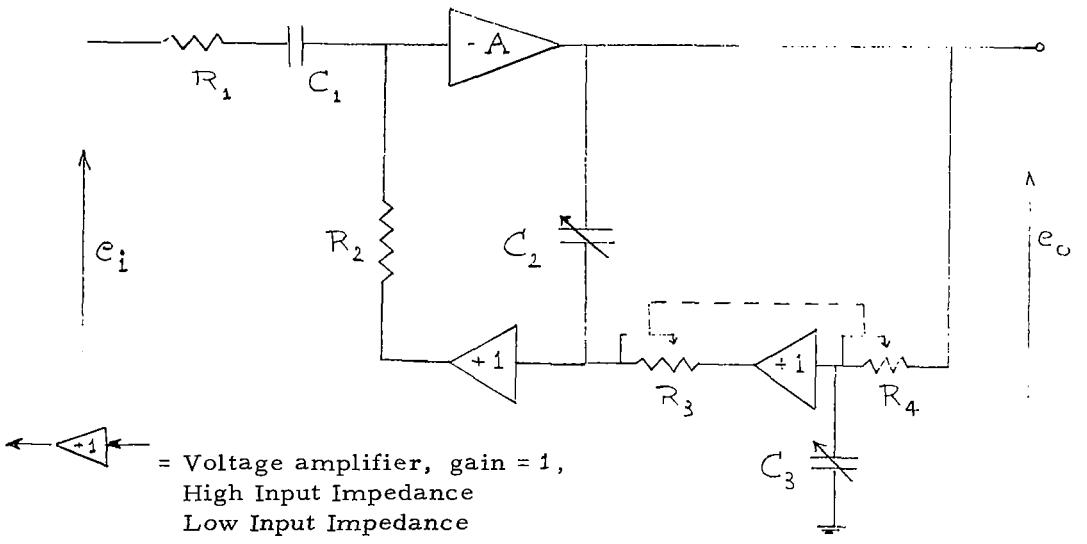

One stage of the active BP filter.

In the vicinity of the passband center, defined by

$$w^2_o\, (R_3C_2)\, (R_4\, C_3) = 1$$

one has the usual RLC-tuned behavior, (normalized):

$$\frac{1}{1 + \theta_o \left(\frac{s}{w_o} + \frac{w_o}{s} \right)}$$

where

$$\theta_o = (R_4 C_3 / R_3 C_2)^{1/2}$$

The resistances R_3, R_4 are used for tuning w_o, while C_2, C_3 are employed for bandwidth choice. The normalized low pass equivalent is of the form

$$\frac{1}{1 + T s}$$

with T being close to $2 \theta_o / w_o$.

Since the BP uses two such stages and since the experimental evidence shows no overshoot in the envelope step response, one may assume for practical purposes nearly zero or zero staggering (see again Chapter 7 of Reference 8). Therefore, one has for the displaced low pass filter

$$\frac{F_{DLP}(s)}{F_{DLP}(o)} = \frac{1}{(1 + T s)^2} \qquad (5\text{-}6)$$

with step response $1 = \exp\left(-\frac{t}{T}\right)\left(1 + \frac{t}{T}\right)$

corresponding with a critically damped second order system

$$\left(\text{i.e., } \zeta = 1.0 \text{ in } \frac{1}{1 + 2\zeta \frac{s}{w_n} \frac{s^2}{w^2_n}}\right) \qquad (5\text{-}7)$$

According to the manufacturer, the BP bandwidth (i.e., the edges) are defined as points approximately 2.5 db (or a factor of $1/1.334 = 0.75$) down from center frequency. For the DLP above this corresponds with

$$W_{E_{LP}} T = 0.578 \quad \text{(subscript E denotes edge)}$$

Since $W_{E_{LP}} = W_{E\ \text{upper, BP}} - W_o$, this gives for a $\pm$ 7.5% BP filter

$$T_{(\pm\ 7.5\%)} = \frac{0.578}{2\pi\ 0.075 \times F_c} = \frac{0.578}{0.075\ w_o}$$

and for a ± 15% BP filter

$$T_{(\pm 15\%)} = \frac{0.578}{2\pi\ 0.15\ F_c} = \frac{0.578}{0.15\ w_o}$$

where $F_c = \frac{w_o}{2\pi}$ is, as before, the center-frequency of the pertinent channel.

Particularly, for channel #6, F_c = 1,700 Hz.
w_o = 10,700 rad/sec

and $T_{(\pm 7.5\%,\ \text{ch. \#6})} = 0.72$ msec.

$T_{(\pm 15\%,\ \text{ch. \#6})} = 0.36$ msec.

As a verification, $(1 + Ts)^{-2}$ is down by a factor $\frac{1}{3.376}$ or 10.57 db (more than 10 db imposed by the specifications) for

$$\frac{w}{W_{E,LP}} = \frac{20}{7.5}$$

corresponding with a 20% shift in carrier-frequency for the BP filter. The DLP characteristic $(1 + Ts)^{-2}$ or rather the RLC-BP characteristic $(1 + \theta_o(\frac{s}{w_o} + \frac{w_o}{s}))^{-2}$ from which it was derived, also shows a satisfactory numerical agreement with the experimental frequency response of the BP exhibited in Figure 5-16.

In the table below, for channel #6, we now present a comparison between theoretical predictions for a step response using the T-values derived above and the experimental evidence, which is also shown in Figure 5-17.

TABLE
Channel #6 Step-Response

Lab. Experiments		Theoretical Value
± 7.5% filter: (average of 4 measurements)		
Time 1/2 Full Scale is reached	1.4 ± 0.3	1.7 T = 1.23 msec.
Time response is fully settled (take 97.5%, midway error)	3.7 ± 0.3	5.5 T = 3.98 msec.
± 15% filter: (average of measurements)		
Time 0.5 full scale	0.8 ± 0.3	1.7 T = 0.615 msec.
Time fully settled	1.8 ± 0.3	5.5 T = 1.99 msec.

Figure 5-16, Frequency Response Bandpass Filter

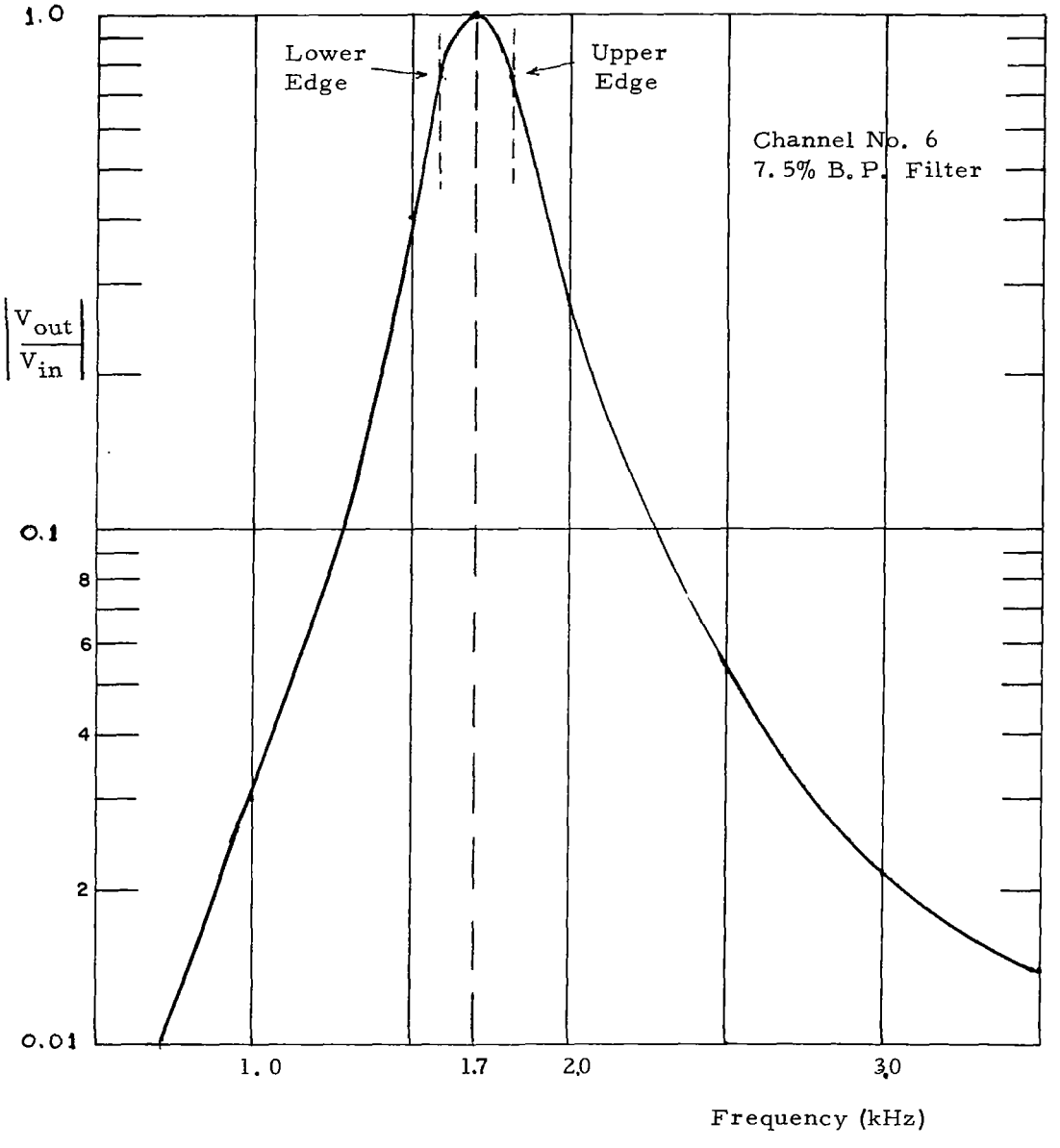

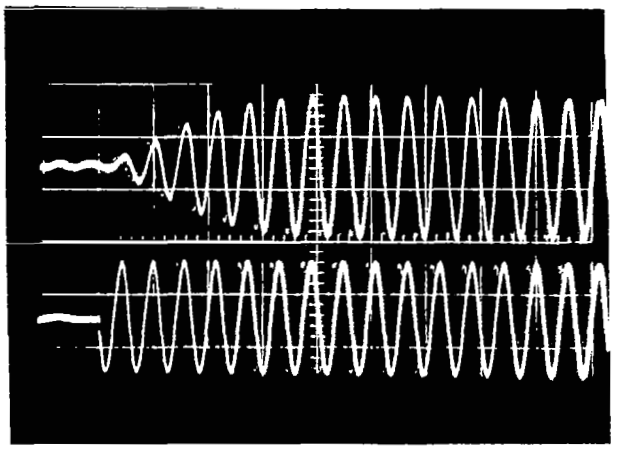

FIGURE 5-17A STEPRESPONSE OF 7.5% BP FILTER OF CHANNEL #6
TIME SCALE 1 ms/DIVISION
LOWER TRACE: INPUT TO BP (CENTERED CARRIER WITH STEP IN ENVELOPE)
UPPER TRACE: BP RESPONSE

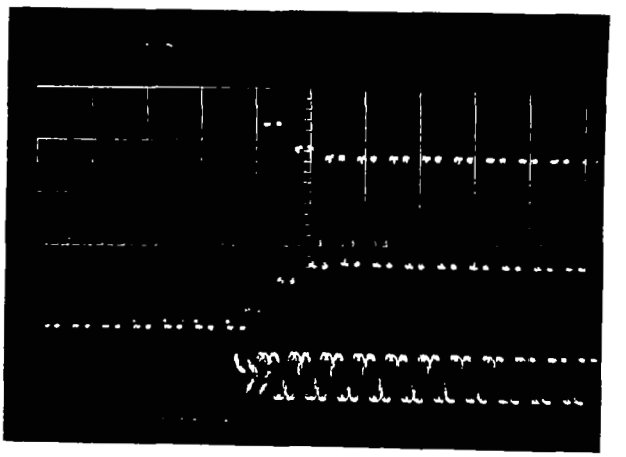

FIGURE 5-17B STEPRESPONSE OF 15% BP FILTER OF CHANNEL #6
SAME TIME SCALE AND COMMENTS AS FIGURE 5-17A

The agreement is quite satisfactory (within the accuracy of the measurements). The smallness of T shows, moreover, that the bandpass filter introduces only a small amount of lag and distortion when compared to the low pass filter (if the standard filters are used, of course).

It is interesting to display the non-linear dependence of the BP output on the magnitude of the frequency swing at its input (in the signal coming from the S. C. O.) a feature discussed in Appendix A. This is done in Figure 5-18. Channel #6 was isolated there to avoid interference from its neighbors. The extra-wide 125 Hz (constant delay) LP filter was used, instead of the standard 25 Hz LP in order to minimize the distortion in the LP. Trace A of Figure 5-18 corresponds with a small swing of 2V to 3V (centered around the middle of the range at 2. 5V) at the input of the S. C. O. , i. e. , a small swing Δw_{in} at the input to the BP. In fact, with the notations of this section and of Appendix A

$$\frac{|\Delta w_{in}|}{w_{E,LP}} = \frac{1}{5} = 0.2$$

Then the small signal approximation of Appendix A is valid, i. e. , the "second property" of this section applies, and the response of Trace A agrees with the normalized step-response derived above as $|\angle w_{in}|\ (1 - \exp(-\frac{t}{T})(1 + \frac{t}{T}))$ (also shown in Figure 5-17), except, of course, for some additional delay introduced by the LP.

For trace B and a fortiori for trace C, the frequency swing is large

$$\frac{|\Delta w_{in}|}{w_{E,LP}} = 1$$

and non-linear effects appear clearly. Just as for the ideal case mentioned in the Appendix A and discussed in Reference 9, a marked overshoot appears (symmetric for this type of input swing which is itself symmetric about the center frequency). The experimental overshoot of trace A is approximately 10% and some rather lengthy calculations indicate that this overshoot is quite compatible with the theory, given the uncertainties in the quantities measured.

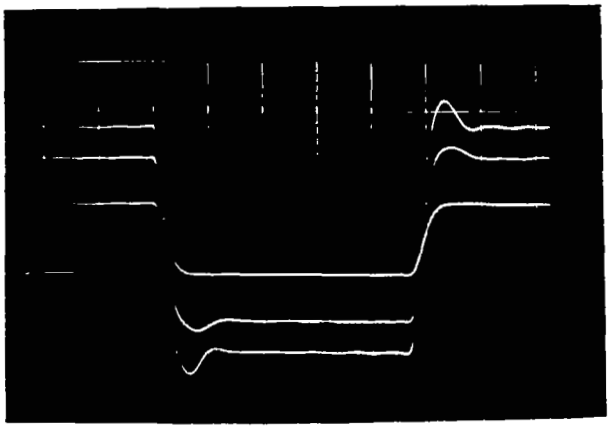

FIGURE 5-18 DEPENDENCE OF B. P. ON MAGNITUDE OF ITS INPUT FREQUENCY SWING (i.e., MAGNITUDE OF INPUT VOLTAGE SWING TO S. C. O.)

ISOLATED CHANNEL #6; 7.5% B. P., 125 Hz CONSTANT DELAY L. P.

TRACE A	INPUT SWING	2V to 3V
TRACE B	INPUT SWING	1V to 4V
TRACE C	INPUT SWING	0V to 5V

TIME SCALE 10 ms/DIVISION

5.8 Discriminators

EMR 229 employs a phase lock-loop discriminator. The dynamic effects are described mainly by the loop filter and the total loop gain. A linearized model of the discriminator is shown (compare with Reference 7, Chapter 8).

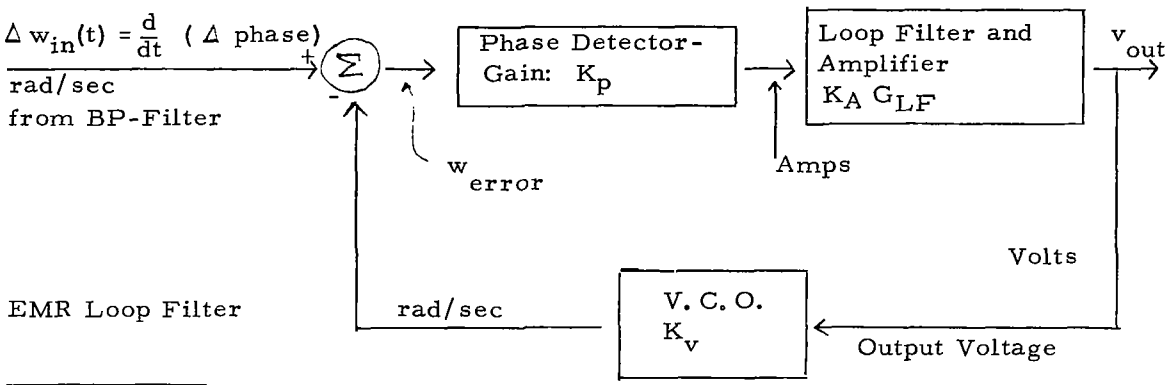

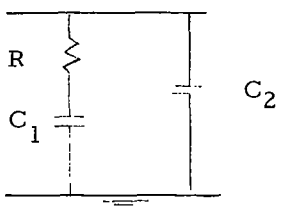

$(K_p K_v)^{-1}$ has dimension ohm

K_A is dimensionless $\frac{\text{volt}}{\text{volt}}$

Fig. Linearized Model of the Discriminator

With these notations one has

$$G_{LF} = \frac{1}{(C_1+C_2)s} \quad \frac{1 + R C_1 s}{1 + RC_1 \frac{C_2}{C_1+C_2} s} \tag{5-8}$$

$$\frac{V_{out}(s)}{\angle w_{in}(s)} = \frac{1 + RC_1 s}{K_v \left(1 + \left(RC_1 + \frac{C_{1+}C_2}{K_A K_p K_v}\right)s + \frac{RC_1C_2}{K_A K_p K_v} s^2\right)} \tag{5-9}$$

The loop gain is generally sufficiently large such that

$$\frac{K_A K_p K_v}{C_1 + C_2} \gg \frac{1}{RC_1}$$

Therefore, the resulting transfer function takes the standard form

$$w^2_n = \frac{K_A K_p K_v}{R C_1 C_2}, \quad \frac{2\zeta}{w_n} = R C_1$$

$$\frac{V_{out}(s)}{\Delta w_{in}(s)} = \frac{1}{K_v} \frac{1 + 2\zeta \frac{s}{w_n}}{1 + 2\zeta \frac{s}{w_n} \left(1 + \frac{C_1 + C_2}{C_1 R K_p K_v K_A}\right) + \frac{s^2}{w^2_n}} \tag{5-10}$$

$\Delta w_{in}(t)$ is measured from the center frequency of the corresponding channel.

The phase error in the loop (see diagram above) is given by

$$\frac{\varphi_E(s)}{\Delta w_{in}(s)} = \frac{\frac{1}{s} w_{error}(s)}{\Delta w_{in}(s)} = \frac{\frac{s}{w^2_n} + \frac{C_1 + C_2}{K_A K_p K_v}}{1 + 2\zeta \frac{s}{w_n} + \frac{s^2}{w^2_n}}$$

The static phase error at band edge $\Delta w_{in} = w_{E,\,LP}$ is given by the manufacturer as less than $2^o = 0.035$ rad.

Therefore,

$$\frac{0.035}{w_{E,\,LP}} > \frac{C_1 + C_2}{K_A K_p K_v} = \frac{1}{\text{Loop Gain (rad/sec)}}$$

For Channel #6, as an example

$$\frac{K_A K_p K_v}{C_1 + C_2} > \frac{2\pi \cdot 0.075 F_c}{0.035} = \frac{800}{0.035} = 2.3 \times 10^4 \text{ rad/sec}$$

During normal operation, the dynamic phase error should be less than $90^o = \frac{\pi}{2}$ rad (no lock-loss).

For infinite loop gain, this amounts to the following condition, derived from the transient response of $\mathscr{E}_E(t)$

$$\frac{|\Delta w_{in}|_{max,\ normal}}{w_n} \exp\left(-\zeta \frac{\left(\frac{\pi}{2} - \text{Arc sin}\,\zeta\right)}{\sqrt{1-\zeta^2}}\right) < \pi/2 \quad (\text{if } \zeta \leq 1)$$

With $|\Delta w_{in}|_{max,\ normal} = w_{E,\ LP} = (800$ rad/sec for channel #6)

one finds (if $\zeta < 1$)

$$w_n > 0.64\ w_{E,LP} \exp\left(-\frac{\zeta}{\sqrt{1-\zeta^2}}\left(\frac{\pi}{2} - \text{Arc sin}\,\zeta\right)\right)$$

One has also

$$2\zeta w_n = \frac{K_A K_p K_v}{C_1 + C_2} \cdot \frac{C_1 + C_2}{C_2} = \frac{C_1 + C_2}{C_2} \text{ Loop Gain} > \text{Loop Gain}$$

The preceding two inequalities indicate that the discriminator has proper frequencies of an order of magnitude higher than those of the BP filter ($\pm$ 7.5%) and thus responds about ten times faster, i.e., even faster than the S.C.O. Therefore, within the accuracy of the experimentation, the discriminator dynamics may be neglected entirely. (Transfer function is unity).

5.9 The Low Pass Filters (LP-F)

The output from the discriminator still contains spurious components such as a ripple at twice the frequency of the subcarrier. The purpose of the LP-F is to remove such unwanted components, while distorting the true signal as little as possible.

Basically, the 210 C-01 LPF's in the EMR 229 have the schematics shown below.

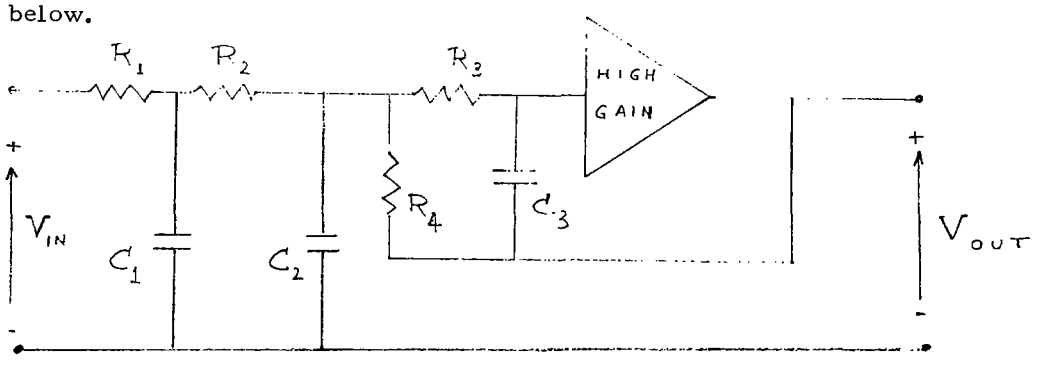

Low Pass (Output) Filter
Diagram

The transfer function is a third-order function

$$\frac{V_{out}(s)}{V_{in}(s)} = -\frac{R_4}{R_1 + R_2} \qquad \frac{1}{1 + a_1 s + a_2 s^2 + a_3 s^3}$$

$$a_1 = \frac{R_1 R_2}{R_1+R_2} C_1 + (R_3 + R_4) C_3 + \frac{R_3 R_4}{R_1+R_2} C_3$$

with

$$a_2 = C_3 C_2 R_3 R_4 + C_3 C_1 \frac{R_1}{R_1+R_2} (R_2 R_3 + R_3 R_4 + R_4 R_2)$$

$$a_3 = \frac{C_1 C_2 C_3 R_1 R_2 R_3 R_4}{R_1 + R_2}$$

Through an appropriate choice of component values, two basic types of filters are realized by the same diagram.

1) Constant Amplitude or Butterworth Filters, with general transfer-function (normalized).

$$B_U(s) = \frac{1}{1 + 2 T_{BU} s + 2 T^2_{BU} s^2 + T^3_{BU} s^3} \qquad (5\text{-}11)$$

$$= \frac{1}{(1+T_{BU} s)(1+T_{BU} s + T^2_{BU} s^2)}$$

2) Constant Delay or Linear Phase or Bessel Filters, with general (normalized) transfer-function.

$$B_E(s) = \frac{15}{15 + 15 T_{BE} s + 6 T^2_{BE} s^2 + T^3_{BE} s^3} \qquad (5\text{-}12)$$

The preceding filters are discussed in References 8 and 10 and useful transient (including step) responses are shown in Reference 11.

Determination of Parameter Values

Everything is reduced to an estimation of two time-constants T_{BU}, T_{BE} (provided the real filter behavior approaches the theoretical one).

The filters were subjected to rectangular inputs of sufficiently low repetition rate to constitute nearly perfect step inputs.

For the Butterworth filter, the manufacturer specifies the cutoff-frequency $w_{co} = 2\pi f_{co}$ by an attenuation of 0.5 db (a factor of $\frac{1}{1.059}$). This gives

$$T_{BU}\, w_{co} = 0.704$$

The following table gives a comparison of theoretical and experimental results, based on the preceding relation.

TABLE
Step Response of Butterworth Filter

Channel #6 f_{co} = 25 Hz (standard filter)

w_{co} = 157 rad/sec

T_{BU} = 4.5 msec

	Theoretical	Experimental
Overshoot	8.15%	(8.1 ± 1%)
Time of Overshoot	4.8 T_{BU}= 21.6 msec	(22 ± 1) msec
Time full-scale is reached first	3.8 T_{BU}=17.1 msec	(17 ± 1) msec
Time full-scale is reached second time	7.2 T_{BU}= 32.4msec	(30 ± 2) msec
Time full-scale is reached third time (essentially settled)	10.5 T_{BU}= 47.4 msec	(46 ±3) msec

The agreement is excellent, and the general formula above for T_{BU} is valid for all channels.

For the Bessel-filter, the manufacturer's amplitude response curves give 3.35 db at w_{co} (cutoff), 12.3 db at twice cutoff and 20.9 db at three times cutoff. This leads to

$$T_{BE}\, w_{co} = 1.8$$

The table below gives again a comparison of theoretical and experimental results.

TABLE
Step Response of Bessel-Filter

Channel #6 $f_{co} = 25$ Hz

$w_{co} = 157$ rad/sec

$T_{BE} = 11.5$ msec

	Theoretical	Experimental
Time half-scale is reached	$0.96\, T_{BE} = 11.0$ msec	(9.6 ± 1.5) msec
Time of settling (within accuracy)	$2.3\, T_{BE} = 26.4$ msec	(26.6 ± 1.5) msec
Overshoot	0.75%	Not noticeable

Other experiments for other cutoff-frequencies gave similar satisfactory agreements such that the general formula above for T_{BE} is an acceptable formula. Experimental step responses for both Butterworth and Bessel filters are shown in Figure 5-19 A & B, and the analog computer verification is exhibited in Figure 5-20.

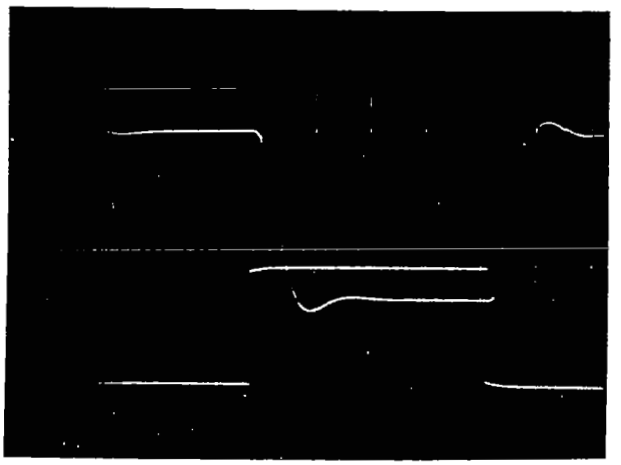

FIGURE 5-19A STEPRESPONSE OF 25 Hz CONSTANT AMPLITUDE LOW PASS FILTER . TIME SCALE 20 ms/DIVISION

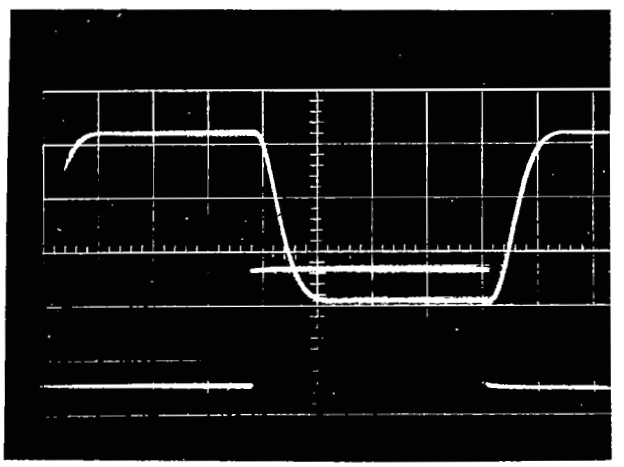

FIGURE 5-19B STEPRESPONSE OF 25 Hz CONSTANT DELAY LOW PASS FILTER TIME SCALE 20 ms/DIVISION

Figure 5-20, Step Responses of Low Pass Filters

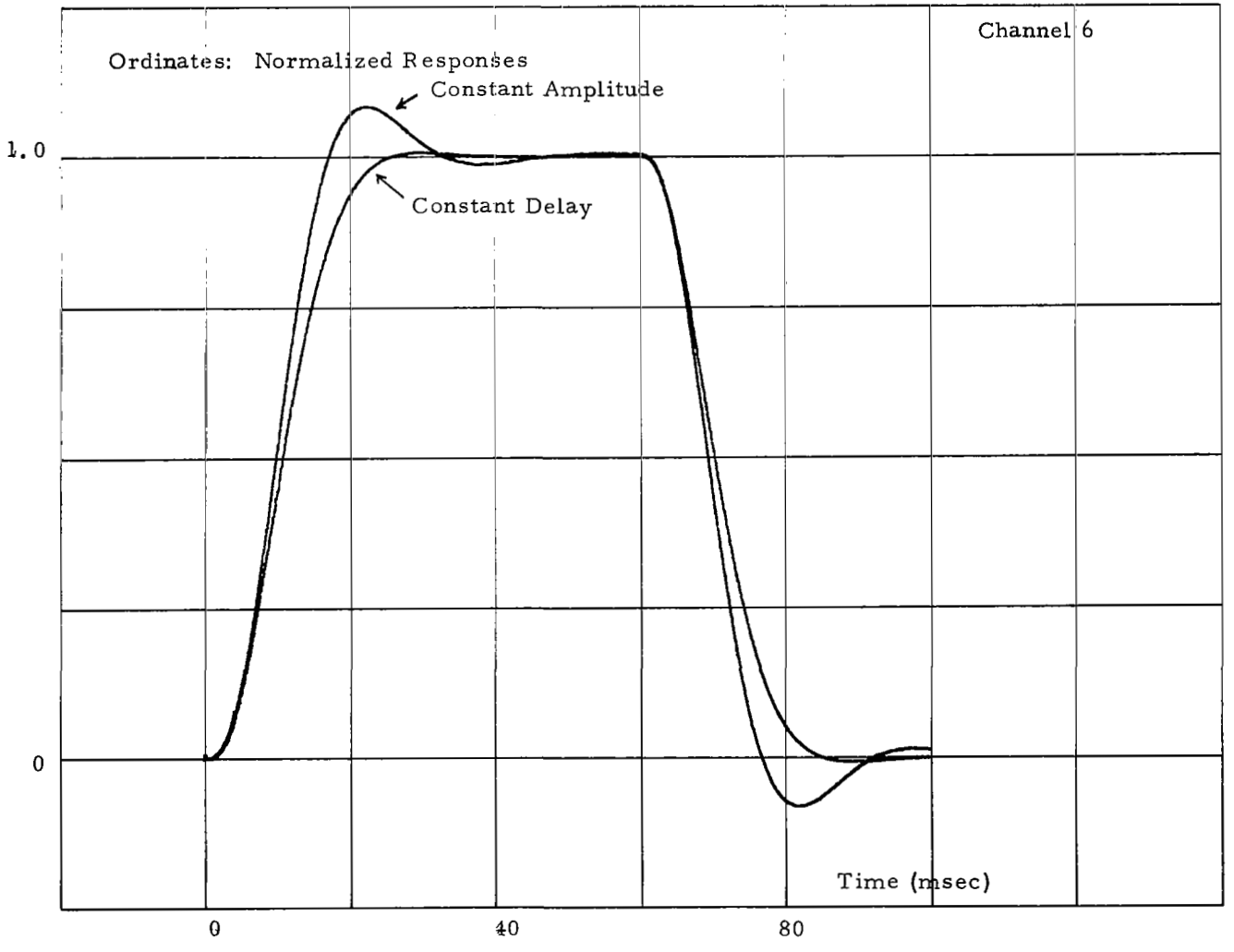

5.10 Complete Telemetry Chain

After the individual components were tested and their characteristics determined, the transmission of signals through the entire cascade of T/M components was studied. For analog computer verification, the separate models of each individual successive component (P. S. D., S. C. O, B. P., L. P.) were simply cascaded.

Because of interaction of successive stages, the entire chain might a priori have a transfer function different from the product of the individual transfer-functions. Such interaction was observed for the pressure-transducers. However, for the T/M chain, the interaction turned out to be negligible and the cascading of individual component models is a valid procedure. Moreover, for standard filters, the LP filter is by far slower than the other components, except the P. S. D. (where used) and therefore the entire chain will behave very much as the LP-F with some relatively small additional lags superimposed, or, in the case of channels #6, 7 and 8 the entire chain will behave very nearly as the LP-F combined with P. S. D. (if used).

Experimental results and the analog simulation corroborating the statements made above are shown:

a) For trapezoidal inputs in Figures 5-21 A & B, 5-22.

The agreement is very good. Figure 5-23 shows the response of the LP alone to the same input, proving indeed that the LP is by far the major contributor of dynamic distortion in the T/M chain. Results for other channels can be simply obtained by correct time scaling.

b) For triangular inputs in Figures 5-24 A & B, 5-25 and 5-26. The same comments apply as in the preceding case of trapezoids.

c) For rectangular (step) inputs, in Figure 5-20 seen before and also in Figures 5-27 A & B, 5-28 and 5-29, with the same comments as above.

d) For rectangular (step) inputs, but now with P. S. D. included, see Figures 5-30 A & B, 5-31 and 5-32. It is obvious that indeed, as mentioned before, the P. S. D. constituted a noticeable part of the dynamic lag, comparable to that of the LP itself.

NOTE: Experimental data for other channels were obtained, but they offer nothing new, since these results can be obtained simply by rescaling times, inversely proportional to the center-frequency.

Peculiar effects in the total T/M chain are now discussed in the next sub-sections 5.11 and 5.12.

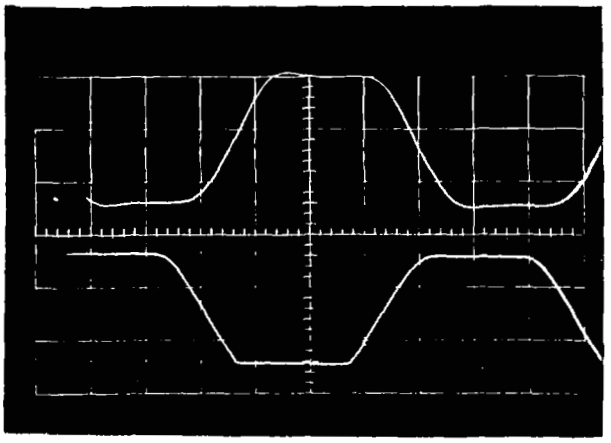

FIGURE 5-21A RESPONSE OF CHANNEL #6 TO TRAPEZOIDAL INPUTS (P.S.D.. EXCLUDED)
7.5% B.P., 25 Hz CONSTANT AMPLITUDE L. P.
TIME SCALE 20 ms/DIVISION

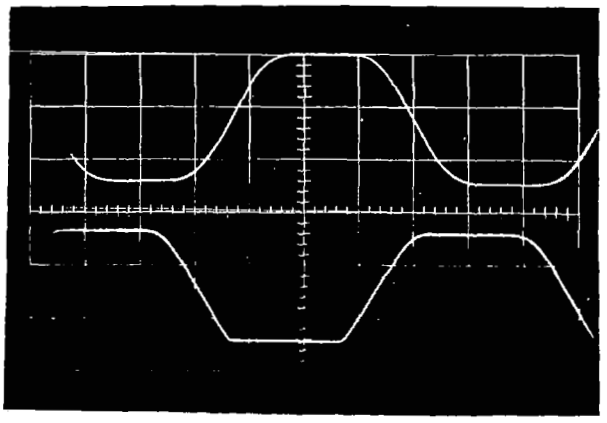

FIGURE 5-21B SAME AS FIGURE 5-21A EXCEPT THAT CONSTANT DELAY L. P. WAS USED

Figure 5-22, Responses of Channel 6 to Trapezoidal Inputs

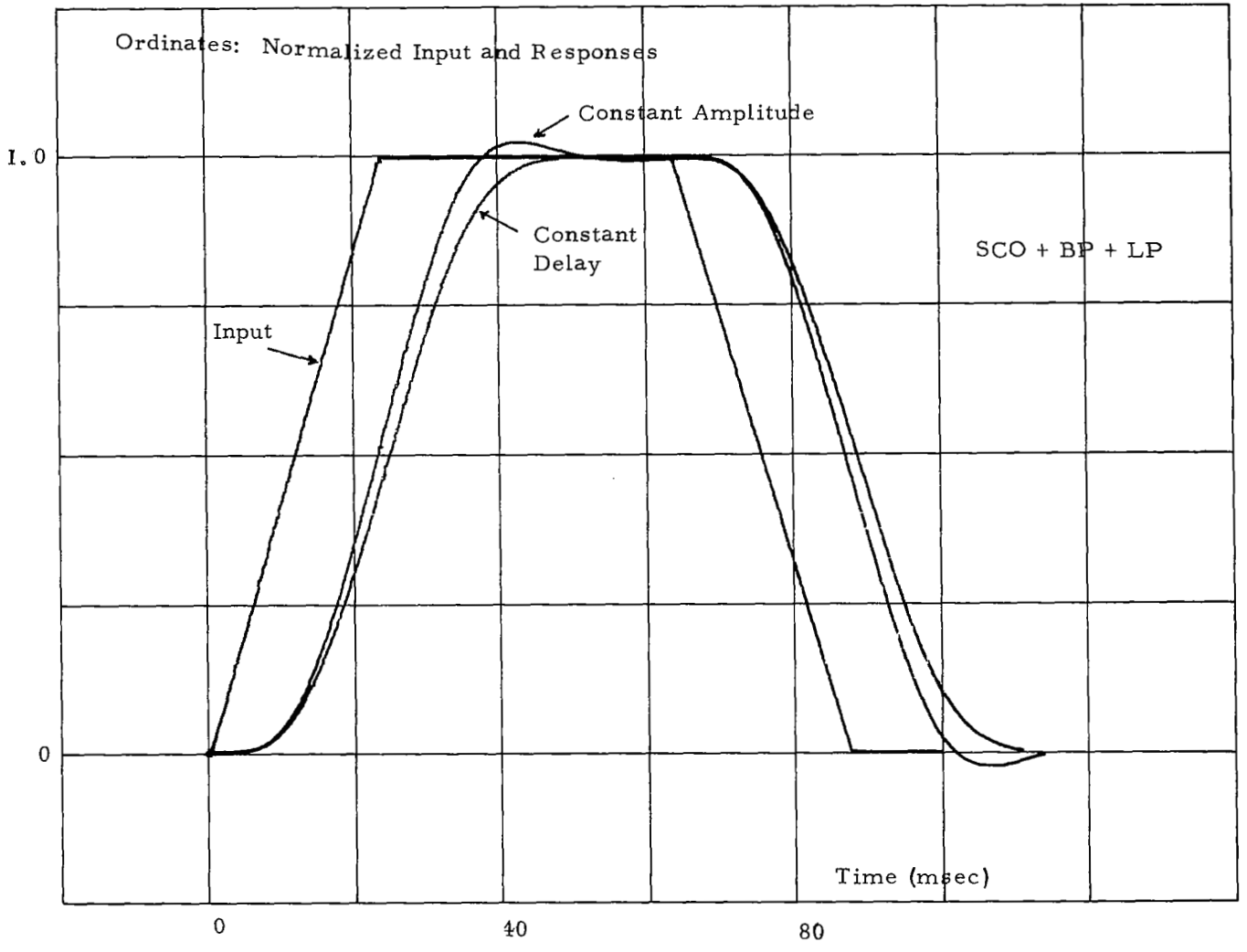

Figure 5-23, Response of L. P. (Channel 6) to Trapezoidal Inputs

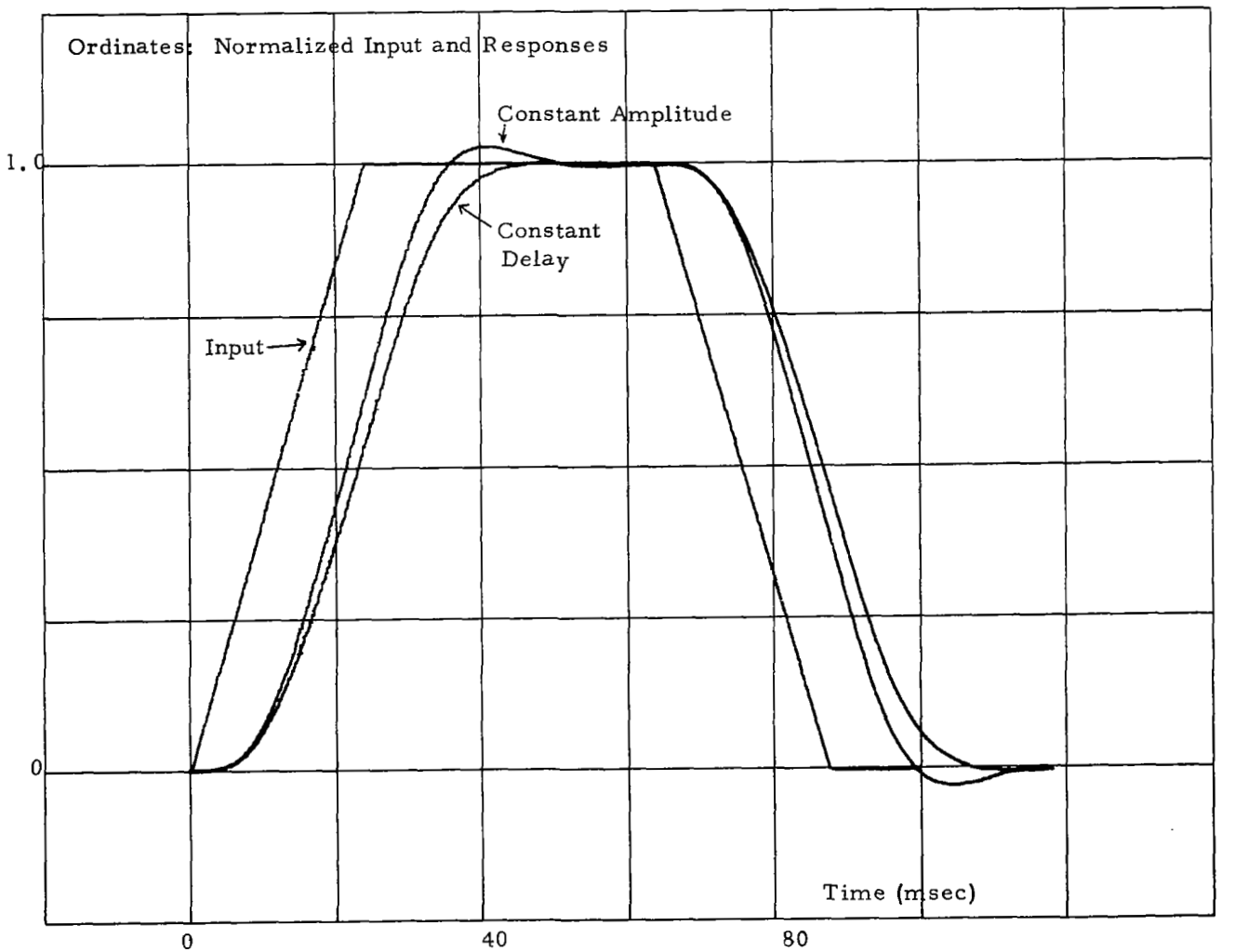

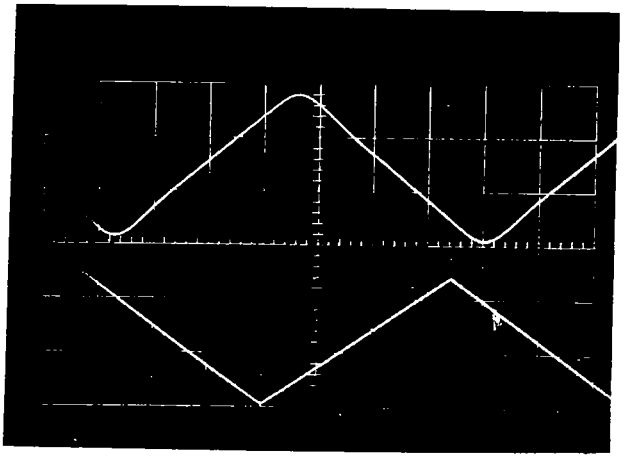

FIGURE 5-24A RESPONSE OF CHANNEL #6 (P.S.D. EXCLUDED) TO TRIANGULAR INPUTS
7.5% B.P., 25 Hz CONSTANT AMPLITUDE L. P.
TIME SCALE 20 ms/DIVISION

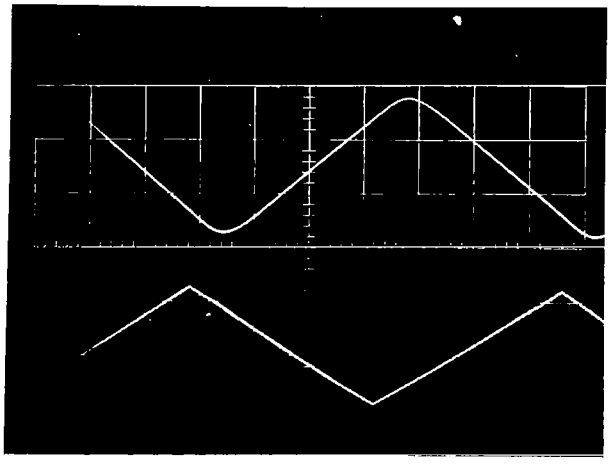

FIGURE 5-24B SAME AS FIGURE 5-24A, EXCEPT THAT CONSTANT DELAY L. P. WAS USED

Figure 5-25, *Responses of Channel 6 to Triangles*

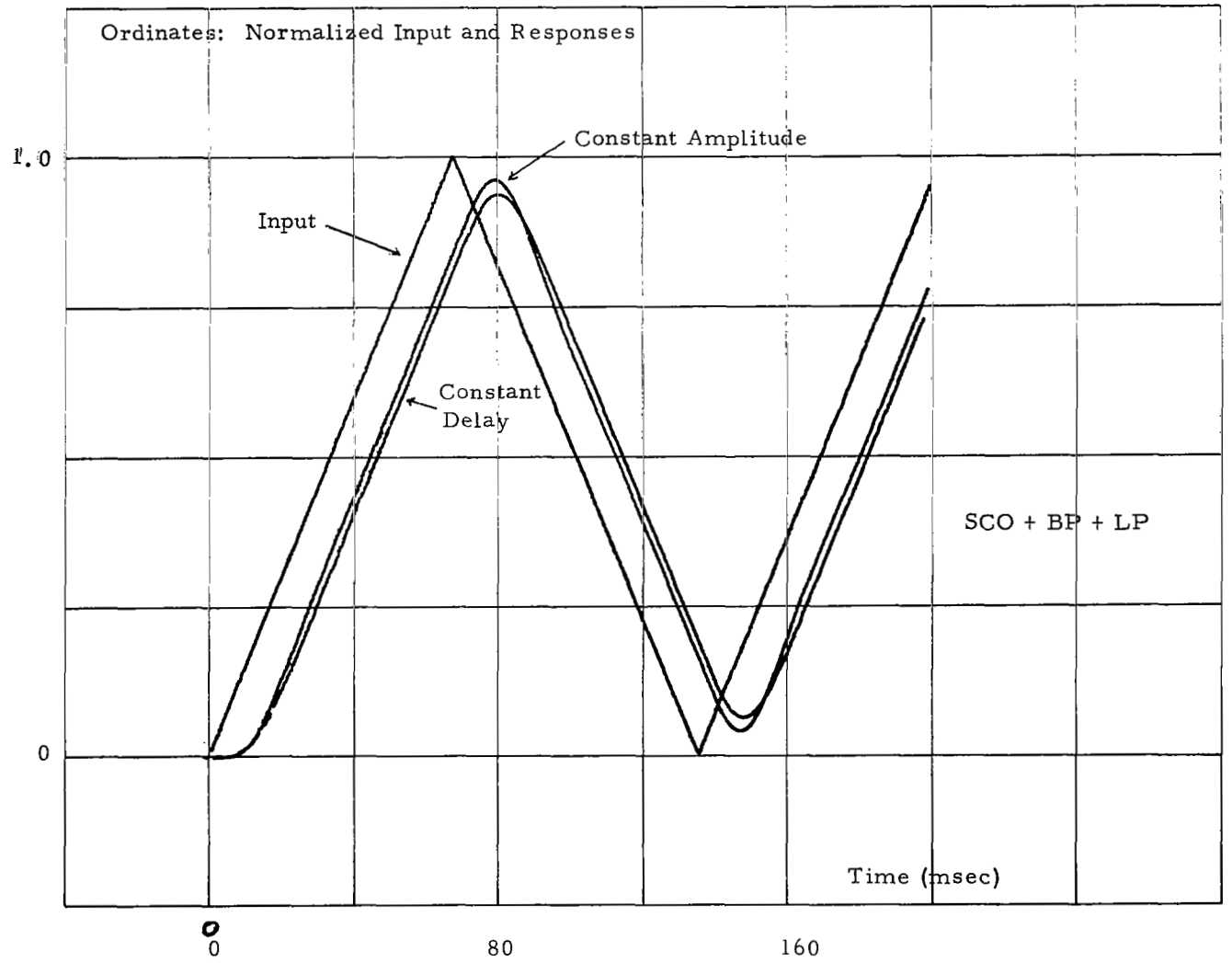

Figure 5-26, Response of L. P. (Channel 6) to Triangles

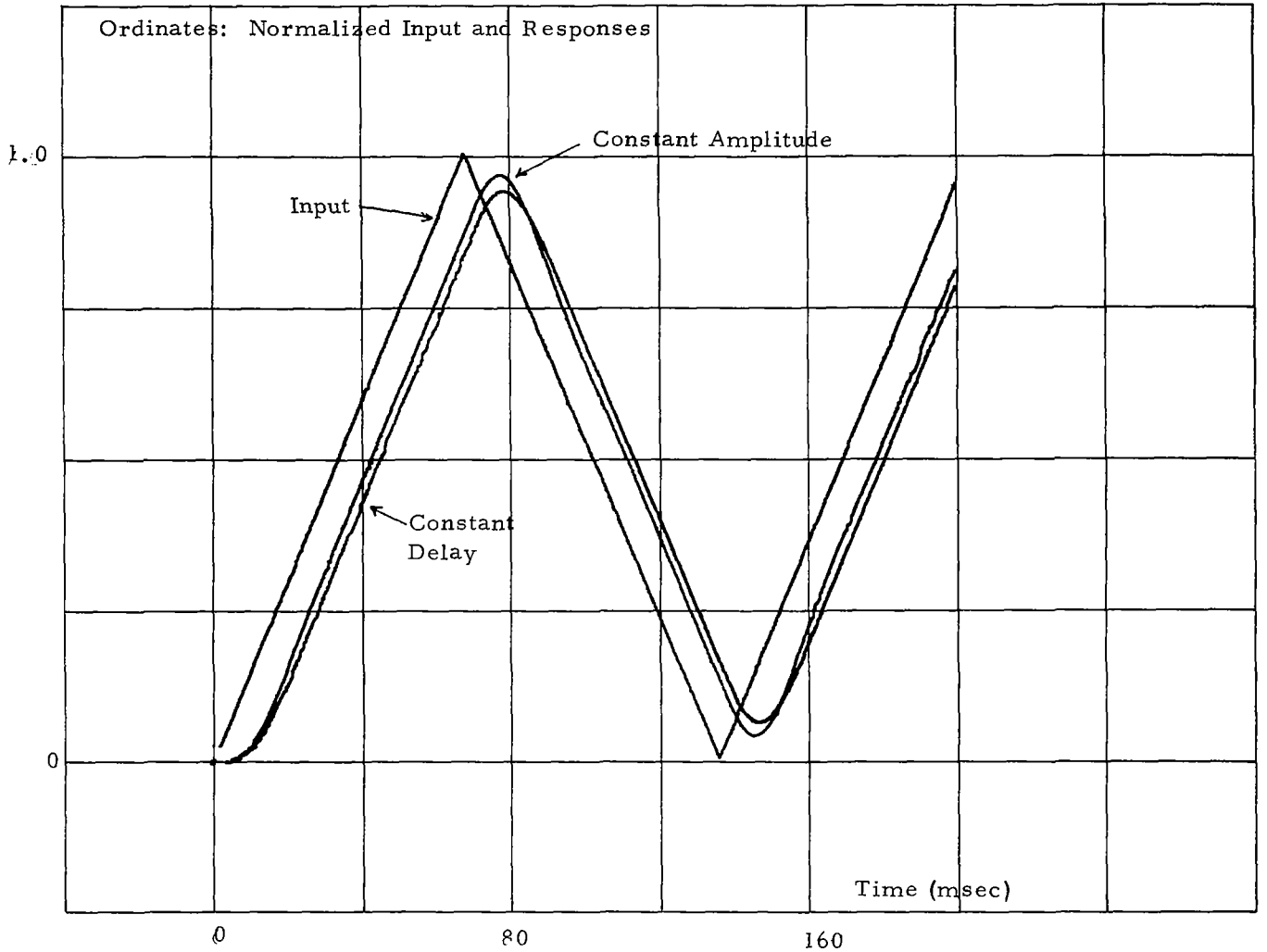

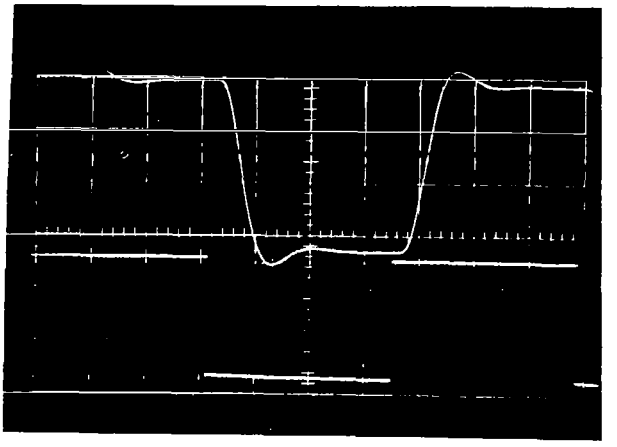

FIGURE 5-27A STEPRESPONSE OF CHANNEL #6 (EXCLUDING P.S.D.)
7.5% B.P., 25 Hz CONSTANT AMPLITUDE L. P.
TIME SCALE 20 ms/DIVISION

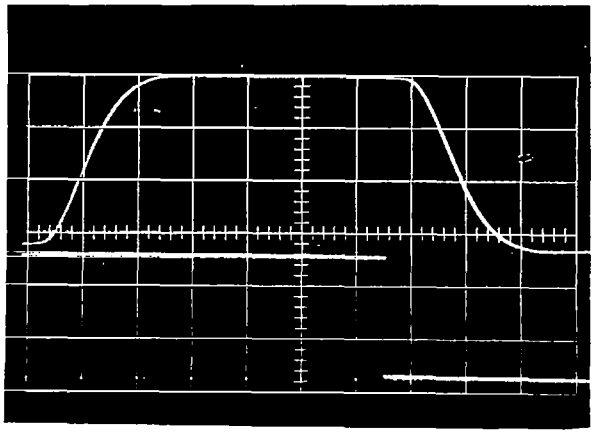

FIGURE 5-27B STEPRESPONSE OF CHANNEL #6 (EXCLUDING P.S.D.)
7.5% B. P., 25 Hz CONSTANT DELAY L. P.
TIME SCALE 10 ms/DIVISION

Figure 5-28, Step Responses of Channel 6

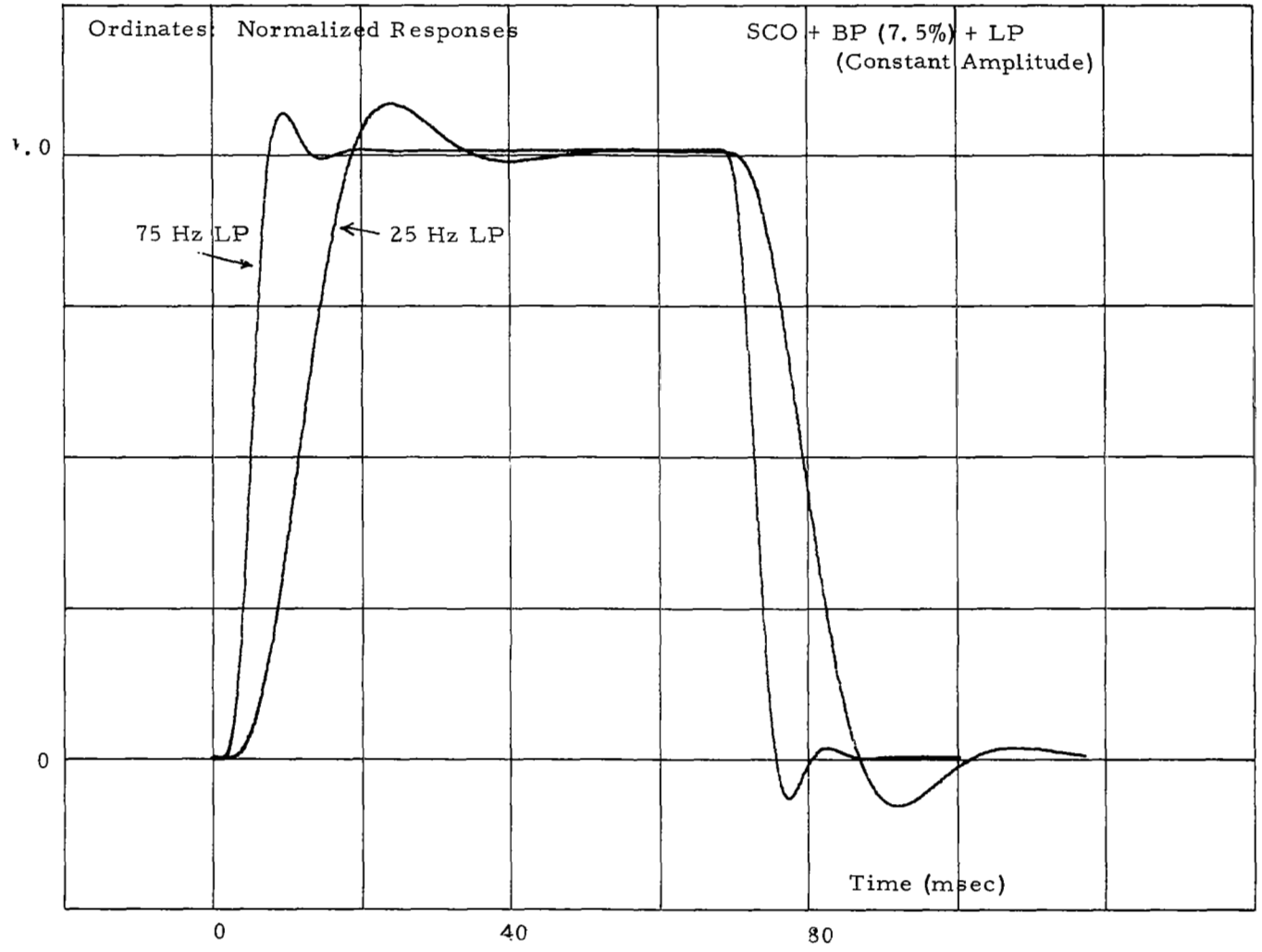

Figure 5-29, Step Responses of Channel 6

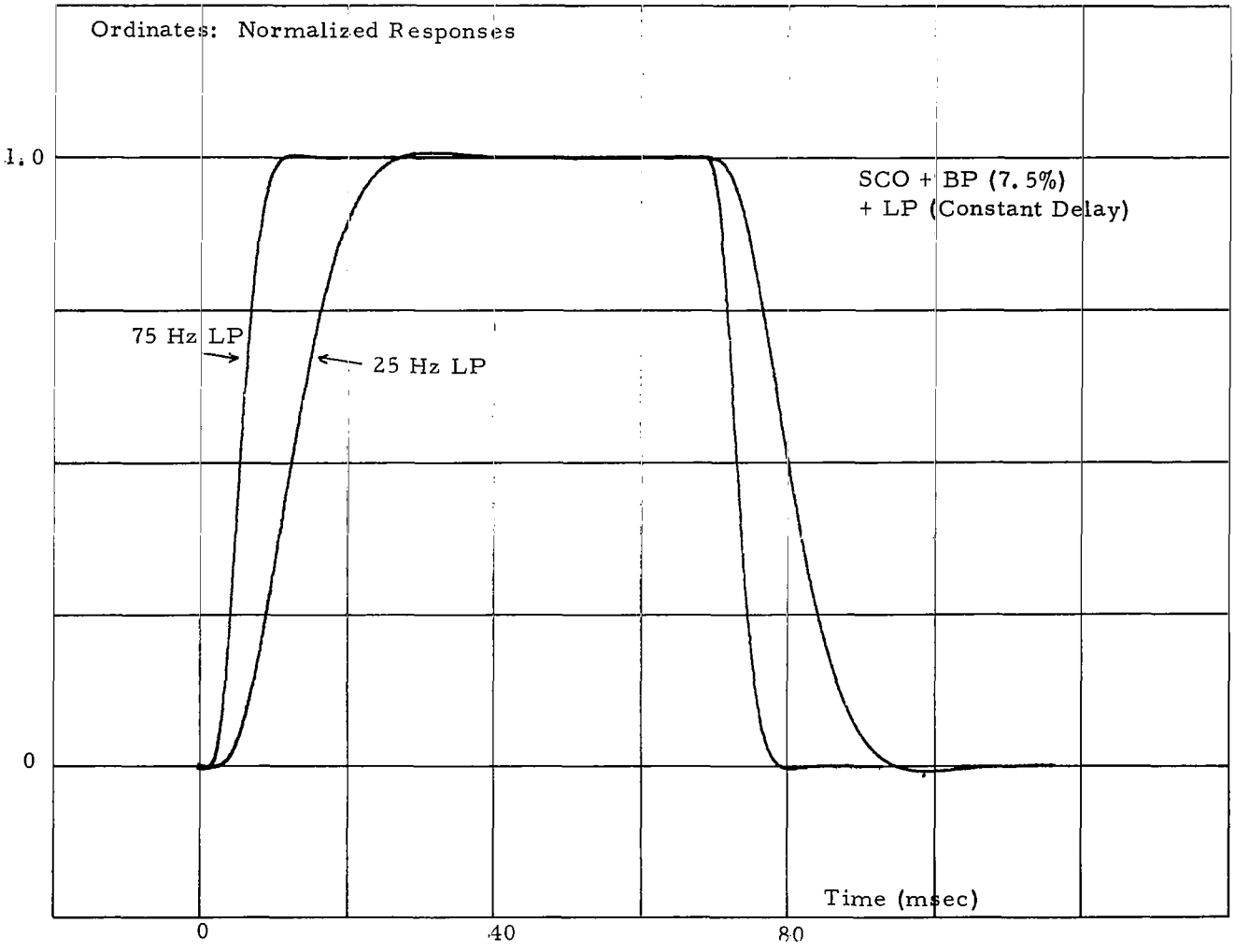

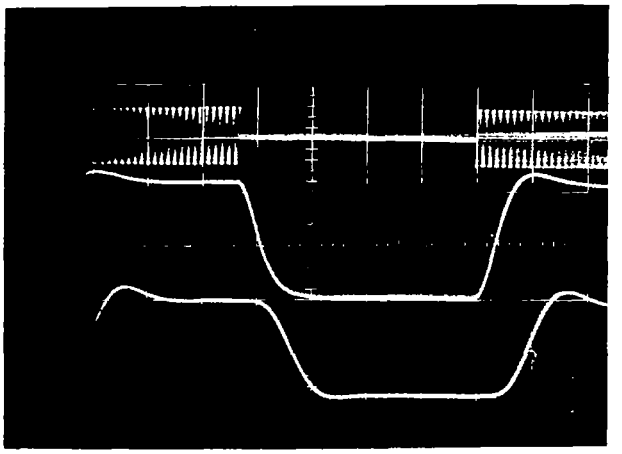

FIGURE 5-30A STEP INPUT OF CHANNEL #6, INCLUDING P.S.D. #1
7.5% B. P., 25 Hz CONSTANT AMPLITUDE L. P.
TIME SCALE 20 ms/DIVISION

TRACE 1 INPUT TO P. S. D.
TRACE 2 OUTPUT OF P. S. D.
TRACE 3 OUTPUT FROM L. P.

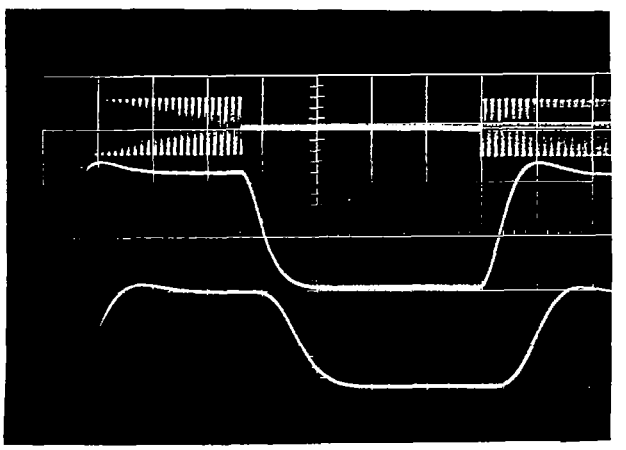

Figure 5-30B SAME AS FIGURE 5-30A EXCEPT THAT CONSTANT DELAY FILTER WAS USED.

Figure 5-31, Step Responses of P. S. D. and Channel 6

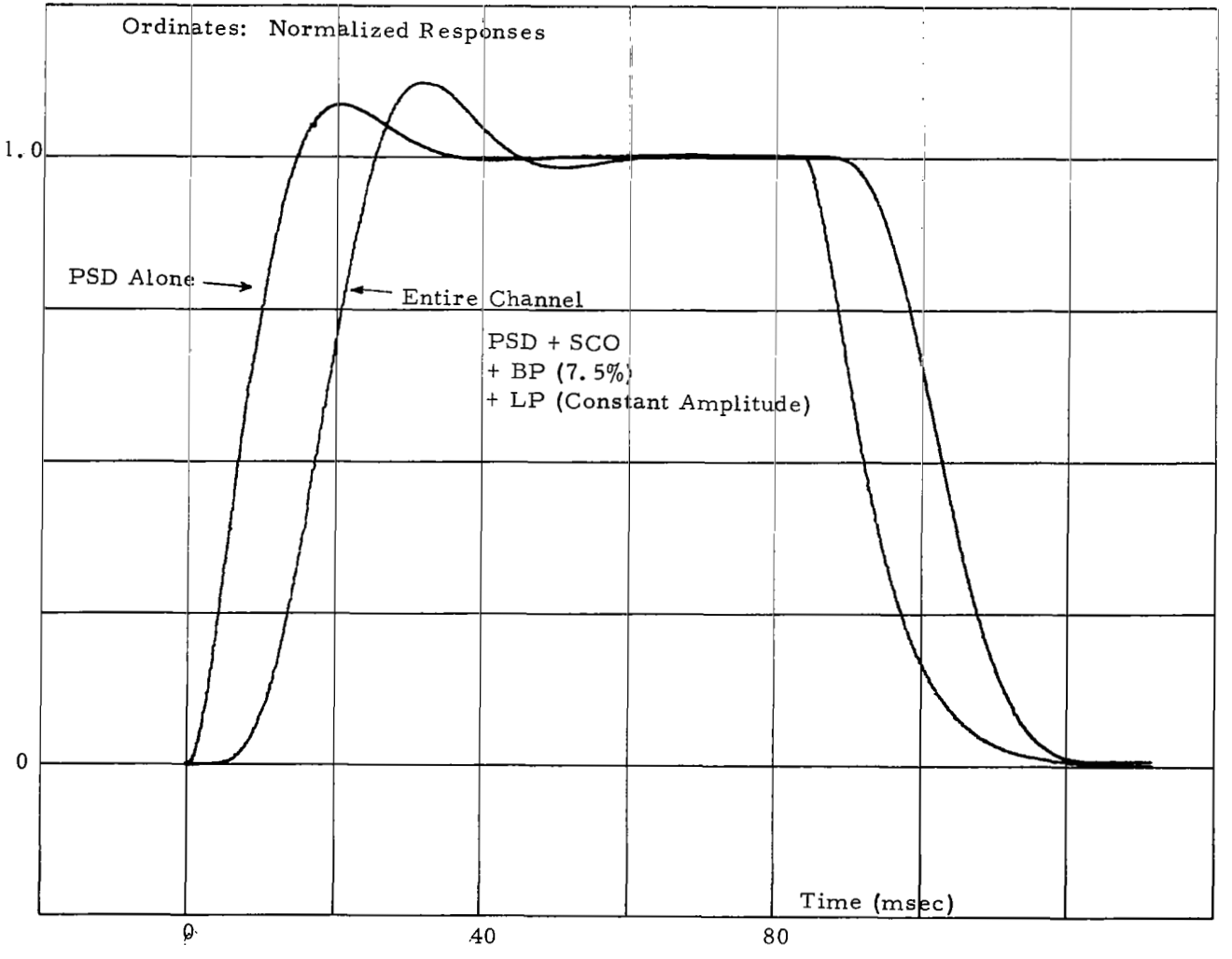

Figure 5-32, Step Responses of P. S. D. and Channel 6

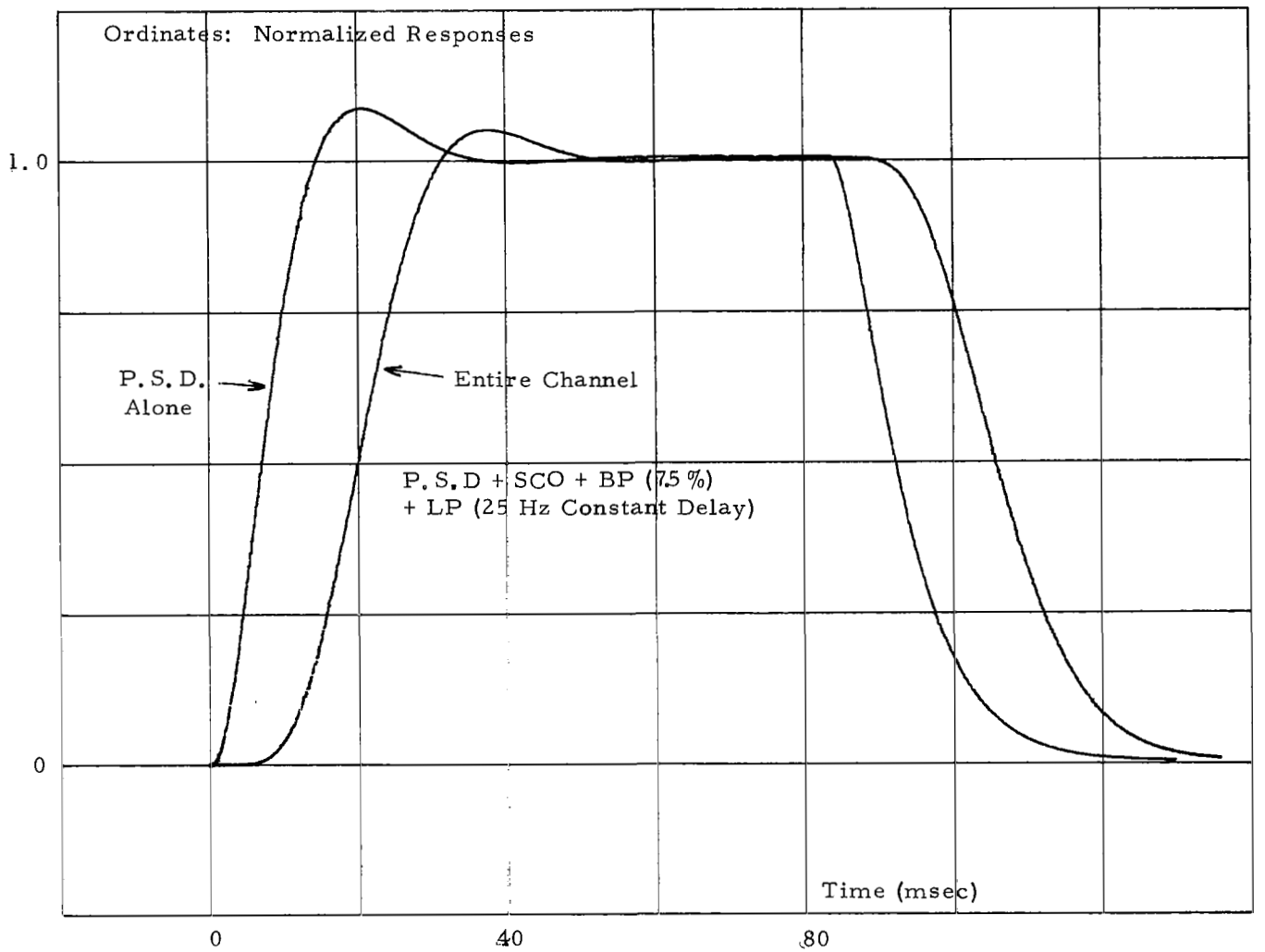

5.11 *Choice of Filters, and Channel Interference*

The discussion of Section 5.1 mentioned that the standard frequency response of each channel (as listed in column 5 of table 5.1) was based upon the assumption of a deviation ratio of 5. It was also pointed out that this standard frequency response (such as 25 Hz for channel #6) is not necessarily compatible with the transducers used (in this case a yaw rate gyro of natural frequency 26 Hz, which can certainly transmit signals higher than 26 Hz without excessive attenuation). Therefore, the user might think of using non-standard filters (both BP and LP) to fit the transducer bandwidth more closely. To illustrate this point, Figures 5-33 A through F, 5-34 A through F show various step responses of channel #6 (with all other channels under power, and zero inputs) for 7.5% and 15% BP and for LP going from 15 Hz to 125 Hz cut-off frequency (NOTE: 25 Hz is the standard LP). It is clear that the use of wider band LP permits a faster response and a smaller dynamic lag and distortion, but the figures show that there is a limitation to that procedure. Indeed, as the LP becomes much wider than the standard LP, a ripple appears (see Figures 5-34D and 5-34C), which becomes very objectionable for very wide band LP (see the 125 Hz LP filters). It will be shown further that this ripple is due to interference from adjacent channels. Pictures such as Figure 5-33 and 5-34 permit the user to make a trade-off between desired speed of response (lack of dynamic distortion) and interference-ripple (or noise). The user's choice would, of course, depend on his particular preferences and on the expected types of signals. Comparison of the pictures also show that, for the same LP bandwidth, the ripple increases with bandwidth of the BP.

The Figures 5-35 A & B, giving step responses of the same channel #6, but now isolated (i.e., all other channels are completely removed) show no ripple for a 125 Hz LP (to be compared with Figure 5-34 F) and only very little ripple for the extremely wide band filter with 500 Hz cut-off frequency. This proves that the ripple discussed here is indeed due to interference from other channels. These pictures of Figure 5-35 further indicate, that if the user has to transmit only a few signals, the response can be speeded up by the use of wider LP filters, provided the channels used (and powered) are spaced farther apart.

In order to show the influence and importance of the ground equipment used, the pictures in Figure 5-36 A & B, give again the step responses of channel #6, but now with a different discriminator (the EMR Model 210 Fixed Discriminator). Comparison with Figures 5-33 shows less ripple for the fixed discriminator, due to the fact that the BP filters differ from the ones of the tunable discriminator used in all other experiments. (The fixed discriminator BP has a much sharper cut-off slope than the tunable BP).

Finally, Figure 5-37 A through D proves that among all channels, it is the nearest neighbors which contribute most or all of the interference ripple.

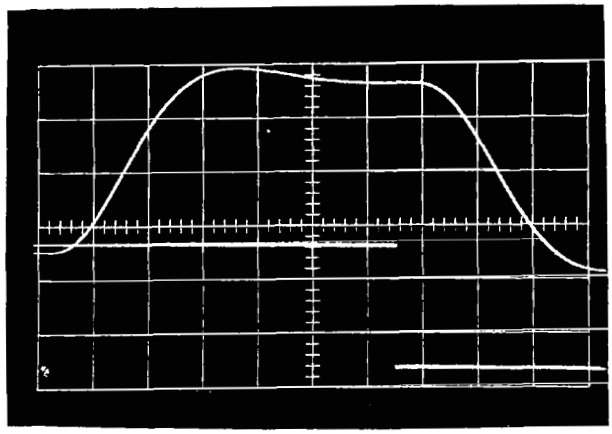

FIGURE 5-33

STEP RESPONSE OF CHANNEL 6, 7.5% B.P., CONSTANT AMPLITUDE L.P., (NO P.S.D.) TIME SCALES 10 ms/DIVISION

A) 15 Hz L.P.

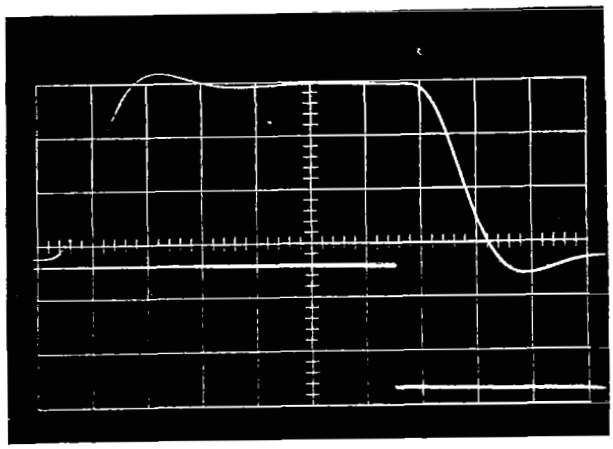

B) 25 Hz L.P. (STANDARD)

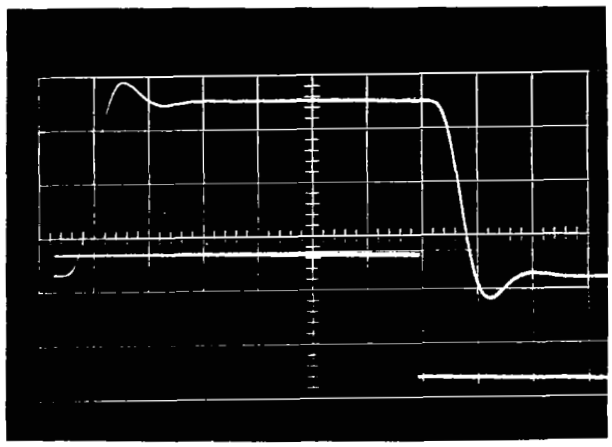

C) 50 Hz L.P.

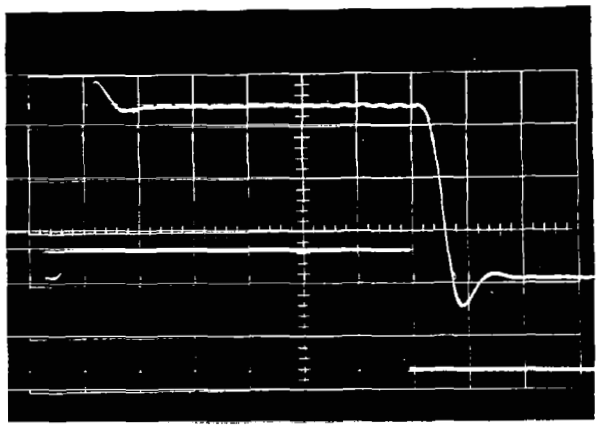

FIGURE 5-33 CONTINUED

D) 75 Hz L. P.

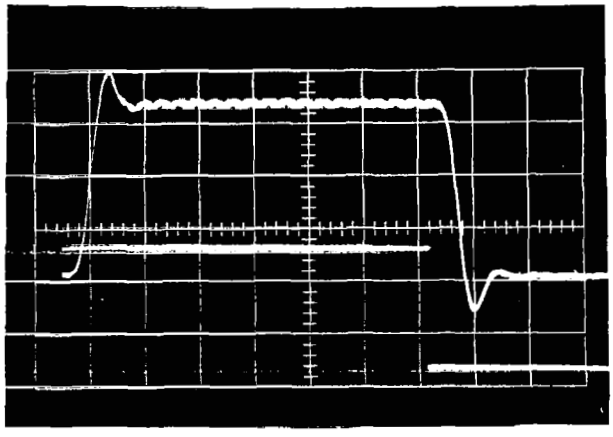

E) 100 Hz L. P.

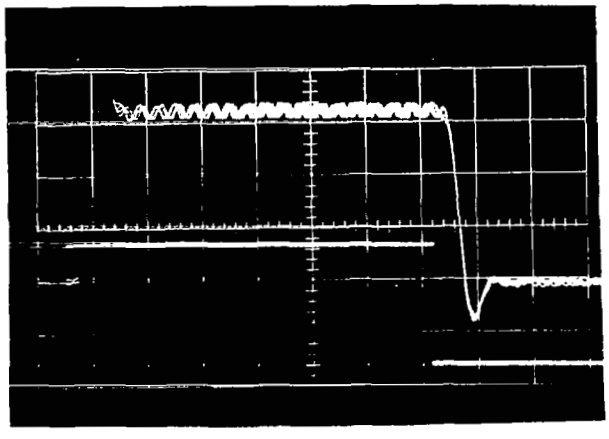

F) 125 Hz L. P.

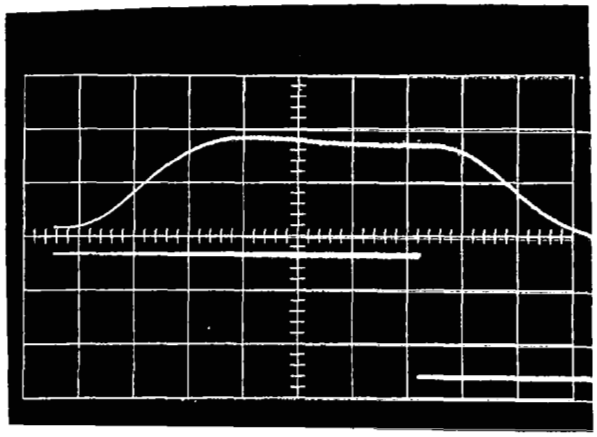

FIGURE 5-34

STEP RESPONSE OF CHANNEL #6, 15% B.P. CONSTANT AMPLITUDE L.P. (NO P.S.D.) TIME SCALES 10 ms/DIVISION

A) 15 Hz L.P.

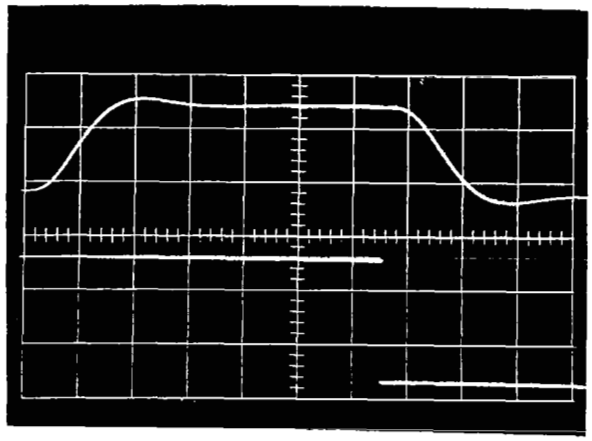

B) 25 Hz L.P. (STANDARD)

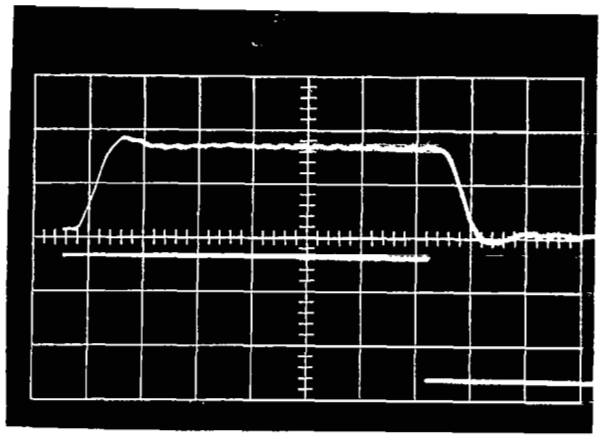

C) 50 Hz L.P.

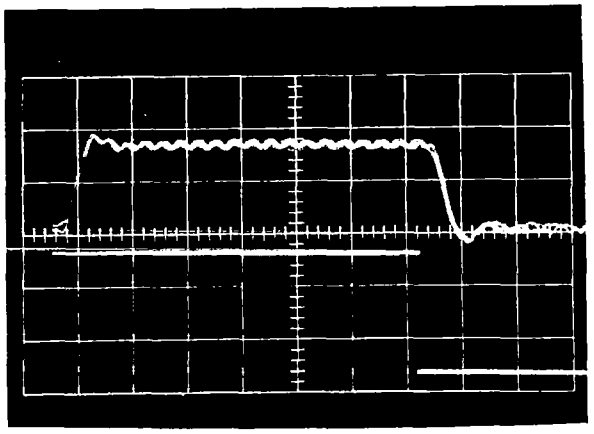

FIGURE 5-34CONTINUED

D) 75 Hz L. P.

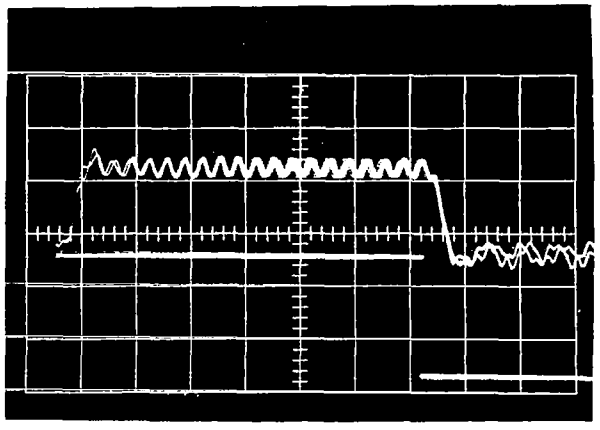

E) 100 Hz L. P.

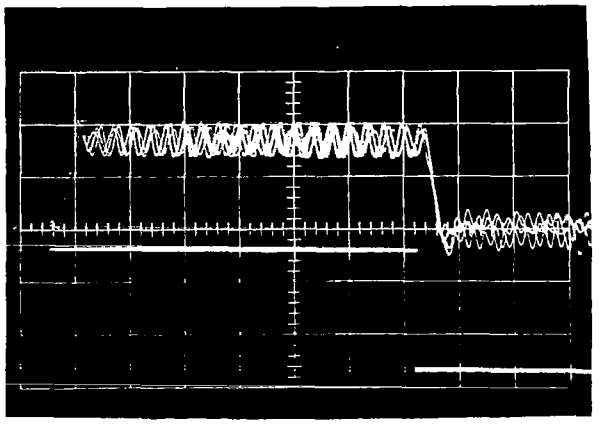

F) 125 Hz L. P.

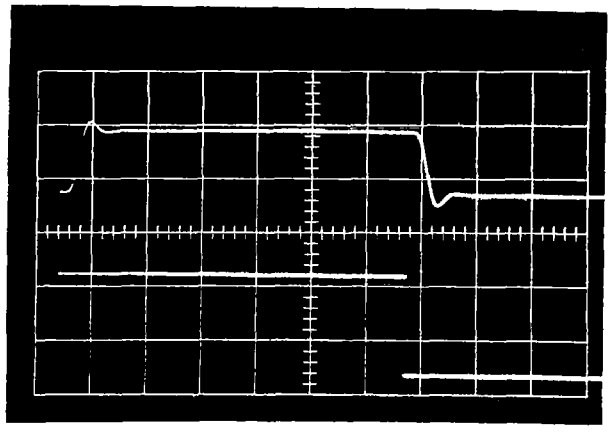

FIGURE 5-35

STEPRESPONSE OF THE ISOLATED CHANNEL #6

15% B. P., CONSTANT AMPLITUDE L. P.
(NO P. S. D.)
TIME SCALES: 10 ms/DIVISION

A) 125 Hz L. P.

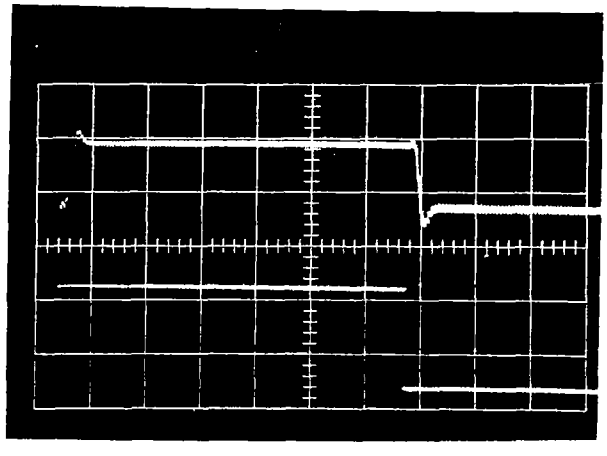

B) 500 Hz L. P.

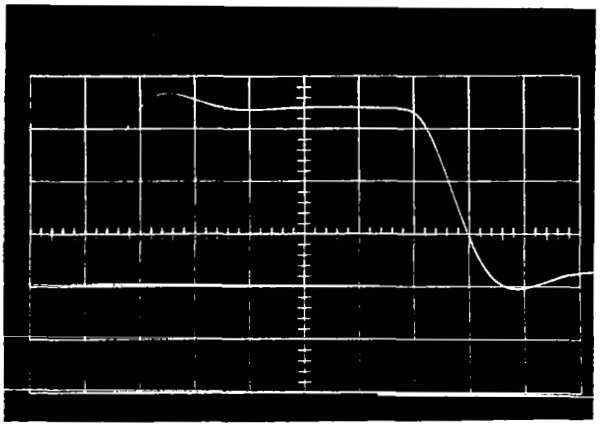

FIGURE 5-36

STEPRESPONSE OF CHANNEL #6, 7.5 % B. P., CONSTANT AMPLITUDE L. P., (NO P.S.D.)
TIME SCALES: 10 ms/DIVISION
FIXED DISCRIMINATOR

A) 25 Hz L. P.

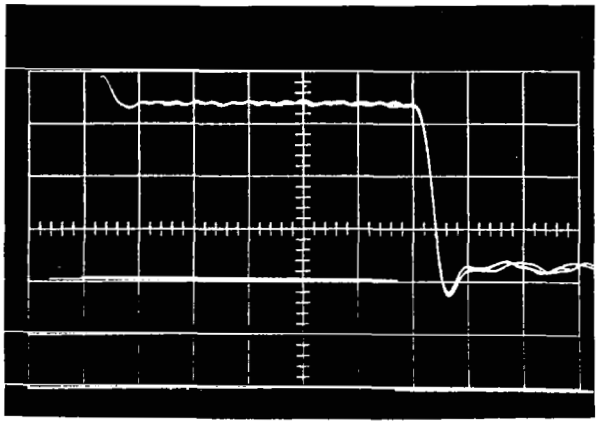

B) 110 Hz L. P.

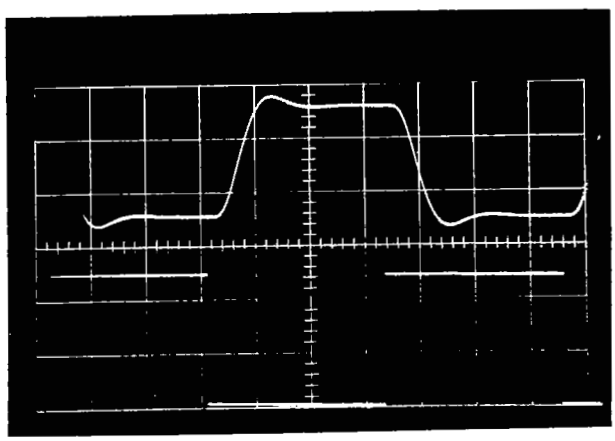

FIGURE 5-37

STEPRESPONSE OF CHANNEL #6
TIME SCALES: 20 ms/DIVISION
7.5% B. P, CONSTANT AMPLITUDE
L. P.

A) 25 Hz L.P. (STANDARD)

CHANNEL #5: 0V D.C.
CHANNEL #7: 5V D.C.
(BEST CASE)

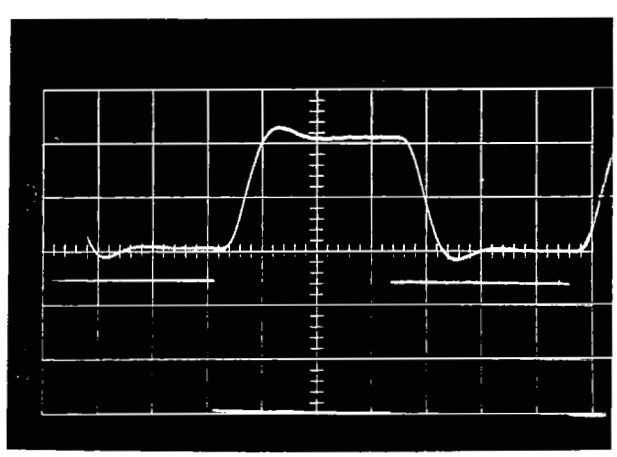

B) 25 Hz L. P. (STANDARD)

CHANNEL #5: 5V D. C.
CHANNEL #7: 0V D. C.
(WORST CASE)

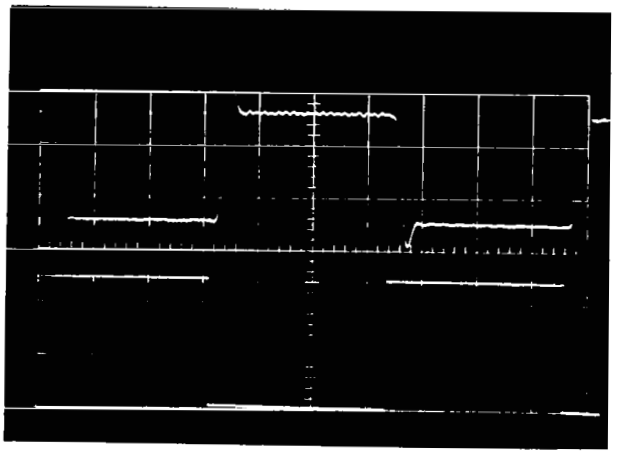

FIGURE 5-37 CONTINUED

C) 125 Hz L. P. (WIDE)

CHANNEL 5: 0V D. C.

CHANNEL 7: 5V D.C.
(BEST CASE)

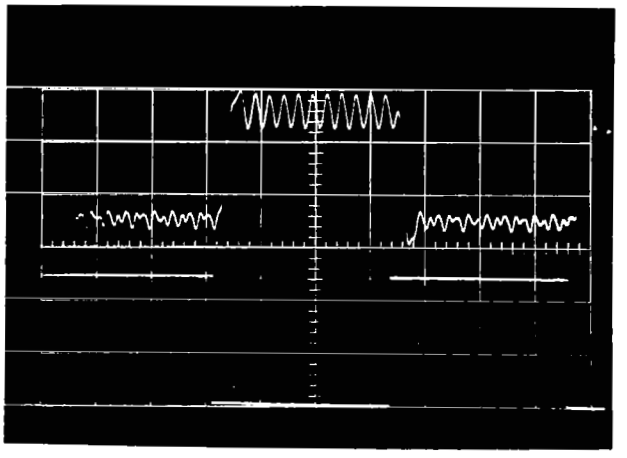

D) 125 Hz L. P. (WIDE)

CHANNEL 5: 5V D. C.

CHANNEL 7: 0V D. C.
(WORST CASE)

This interference is easily explained theoretically. Consider the channel #6 and its two neighbors #5 and #7.

Channel	Lower Edge (Hz)	Center (Hz)	Upper Edge (Hz)
5	1202	1300	1399
6	1572	1700	1828
7	2127	2300	2473

In Figure 5-37 D (worst case with wide LP Filter) one observes on one side of the square wave a ripple with frequency of approximately 190 Hz (= 1572 - 1399 = 173) and on the other side a ripple at nearly 290 Hz (= 2127 - 1828 = 299). With the figure below one has (neglecting phase shifts in the BP, which are immaterial here)

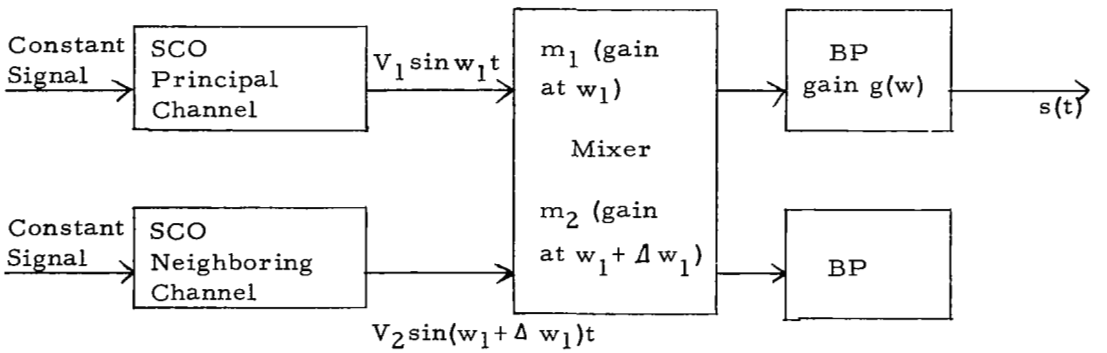

an output signal from the BP given by

$$s(t) = (g(w_1)\, m_1 v_1) \sin w_1 t + (g(w_1 + \Delta w_1) m_2 v_2) \sin (w_1 + \Delta w_1)t$$

Because of the selectivity of the BP,

$$| g (w_1 + \Delta w_1) | \ll | g (w_1) |$$

must be satisfied.

Therefore, one has, since $m_2 = \bigcirc (m_1)$, $V_1 = \bigcirc (V_2)$

$$\frac{g(w_1 + \Delta w_1)\, m_2\, V_2}{g(w_1)\, m_1\, V_1} = \varepsilon \quad , \qquad |\varepsilon| << 1$$

We can restrict our attention to the input signal

$$s_1(t) = \sin(w_1 t) + \varepsilon \sin(w_1 + \Delta w_1)t$$

to the discriminator.

For neighboring channels $\frac{\Delta w_1}{w_1} < 1$, but not necessarily small.

Many discriminators, and particularly, the ones used in this study, basically detect phase differences or frequency differences by changes in zero-crossings. For the EMR 229, e.g., phase detection is based on comparison of pulsed signals from a limiter and from a V.C.O. (multi-vibrator) in the feedback loop (See Section 5.8).

If $\varepsilon = 0$, zero crossings t_n of $s_1(t)$ are given by $t_n = n\pi / w_1$ $(n = 0, 1, 2, \ldots)$ and spacing $t_{n+1} - t_n = \pi / w_1$.

For ε non-zero, but small relative to unity, zero crossings are shifted by an amount Δt_n given by $s_1(t_n + \Delta t_n) = 0$

Using the fact that $|\varepsilon| << 1$ and hence $w_1 |\Delta t_n| << 2\pi$, this leads to

$$w_1 \Delta t_n + \varepsilon \sin \left(\frac{\Delta w_1}{w_1} n\pi \right) \cong 0$$

Hence the new spacing between zero crossings becomes

$$t_{n+1} + \Delta t_{n+1} - (t_n + \Delta t_n) = \frac{\pi}{w_1} - \frac{\varepsilon}{w_1} \left(\sin \frac{\Delta w_1}{w_1} (n+1)\pi - \sin \frac{\Delta w_1}{w_1} n\pi \right)$$

$$= \frac{\pi}{w_1} - \frac{2\varepsilon}{w_1} \sin \frac{\Delta w_1}{w_1} \frac{\pi}{2} \cos \frac{\Delta w_1}{w_1} \left(n + \frac{1}{2} \right) \pi$$

Since the signal (frequency shift) given as output by the discriminator is inversely proportional to the length between zero crossings, one gets

$$\frac{f\ (\text{output discriminator})}{f\ (\text{same for } \varepsilon = 0)} = \frac{\pi / w_1}{\frac{\pi}{w_1} - \frac{2\varepsilon}{w_1} \sin \frac{\Delta w_1}{w_1} \frac{\pi}{2} \cos \frac{\Delta w_1}{w_1} (n+\frac{1}{2})\pi}$$

or, for running time t ($\frac{n\pi}{w_1}$ t)

$$\frac{f\ (t)}{f\ (\varepsilon = 0)} = 1 + (\frac{2\varepsilon}{\pi} \sin \frac{\Delta w_1}{w_1} \frac{\pi}{2}) \cos (\Delta w_1 t + \frac{\Delta w_1}{w_1} \frac{\pi}{2})$$

One obtains indeed a ripple with frequency $\frac{\Delta w_1}{2\pi}$ and with amplitude

$$\frac{2\varepsilon}{\pi} \sin \frac{\Delta w_1}{w_1} \frac{\pi}{2}$$

Due to the presence of ε , the ripple amplitude depends on the bandwidth of the BP filters (for narrow BP, ε decreases and there is less ripple amplitude). Moreover, the LP filter following the discriminator also helps in suppressing the ripple. Those statements are confirmed by inspection of the Figures 5-33 and 5-34, showing the influence of BP and LP respectively.

5.12 Power-Interruption

In order to observe the effect of power interruptions on the signal transmission, several tests were run under a variety of conditions. Some results are shown in Figure 5-38 A through E. Inspection of these pictures demonstrates that power interruptions can give rise to signals at the discriminator output resembling normally transmitted signals. One possibility of distinguishing between genuine transmitted signals and power-interruption signals exists in the fact that the latter category would show up as a simultaneous disturbance in all channels. However, in the case of catastrophic events sensed by the transducers, such simultaneity may also arise in regular signals not due to power interruption.

Figures 5-39 and 5-40 give the output frequency of the SCO's in channels 6 and 15 as a function of power supply voltage. Clearly there is a wide range of supply variations (from 22V to 37V) where the output frequency is indeed independent of supply voltage, indicating the good quality of the SCO's.

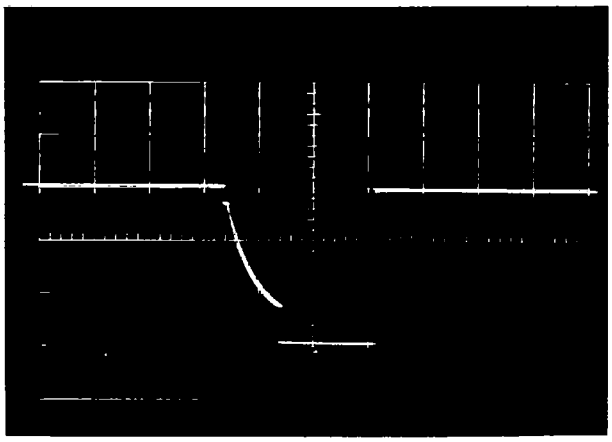

FIGURE 5-38A

POWER PULSE FROM 32V TO GROUND

TIME SCALE: 1 ms/DIVISION

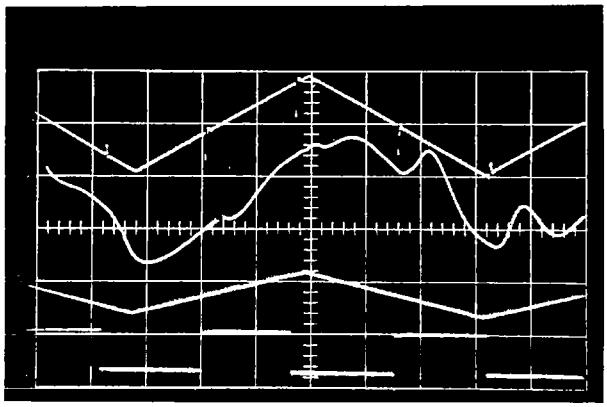

FIGURE 5-38B

TRACE #1 CHANNEL #15
TRACE #2 CHANNEL #6
TRACE #3 INPUT SIGNAL 0-4V D. C.
TRACE #4 POWER SUPPLY 24 V - 32V

TIME SCALE: 20 ms/DIVISION

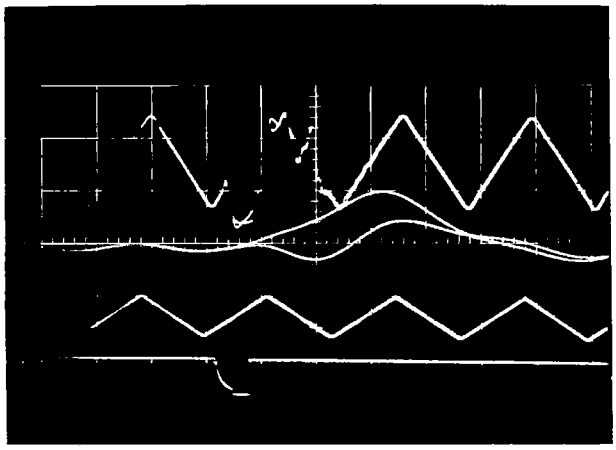

FIGURE 5-38C

TRACE 1 CHANNEL #15
TRACE 2 CHANNEL #6
TRACE 3 INPUT SIGNAL AT 86 Hz REPETITION RATE
TRACE 4 POWER INTERRUPTION 32 V TO GROUND

TIME SCALE: 5 ms/DIVISION

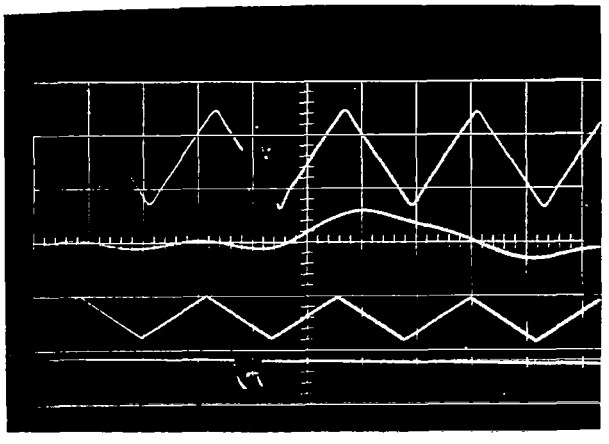

FIGURE 5-38D

TRACE 1 CHANNEL #15
TRACE 2 CHANNEL #6
TRACE 3 INPUT SIGNAL AT 86 Hz REPETITION RATE
TRACE 4 POWER INTERRUPTION 32V to 24V

TIME SCALE 5ms/DIVISION

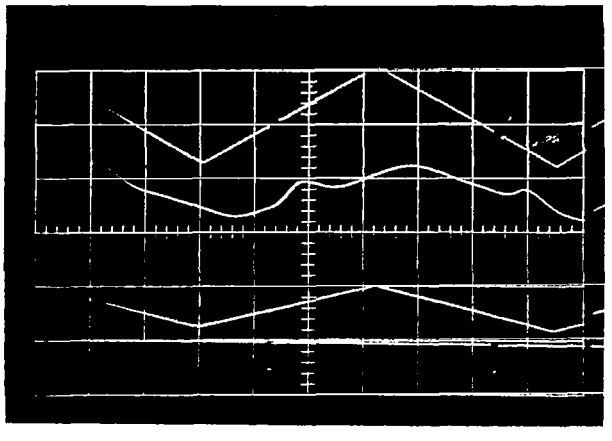

FIGURE 5-38E

TRACE 1 CHANNEL #15
TRACE 2 CHANNEL #6
TRACE 3 INPUT SIGNAL AT 7.8 Hz REPETITION RATE
TRACE 4 POWER INTERRUPTION FROM 32V to 24V

TIME SCALE 20 ms/DIVISION

Figure 5-39

V. C. O. Channel #6 Power Supply Variations

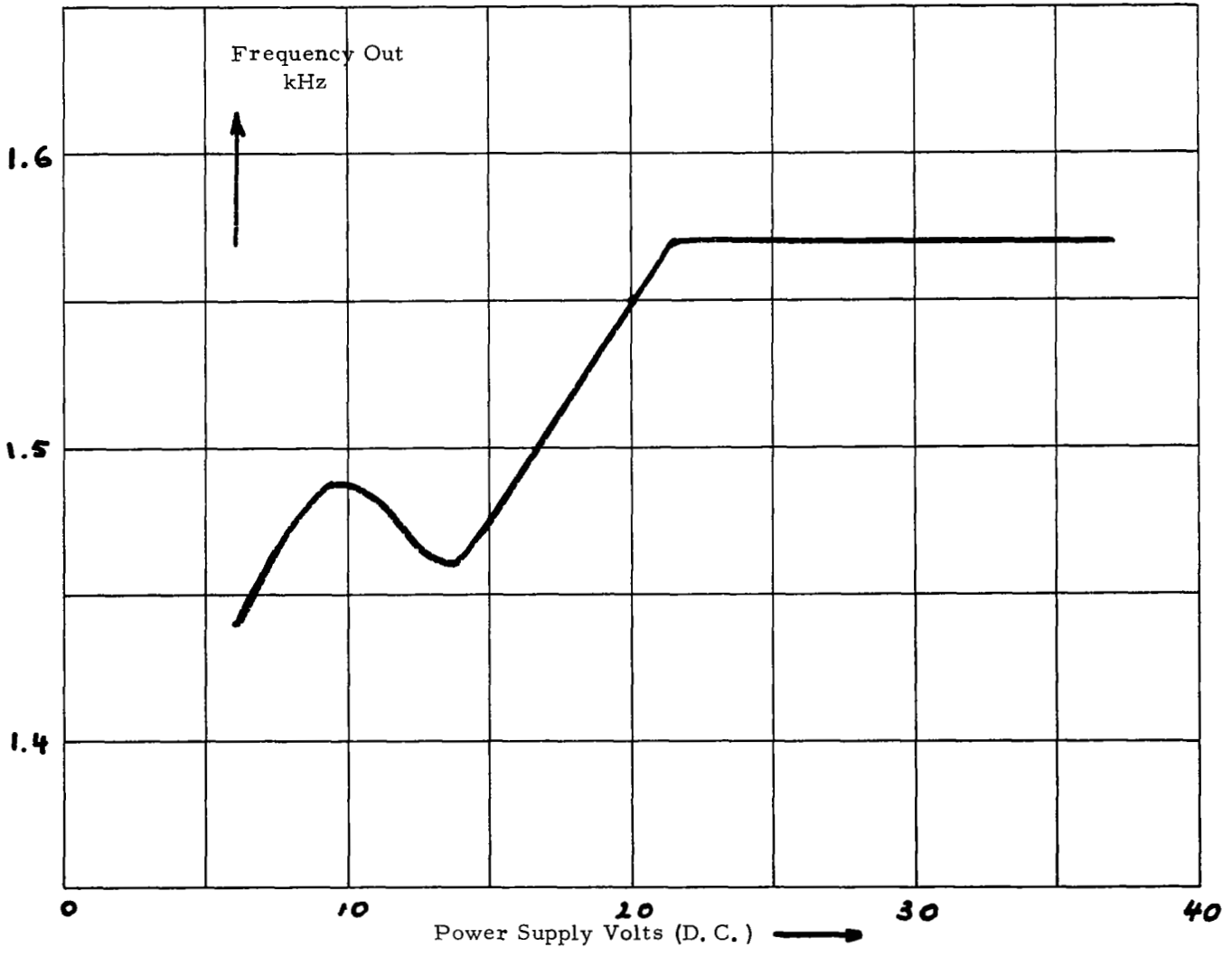

Figure 5-40, S. C. O. Channel 15 Power Supply Variations

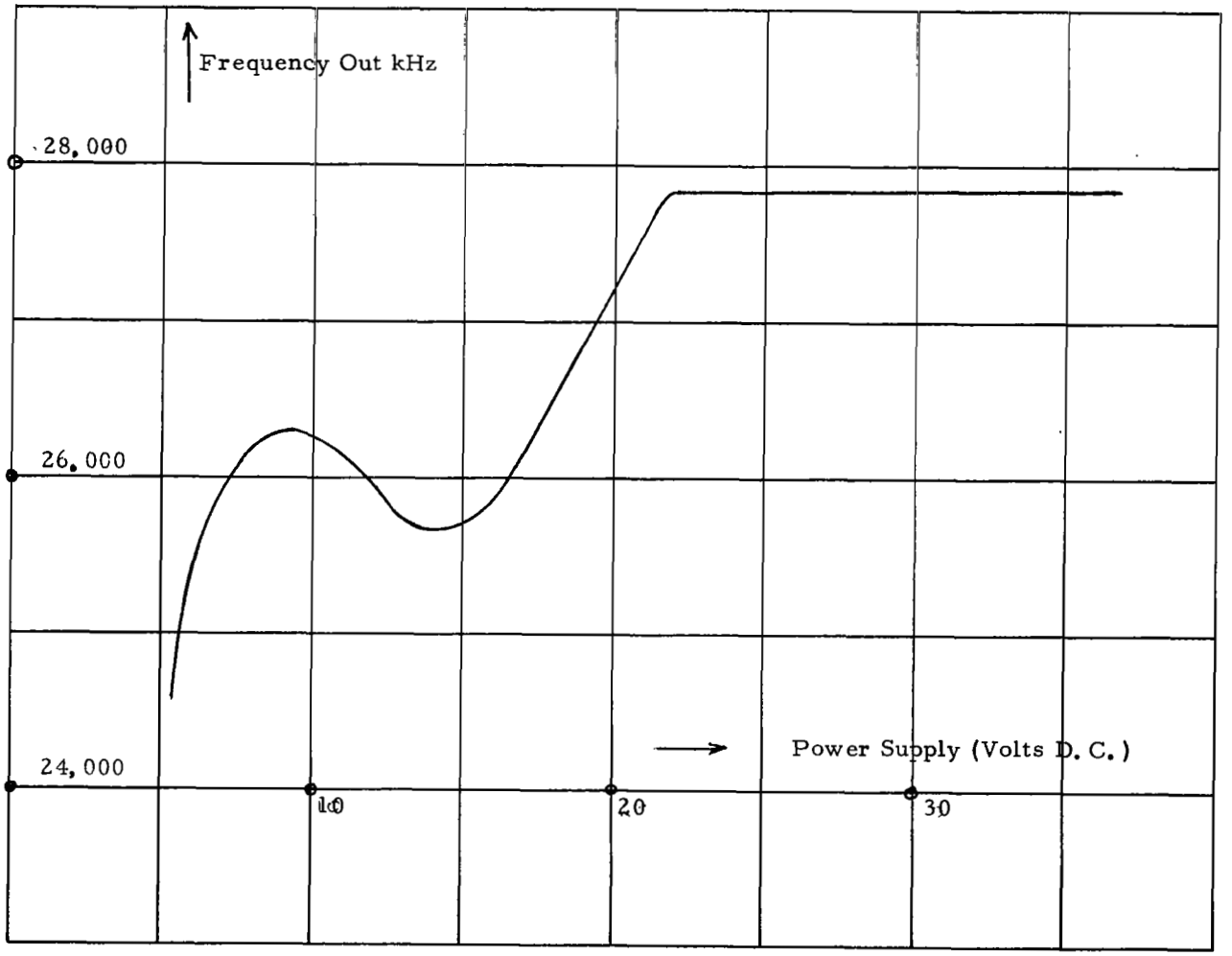

6. THE INVERSION PROBLEM

6.1 Introduction

In previous sections 2, 3, and 4 analytical models were derived for the three categories of instruments; rate gyros, accelerometers, and pressure transducers, including appendages such as mounting brackets and connecting tubings. These models permit direct calculation of the instrument outputs for given input signals, say, by means of analog simulation. However, in order to find out what really happens in the vehicle carrying the instruments, the inverse problem of calculating input signals for known (recorded) output signals is what matters. This report describes an inversion process for the above-mentioned instruments, under the following assumptions and rules.

A. The recorded output data are available as equidistant, sampled quantities in engineering units, presented in tables or as graphs. (These data come from continuous traces having finite bandwidth).

B. All instrument models are, where necessary, simplified to single-input, linear time-invariant systems (zero order model). This means that parasitic inputs such as accelerations for the gyro and pressure transducer, and transverse acceleration for the accelerometer, are neglected. The neglected secondary effects are small.

C. The inversion is performed on a digital computer. It is an optimum inverted filtering, in a minimax sense.

D. The reconstructed input signals are obtained as equidistant/sampled quantities in engineering units, displayed in tabular form or as computer plots. Error bounds are given. The inversion process can be used to study the uncertainty with which the reconstruction is found, and the sensitivity of the results to changes in the system parameter values. It can also yield information on statistical effects by means of so-called Monte Carlo simulations.

The testing of instruments, coupled with theoretical analysis, has resulted in the following typical (zero order) transfer-functions: (x is input signal , y = output signal, s = transform variable).

Rate Gyros

$$\frac{y(s)}{x(s)} = \frac{K}{1 + 2\zeta_n \frac{s}{w_n} + \frac{s^2}{w^2_n}} \qquad (6\text{-}1)$$

The bracket effects are negligible for the main input. The electro-mechanical output device is considerably faster than the mechanical response of the gyro; moreover, the device forms an entity with the phase-sensitive demodulator (not included in the inversion task statement). Therefore (6-1) reflects the dominant part played by the mechanical response only.

Accelerometers

$$\frac{y(s)}{x(s)} = \frac{K}{1+2\zeta_n \frac{s}{w_n} + \frac{s^2}{w^2_n}} \qquad (6\text{-}2)$$

The bracket-effects are negligible for the main input. The damping ζ_n tends to decrease as inputs vary faster (a non-linear effect).

Pressure Transducers

Giannini $500 \frac{lb}{in^2}$ transducer

$$\frac{y(s)}{x(s)} = \frac{K}{(1+2\zeta_n \frac{s}{w_n} + \frac{s^2}{w^2_n})(1+2\zeta_{or} \frac{s}{w_{or}} + \frac{s^2}{w^2_{or}})} \qquad (6\text{-}3A)$$

The parameters ζ_n, w_n represent the basic Bourdon tube, while ζ_{or}, w_{or} represent the connecting orifice. However, this interpretation is somewhat artificial, since both elements interact and (6-3A) is to be regarded as an entity which should not be split, in physical interpretations. The damping ζ_{or} tends to increase as the inputs vary faster (a non-linear effect).

Bourns 800 $\frac{lb}{in^2}$ transducer

$$\frac{y(s)}{x(s)} = K \frac{1 + 2\zeta_a \frac{s}{w_a} + \frac{s^2}{w^2_a}}{(1 + 2\zeta_n \frac{s}{w_n} + \frac{s^2}{w^2_n})(1 + 2\zeta_b \frac{s}{w_b} + \frac{s^2}{w^2_b})} \qquad (6\text{-}3B)$$

The parameters $\zeta_n w_n$ represent the basic Bourdon tube; while ζ_a, w_a and ζ_b, w_b model a low frequency approximation of the T-tubing and orifice. Again, there is interaction and (6-3B) should also be regarded as a single unit. Of course, for purely mathematical purposes splitting is allowed.

The preceding results show that all instruments (as was obviously expected) smooth out the input wave form x(t) into more gradually varying output waveforms y(t). Inversion therefore requires reconstruction of a rougher signal shape from smoothed data, and is in fact equivalent with differentiation of recorded signals. All the problems attending differentiation do show up in the inversion process.

Observe that, with one exception, all transfer functions to be inverted are second order systems. The one exception is the factor $1 + 2\zeta_a \frac{s}{w_a} + \frac{s^2}{w^2_a}$ in the T-tubing of the Bourns transducer, which, when inverted, becomes a classical, smoothing second order dynamic system.

The next sections discuss the basic inversion relations, the error-analysis, interpolation and shifting, the cascading, the inversion of the numerator, etc.

6.2 Theory

6.2.1 Basic Inversion Relations of the Second Order System

Consider the normalized system (K = 1)

$$\frac{y(s)}{x(s)} = \frac{1}{1 + 2\zeta_n \frac{s}{w_n} + \frac{s^2}{w^2_n}} \qquad (6\text{-}4)$$

corresponding with the relationship

$$y(t) + \frac{2}{w_n}\zeta_n y'(t) + \frac{y''(t)}{w^2_n} = x(t)$$

The output data y(t) are available as N equidistant samples (directly measured or obtained by interpolation; see section 6.2.2).

$$y_1 = y(t_o);\ y_2 = y(t_o + T);\ldots;\ y_k = y(t_o + (k-1)T);\ldots$$

$$\ldots\ y_N = y(t_o + (N-1)T)$$

We approximate the continuous second order operator (6-4) by a discrete second order operator:

$$x_k = \alpha y_{k+1} + \beta y_k + \gamma y_{k-1} \tag{6-5}$$

where $x_k = x(t_o + (k-1)T)$ is the input sample to be reconstructed, at the same sampling instant as y_k. If $y(t)$ is decomposed in its harmonic components $\frac{y(w)}{2\pi} e^{iwt}$, one finds the conditions

$$\alpha e^{iwt} + \beta + \gamma e^{-iwt} = 1 + i \frac{2\zeta}{w_n} w - \left(\frac{w}{w_n}\right)^2$$

and, for zero-frequency accuracy,

$$\alpha + \beta + \gamma = 1 \tag{6-6}$$

The foregoing conditions lead to:

$$\alpha + \gamma = \frac{\left(\frac{w}{w_n}\right)^2}{1 - \cos(wT)} = \frac{2}{(w_n T)^2} \left(\frac{WT/2}{\sin(wT/2)}\right)^2$$

$$\alpha - \gamma = \frac{2\zeta_n \frac{w}{w_n}}{\sin(wT)} = \frac{2\zeta_n}{w_n T} \frac{wT}{\sin(wT)}$$

or

$$\alpha = \frac{1}{(w_n T)^2} \left(\frac{wT/2}{\sin(wT/2)}\right)^2 + \frac{\zeta_n}{w_n T} \frac{wT}{\sin(wT)}$$

$$\gamma = \frac{1}{(w_n T)^2} \left(\frac{wT/2}{\sin(wT/2)}\right)^2 - \frac{\zeta_n}{w_n T} \frac{wT}{\sin(wT)}$$

Clearly α and γ depends on frequency w. A low-frequency approximation (Taylor - development around w = 0) gives

$$\alpha_o = \frac{1 + \zeta_n (w_n T)}{(w_n T)^2}$$

$$\gamma_o = \frac{1 - \zeta_n (w_n T)}{(w_n T)^2} \qquad (6\text{-}7)$$

$$\beta_o = 1 - \alpha_o - \gamma_o = \frac{(w_n T)^2 - 2}{(w_n T)^2}$$

These relations correspond to the choice of symmetric differences to approximate derivatives. Formula (6-5) is not valid for the two extreme data points. For the leftmost point we use

$$x_1 = \alpha_L y_3 + \beta_L y_2 + \gamma_L y_1 \qquad (6\text{-}8)$$

and for the rightmost point

$$x_N = \alpha_R y_N + \beta_R y_{N-1} + \gamma_R y_{N-2} \qquad (6\text{-}9)$$

The corresponding coefficients are given by

$$\alpha_L = \frac{1}{(w_n T)^2} \left(\frac{w T/2}{\sin (w T/2)} \right)^2 - \frac{\zeta_n}{w_n T} \frac{w T}{\sin (w T)} = \gamma$$

$$\beta_L = - \frac{2 \cos w T}{(w_n T)^2} \left(\frac{w T/2}{\sin (w T/2)} \right)^2 + \frac{4 \zeta_n}{w_n T} \frac{w T/2}{\tan (w T/2)}$$

$$\gamma_L = 1 - \alpha_L - \beta_L$$

Hence,

$$\beta_R = \beta_L \text{ with } \zeta_n \text{ replaced by } -\zeta_n$$

$$\gamma_R = \alpha_L \text{ with } \zeta_n \text{ replaced by } -\zeta_n$$

$$\alpha_R = 1 - \beta_R - \gamma_R$$

The low-frequency approximations are:

$$\alpha_{Lo} = \gamma_o$$

$$\beta_{Lo} = \frac{-2 + 4\zeta_n (w_n T)}{(w_n T)^2} \qquad (6\text{-}10)$$

$$\gamma_{Lo} = 1 - \alpha_{Lo} - \beta_{Lo}$$

and

$$\beta_{Ro} = \frac{-2 - 4\zeta_n (w_n T)}{(w_n T)^2}$$

$$\gamma_{Ro} = \frac{1 + \zeta_n (w_n T)}{(w_n T)^2} \qquad (6\text{-}11)$$

$$\alpha_{Ro} = 1 - \beta_{Ro} - \gamma_{Ro}$$

6.2.2 Interpolation and Shifting of Sampling Instants

References 12, 13 and 14 are very useful for this section. Assume the original output data to be N_s equidistant samples $\{\hat{y}k\}$:

$$\hat{y}k = y((k-1)\,T_s)\,, \qquad 1 \leqslant k \leqslant N_s \tag{6-12}$$

While these original output samples $(\hat{y}k)$ are found at instants $t = o$, $t = T_s$, ... $t = (N_s-1)\,T_s$, the error-analysis (see next section 6.2.3) or the preference of the user may dictate a different origin and/or different spacing (see section 6.2.1).

$$t = t_o, \quad t = t_o + T, \ \ldots, \ t = t_o + (N-1)\,T$$

We may assume that the signals y(t) are bandlimited for practical purposes, with finite energy (if necessary, after subtracting the average value). This means that if the Fourier transform of y(t) is

$$Y(w) = \int_{-\infty}^{\infty} y(t) e^{-iwt}\, dt$$

then $Y(w) = 0$ for $|w| >$ a minimum value which we can set equal to $\mu\, w_n$.

Then μ is a number, often larger than one. The energy is

$$E_y = \int_{-\infty}^{\infty} y^2(t)\, dt = \frac{1}{2\pi}\int_{-\mu w_n}^{\mu w_n} |\, y\,(w)|^2\, dw \quad < \quad \infty$$

For the samples $\{\hat{y}k\}$, one has approximately (exactly, if T_s is sufficiently small; $T_s < \frac{\pi}{2\,\mu\, w_n}$ and if y(t) is truly band-limited):

$$E_y \simeq T_s \sum_{k=1}^{N_s} \hat{y}\,k^2$$

The bandwidth $\mu\, w_n$ can, if necessary, be estimated by a discrete Fourier-analysis (preferably the Fast Fourier transform techniques) on $\{\hat{y}k\}$. The Nyquist-Shannon sampling theorem says that, in order not to lose information concerning y(t), the sampling interval T_s must satisfy

$$T_s \leqslant \frac{\pi}{\mu\, w_n}$$

If this inequality is not satisfied, aliasing occurs and even an ideal (low pass) filter cannot reconstitute y(t) exactly from $\{\hat{y}k\}$. Since the reconstruction is not performed in real time, a non-causal interpolating operator can be used.

Therefore, one uses here the interpolating function (corresponding to an ideal low pass filter for $w \leq w_{INT}$).

$$\frac{\sin w_{INT}\, t}{\frac{\pi}{T_s}\, t} \qquad \text{with } \mu w_n \leq w_{INT} \leq 2\frac{\pi}{T_s} - \mu w_n$$

One has the interpolating operator with the narrowest bandwidth if $w_{INT} = \mu w_n$. For any time $\bar{t}$ the interpolated value $\bar{y}$ of $y(\bar{t})$ is taken as

$$\bar{y}(\bar{t}) = \sum_{k=1}^{N_s} \hat{y}((k-1)\, T_s)\, \frac{\sin w_{INT}\, (\bar{t} - (k-1)\, T_s)}{\frac{\pi}{T_s}\, (\bar{t} - (k-1)\, T_s)}$$

The interpolated and shifted values y_k are now given by

$$y_j = \sum_{k=1}^{N_s} \hat{y}_k\, \frac{\sin w_{INT}\, (t_o + (j-1)T - (k-1)\, T_s)}{\frac{\pi}{T_s}\, (t_o + (j-1)\, T - (k-1)\, T_s)}$$

T can be larger, equal or smaller than T_s. In some cases, to avoid the Gibbs phenomenon, the interpolation formula might be changed slightly to produce a Fejèr sum.

This interpolation formula can be used for a variety of values of t_o in an interval of length T to obtain shifted sample instants of the output (y_k) and hence input (x_k), for the same set of original $(\hat{y}_k)$.

6.2.3 Error Analysis for Single Second Order Dynamic Systems

The equation (6-4) models the rate gyros and accelerometers (but not the pressure transducers). Looking at the discrete relationship (6-5) used for inversion, one observes three immediate sources of error.

A. Quantization Error

Disregarding the inaccuracies in α, β, γ there will be an error ε_{qx} in x_k due to quantization, roundoff, reading error and noise in $\{\hat{y}_k\}$.

The following reasonable model is used to describe those errors in $\{\hat{y}_k\}$. One assumes that the errors have a mean value $\hat{\varepsilon}_y$ and further that the deviations around this mean have an upper bound $\hat{h}_y$.

In other words, for each k :

$$\text{average of } \hat{y}\,k - (\hat{y}\,k)_{true} = \hat{\varepsilon}_y$$

$$\left| \hat{y}\,k - (\hat{y}\,k)_{true} - \hat{\varepsilon}_y \right| \leq \hat{h}_y$$

As a result, because of the interpolation formula established in section 6.2.2, the $\{y_k\}$ values have errors with mean $\varepsilon_y = \hat{\varepsilon}_y$ and with an upper bound on deviations around that mean which is strictly speaking infinite. However, use of the statistical formulas derived in the Reference 12, combined with the fact that $\varepsilon_y = \hat{\varepsilon}_y$ already takes care of systematic bias, shows that $\hat{h}_y$ may also be taken as a realistic "bound" on deviations around the mean for $\{y_k\}$, except for infrequently occurring highly unfavorable error distributions.

Then, the x_k samples have errors with mean

$$\varepsilon_x = \varepsilon_y = \hat{\varepsilon}_y$$

because of condition (6-6), and deviation around the mean bounded by

$$c_q \hat{h}_y$$

where

$$c_q = |\alpha_o| + |\beta_o| + |\gamma_o| = \frac{1 + \gamma_n(w_n T) + |1 - \gamma_n(w_n T)| + |2 - (w_n T)^2|}{(w_n T)^2}$$

Clearly c_q increases as $(w_n T)$ decreases to zero and c_q becomes infinite for $w_n T = o$.

(see also Figure 6-1). This consideration imposes a lower bound on $(w_n T)$. Since the purpose of this error analysis is only to establish a compromise value for T and no exact knowledge of the error is required, we will use here for the quantization error the following relation:

$$\varepsilon_{qx} \leq |\hat{\varepsilon}_y| + c_q \hat{h}_y$$

a conservative bound, reached only in rare cases with a very unfavorable distribution of noise errors.

Figure 6-1, Quantization Error

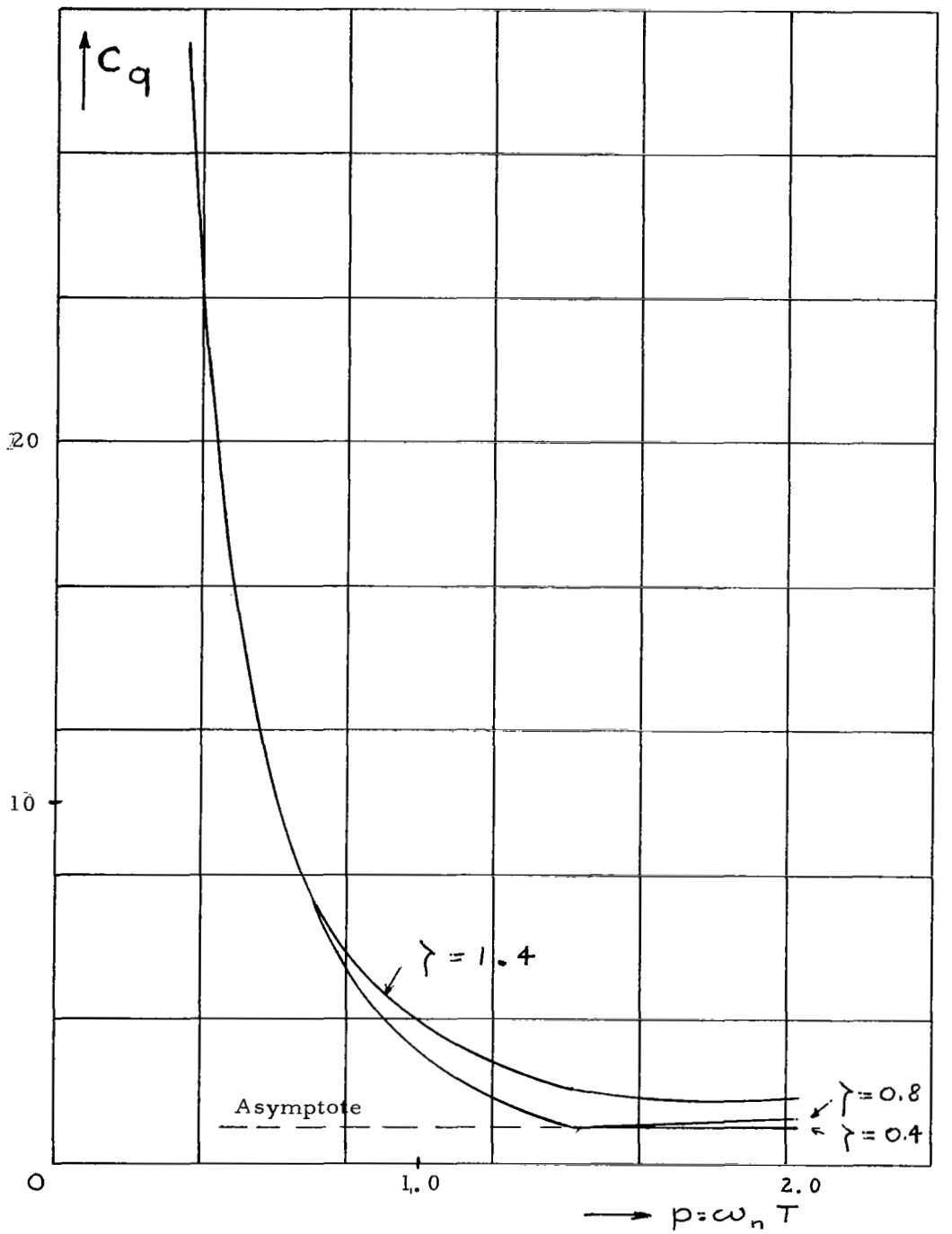

B. Operator Error

Besides the quantization error, there is still an operator error ε_{DX} in X_K due to replacement of the operators α, β, γ by the low frequency constant multipliers $\alpha_o, \beta_o, \gamma_o$. Again Reference 12 gives background information for the following developments.

For the system modeled by equation (6-4), the true inverse operator is:

$$G(w) = 1 + i\, 2\zeta_n (w/w_n) - (w/w_n)^2$$

The approximate inverse operator is:

$$D(w) = \alpha_o \exp(iwT) + \beta_o + \gamma_o \exp(-iwT)$$

$$= 1 - 2\frac{(1 - \cos w T)}{(w_n T)^2} + i\, 2\zeta_n \frac{\sin w T}{w_n T}$$

One has

$$\varepsilon_{DX}^2 \leq \frac{E_y}{2\pi} \int_{-\mu w_n}^{\mu w_n} |G(w) - D(w)|^2 \, dw$$

The operator error ε_{DX} increases when T increases (for fixed μw_n of course), unlike ε_{qx} which decreases under these circumstances.

Indeed, to find ε_{DX} one needs an expression for

$$\int_{-\mu w_n}^{\mu w_n} |G(w) - D(w)|^2 \, dw = w_n \int_{u=-\mu}^{u=\mu} |G(u w_n) - D(u w_n)|^2 \, du$$

$$= w_n I_\mu (p, \zeta)$$

where $p = w_n T$

Then $$I_\mu(p,\zeta) = 2\int_0^\mu \left\{\left[\frac{2}{p^2}(1-\cos p u) - u^2\right]^2 + 4\zeta^2\left(\frac{\sin pu}{p} - u\right)^2\right\} du$$

$$= \frac{4\mu^5}{(\mu p)^5}\left[3(\mu p) - 8\sin(\mu p) + 4(\mu p)\cos(\mu p) + \sin(\mu P)\cos(\mu p) + 2(\mu p)^2\sin(\mu p) + \frac{(\mu p)^5}{10} - \frac{2}{3}(\mu p)^3\right]$$

$$+ \frac{4\zeta^2\mu^3}{(\mu p)^3}\left[(\mu p) - 4\sin(\mu p) + 4(\mu p)\cos(\mu p) - \sin(\mu p)\cos(\mu p) + \frac{2}{3}(\mu p)^3\right]$$

A series development shows that

$$I_\mu(p,\zeta) = \frac{2}{63}\zeta^2\mu^3((\mu p)^4 + \ldots) + \frac{\mu^5}{648}((\mu p)^4 + \ldots)$$

Now $$\varepsilon_{DX}^2 \leqslant \frac{E_y w_n}{2\pi} I_\mu(p,\zeta)$$

Figure 6-2 shows the increase of $\left(I_\mu(p,\zeta)\right)^{1/2}$ with $p = w_n T$, for a fixed value of μ ($\mu = 2$). The bound ε_{DX} is also very conservative, being reached only by the rarely occurring most unfavorable combination of signal and transfer function.

Because of the linearity of the system model the worst total error on x(t) is given by the sum

$$\varepsilon_x = \varepsilon_{qx} + \varepsilon_{Dx}$$

Due to the different behavior of ε_{qx} and ε_{DX} with varying T, ε_x, will reach a minimum for a finite optimum value of T, say T_o.

The preceding discussion on how to find T_o is based on the idea that for this particular application a minimax formulation:

find: $\min_T$ | max error on x(t) any time t in the record |

is more appropriate than, say, a least integral squared error criterion. Indeed, one wants to discover what exactly happened in the vehicle in case of an accident, where large peak signals can be expected and one wants to find these peaks as accurately as possible, rather than obtain a good average fit (which would give too much importance to more trivial portions of the signal x).

Figure 6-2, Operator Error

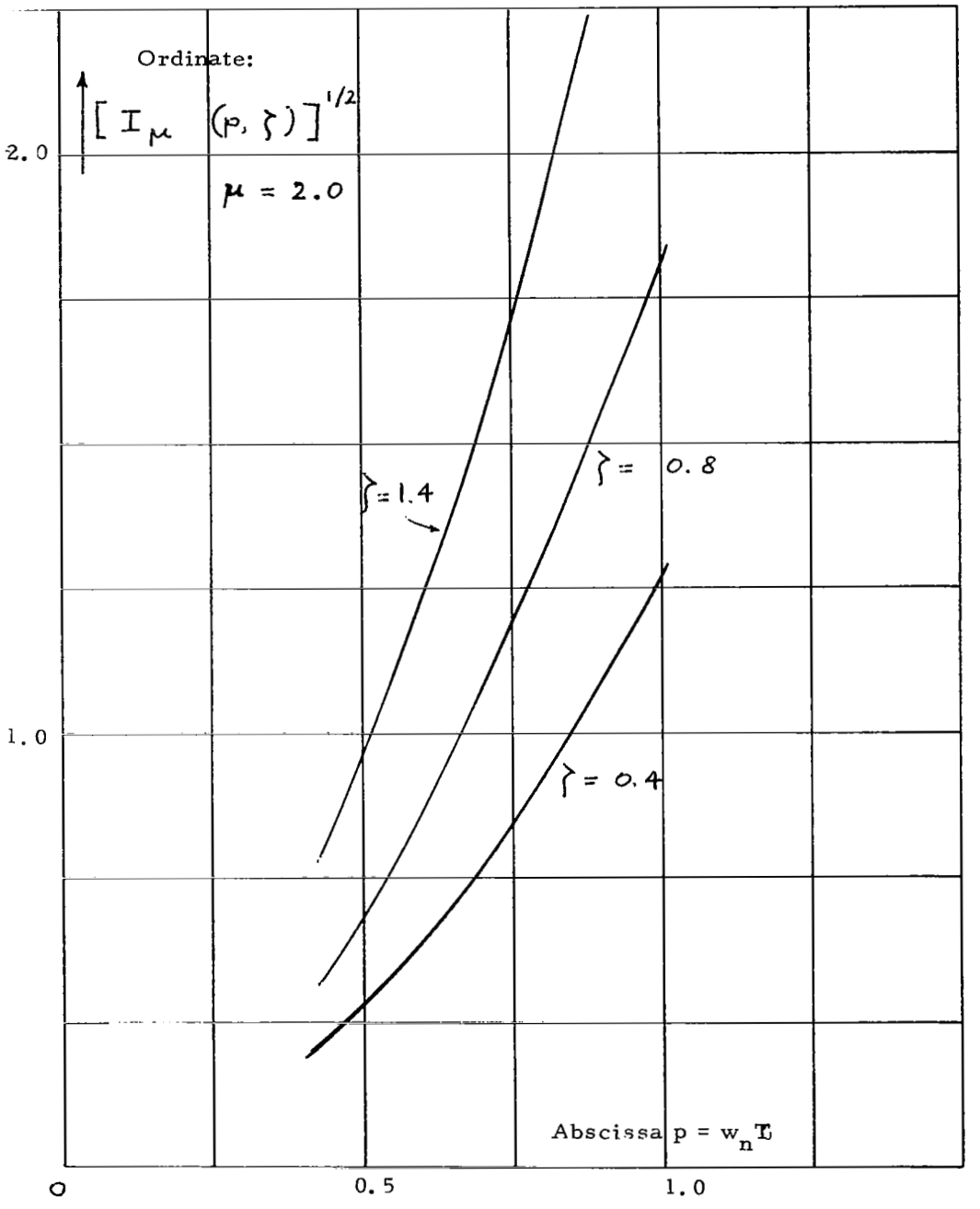

Since both $\mathcal{E}_{qx}$ and $\mathcal{E}_{DX}$ are conservative, $\mathcal{E}_x$ will be a very conservative estimate, reached only in rarely occurring most unfavorable combinations. Actual errors can be expected to be quite smaller in most examples (see examples in this report). However, regardless of the conservatism of $\mathcal{E}_x$, the formulas for this bound are useful in establishing a best compromise T_o.

It is possible to find less conservative error estimates by different means. These means include "Monte Carlo" runs to establish expected values for the quantization error, and approximate calculation of the spectrum y(w) of y(t) by means of fast Fourier transforms, followed by numerical calculation of the exact formula for $\mathcal{E}_{DX}$. If the probabilistic structure of the errors is known, more refined statistical modeling becomes possible.

Note that $\mathcal{E}_x$ bounds the error at input sampling instants on $\{x_k\}$. The inversion results are recorded as samples $\{x_k\}$ and no interpolation is performed on x. Note that if y(t) were truly band limited, then x(t) would also be truly band limited, with the same bandwidth. However, y(t) is only approximately bandlimited, and therefore the approximate assumption of finite bandwidth is better satisfied by y(t) than by x(t). Therefore, it is preferable to avoid making any assumptions about the spectrum of x(t). Values of x(t) at new instants of time are better obtained by interpolation and shifting on $\{\hat{y}k\}$.

C. Parameter Error

The third kind of error is due to errors in the values taken for the system parameters $w_{n,} \rangle_{n}$, and, more generally errors due to replacement of the true system equations by (6-4). One can get an idea of the importance of this error by making parametric runs with neighboring values for $w_{n,} \rangle_{n}$. Note that one obvious reason for parameter error is the fact that we use average parameters for all instruments of the same class, say all (-3g, +3g) accelerometers, while tests have shown that there may be a noticeable variation (more than 10%) among individual members of that class.

There is also a fourth type of error, less obvious than the preceding ones.

D. Inaccuracy Due to Truncation of Data (Edge Effects)

If the true output samples $\{\hat{y}_k\}$ contain non-zero elements for $t < o$ or for $t > (N_s - 1)T_s$, then the interpolation formula produces an error in the values of y_j due to truncation. Because of the shape of the interpolating function, this truncation effect is largest at the edges of the record and very much suppressed toward the middle of the record. A simplified estimation of this truncation effect is obtained below. The influence of the first omitted sample $\hat{y}_o$ at $t = -T_s$ (left) or $\hat{y}_{Ns+1}$ at $t = N_s T_s$ (right) is the most important. Assume that $|\hat{y}_o| \simeq |\hat{y}_1|$ and $|\hat{y}_{Ns+1}| \simeq |\hat{y}_{Ns}|$. Use an average for the absolute value of the interpolating function.

$$\left| \frac{\sin w_{INT}\, t}{\frac{\pi}{T_s}\, t} \right|_{av} \simeq \frac{T_s}{1.5\pi\, t}$$

Then, at a distance $|\Delta t|$ from the edges, one finds an error

$$(|\hat{y}_1| \text{ or } |\hat{y}_{N_s}|) \cdot \frac{T_s}{1.5\pi\,(T_s + |\Delta t|)}$$

If $w_{INT} \ll \pi/T_s$ several truncated values will contribute; however, there will also be more correlation of errors. For this reason the error can be estimated as

$$(|\hat{y}_1| \text{ or } |\hat{y}_{N_s}|) \quad \frac{\gamma\, T_s}{1.5\pi\,(T_s + |\Delta t|)}$$

with

$$\gamma = 1 \text{ if } w_{INT}\, T_s > \frac{\pi}{5}$$

$$\gamma = 3 \text{ if } w_{INT} T_s < \frac{\pi}{5}$$

In order to have compatibility with the rest of the inversion, the truncation error should be of the order of $\hat{h}_y$. But, due to the worst case assumptions of the error analysis, one may allow truncation error estimates an order of magnitude larger than $\hat{h}_y$, say $10\,\hat{h}_y$. Then one finds

$$(\Delta t)_{\substack{\text{left or} \\ \text{right}}} = T_s \left\{ \left(\begin{matrix} |\hat{y}_1| \\ \text{or } |\hat{y}_{N_s}| \end{matrix} \right) \frac{\gamma}{15\pi\,\hat{h}_y} - 1 \right\}$$

as an estimate of the distance from both edges where results for $\{ x\ k \}$ must be treated with caution. If no interpolation is used in the inversion, the truncation error does not arise. In many cases of truncated records, extrapolation by eye of $\{ \hat{y}\ k \}$ before inversion can be used to decrease the truncation error.

6.2.4 Inversion of a Cascade of Second Order Systems (Giannini Pressure Transducers)

Now we take up the case of a cascade of two systems like (6-4), as exemplified by (6-3A)., or part of (6-3B). Such a system can be decomposed in two subsystems, at least for the purely mathematical part of the reconstruction as shown in the normalized diagram below:

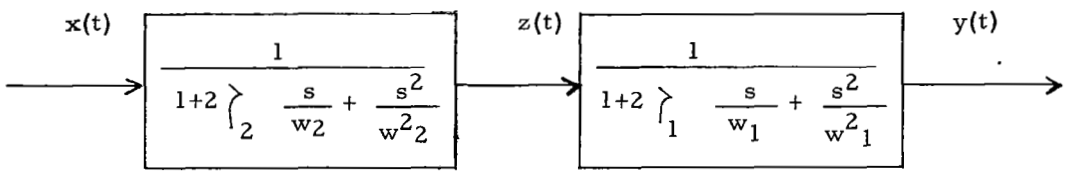

Hence

$$\frac{Z(s)}{X(s)} = \frac{1}{1+2\zeta_2 \frac{s}{w_2} + \frac{s^2}{w^2_2}}$$

$$\frac{Y(s)}{Z(s)} = \frac{1}{1+2\zeta_1 \frac{s}{w_1} + \frac{s^2}{w^2_1}}$$

For each subsystem the formulas of Section 6.2.1 can be applied immediately. However, the error analysis is somewhat different. First, in order to have the intermediate signal z(t) as smooth as possible, one chooses the following order for inversion:

First: $w_1 = \max (w_n, w_{or})$ or $\max (w_n, w_b)$

ζ_1 is the corresponding damping coefficient

followed by: $w_2 = \min (w_n, w_{or})$ or $\min (w_n, w_b)$

ζ_2 is the corresponding damping coefficient.

Hence, $w_1 \geq w_2$. If $w_1 = w_2$, then ζ_1 is taken as the lower damping coefficient.

We can assume a bandwidth of y(t) in the form

$$\mu w_2$$

requiring a sampling interval T_s for $(\hat{y}_k)$ given by

$$T_s \leq \frac{\pi}{\mu w_2}$$

Then the intermediate signal z(t) has approximately the same bandwidth μw_2 and the same interpolating function can be used for both z(t) and y(t).

Assume that a sampling interval T_1 is used from y_k to $\hat{z}_k$, and an interval T_2 from z_k to x_k. We now calculate the error bounds.

A. Quantization Error

One gets in the same manner as in Section 6.2.3 that

$$\varepsilon_{qx} \leq |\hat{\varepsilon}_y| + (c_q)_1 (c_q)_2 \hat{h}_y$$

where

$$(c_q)_1 = \frac{1 + \zeta_1 (w_1 T_1) + |1 - \zeta_1 (w_1 T_1)| + |2 - (w_1 T_1)^2|}{(w_1 T_1)^2}$$

and $(c_q)_2$ is given by a similar relation, where index 1 is replaced by index 2.

This is again a conservative bound.

B. Operator Error

Proceeding as in Section 6.2.3, one finds (see Reference 12)

$$\pm \varepsilon_{DX} = \frac{1}{2\pi} \int_{-\mu w_2}^{\mu w_2} [G_2 G_1 - D_2 D_1] Y e^{iwt} dw$$

$$= \frac{1}{2\pi} \int_{-\mu w_2}^{\mu w_2} [(G_2 - D_2) G_1 + (G_1 - D_1) D_2] Y e^{iwt} dw$$

then

$$\varepsilon_{DX}^2 \leq \frac{E_y}{2\pi} \int_{-\mu w_2}^{\mu w_2} |(G_2 - D_2) G_1 + (G_1 - D_1) D_2|^2 dw$$

or

$$\varepsilon_{DX} \leq \left(\frac{E_y}{2\pi}\right)^{1/2} \left\{ \left(\int_{-\mu w_2}^{\mu w_2} |(G_2 - D_2)\, G_1|^2\, dw \right)^{1/2} + \left(\int_{-\mu w_2}^{\mu w_2} |(G_1 - D_1)\, D_2|^2\, dw \right)^{1/2} \right\}$$

While the preceding expressions can be calculated exactly, the results are fairly complicated and more precise than is needed here. Therefore, we replace them by a simpler approximate relation (with some compensation of errors)

$$\varepsilon_{DX_{approx}} \leq \left(\frac{E_y}{2\pi}\right)^{1/2} \left[\left(\int_{-\mu w_2}^{\mu w_2} |G_2 - D_2|^2\, dw \right)^{1/2} + \left(\int_{-\mu w_1}^{\mu w_1} |G_1 - D_1|^2\, dw \right)^{1/2} \right]$$

In terms of the pre-calculated expression for $I_\mu(p, \gamma)$, one can rewrite the last inequality as

$$\varepsilon_{DX_{approx}} \leq \left(\frac{E_y}{2\pi}\right)^{1/2} \left(\left[w_2 I_\mu(w_2 T_2, \gamma_2) \right]^{1/2} + \left[w_1 I_\mu(w_1 T_1, \gamma_1) \right]^{1/2} \right)$$

The minimum of $\varepsilon_x = \varepsilon_{qx} + \varepsilon_{DX}$ can be found by calculating both sources of error for a net of values of T_1 and T_2. The bound ε_x for the cascade will be even more conservative than for the single second order system.

The spacing T_1 for the first inversion can be obtained if necessary by interpolating $(\hat{y}_k)$ into (y_k) with T_s satisfying

$$T_s \leq \pi / (\mu w_2)$$

This gives $(\hat{z}_k)$ at a spacing T_1. The distance T_2 for the second inversion can be obtained if necessary, by interpolating these $(\hat{z}_k)$ into a new set (z_k) with distance T_2 provided $T_1 \leq T_s$.

If $T_1 > T_s$, another set of $(\hat{z}_k)$ is to be calculated, say by shifting the origin (and sampling times) of the new $(\hat{z}_k)$ to half way points of the sampling times of the old $\{\hat{z}_k\}$. This process can be repeated until one has a combined set of $\{\hat{z}_k\}$ values with spacing smaller than T_s.

For many applications one can expect larger inversion errors for the cascade than for a single second order system, due to the need for higher order derivatives in the inversion process. This observation implies that, unless the transducer models are exactly known, and there is very little noise, it is preferable by far to restrict oneself to low order approximating models and that the supposed gain in knowledge of the real physical device by means of a high order model may be illusory in practical applications. Therefore, if a physical system consists of a large number of cascaded devices, it may be preferable, at least for the purpose of inversion, to take only the dominant blocks, i.w., the slowest ones, and, where possible, to lump several fast blocks into a single lower order approximating block. Such long chains do indeed occur in the Scout System, where the entire telemetry transmission follows the transducer.

In fact, a general theory exists for such inversion problems.

6.2.5 Inversion of a Numerator in the Direct Transfer Function

(T-Tubing of Bourns pressure transducers)

The numerator factor

$$\frac{Y(s)}{V(s)} = 1 + 2\zeta_a \frac{s}{w_a} + \frac{s^2}{w_a^2}$$

in the transfer-function (6-3B) gives rise to a conventional second order dynamical system when inverted. Here V(t) is defined as an intermediate (mathematical) signal, such that inversion of V(s)/X(s) becomes the problem treated in Section 6.2.4. The order of inversion, with Y/V inverted first, then followed by inversion of V/X is again chosen to find the intermediate signal v(t) as smooth as possible.

Assume that y(t) has a bandwidth

$$\mu \min (w_n, w_b)$$

Then v(t) will have approximately similar bandwidth. For the inverstion of V/X that bandwidth implies a spacing in v(t) - samples $T_{s,v}$ satisfying

$$T_{s,v} \leqslant \pi / (\mu \min (w_n, w_b))$$

A similar spacing $T_{s,y} = T_{s,v}$ is needed for $\{ \hat{y}\, k \}$ to avoid aliasing. If $h_a(t)$ is the impulse response connected with the transfer function of V(s)/Y(s) then one has for the forced part of v(t)

$$v(t)_{forced} = \int_{t'=o}^{t'=t} h_a(t')\, y\,(t-t')\, dt'$$

(A free solution with 2 arbitrary constants could be added, see further).

If now one has a set of $\{ yk \}$ with spacing T

$$yk = y\,(t_o + (k-1)T), \quad t_o = o$$

one can replace the integral for v(t) forced by the discrete approximation:

$$v_K = \frac{1}{2} \sum_{n=1}^{n=k} y_{k+1-n}\,(H_n - H_{n-2}) - \frac{1}{2}\, y_1\,(H_k - H_{k-1})$$

where

$$H_j = \int_{t'=o}^{t'=jT} h_a\,(t')\, dt' = H\,(jT)_j \quad j > o$$

$$H_j = o \quad \text{if } j \leqslant o$$

i.e., $H_j(t)$ is the step response, and T is sufficiently small such that y(t+T)-y(t) is nearly zero over the record-length, (i.e., y(t) is nearly constant over a length T). The latter condition is satisfied if $T \cdot \mu \cdot \min (w_n, w_b) \ll 1$ (See Reference 12). As an example, one might take

$$T \leqslant \frac{0.2}{\mu \cdot \min (w_n, w_b)}$$

while, for simplicity, T is also taken as a submultiple of T_s. For H_j one has further, explicitly

$$H_j = 1 - \frac{e^{-\zeta_a w_a (jT)} \cos (\sqrt{1-\zeta_a^2}\, w_a\, j\, T - \text{Arc sin } \zeta_a)}{(1 - \zeta_a^2)^{1/2}}$$

Once $\{ v_k \}$ is found, the rest of the inversion proceeds as outlined in Section 6.2.4.

However, there is one particularity already mentioned before. Since only the forced part of v(t) was used, assuming v(t = o) = o and $\dot{v}$(t = o) = o, one can add a free solution corresponding to

$$\frac{\ddot{v}}{w_a^2} + 2\zeta_a \frac{\dot{v}}{w_a} + v \equiv o$$

This means that as far as x(t) is concerned, one can add a free solution of the same differential equation with x replacing v.

If somehow x(o) and $\dot{x}$ (o) are known, then

$$x_{free}(o) = x(o) - x_{forced}(o)$$

$$\dot{x}_{free}(o) = \dot{x}(o) - \dot{x}_{forced}(o)$$

The free solution to be added, at the sampling times of xk is:

$$x_{free}(t) = e^{-\zeta_a w_a t} \left[x_{free}(o) \cos \sqrt{1 - \zeta_a^2}\, w_a t \right.$$

$$\left. + \left(\frac{\dot{x}_{free}(o)}{w_a} + \zeta_a x_{free}(o) \right) \sin \left(\sqrt{1 - \zeta_a^2}\, w_a t \right) / \sqrt{1 - \zeta_a^2} \right]$$

In some cases x(o) and $\dot{x}$ (o) can be estimated. Say, that before t = o a steady regime is established, x(t) is a constant or a ramp for t < o

$$x(t) = x(o) + \dot{x}(o)t \quad , \quad t \leqslant o$$

then y(t) is also a constant or a ramp with

$$y(t) = y(o) + \dot{y}(o)\, t \quad , \quad t \leqslant o$$

where, for K = 1,

$$\dot{x}(o) = \dot{y}(o)$$
$$x(o) = y(o) + \dot{y}(o)\ 2 \left(\frac{\zeta_n}{w_n} + \frac{\zeta_b}{w_b} - \frac{\zeta_a}{w_a} \right)$$

$x_{forced}(o)$ is obtained directly from $\{ x_k \}$, if no shift is made in origin, while $\dot{x}_{forced}(o) \simeq \frac{x_2 - x_1}{T_x}$ ($T_x \mu w_n \ll 1$) or some other relationship, but this is subject to large errors!

Other known boundary conditions can also occur, e.g., at the tail end of the record to be inverted. In all cases two boundary conditions are needed to specify x(t) completely. Superposition can be used to eliminate the need for specific formulas for other boundary conditions.

The error analysis for this case is not complicated. One needs an estimate of errors in v(t) based on the errors in y(t), in order to be able to use the results obtained for the simple case (Section 6.2.4) of the Giannini models.

Using the formula for v_k, one finds immediately for the bias in the error

$$\varepsilon_{vk} = \hat{\varepsilon}_y H_{k-1}$$

Hence

$$|\varepsilon_{vk}| < |\hat{\varepsilon}_y| \, |H_{k-1}|_{max} = |\hat{\varepsilon}_y| \, (1 + \text{overshoot})$$

A good value, for k not very small (neglecting boundary effects) is then

$$\varepsilon_{vk} = \hat{\varepsilon}_y$$

As for the unbiased part of the error, one obtains the bound

$$h_v \ll \hat{h}_y$$

using the fact that the step response $\int h_a \, dt$ was normalized. Finally, because of the normalization of $h_a(t)$ again, one may take very approximately

$$E_v = E_y$$

for the signal energy.

Hence, one simply uses the error description of $\hat{y}$ also for v, without any change at all.

6.2.6 Some Remarks on Inversion

This section discusses a few problems arising in the inversion process.

A. Order of the Discrete Inversion Operator

In Section 6.2.1, a discrete second order operator (i.e., second order in the basic delay operator e^{-Ts}) replaced a continuous second order operator (second order in the basic differential operator s). A higher order discrete operator could, in fact, approximate the ideal operator better. However, better inversion results generally would only be obtained if y(t) were known exactly, without any error or noise, or with very little noise. With noise present, a higher order discrete operator leads to a larger coefficient C_q (see the results for the cascade) and hence larger errors.

To offset this, one would have to take a larger value of T and this would then negate the apparent gain produced by the higher order inversion operator. In fact, if signal and noise description are known, one can find the optimum order of the discrete inversion operator, but it would often be rather small in practical cases.

There exists a more general theory covering this aspect. We refer to the end of Section 6.2.4 for a brief discussion of what to do with high order models, and the desirability to collapse long chains of devices into a low order approximation, in cases where noise and parameter uncertainties are significant, as is usually the case.

B. Interesting recent general results of a theoretical nature on inversion of linear systems can be found in the references listed under 15, 16 and 17.

C. The present formulation was made with the models of the Scout instruments as specific applications. Therefore, the inversion of the fourth order Giannini model was reduced to successive application of the second order accelerometer model. However, one can also directly obtain inversions for higher order models, without the use of factoring.

D. For very fast inputs (i.e., fast compared with the response of the transducer), the reconstruction of the actual waveform is very dubious and is not even to be considered a well-posed physical problem. What counts is the total area under the fast pulse which acts more like a mathematical impulse.

This effect is also demonstrated in Figure 6-3 for an accelerometer with $w_n = 850$ rad/sec, $\zeta_n = 0.55$ where all the inputs have equal area. Since output area is nearly proportional to input area, the strength of the impulse can be calculated, without any need for inversion by direct simulation and area-measurement with a planimeter (after the fact has been established that this is indeed a very fast input).

Figure 6-3, Uncertainty for Nearly Impulsive Inputs

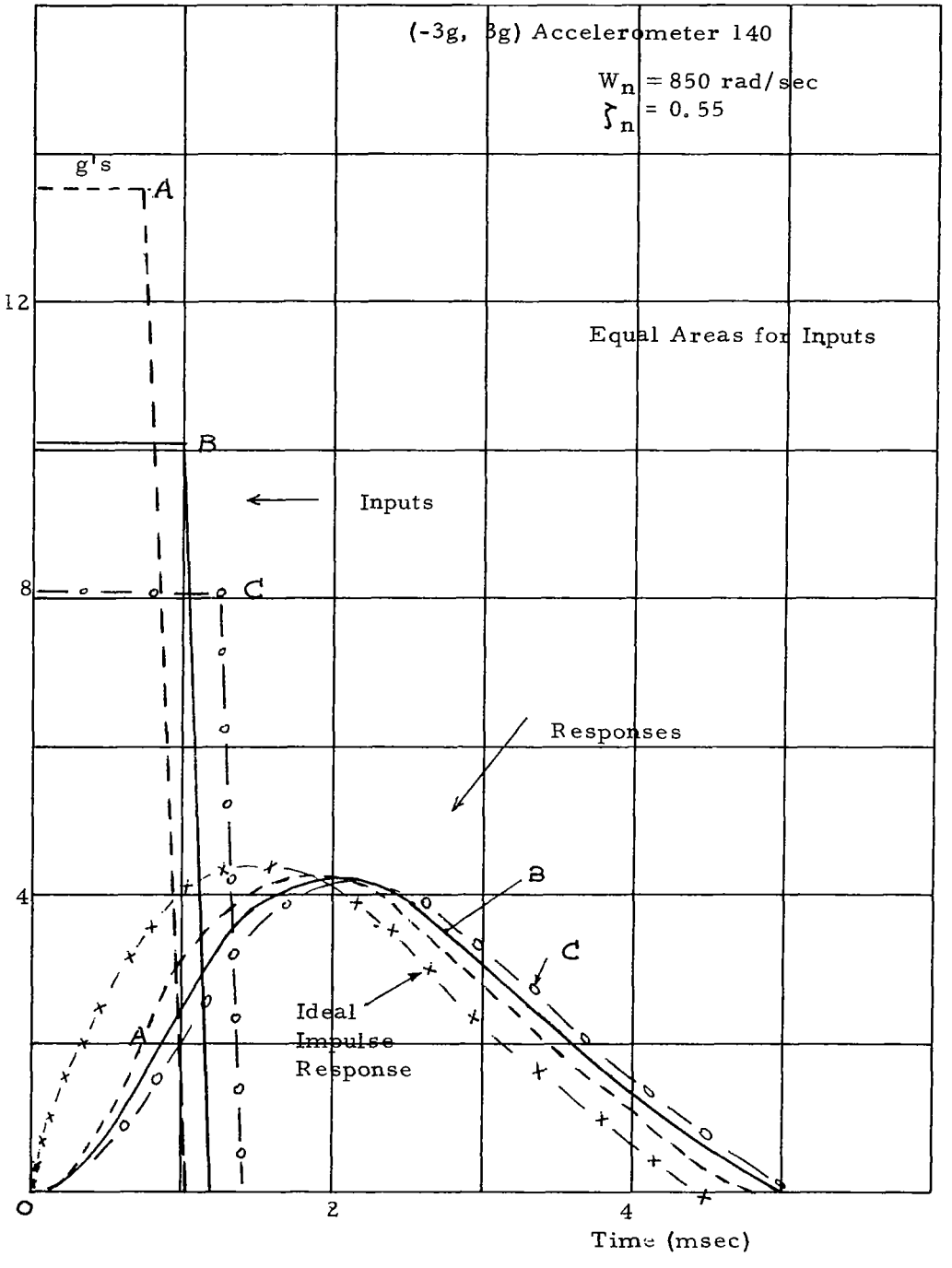

E. In the present version of the digital program, the bandwidth of the transducer output signal is estimated by the user through the input μ. A poor choice of μ can lead to erroneous results (especially in interpolation). It would be useful, in an enlarged version of the inversion program, to have the computer estimate μ by means of a spectral analysis. Such an analysis can be performed fast by the use of the fast Fourier transform.

F. Edge-Effects

The fourth type of error discussed in Section 6.2.3, due to truncation of $\hat{y}_k$ data can be (partially) removed in some ways. One method is to use such sampling of the original y(t)-record that interpolation becomes unnecessary. Another method consists of using a different interpolation scheme near the edges, such as spline functions. However, this approach requires further study to estimate best choice of order and type of interpolating function. A simple, but efficient way of alleviating edge-effects was mentioned at the end of Section 6.2.3; it can be used in the present program.

6.3 Organization of the Digital Inversion Program

The theory of the inversion process used was given in Section 6.2. While the purely computational (numerical) aspects are very simple and straight-forward, the logic is a little more complex. Therefore, the present section describes the logical organization of the digital program for the reader who wishes to know its details.

Inversion Program

Inputs: t_{so}
N_s
T_s
$\{\hat{y}_k\}$, $1 \leq k \leq N_s$
gain K

Errors $\hat{\varepsilon}_y$, $\hat{h}_y$

Bandwidth $\{\mu\}$

t_o: optional
t_{max}: optional

Choice w_{INT} (IWINT)

Option to stop after error calculation (ISTOP)
Type of instruments: Class CA: Gyro, accelerometer
Class CB: (Giannini) pressure transducer without T-tube
Class CC: (Bourns) pressure transducer with T-tube

Special Inputs

If CA: $w_n, \zeta_n; \{T\}; \{T_{ch}\}$

If CB: $w_n, \zeta_n; w_{or}, \zeta_{orj} \{T_1\}, \{T_2\}; \{T_{1\,ch}, T_{2\,ch}\}$

If CC: $w_n, \zeta_n; w_b, \zeta_b; w_a, \zeta_a; \{T_1\}, \{T_2\};$

$\{T_{1\,ch}, T_{2\,ch}\}$

α (optional)

y_o (optional)

$\dot{y}_o$ (optional)

Notes:

1. $\{T_{ch}\}$; $\{T_{1\,ch}, T_{2\,ch}\}$ are optional (NOPT1)

   If they are used, they should have values covered by $\{T\}$ or $\{T_1\}, \{T_2\}$ if one wishes to have an error calculation.

2. One should have

$$t_{so} \leq t_o \leq t_{max}$$

Main Program

Calculate E_y

If t_o not listed: $t_o = t_{so}$

If t_{max} not listed: $t_{max} = t_{so} + (N_{s-1})T_s$

Check if Class CA, CB, CC, then go to appropriate subprogram (CA), (CB), (CC).

* Calculate $\{x_k/K\}$ call results $\{x_k\}$

Print Δt_L, Δt_R (edge effects) if applicable

Print t_o, T, N

Print / Plot $\{t_k, x_k\}$

If Class CC, moreover, (for formulas see section 6.2.5)

Read y_o, $\dot{y}_o$ (set zero, if not given)

Calculate $x(o)$, $\dot{x}(o)$

Calculate $x_{free,\ 1} = x_{free}(o)$, $x_{forced}(o) = x_1$

$\dot{x}_{free,\ 1} = \dot{x}_{free}(o)$, $\dot{x}_{forced}(o) = \frac{x_2 - x_1}{T_x}$

Calculate $\left\{\frac{x_{free}}{K}\ (t_o + (k-1)\ T)\right\}$ $1 \leqslant k \leqslant N$

call results $\{x_{free,\ k}\}$

Print $\{t_k, x_{free,\ k}\}$

Print/Plot $\{t_k, x_{free,\ k} + x_k\}$

Stop

Subprogram (CA)

For $\{T\}$, $\{\mu\}$: Calculate $I_{\mu}(p, \gamma_n)$

$p = w_n T$

ε_{DX}

Calculate c_q, ε_{qx}, ε_x

Print $\frac{\varepsilon_x}{K}$; T; μ (call results ε_x)

Check ISTOP (stop
or
(continue

If continue, then

Choose T_{opt} for each μ, unless overridden

by $\{T_{ch}\} \rightarrow \{T'\}$ is ultimate choice

E_1 —— —— —— ——

If $T' = T_s$ and $t_o = t_{so}$

Then $[t_o, N, T, t_k, x_k] = BASINV [t_o, N_s, T_s, \hat{y}k, w_n, \gamma_n]$

(see subroutine BASINV further on)

and return to MAIN at point*

Otherwise $[t_o, T, N, t_k, yk] = INTERP [t_{so}, N_s, T_s, \hat{y}k, \mu, w_n, T', t_o, t_{max}, w_{INT}]$

(see subroutine INTERP further on)

$[t_o, N, T, t_k, x_k] = BASINV [t_o, N, T, yk, w_n, \gamma_n]$

L_1 —— —— —— —— —— —— ——

and return to MAIN at point*

Subprogram (CB)

E_2 —— —— —— —— ——

Calculate w_1, w_2 and γ_1, γ_2

according to section 6.2.4.

For $\{T_1\}$, $\{T_2\}$; $\{\mu\}$ calculate p_1, p_2

$I_\mu(p_1, \gamma_1)$, $I_\mu(p_2, \gamma_2)$

ε_{DX}

Calculate $(c_q)_1$, $(c_q)_2$, ε_{qx}

Calculate ε_x

Print $\frac{\varepsilon_K}{K}$, T_1, T_2, μ (call results ε_x)

Check ISTOP (stop
L_2 —— —— —— —— or
(continue

If continue, then

E_3 —— —— —— —— ——

Choose $T_{1\,opt}$, $T_{2\,opt}$ for each μ, unless overridden by

$\{T_{1\,ch}, T_{2\,ch}\} \rightarrow \{T'_1, T'_2\}$ is ultimate choice

Now, for each μ, enter (CA) at point E_1

with $\begin{cases} T' = T'_1, \quad w_n = w_1, \quad \gamma_n = \gamma_1, \\ \mu = \frac{w_2}{w_1}\mu_{input}, \text{ other symbols are correct} \end{cases}$

and leave at L_1 with $\begin{cases} N_1 = N, \quad T_1 = T, \quad \hat{z}_k = x_k \\ \text{other symbols unchanged} \end{cases}$

Then, check whether $T_1 \leq \pi/(\mu w_2)$

If yes, go to P_2

If not, determine whether $T_1 = T'_2$

If yes, go to P_2

If not, find smallest integer $p \geq 1$, such that $T_1 2^{-p} \leq \pi/(\mu w_2)$ and then for $j = 1, 2, \ldots, 2^p - 1$ go to E_1 with t_o replaced by $t_o + j\, T_1 2^{-p}$ and otherwise same conditions as first entry at E_1 above.

Leave again each time at L_1 with $\hat{z}_{k,j} = x_k$, $t_{k,j} = t_k$ and otherwise conditions as above.

Now, reorder all $\{\hat{z}_{k,j}\}$ in order of increasing time

$t_o < t_{o,1} < t_{o,2} < \cdots < t_1 < t_{1,1} \cdots$

$\hat{z}_1 \quad \hat{z}_{1,1} \quad \hat{z}_{1,2} \cdots \quad \hat{z}_2 \quad \hat{z}_{2,1} \cdots$

Call new series $\{\hat{z}_k, t_k\}$

P_2 — — (Still for each μ)

Enter (CA) at point E_1

with $\begin{cases} T' = T'_2, \; w_n = w_2, \; \}_n = \}_2 \\ t_{so} = t_o, \; N_s = N_1 \text{ or } N_1 2^p \end{cases}$

Values for w_{INT}, t_{max}, t_o, μ are correct

$\{\hat{y}k\} = \{\hat{z}k\}$

$T_s = T_1$ or $T_1 2^{-p}$

Leave at point L_1 with N, T

L_3 — — —

Return to MAIN at point *

Subprogram (CC)

Take $T_v = \frac{T_s}{m}$, with m smallest integer ($m \geqslant 1$) for which

$$\frac{T_s}{m} \leqslant \frac{\alpha}{\max(\mu) \cdot \min(w_n, w_b)}$$

(if α is not input, use $\alpha = 0.2$)

Print T_v

Enter (CB) at point E_2 , leave at point L_2

Check if $T_v = T_s$.

If yes, proceed to P_1

If not, then for each μ

$$[t_{so}, T_s, N_s, \hat{t}_k, \hat{y}k] = \text{INTERP}\,[t_{so}, N_s, T_s, \hat{y}k, \frac{w_2}{w_1}\mu\,,$$

$$w_1, T_v, t_{so}, t_{max}, w_{INT}\,]$$

P_1 -- Calculate $\{v_k\}$, see section 6.2.5

Set new $\{\hat{y}k\} = \{vk\}$, and enter (CB) at E_3

Leave at L_3

Print "forced solution"

Return to MAIN at point *

Subroutine for Basic Inversion -"BASINV"

Inputs $\left\{ \begin{array}{l} t_o,\ N,\ T \\ \{yk\},\ w_n,\ \rangle_n \end{array} \right.$

Calculate tk

$\alpha_o\ \beta_o\ \gamma_o$

$\alpha_{Lo}\ \beta_{Lo}\ \gamma_{Lo}$

$\alpha_{Ro}\ \beta_{Ro}\ \gamma_{Ro}$

$x_k\ (k \neq 1,\ k \neq N)$

$x_1,\ x_N$

Outputs $\left\{ \begin{array}{l} t_o,\ N,\ T \\ \{t_k,\ x_k\} \end{array} \right.$

Symbolically:

$$[\, t_o,\ N,\ T,\ t_k,\ x_k \,] = \text{BASINV}\ [\, t_o,\ N,\ T,\ yk,\ w_n\ ,\ \rangle_n \,]$$

Subroutine for Interpolation - "INTERP"

Inputs t_{so}, N_s, T_s

$\{\hat{y}k\}$

μ, w_n

t_o, T, t_{max}

w_{INT}; optional

Verify: $T_s \leq \pi / (\mu w_n)$

If no: warning "sampling interval too large"

If yes: proceed

$w_{INT} = \mu w_n$, unless input (IWINT) commands

$w_{INT} = \pi / T_s$ (wideband)

N largest integer such that

$t_o + (N-1)T \leq (t_{max}; t_{so} + (N_s-1) T_s)$

$\hat{t}_k = t_{so} + (k-1)T_s$ belongs to $\hat{y}k$

$t_j = t_o + (j-1)T$ belongs to y_j

Interpolate

$$y_j = \sum_{k=1}^{N_s} \hat{y}k \quad \frac{\sin w_{INT} (t_j - \hat{t}_k)}{\frac{\pi}{T_s} (t_j - \hat{t}_k)} \qquad 1 \leq j \leq N$$

Outputs $\left\{ \begin{array}{l} t_o, T, N \\ \{ t_k, yk \} \end{array} \right.$

Symbolically:

$[t_o, T, N, t_k, yk] =$

INTERP $[t_{so}, N_s, T_s, \hat{y}k, \mu, w_n, T, t_o, t_{max}, w_{INT}]$

RAD 2-0963
9-63

DIGITAL COMPUTER INPUT REQUEST FORM	PROBLEM NO: 2894	PROGRAMMER: D. Gootkind
	TITLE: Inversion Algorithm for Filters	

MEMO NO.	SECTION NO.	WORK ORDER NO.	(E240 USE ONLY)	REQUESTED BY:	EXT.	EST. TIME	PAGE 1 OF 5 PAGES

*NS _____ TS _____ *NMU _____ *ICLASS _____

*NØPT1 _____ *NPLØT _____ *ISTØP _____ TS0 _____

T0(1) _____ KGAIN _____ TMAX(2) _____ ALPHA(3) _____

*IWINT _____ EBY _____ HBY _____ *NTCH _____

WN _____ ZETAN _____

YBK _____ _____ _____ _____ _____ _____ _____ _____ _____ _____

_____ _____ _____ _____ _____ _____ _____ _____ _____ _____

_____ _____ _____ _____ _____ _____ _____ _____ _____ _____

_____ _____ _____ _____ _____ _____ _____ _____ _____ _____

_____ _____ _____ _____ _____ _____ _____ _____ _____ _____

MU _____ _____ _____ _____ _____ _____ _____ _____ _____ _____

*NT _____

TCH _____ _____ _____ _____ _____ _____ _____ _____ _____ _____

T _____ _____ _____ _____ _____ _____ _____ _____ _____ _____

T1 _____ _____ _____ _____ _____ _____ _____ _____ _____ _____

T2 _____ _____ _____ _____ _____ _____ _____ _____ _____ _____

*NT1 _____ *NT2 _____

T1CH _____ _____ _____ _____ _____ _____ _____ _____ _____ _____

T2CH _____ _____ _____ _____ _____ _____ _____ _____ _____ _____

WØR _____ ZETAØR _____ WA _____ ZETAA _____

WB _____ ZETAB _____ Y0(4) _____ Y0D(5) _____

INPUT SHEETS FOR DIGITAL INVERSION PROGRAM

* Takes integer value

(1) Preset to TS0

(2) Preset to TS0 + (NS - 1)*TS

(3) Preset to 0.2

(4) Preset to 0.0

(5) Preset to 0.0

DESCRIPTION OF INPUT

Input Common to Classes CA , CB , CC

*NS	Number of points of Y (500 max.)
TS	Time spacing of points of Y
*NMU	Number of values of μ (10 max.)
*ICLASS	Values of 1, 2, 3 choose CA, CB, CC respectively
*NØPT1	Value 1 allows program to choose its own time spacing; value 2 imposes choice of spacing by user
*NPLØT	Value 1 allows for plotting; value 2, no plotting
*ISTØP	Value 0 bypasses determination of (KX); value 1 calculates (KX) . Values 0 and 1 both allow for error calculations
TS0	Initial value of time for Y
T0	Initial value of time for (KX) (preset to TS0)
KGAIN	Value of gain K of instrument
TMAX	Value of maximum time for (KX) (preset by program)
ALPHA	Value of α (preset to 0.2)
*IWINT	Value 1 allows for narrow band , value 2 allows for wide band-
EBY	Value of $\hat{\mathcal{E}}_y$
HBY	Value of $\hat{h}_y$
*NTCH	Number of chosen values of spacing imposed by user (10 max.)
YBK	Values of Y (500 max.)

WN	Value of ω_n
ZETAN	Value of ζ_n
MU	Values of μ (10 max.)

Input for Class CA Only

TCH	Values of chosen time spacing imposed by user (10 max.)
*NT	Number of values of T (10 max.)
T	Values of time spacing , T (10 max.)

Input Common to Classes CB , CC

T1	Values of T_1 (10 max.)
T2	Values of T_2 (10 max.)
*NT1	Number of values of T_1 (10 max.)
*NT2	Number of values of T_2 (10 max.)
T1CH	Values of T_{1ch} imposed by user (10 max.)
T2CH	Values of T_{2ch} imposed by user (10 max.)

Input for Class CB Only

WØR	Value of ω_{or}
ZETAØR	Value of ζ_{or}

Input for Class CC Only

WA	Value of ω_a
ZETAA	Value of ζ_a

WB	Value of ω_b
ZETAB	Value of ζ_b
Y0	Value of Y_o (preset to 0.0)
Y0D	Value of $\dot{Y}_o$ (preset to 0.0)

* Must be integer

Warnings

(1) $TS0 < T0 < TMAX$

(2) Program stops if number of interpolated points exceeds 500 and prints "Number of points are too great"

(3) MU, WN, WØR, WA, and WB must be positive and have exponents between -3 and +10 in order for the plotting routines to work.

6.4 Illustrative Examples

First Example:

Take the accelerometer with w_n = 850 rad/sec = 0.85 rad/msec, γ_n = 0.55; triangular input. The computer plotting routine plots the transducer output ($\hat{y}$) and the reconstructed input (x). The plotter also connects x-samples by straight lines, to facilitate reading. The true input has been added (by hand) to provide an immediate criterion of the quality of the reconstruction. All necessary parameter values are given in the computer printout: among them, bandwidth μ = 2, error $\hat{h}_y$ = 0.025, sampling time T_s = 0.5 ms.

Figures 6-4 and 6-5 give the reconstruction for smallest total error $\mathcal{E}_x$, corresponding with T = 0.6 msec; for interpolation with $w_{INT} = \mu\ w_n$ = 1,700 rad/sec (narrowband) and $w_{INT} = \frac{\pi}{T_s}$ = 6,280 rad/sec (wideband) respectively. Figure 6-6 shows the reconstruction for $T = T_s$ avoiding interpolation. All three results are quite acceptable, indicating that in this case the bandwidth was properly estimated.

Second Example:

This is a Giannini pressure transducer with ω_n = 1,300 rad/sec, γ_n = 0.2, w_{or} = 1,300 rad/sec, γ_{or} = 0.3, the bandwidth factor μ is taken as either 1 or 2. Results are shown in Figures 6-7 and 6-8 for T_1 and T_2 selected for minimum total error. Clearly, μ = 1 is a better choice here; the edge effect is very noticeable at the right end. Figure 6-9 pictures the reconstruction for $T_1 = T_2 = T_s$ = 0.625 msec, avoiding interpolation: obviously no edge effect appears.

Third Example:

This deals with a Bourns pressure transducer, together with its T-tubing.

One has w_n = 400 rad/sec, w_a = 1,000 rad/sec, w_b = 200 rad/sec,
γ_n = 0.3, γ_a = 0.8, γ_b = 0.8

T_s = 1 msec, $\hat{h}_y$ = 0.015, μ = 1 and 2, y_o = 1.0 (initial value)

The results for the total solution (forced plus free) x are shown in Figures 6-10 and 6-11 for μ = 1 and 2 respectively, with narrowband interpolation ($w_{INT} = \mu\ w_b$). There is a very strong edge effect. Figure 6-12 gives a much better reconstruction with $w_{INT} = \pi / T_s$ (wide band interpolation) indicating that μ should be chosen larger here than 2.0.

NOTE:

All examples show that the calculated error bound is indeed quite conservative, as predicted. However, the choice of spacing intervals found by minimizing this worst error is quite good and this is the main purpose of the error calculation. It would be possible to find smaller error estimates by use of statistical methods. However, to maintain generality, a non-statistical error calculation was preferred here. This made possible avoidance of additional hypotheses about signal and error distribution.

The computer printout corresponding to the plots follows after Figure 6-12.

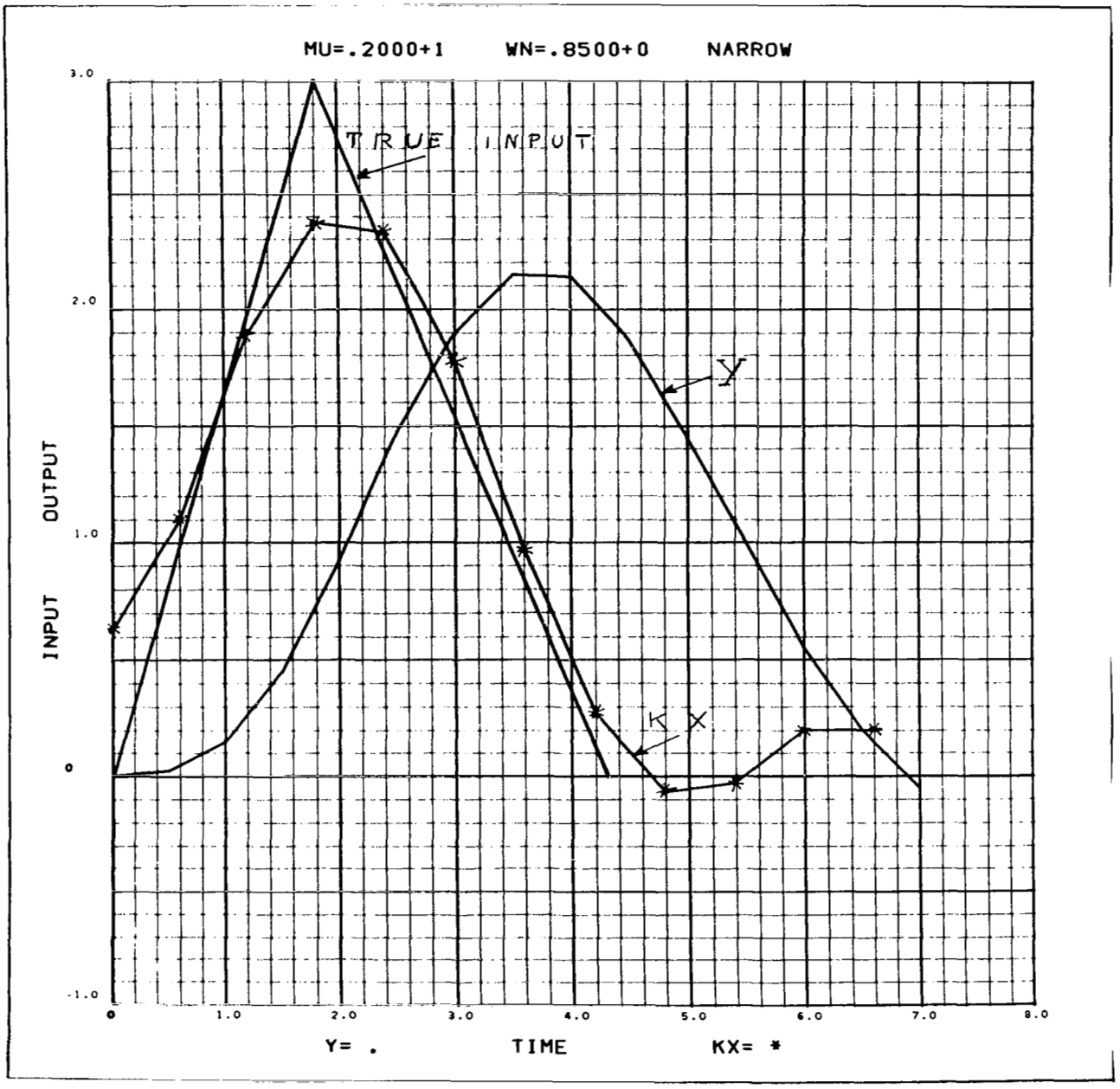
MU=.2000+1
WN=.8500+0
NARROW
TRUE INPUT
Y
KX
INPUT OUTPUT
3.0
2.0
1.0
0
-1.0
0
1.0
2.0
3.0
4.0
5.0
6.0
7.0
8.0
Y= .
TIME
KX= *

Figure 6-4

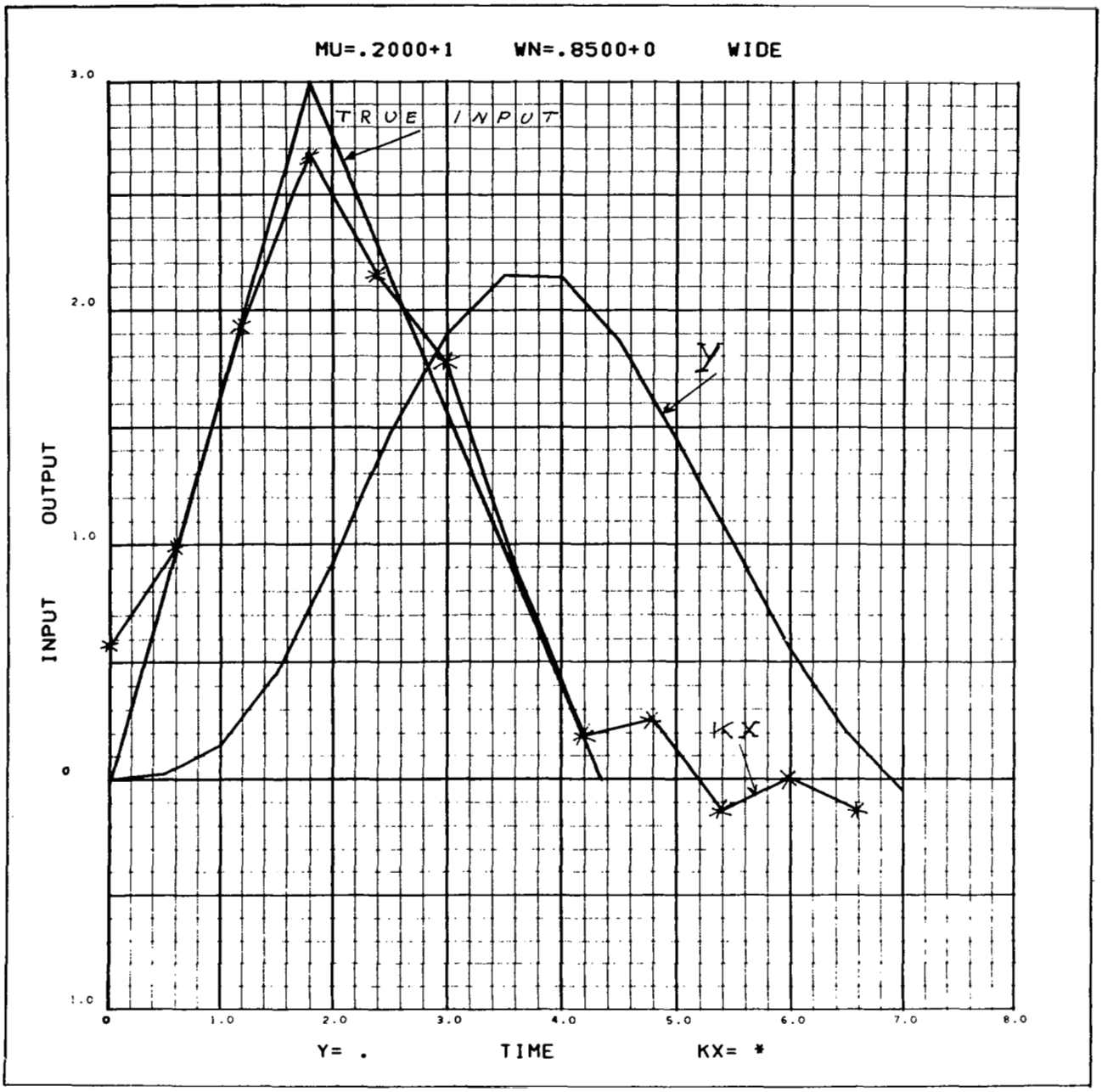
MU=.2000+1
WN=.8500+0
WIDE
TRUE INPUT
Y
KX
INPUT OUTPUT
3.0
2.0
1.0
0
1.0
0
1.0
2.0
3.0
4.0
5.0
6.0
7.0
8.0
Y= .
TIME
KX= *

Figure 6-5

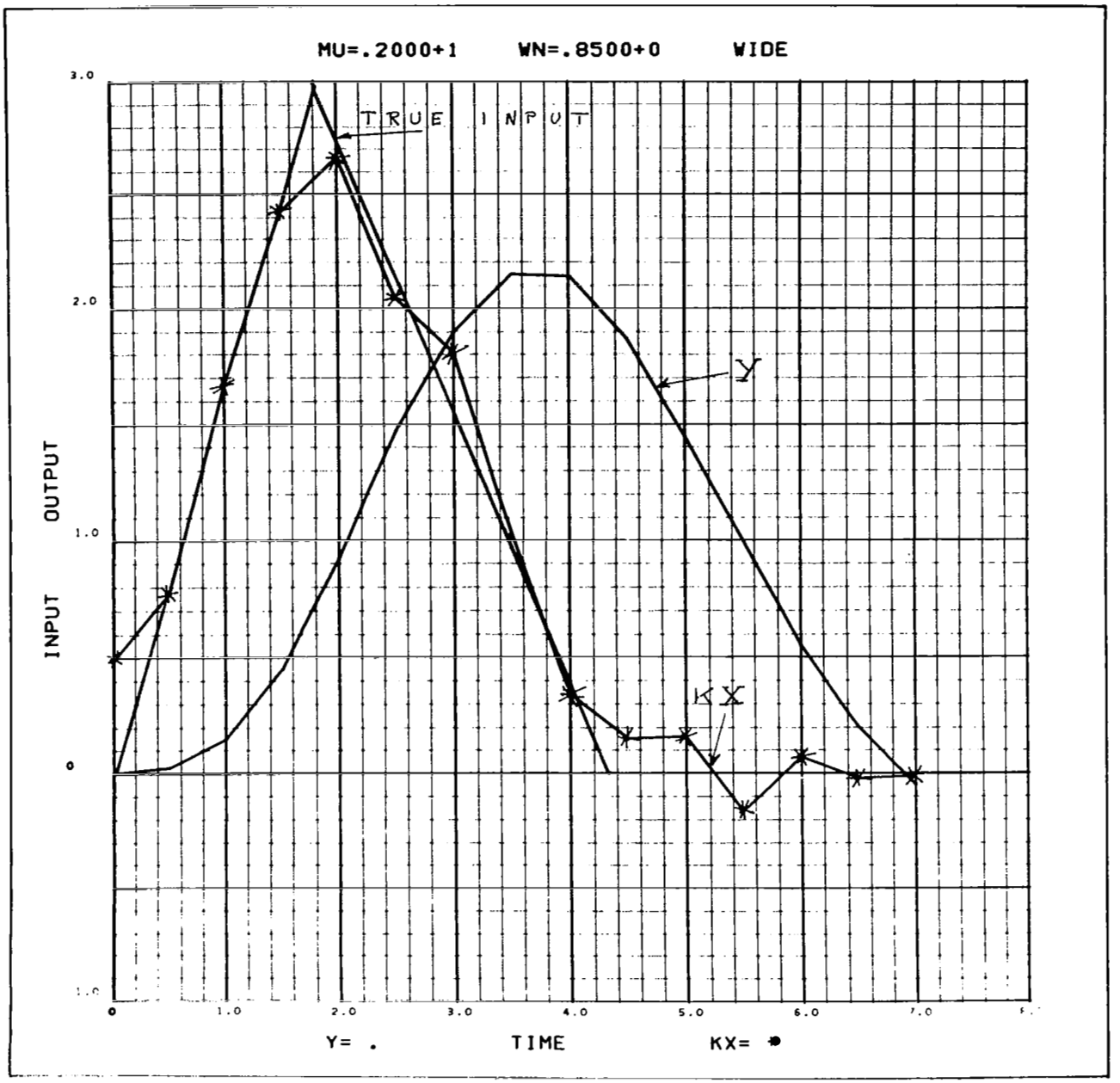
MU=.2000+1
WN=.8500+0
WIDE
TRUE INPUT
Y
KX
INPUT OUTPUT
3.0
2.0
1.0
0
1.0
0
1.0
2.0
3.0
4.0
5.0
6.0
7.0
Y= .
TIME
KX= *

Figure 6-6

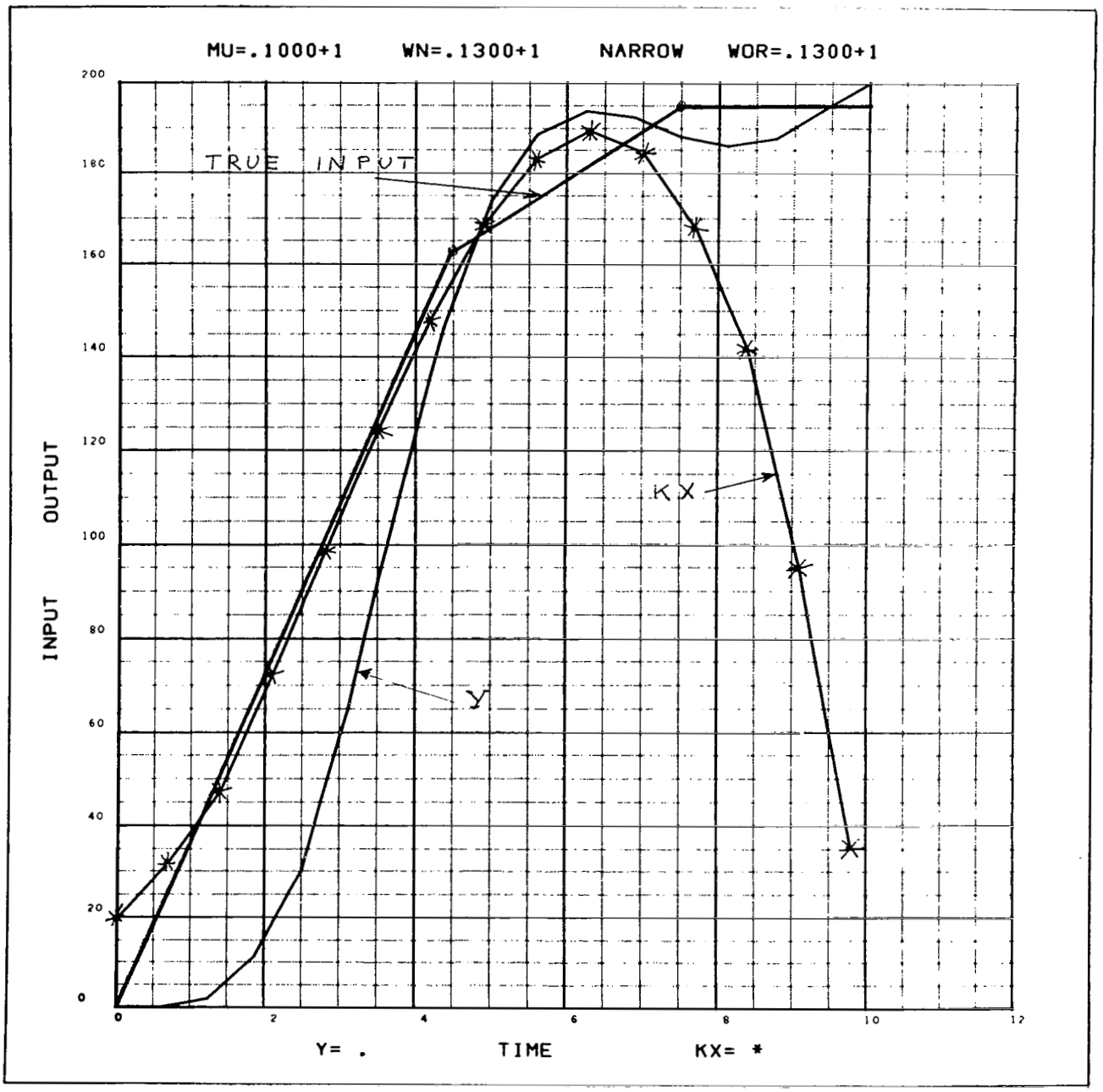
MU=.1000+1
WN=.1300+1
NARROW
WOR=.1300+1
TRUE INPUT
KX
Y
INPUT OUTPUT
200
180
160
140
120
100
80
60
40
20
0
0
2
4
6
8
10
12
Y= .
TIME
KX= *

Figure 6-7

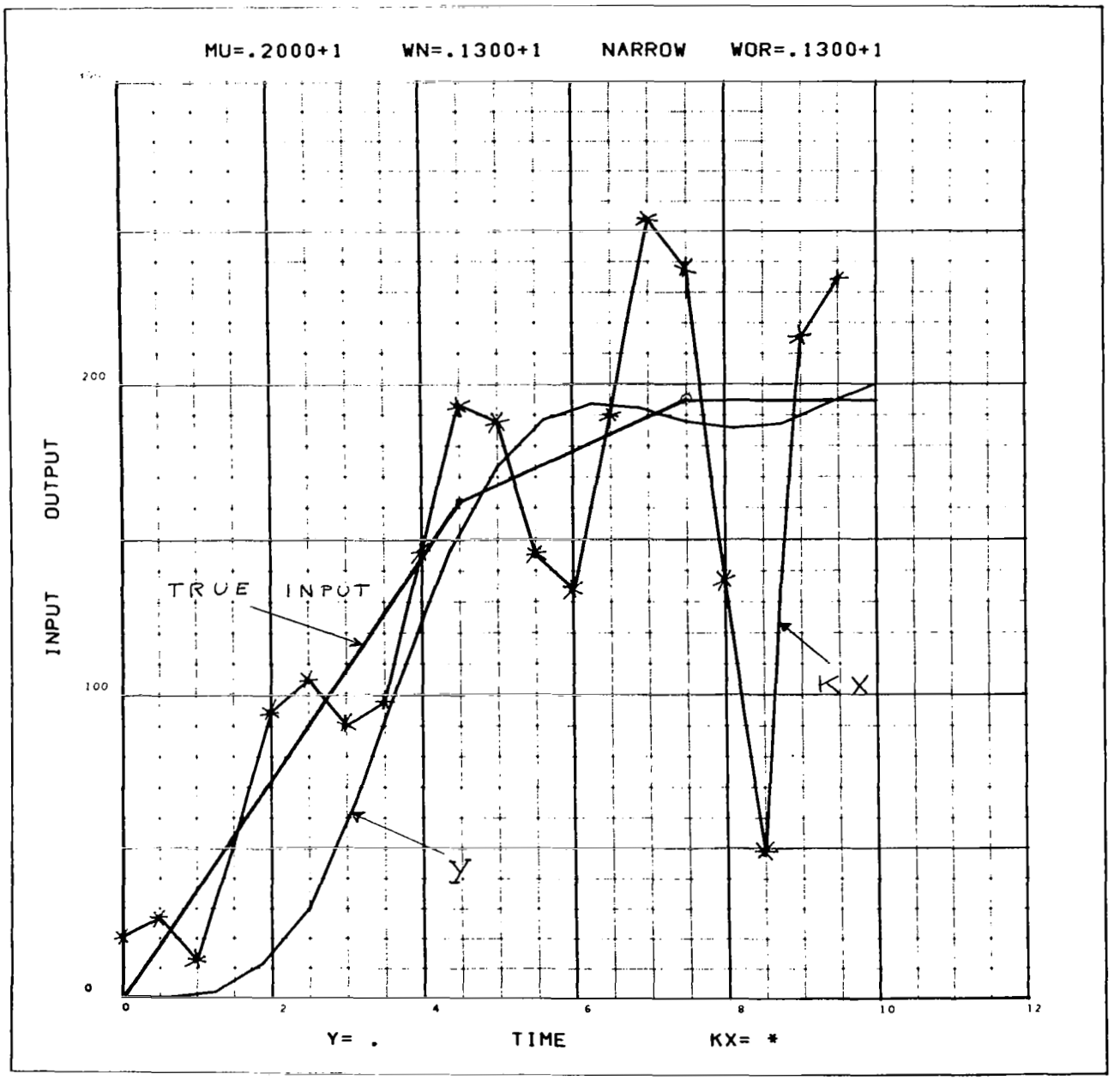
MU=.2000+1
WN=.1300+1
NARROW
WOR=.1300+1
INPUT OUTPUT
200
100
0
TRUE INPUT
KX
Y
0
2
4
6
8
10
12
Y= .
TIME
KX= *

Figure 6-8

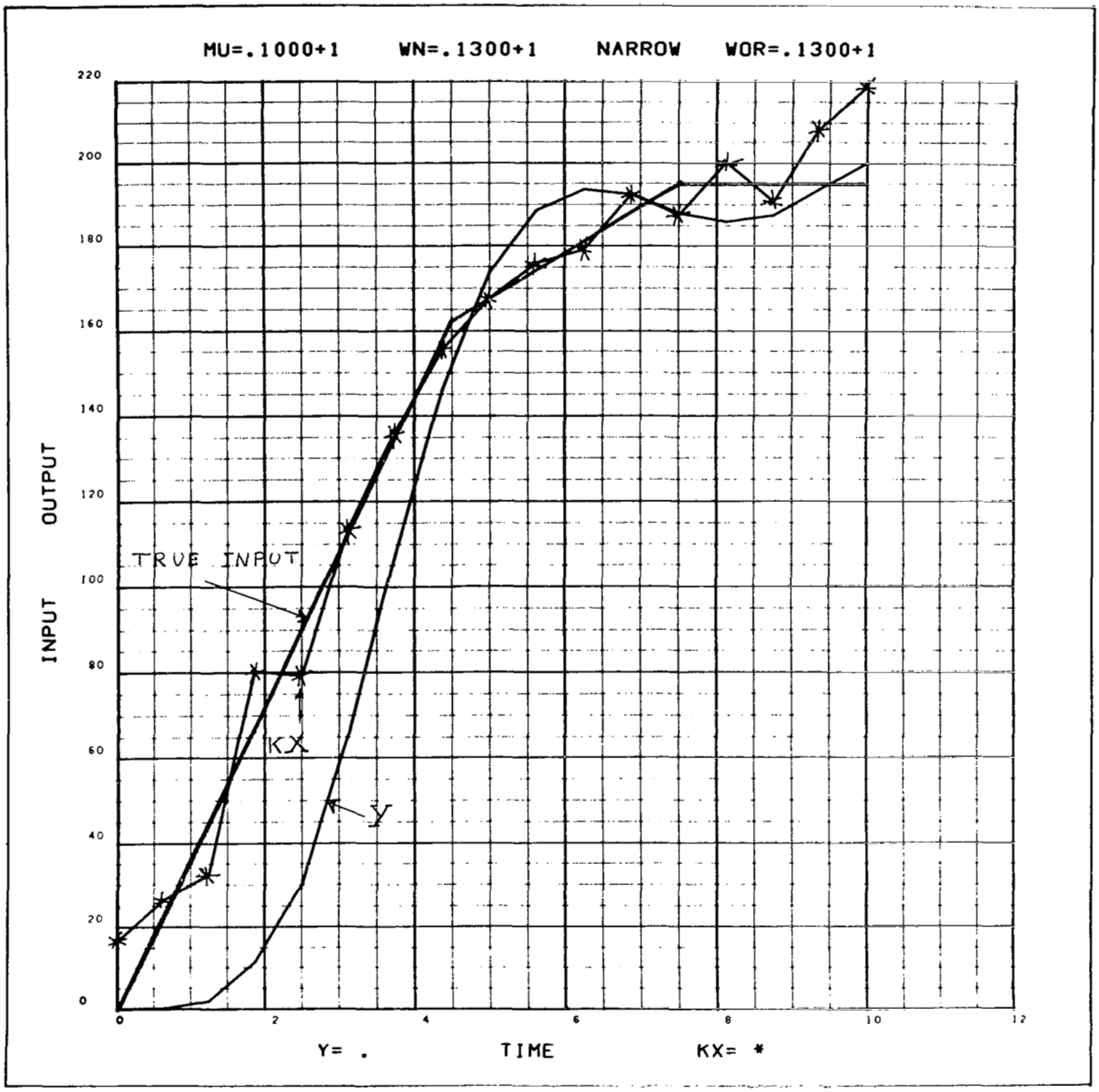
MU=.1000+1
WN=.1300+1
NARROW
WOR=.1300+1
INPUT OUTPUT
TRUE INPUT
KX
Y
Y= .
TIME
KX= *
0
20
40
60
80
100
120
140
160
180
200
220
0
2
4
6
8
10
12

Figure 6-9

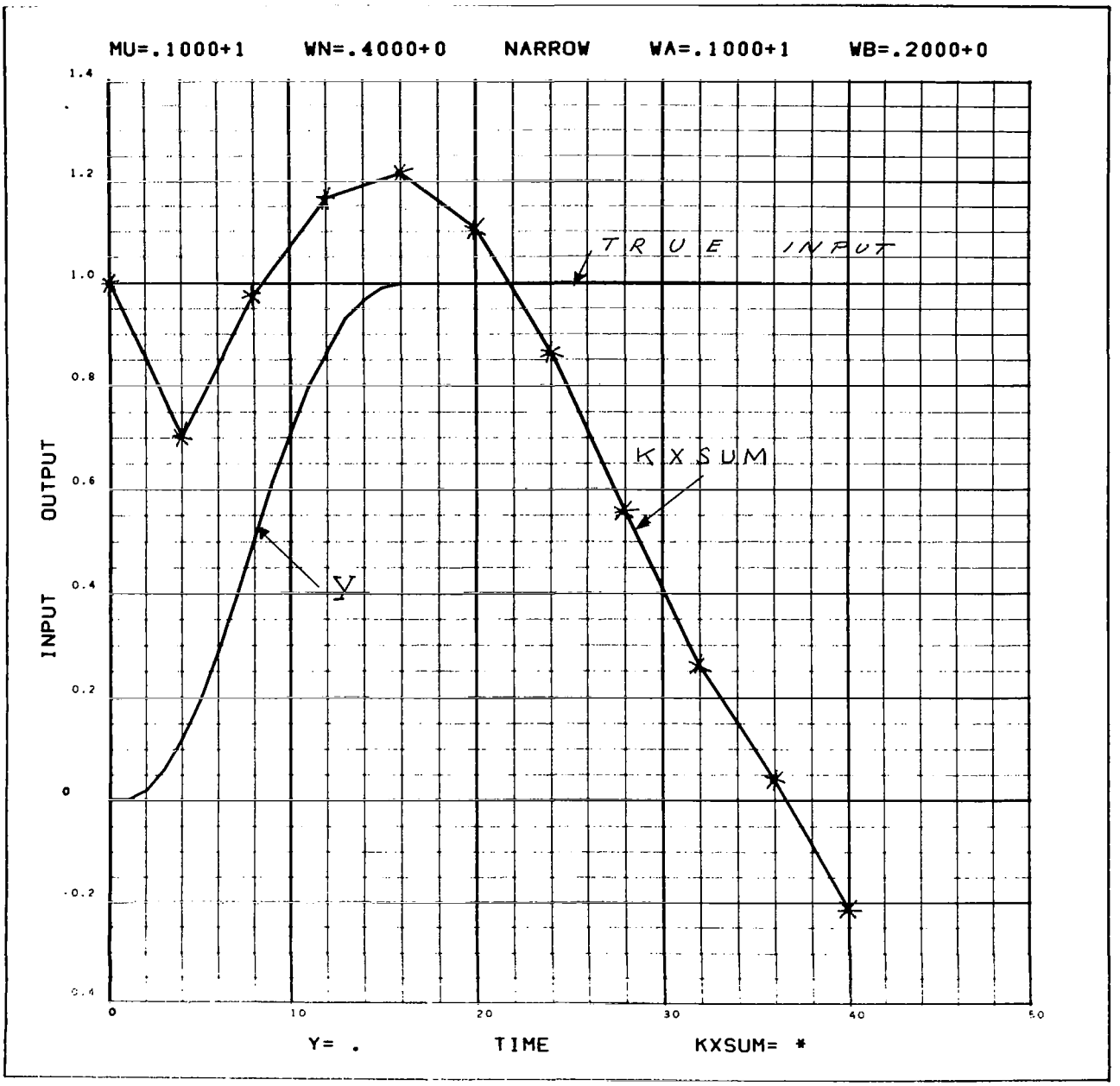
MU=.1000+1
WN=.4000+0
NARROW
WA=.1000+1
WB=.2000+0
TRUE INPUT
KXSUM
Y
OUTPUT
INPUT
1.4
1.2
1.0
0.8
0.6
0.4
0.2
0
-0.2
-0.4
0
10
20
30
40
50
Y= .
TIME
KXSUM= *

Figure 6-10

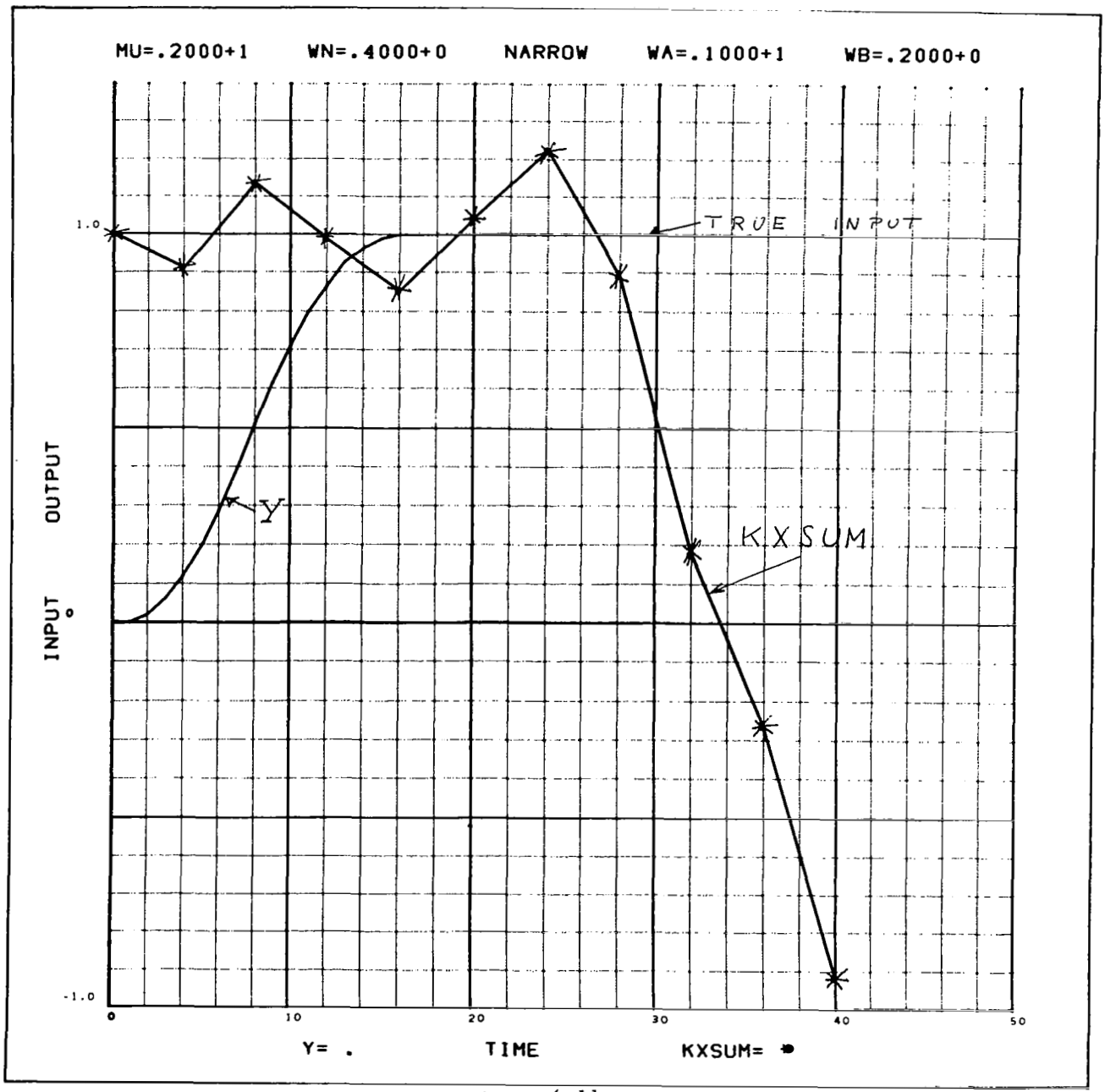
MU=.2000+1
WN=.4000+0
NARROW
WA=.1000+1
WB=.2000+0
TRUE INPUT
Y
KXSUM
INPUT OUTPUT
1.0
-1.0
0
10
20
30
40
50
Y= .
TIME
KXSUM= *

Figure 6-11

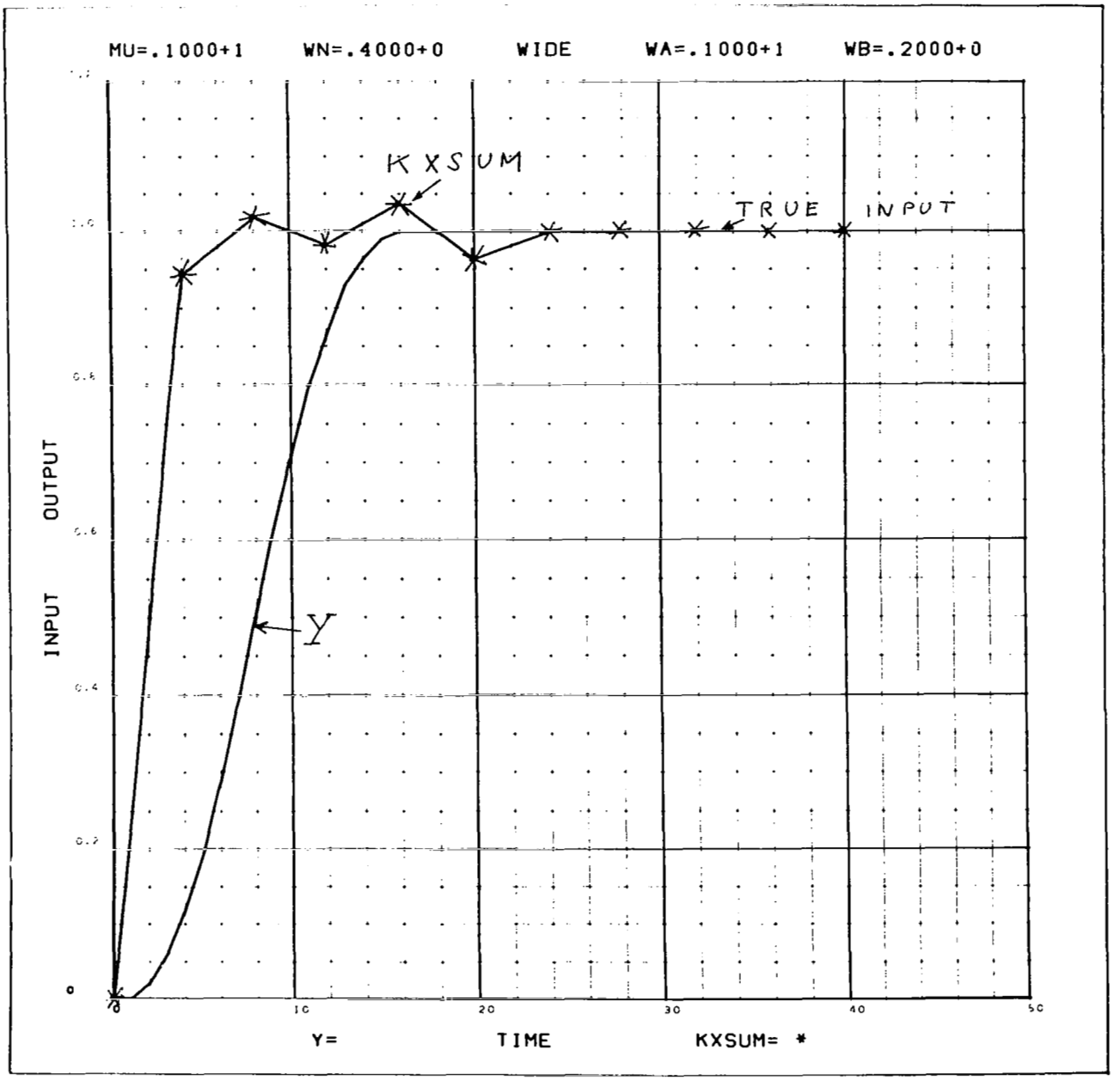
MU=.1000+1
WN=.4000+0
WIDE
WA=.1000+1
WB=.2000+0
KXSUM
TRUE INPUT
Y
OUTPUT
INPUT
0
0.2
0.4
0.6
1.0
10
20
30
40
50
Y=
TIME
KXSUM= *

Figure 6-12

```
INPUT CARDS READ                                                    14.44.22.05
DATA*   NS 15 TS 0.5D0 NMU 1 ICLASS 1 NOPT1 1 ISTOP 0 TS0 0.0D0 TCH 0.5D0
DATA*   NTCH 1 IWINT 1 KGAIN 1.0D0 EBY 0.0D0 HBY 0.025D0 YBK 0.0D0 0.025D0
DATA*   0.15D0 0.45D0 0.925D0 1.475D0 1.90D0 2.15D0 2.14D0 1.87D0 1.45D0
DATA*   1.0D0 0.55D0 0.20D0 -0.05D0 MU 2.0D0 NT 10 T 0.1D0(0.1D0)1.0D0
DATA*   WN 0.850D0 ZETAN 0.55D0 NPLOT 1
DATA*1

                    T0 LIES IN THE INTERVAL (TSC,TMAX)

        MU = 0.200000D 01     T = 0.100000D 00     EX =  0.13829D 02
        MU = 0.200000D 01     T = 0.200000D 00     EX =  0.34862D 01
        MU = 0.200000D 01     T = 0.300000D 00     EX =  0.16271D 01
        MU = 0.200000D 01     T = 0.400000D 00     EX =  0.10418D 01
        MU = 0.200000D 01     T = 0.500000D 00     EX =  0.84104D 00
        MU = 0.200000D 01     T = 0.600000D 00     EX =  0.80447D 00
        MU = 0.200000D 01     T = 0.700000D 00     EX =  0.85544D 00
        MU = 0.200000D 01     T = 0.800000D 00     EX =  0.96083D 00
        MU = 0.200000D 01     T = 0.900000D 00     EX =  0.11037D 01
        MU = 0.200000D 01     T = 0.100000D 01     EX =  0.12741D 01

        T0 = 0.0              TF = 0.600000D 00    N =12    MU = 0.200000D 01

              DTLEFT =-0.500000D 00    DTRIGHT =-0.47878D 00

        TSUB( 1) = 0.0              X = 0.62673D 00
        TSUB( 2) = 0.600000D 00     X = 0.11016D 01
        TSUB( 3) = 0.120000D 01     X = 0.18856D 01
        TSUB( 4) = 0.180000D 01     X = 0.23769D 01
        TSUB( 5) = 0.240000D 01     X = 0.23348D 01
        TSUB( 6) = 0.300000D 01     X = 0.17743D 01
        TSUB( 7) = 0.360000D 01     X = 0.96412D 00
        TSUB( 8) = 0.420000D 01     X = 0.26782D 00
        TSUB( 9) = 0.480000D 01     X =-0.65515D-01
        TSUB(10) = 0.540000D 01     X =-0.24631D-01
        TSUB(11) = 0.600000D 01     X = 0.19974D 00
        TSUB(12) = 0.660000D 01     X = 0.20307D 00
```

FOR FIG 6-4

```
INPUT CARDS READ                                                14.44.26.01
DATA*    IWINT 2
DATA*1

                    TO LIES IN THE INTERVAL (TSO,TMAX)

      MU = 0.20000D 01     T = 0.10000D 00     EX =  0.13829D 02
      MU = 0.20000D 01     T = 0.20000D 00     EX =  0.34862D 01
      MU = 0.20000D 01     T = 0.30000D 00     EX =  0.16271D 01
      MU = 0.20000D 01     T = 0.40000D 00     EX =  0.10418D 01
      MU = 0.20000D 01     T = 0.50000D 00     EX =  0.84104D 00
      MU = 0.20000D 01     T = 0.60000D 00     EX =  0.80447D 00
      MU = 0.20000D 01     T = 0.70000D 00     EX =  0.85544D 00
      MU = 0.20000D 01     T = 0.80000D 00     EX =  0.96083D 00
      MU = 0.20000D 01     T = 0.90000D 00     EX =  0.11037D 01
      MU = 0.20000D 01     T = 0.10000D 01     EX =  0.12741D 01

TO = 0.0          TF = 0.60000D 00     N =12     MU = 0.20000D 01

          DTLEFT =-0.50000D 00     DTRIGHT =-0.47878D 00

TSUB( 1) = 0.0                X = 0.56901D 00
TSUB( 2) = 0.60000D 00        X = 0.98747D 00
TSUB( 3) = 0.12000D 01        X = 0.19343D 01
TSUB( 4) = 0.18000D 01        X = 0.26807D 01
TSUB( 5) = 0.24000D 01        X = 0.21464D 01
TSUB( 6) = 0.30000D 01        X = 0.17655D 01
TSUB( 7) = 0.36000D 01        X = 0.90034D 00
TSUB( 8) = 0.42000D 01        X = 0.18293D 00
TSUB( 9) = 0.48000D 01        X = 0.25484D 00
TSUB(10) = 0.54000D 01        X =-0.13549D 00
TSUB(11) = 0.60000D 01        X = 0.43067D-02
TSUB(12) = 0.66000D 01        X =-0.13669D 00
```

FOR FIG. 6-5

```
INPUT CARDS READ                                                14.44.26.61
DATA*    NOPT1 2
DATA*1

                    TO LIES IN THE INTERVAL (TSC,TMAX)

      MU = 0.200000D 01     T = 0.100000D 00     EX = 0.13829D 02
      MU = 0.200000D 01     T = 0.200000D 00     EX = 0.34862D 01
      MU = 0.200000D 01     T = 0.300000D 00     EX = 0.16271D 01
      MU = 0.200000D 01     T = 0.400000D 00     EX = 0.10418D 01
      MU = 0.200000D 01     T = 0.500000D 00     EX = 0.84104D 00
      MU = 0.200000D 01     T = 0.600000D 00     EX = 0.80447D 00
      MU = 0.200000D 01     T = 0.700000D 00     EX = 0.85544D 00
      MU = 0.200000D 01     T = 0.800000D 00     EX = 0.96083D 00
      MU = 0.200000D 01     T = 0.900000D 00     EX = 0.11037D 01
      MU = 0.200000D 01     T = 0.100000D 01     EX = 0.12741D 01


      TC = 0.0          TF = 0.500000D 00     N =15     MU = 0.200000D 01

      TSUB( 1) = 0.0                X = 0.48893D 00
      TSUB( 2) = 0.500000D 00       X = 0.77275D 00
      TSUB( 3) = 0.100000D 01       X = 0.16689D 01
      TSUB( 4) = 0.150000D 01       X = 0.24218D 01
      TSUB( 5) = 0.200000D 01       X = 0.26667D 01
      TSUB( 6) = 0.250000D 01       X = 0.20447D 01
      TSUB( 7) = 0.300000D 01       X = 0.18047D 01
      TSUB( 8) = 0.350000D 01       X = 0.10211D 01
      TSUB( 9) = 0.400000D 01       X = 0.33820D 00
      TSUB(10) = 0.450000D 01       X = 0.14661D 00
      TSUB(11) = 0.500000D 01       X = 0.15803D 00
      TSUB(12) = 0.550000D 01       X =-0.16471D 00
      TSUB(13) = 0.600000D 01       X = 0.68339D-01
      TSUB(14) = 0.650000D 01       X =-0.22837D-01
      TSUB(15) = 0.700000D 01       X =-0.14014D-01
```

FOR FIG. 6-6

```
 INPUT CARDS READ                                                    14.44.27.09     3/03/70
 DATA*   NS 17 TS 0.625D0 NMU 2 ICLASS 2 NCPT1 1 ISTOP 0 WOR 1.3D0 KGAIN 1.0D0          *DATA
 DATA*   ZETAOR 0.3D0 NT1 3 NT2 3 NTCH 1 T1CH 0.625D0 T2CH 0.625D0 IWINT 1              *DATA
 DATA*   TSC 0.0D0 EBY 0.0D0 HBY 0.625D0 YBK 0.0D0 0.0D0 1.88D0 11.25D0 30.0D0         *DATA
 DATA*   65.0D0 107.5D0 146.25D0 173.75D0 188.75D0 193.75D0 192.5D0 188.0D0            *DATA
 DATA*   186.0D0 187.5D0 193.75D0 200.0D0 MU 1.0D0 2.0D0 WN 1.3D0 ZETAN 0.2D0         *DATA
 DATA*   T1 0.5D0 0.625D0 0.7D0 T2 0.5D0 0.625D0 0.7D0                               *DATA
 DATA*1                                                                              *DATA
```

TC LIES IN THE INTERVAL (TSC,TMAX)

MU = 0.100000D 01	T1 = 0.500000D 00	T2 = 0.500000D 00	EX = 0.55558D 02
MU = 0.100000D 01	T1 = 0.500000D 00	T2 = 0.625000D 00	EX = 0.40801D 02
MU = 0.100000D 01	T1 = 0.500000D 00	T2 = 0.700000D 00	EX = 0.36584D 02
MU = 0.100000D 01	T1 = 0.625000D 00	T2 = 0.500000D 00	EX = 0.40150D 02
MU = 0.100000D 01	T1 = 0.625000D 00	T2 = 0.625000D 00	EX = 0.32654D 02
MU = 0.100000D 01	T1 = 0.625000D 00	T2 = 0.700000D 00	EX = 0.31055D 02
MU = 0.100000D 01	T1 = 0.700000D 00	T2 = 0.500000D 00	EX = 0.35481D 02
MU = 0.100000D 01	T1 = 0.700000D 00	T2 = 0.625000D 00	EX = 0.30603D 02
MU = 0.100000D 01	T1 = 0.700000D 00	T2 = 0.700000D 00	EX = 0.29947D 02

MU = 0.200000D 01	T1 = 0.500000D 00	T2 = 0.500000D 00	EX = 0.22285D 03
MU = 0.200000D 01	T1 = 0.500000D 00	T2 = 0.625000D 00	EX = 0.25306D 03
MU = 0.200000D 01	T1 = 0.500000D 00	T2 = 0.700000D 00	EX = 0.27895D 03
MU = 0.200000D 01	T1 = 0.625000D 00	T2 = 0.500000D 00	EX = 0.24894D 03
MU = 0.200000D 01	T1 = 0.625000D 00	T2 = 0.625000D 00	EX = 0.28641D 03
MU = 0.200000D 01	T1 = 0.625000D 00	T2 = 0.700000D 00	EX = 0.31491D 03
MU = 0.200000D 01	T1 = 0.700000D 00	T2 = 0.500000D 00	EX = 0.27215D 03
MU = 0.200000D 01	T1 = 0.700000D 00	T2 = 0.625000D 00	EX = 0.31224D 03
MU = 0.200000D 01	T1 = 0.700000D 00	T2 = 0.700000D 00	EX = 0.34168D 03

TC = 0.0 TF1 = 0.700000D 00 TF2 = 0.700000D 00 N =15 MU = 0.100000D 01

TSUB(1) = 0.0 X = 0.19628D 02
TSUB(2) = 0.700000D 00 X = 0.31980D 02
TSUB(3) = 0.140000D 01 X = 0.47203D 02
TSUB(4) = 0.210000D 01 X = 0.72317D 02
TSUB(5) = 0.280000D 01 X = 0.99599D 02
TSUB(6) = 0.350000D 01 X = 0.12431D 03
TSUB(7) = 0.420000D 01 X = 0.14812D 03
TSUB(8) = 0.490000D 01 X = 0.16850D 03
TSUB(9) = 0.560000D 01 X = 0.18318D 03
TSUB(10) = 0.630000D 01 X = 0.18935D 03
TSUB(11) = 0.700000D 01 X = 0.18456D 03
TSUB(12) = 0.770000D 01 X = 0.16807D 03
TSUB(13) = 0.840000D 01 X = 0.14167D 03
TSUB(14) = 0.910000D 01 X = 0.94873D 02
TSUB(15) = 0.980000D 01 X = 0.35170D 02

FOR FIG 6-7

TC = 0.0 TF1 = 0.500000D 00 TF2 = 0.500000D 00 N =20 MU = 0.200000D 01

TSUB(1) = 0.0 X = 0.20344D 02
TSUB(2) = 0.500000D 00 X = 0.26413D 02
TSUB(3) = 0.100000D 01 X = 0.12526D 02
TSUB(4) = 0.150000D 01 X = 0.51425D 02
TSUB(5) = 0.200000D 01 X = 0.94515D 02
TSUB(6) = 0.250000D 01 X = 0.10458D 03
TSUB(7) = 0.300000D 01 X = 0.89950D 02
TSUB(8) = 0.350000D 01 X = 0.97352D 02
TSUB(9) = 0.400000D 01 X = 0.14608D 03
TSUB(10) = 0.450000D 01 X = 0.19357D 03
TSUB(11) = 0.500000D 01 X = 0.18822D 03
TSUB(12) = 0.550000D 01 X = 0.14454D 03
TSUB(13) = 0.600000D 01 X = 0.13371D 03
TSUB(14) = 0.650000D 01 X = 0.19005D 03
TSUB(15) = 0.700000D 01 X = 0.25413D 03
TSUB(16) = 0.750000D 01 X = 0.23759D 03
TSUB(17) = 0.800000D 01 X = 0.13680D 03
TSUB(18) = 0.850000D 01 X = 0.48147D 02
TSUB(19) = 0.900000D 01 X = 0.21533D 03
TSUB(20) = 0.950000D 01 X = 0.23426D 03

FOR FIG. 6-8

INPUT CARDS READ 14.44.28.69 3/03/70
DATA* NOPT1 2 *DATA
DATA*1 *DATA

TC LIES IN THE INTERVAL (TSC,TMAX)

MU = 0.100000D 01 T1 = 0.500000D 00 T2 = 0.500000D 00 EX = 0.55558D 02
MU = 0.100000D 01 T1 = 0.500000D 00 T2 = 0.625000D 00 EX = 0.40801D 02
MU = 0.100000D 01 T1 = 0.500000D 00 T2 = 0.700000D 00 EX = 0.36584D 02
MU = 0.100000D 01 T1 = 0.625000D 00 T2 = 0.500000D 00 EX = 0.40150D 02
MU = 0.100000D 01 T1 = 0.625000D 00 T2 = 0.625000D 00 EX = 0.32654D 02
MU = 0.100000D 01 T1 = 0.625000D 00 T2 = 0.700000D 00 EX = 0.31055D 02
MU = 0.100000D 01 T1 = 0.700000D 00 T2 = 0.500000D 00 EX = 0.35481D 02
MU = 0.100000D 01 T1 = 0.700000D 00 T2 = 0.625000D 00 EX = 0.30603D 02
MU = 0.100000D 01 T1 = 0.700000D 00 T2 = 0.700000D 00 EX = 0.29947D 02

MU = 0.200000D 01 T1 = 0.500000D 00 T2 = 0.500000D 00 EX = 0.22285D 03
MU = 0.200000D 01 T1 = 0.500000D 00 T2 = 0.625000D 00 EX = 0.25306D 03
MU = 0.200000D 01 T1 = 0.500000D 00 T2 = 0.700000D 00 EX = 0.27895D 03
MU = 0.200000D 01 T1 = 0.625000D 00 T2 = 0.500000D 00 EX = 0.24894D 03
MU = 0.200000D 01 T1 = 0.625000D 00 T2 = 0.625000D 00 EX = 0.28641D 03
MU = 0.200000D 01 T1 = 0.625000D 00 T2 = 0.700000D 00 EX = 0.31491D 03
MU = 0.200000D 01 T1 = 0.700000D 00 T2 = 0.500000D 00 EX = 0.27215D 03
MU = 0.200000D 01 T1 = 0.700000D 00 T2 = 0.625000D 00 EX = 0.31224D 03
MU = 0.200000D 01 T1 = 0.700000D 00 T2 = 0.700000D 00 EX = 0.34168D 03

T0 = 0.0 TF1 = 0.62500D 00 TF2 = 0.62500D 00 N =17 MU = 0.20000D 01

TSUB(1) = 0.0	X = 0.16535D 02	
TSUB(2) = 0.62500D 00	X = 0.26148D 02	
TSUB(3) = 0.12500D 01	X = 0.32335D 02	
TSUB(4) = 0.18750D 01	X = 0.89428D 02	FOR FIG. 6-9
TSUB(5) = 0.25000D 01	X = 0.79202D 02	
TSUB(6) = 0.31250D 01	X = 0.11353D 03	
TSUB(7) = 0.37500D 01	X = 0.13624D 03	
TSUB(8) = 0.43750D 01	X = 0.15560D 03	
TSUB(9) = 0.50000D 01	X = 0.16760D 03	
TSUB(10) = 0.56250D 01	X = 0.17593D 03	
TSUB(11) = 0.62500D 01	X = 0.17935D 03	
TSUB(12) = 0.68750D 01	X = 0.19265D 03	
TSUB(13) = 0.75000D 01	X = 0.18744D 03	
TSUB(14) = 0.81250D 01	X = 0.20026D 03	
TSUB(15) = 0.87500D 01	X = 0.19081D 03	
TSUB(16) = 0.93750D 01	X = 0.20835D 03	
TSUB(17) = 0.10000D 02	X = 0.21905D 03	

```
 INPUT CARDS READ                                                    14.44.31.29     3/03/7
DATA*   NS 41 TS 1.0D0 NMU 2     ICLASS 3 NOPT1 2 ISTOP 0 NT1 1 NT2 1                *DATA
DATA*   ZETAB 0.8D0 WB 0.2D0 IWINT 1 KGAIN 1.0D0 TS0 0.0D0 EBY 0.0D0                *DATA
DATA*   HBY 1.5D-2 YBK 0.0D0 0.0D0 0.02D0 0.06D0 0.12D0 0.195D0 0.29D0              *DATA
DATA*   0.395D0 0.51D0 0.615D0 0.71D0 0.8D0 0.865D0 0.93D0 0.965D0 0.99D0           *DATA
DATA*   YBK(17-41) 1.0D0 MU 1.0D0 2.0D0 NTCH 1 T1CH 2.0D0 T2CH 4.0D0                *DATA
DATA*                                   WN 0.4D0 ZETAN 0.3D0 WA 1.0D0               *DATA
DATA*   ZETAA 0.8D0 Y0 1.0D0 T1 2.0D0 T2 4.0D0                                      *DATA
DATA*1                                                                              *DATA


                    TO LIES IN THE INTERVAL (TS0,TMAX)



          TV = 0.50000D 00

          MU = 0.10000D 01     T1 = 0.20000D 01     T2 = 0.40000D 01     EX = 0.56254D 00


          MU = 0.20000D 01     T1 = 0.20000D 01     T2 = 0.40000D 01     EX = 0.23619D 01
```

```
T0 = 0.0          TF1 = 0.20000D 01     TF2 = 0.40000D 01     N =11

                                                          MU = 1.0
          DTLEFT =-0.10000D 01     DTRIGHT = 0.32441D 01

TSUB( 1) = 0.0                 X = 0.41162D 00
TSUB( 2) = 0.40000D 01         X = 0.70146D 00
TSUB( 3) = 0.80000D 01         X = 0.97652D 00
TSUB( 4) = 0.12000D 02         X = 0.11667D 01
TSUB( 5) = 0.16000D 02         X = 0.12158D 01
TSUB( 6) = 0.20000D 02         X = 0.11057D 01
TSUB( 7) = 0.24000D 02         X = 0.86434D 00
TSUB( 8) = 0.28000D 02         X = 0.55625D 00
TSUB( 9) = 0.32000D 02         X = 0.25945D 00
TSUB(10) = 0.36000D 02         X = 0.38433D-01
TSUB(11) = 0.40000D 02         X =-0.21303D 00

          FORCED SOLUTION

TSUB( 1) = 0.0                 XFREE = 0.58838D 00
TSUB( 2) = 0.40000D 01         XFREE = 0.58960D-03
TSUB( 3) = 0.80000D 01         XFREE =-0.10131D-02
TSUB( 4) = 0.12000D 02         XFREE = 0.59922D-04

TSUB( 5) = 0.16000D 02         XFREE =-0.19190D-05
TSUB( 6) = 0.20000D 02         XFREE = 0.15796D-07
TSUB( 7) = 0.24000D 02         XFREE = 0.22389D-08
TSUB( 8) = 0.28000D 02         XFREE =-0.16084D-09
TSUB( 9) = 0.32000D 02         XFREE = 0.59488D-11
TSUB(10) = 0.36000D 02         XFREE =-0.90375D-13
TSUB(11) = 0.40000D 02         XFREE =-0.44514D-14

TSUB( 1) = 0.0                 XSUM = 0.10000D 01   FOR FIG. 6-10
TSUB( 2) = 0.40000D 01         XSUM = 0.70205D 00
TSUB( 3) = 0.80000D 01         XSUM = 0.97551D 00
TSUB( 4) = 0.12000D 02         XSUM = 0.11668D 01
TSUB( 5) = 0.16000D 02         XSUM = 0.12158D 01
TSUB( 6) = 0.20000D 02         XSUM = 0.11057D 01
TSUB( 7) = 0.24000D 02         XSUM = 0.86434D 00
TSUB( 8) = 0.28000D 02         XSUM = 0.55625D 00
TSUB( 9) = 0.32000D 02         XSUM = 0.25945D 00
TSUB(10) = 0.36000D 02         XSUM = 0.38433D-01
TSUB(11) = 0.40000D 02         XSUM =-0.21303D 00
```

T0 = 0.0 TF1 = 0.20000D 01 TF2 = 0.40000D 01 N =11

MU = 2.0

DTLEFT =-0.10000D 01 DTRIGHT = 0.32441D 01

TSUB(1) = 0.0 X = 0.44209D 00
TSUB(2) = 0.40000D 01 X = 0.90598D 00
TSUB(3) = 0.80000D 01 X = 0.11374D 01
TSUB(4) = 0.12000D 02 X = 0.98710D 00
TSUB(5) = 0.16000D 02 X = 0.85247D 00
TSUB(6) = 0.20000D 02 X = 0.10410D 01
TSUB(7) = 0.24000D 02 X = 0.12234D 01
TSUB(8) = 0.28000D 02 X = 0.89135D 00
TSUB(9) = 0.32000D 02 X = 0.17760D 00
TSUB(10) = 0.36000D 02 X =-0.26593D 00
TSUB(11) = 0.40000D 02 X =-0.91882D 00

FORCED SOLUTION

TSUB(1) = 0.0 XFREE = 0.55791D 00
TSUB(2) = 0.40000D 01 XFREE =-0.16558D-02
TSUB(3) = 0.80000D 01 XFREE =-0.82746D-03
TSUB(4) = 0.12000D 02 XFREE = 0.52495D-04
TSUB(5) = 0.16000D 02 XFREE =-0.17809D-05
TSUB(6) = 0.20000D 02 XFREE = 0.19835D-07
TSUB(7) = 0.24000D 02 XFREE = 0.17666D-08
TSUB(8) = 0.28000D 02 XFREE =-0.13916D-09
TSUB(9) = 0.32000D 02 XFREE = 0.54302D-11
TSUB(10) = 0.36000D 02 XFREE =-0.95223D-13
TSUB(11) = 0.40000D 02 XFREE =-0.32983D-14

TSUB(1) = 0.0 XSUM = 0.10000D 01
TSUB(2) = 0.40000D 01 XSUM = 0.90832D 00
TSUB(3) = 0.80000D 01 XSUM = 0.11366D 01
TSUB(4) = 0.12000D 02 XSUM = 0.98716D 00
TSUB(5) = 0.16000D 02 XSUM = 0.85247D 00
TSUB(6) = 0.20000D 02 XSUM = 0.10410D 01
TSUB(7) = 0.24000D 02 XSUM = 0.12234D 01
TSUB(8) = 0.28000D 02 XSUM = 0.89135D 00
TSUB(9) = 0.32000D 02 XSUM = 0.17760D 00
TSUB(10) = 0.36000D 02 XSUM =-0.26593D 00
TSUB(11) = 0.40000D 02 XSUM =-0.91882D 00

FOR FIG. G-11

```
 INPUT CARDS READ                                                14.44.36.13     3/03/70
 DATA*    IWINT 2 NMU 1                                                          *DATA
 DATA*1                                                                          *DATA


                    TC LIES IN THE INTERVAL (TSO,TMAX)


          TV = 0.100000 01

          MU = 0.100000 01     T1 = 0.200000 01     T2 =  0.400000 01     EX =  0.56254D 00
```

TG = 0.0 TF1 = 0.200000D 01 TF2 = 0.400000D 01 N =11

DTLEFT =-0.100000D 01 DTRIGHT = 0.414710 00 MU=1.0

TSUB(1) = 0.0 X = 0.47119D 00
TSUB(2) = 0.400000D 01 X = 0.95238D 00
TSUB(3) = 0.800000D 01 X = 0.10186D 01
TSUB(4) = 0.120000D 02 X = 0.98256D 00
TSUB(5) = 0.160000D 02 X = 0.10378D 01
TSUB(6) = 0.200000D 02 X = 0.96297D 00
TSUB(7) = 0.240000D 02 X = 0.99853D 00
TSUB(8) = 0.280000D 02 X = 0.10001D 01
TSUB(9) = 0.320000D 02 X = 0.99999D 00
TSUB(10) = 0.360000D 02 X = 0.100000D 01
TSUB(11) = 0.400000D 02 X = 0.100000D 01

FORCED SOLUTION

TSUB(1) = 0.0 XFREE =-0.47119D 00
TSUB(2) = 0.400000D 01 XFREE =-0.86553D-02
TSUB(3) = 0.800000D 01 XFREE = 0.13032D-02
TSUB(4) = 0.120000D 02 XFREE =-0.63963D-04
TSUB(5) = 0.160000D 02 XFREE = 0.16798D-05
TSUB(6) = 0.200000D 02 XFREE = 0.52967D-08
TSUB(7) = 0.240000D 02 XFREE =-0.31095D-08
TSUB(8) = 0.280000D 02 XFREE = 0.17813D-09
TSUB(9) = 0.320000D 02 XFREE =-0.55417D-11
TSUB(10) = 0.360000D 02 XFREE = 0.37171D-13
TSUB(11) = 0.400000D 02 XFREE = 0.697320-14

TSUB(1) = 0.0 XSUM = 0.0
TSUB(2) = 0.400000D 01 XSUM = 0.94372D 00 FOR FIG. 6-12
TSUB(3) = 0.800000D 01 XSUM = 0.10199D 01
TSUB(4) = 0.120000D 02 XSUM = 0.98250D 00
TSUB(5) = 0.160000D 02 XSUM = 0.10378D 01
TSUB(6) = 0.200000D 02 XSUM = 0.96297D 00
TSUB(7) = 0.240000D 02 XSUM = 0.99853D 00
TSUB(8) = 0.280000D 02 XSUM = 0.10001D 01
TSUB(9) = 0.320000D 02 XSUM = 0.99999D 00
TSUB(10) = 0.360000D 02 XSUM = 0.10000D 01
TSUB(11) = 0.400000D 02 XSUM = 0.10000D 01

7. CONCLUSIONS

The results obtained in the present study indicate that it is indeed possible to construct successful models of the transducers and telemetry elements included in this report. Furthermore, it is possible to compute most of the necessary coefficients by performing some relatively simple experiments, some of which may destroy the instruments (as happened with the opened transducers here). However, if one models a large series of similar instruments, destructive testing of one or a few is not objectionable. The determination of some other coefficients required more elaborate tests. In all cases, it is desirable to test the model obtained by means of more complex experiments (as was done here) to verify assumptions and the range of validity. For the individual categories the following more detailed conclusions can be drawn:

A. Rate Gyros

The equations of the complete model, in all generality, are given by:

Mechanical part of gyro: equations (2-6), (2-7), (2-8), (2-5)
Electrical output circuit: equations (2-9) through (2-13)
Bracket: equation (2-14)

The corresponding numerical values of all parameters are listed in Sections 2.2.4 and 2.1.2.

However, the response of the entire gyro system to the principal input (angular rate about the input axis) is very well described by the simple second order linar system equation (2-6), where only the first term on the right hand side is retained, i.e., the mechanical response of the gimbal along the output axis is the dominant element in the gyro model. Therefore, a considerable economy is achieved in describing the gyro behavior mainly in terms of only three parameters:

The steady state gain	(volts per deg/sec)
The natural frequency	$w_{gy}/(2\pi)$
The damping factor	ζ_{gy}

The correlation between actual tests in the laboratory and simulations on the analog computer using the best-fit parameter values in the theoretical model was good, and this for a wide variety of signals being applied to the gyroscopes.

The overall accuracy of the three main parameters is of the order of 5%, while it is somewhat lower (10% to 20%) for the secondary parameters.

B. Accelerometers

The equations of the complete model are given by

Accelerometer only:	Equations (3-2), (3-3)
Bracket:	Equation (3-4)

The corresponding numerical values of all parameters are listed in Sections 3.1.1, 3.1.2, 3.2.1.

The response of the entire system to the principal input (linear acceleration along the sensitive axis) is very well described by a simple second order system (the first term is equation (3-2)), with the same three parameters as for the gyros:

Steady state gain
Natural frequency
Damping factor

The correlation between tests on the transducers and simulations based on the theoretical model was good. The overall accuracy for the three main parameters was of the order of 15%, mainly due to spread among individual instruments of the same category. (See Section 3.2.1). An important, and surprising, result was:

a) The low value of the damping coefficient ζ_n (see again section 3.2.1), as opposed to the higher values obtained by the manufacturer for slower, more "normal" signals. As a consequence, the response of the accelerometers exhibits a marked overshoot for very fast transient input signals.

b) A non-linear effect was observed, where the damping factor ζ depends on the speed of variation of the input signals, with ζ decreasing for faster inputs (due to various non-linear effects in the internal structure, such as eddy-currents, etc).

C. Pressure Transducers

The complete theoretical model is described by:

Equation (4-2) for the Bourdon tubes
Equations (4-3) and (4-4) for the T-tubing (Bourns transducer)

The corresponding numerical values of the parameters are listed in Sections 4.1.1 (Bourdon tubes), 4.1.3 (T-tubing). The agreement is very good between experimental data and theoretical predictions for the Bourdon tubes; this is quite satisfactory as no other resonance calculations were found in a literature search for the Bourdon tubes and the present treatment was a first attempt for this problem.

For practical purposes, a sufficient model was found by cascading two second order systems, equation (4-6), depicting Bourdon tube and orifice effect, or else by an added second order numerator, equation (4-7), to include the effect of the T-tubing. Therefore, modeling is mainly reduced to finding

A steady-state gain
Two or three natural frequencies
Two or three damping factors

Because of interaction, these models are to be taken as a whole, and should not be split (except for purely formal operations).

As for the preceding transducers, the correlation between tests in the laboratory on instruments and analog computer simulations, using best fit parameter values was good. The overall accuracy of the parameter values obtained was of the order of 10% to 20%, again mainly due to spread among individual instruments. As for the accelerometers, a surprising result was the low damping for fast input signals, leading to a considerable overshoot in the responses. This contrasts with the much higher damping obtained by the manufacturer for slower, more regular signals. There was also some non-linear effect in damping (now, with damping somewhat increasing for extremely fast inputs) due to non-linear dissipation mechanics in the turbulent fluid flow.

D. Telemetry

A first observation, substantiated in section 5.1, is that some of the transducers have a bandwidth larger than that of the channel assigned to them (under standard IRIG conditions); this holds typically for the Giannini transducer in channel 11 and the roll rate gyro in channel 7.

The following conclusions can be drawn for the present airborne equipment. The phase-sensitive demodulators, used in conjunction with the rate gyros, are modeled by a second order system, equation (5-1), whose damping factor depends on the polarity of the output voltage swing, due to a biasing by means of resistors.

The demodulators introduce a dynamic lag of roughly the same magnitude as the gyros themselves; and, therefore, their presence is important. There was also a noticeable spread in damping among individual devices.

The subcarrier oscillators are modeled by a linear second order system, equations (5-2) and (5-3). For practical purposes, the lag due to SCO's is small compared with the lag of other components and may be neglected in many cases.

The mixer can be considered as an ideal transducer without any lag. The same remark applies to the transmitter.

For the ground equipment used in this study, the following conclusions hold:

The receiver can be considered as an ideal element without any lag. The 300 kHz and 1MHz tape recorders introduce no discernible distortion for the channels studied here under controlled laboratory conditions.

The bandpass filter is modeled as a critically damped linear second order system, which is the same as a cascade of two identical first order systems (equations (5-5), (5-6), and (5-7)); for practical purposes their dynamic lag is small compared to that of other components when standard filters are used. Further analysis showed a pronounced non-linear dependence of the output on the magnitude of the input, which can be approximately described as a lowering of the damping factor (from unity) when the magnitude of the input swing increases. However, with standard filters, this theoretically interesting non-linear effect is rather unimportant in practice since it is nearly entirely suppressed by the low pass filters because of the relative speed of the bandpass response.

The discriminator, in the narrow sense, is modeled by the linear second order model, equation (5-10); however, its response is so fast that, for practical purposes, the discriminator lag is entirely negligible.

The low pass filters can be modeled as linear third order systems, equations (5-11) and (5-12), of two types (constant amplitude or constant delay), each completely described by a single time constant. These low pass filters are the slowest and hence most important components in the ground equipment; their single parameter is determined numerically with excellent accuracy (better than 5%).

The entire telemetry chain can be modeled simply by cascading individual components, if standard filters are used, because there is no interaction then. The agreement between tests and analog computer simulations is very good.

If very wideband, nonstandard bandpass and low pass filters are used, faster response is obtained; but interference from adjacent channels appears, as discussed in section 5.11 with a theoretical explanation.

Power interruptions can create traces resembling useful signals; therefore, one has to monitor different channels as a help in locating power failures.

In what preceeds the tolerance on parameter values varied from a few % to 20%. This accuracy reflects the combined effects of:

a) Spread among individual instruments of the same class.

b) Limit of accuracy of experiments (the generation of precisely known mechanical transients-acceleration and angular rate - is not easy).

c) Inherent limitations in system identification (theoretical limitations).

Note that in several cases, a shift of say 10% in parameter values produces a very much smaller change in output signal. This is a desirable feature for instruments since it obviates the need for fine tuning of components.

E. Inversion Program

The inversion method developed here gives good results when applied to the three kinds of transducers. It appears desirable sometime in the future to add to the present computer program a simple digital spectrum analyzer in order to remove the necessity to have the user estimate signal bandwidth. The present scheme gives the best obtainable results in a minimax sense. It includes an error analysis and can be used for studies of parameter sensitivity, Monte Carlo simulations of random noise effects, etc. In terms of the inversion capabilities in general, one can consider four categories of signals:

a) Signals that are extremely fast, but without large magnitudes (having vanishingly small products of magnitude times duration) will not appear at the output of the transducers and hence will pass unnoticed.

b) Extremely fast signals with large amplitudes (similar to mathematical impulses) are observable; exact input wave form reconstruction is impossible (as it is with any method) but also unnecessary, since such inputs act as mathematical impulses whose strength can be easily determined by the measurement of the area under the output curve.

c) For other fast signals (slower than the preceding categories), the inversion program is fully applicable. The results obtained were very satisfactory after determination of the proper signal bandwidth. Of course, perfect reconstruction is impossible, but under the conditions given here, best possible reconstruction is achieved.

d) Finally, really slow ("normal") signals pose no problem since the transducers transmit them with little or no distortion.

It is interesting to note that for a real system, where noise is unavoidable, a relatively low order, simplified model may give better results in the inversion process than a completely detailed, high order model, which would only be useful for an idealized zero-noise inversion. In fact, the optimum order of the inversion model can be determined in terms of the signal-to-noise ratios for a given system.

Avco Corporation
Wilmington, Massachusetts

June 30, 1970

APPENDIX A

FREQUENCY TRANSFER-FUNCTION OF A BANDPASS FILTER

Consider a BP filter, with input signal $e_{in}(t)$ (as defined in section 5.7) where A_k is considered constant. (This is an approximation in itself, as seen in the discussion and illustrations of the SCO). Then, the output is

$$e_{out}(t) = A\int_{-\infty}^{t} f_{BP}(t-t')\cos\left(w_o t' + \int_{o}^{t'} \Delta w_{in}(t'')\,dt''\right)dt'$$

$$= 2A\int_{-\infty}^{t} f_{DLP}(t-t')\cos\left(w_o(t-t') - \varphi\right)\cos\left(w_o t' + \int_{o}^{t'} \Delta w_{in}(t'')dt''\right)dt'$$

This can be rewritten as

$$e_{out}(t) = A\int_{-\infty}^{t} f_{DLP}(t-t')\cos\left(w_o t - \varphi + \int_{o}^{t'} \Delta w_{in}(t'')dt''\right)dt'$$

$$+ A\int_{-\infty}^{t} f_{DLP}(t-t')\cos\left(w_o(t+2t') - \varphi - \int_{o}^{t'} \Delta w_{in}(t'')dt''\right)dt'$$

Since $|\Delta w_{in}| \ll w_o$ for the telemetry channels, the second term in the preceding formula is nearly zero for a narrow band BP (see explanation related to the "first property" in section 5.7) since the high frequency oscillations $2w_o t'$ approximately cancel contributions from $f_{DLP}(t-t')$.

Therefore,

$$e_{out}(t) \cong A\,Re\,\exp\left(i(w_o t - \varphi)\right)\int_{-\infty}^{t} f_{DLP}(t-t')\exp\left(i\int_{o}^{t'} \Delta w_{in}(t'')dt''\right)dt'$$

$$= A\,Re\,\exp\left(i(w_o t - \varphi)\right)\int_{o}^{\infty} f_{DLP}(u)\exp\left(i\int_{o}^{t-u} \Delta w_{in}(t'')dt''\right)du$$

$$= A\,Re\,\exp\left(i(w_o t - \varphi)\right) M(t)\exp\left(i\,\phi(t)\right)$$

which also defines the real functions M(t) (amplitude) and $\phi(t)$ (phase).

For $\Delta w_{in} \equiv 0$, i.e., no disturbance in frequency, one has

$$\bar{M}(t) \exp(i \bar{\phi}(t)) = \int_0^\infty f_{DLP}(u)\, du = F_{DLP}(0)$$

(for a physically realizable filter)

giving $\begin{cases} \bar{M}(t) = F_{DLP}(0) \\ \bar{\phi}(t) = 0 \end{cases}$

This is the expected steady state response to a sine wave. $A \cos(w_o t - \varphi)$.
Now, for $\Delta w_{in}(t) \not\equiv 0$

$$\frac{d}{dt}\left[M(t) \exp(i \phi(t))\right] = i \int_0^\infty f_{DLP}(u) \exp\left(i \int_0^{t-u} \Delta w_{in}(t'')dt''\right)$$

$$\Delta w_{in}(t-u)\, du$$

Now, provided $|\Delta w_{in}|$ also satisfies the more stringent condition

$$(|\Delta w_{in}|_{average}) \ll \text{edge of D. L. P.}$$

or $(|\Delta w_{in}|_{average}) \ll$ bandwidth of BP filter,

one has

$$\frac{d}{dt}(M(t) \exp(i \phi(t)) = \bar{M} \exp(i \bar{\Phi}) \, i \frac{d\phi}{dt} + \exp(i \bar{\Phi}) \frac{dM}{dt}$$

$$= \frac{dM}{dt} + F_{DLP}(0)\, i \frac{d\phi}{dt} = i \int_0^\infty f_{DLP}(u)\, \Delta w_{in}(t-u)\, du$$

or $\frac{dM}{dt} = 0$

$$\frac{d\phi}{dt} \cong \frac{1}{F_{DLP}(0)} \int_0^\infty f_{DLP}(u)\, \Delta w_{in}(t-u)\, du$$

which proves the "Second Property" of Section 5. 7.

If $|\Delta w_{in}|$ approaches the band edge of BP for an extended time, this is not longer valid. This fact is clearly illustrated, for the case of an ideal bandpass filter and a symmetric step in $w_{in}(t)$, in the above mentioned reference (in a figure shown there, taken from Salinger's article in Proc. I. R. E. 30, 378-383, August 1942). Therefore, for frequency swings $|\Delta w_{in}|_{average}$ which are comparable with the bandwidth of the BP, pronounced non-linear effects appear. They can be calculated numerically for each particular case, by the methods used in this appendix if the first formula of this appendix is employed and all subsequent simplifications based on the smallness of $|\Delta w_{in}|$ are omitted. An example of such a calculation is given in section 5. 7.

APPENDIX B

GENERAL DESCRIPTION OF TESTS ON TRANSDUCERS

Open Instrument Testing: See Figures B1 through B4 on Pages 247 and 248 for pictures.

The three types of instruments were opened to further evaluate their physical dimensions, electrical circuits and undamped natural frequencies. These dimensions were compared with available vendor information and where necessary vendor information was not available the model was updated from actual dimensions. The electrical circuit for the accelerometers was also traced out.

Accelerometer:

The cover of the accelerometer was machined off. The circuit was traced from the two control circuit boards. The power supply board was not traced.

The output of the signal generator was measured as a function of the angle of the pendulum. The high frequencies used in the signal generator precluded the use of a scope probe and so the torquer current was measured as a function of pendulum displacement using a dummy load.

The torque of the torque generator was also determined as a function of input current.

Pressure Transducer:

A small clean hole was machined in the pressure transducer housing. The moving element was moved away from its null point and then the restraint was removed. The moving member then moved to its normal position. This mechanical step function showed the response of the pressure transducer very well.

The dampening fluid was then removed and the process was repeated. The undamped material frequency was clearly indicated.

The pressure transducer was then disassembled and the dimensions and weights of the moving elements were determined. These figures were compared with the vendor's data where available and the inertias were compared to refine the mathematical model.

Gyro:

A small clean hole was machined in the gyro housing. The entire gimbal assembly was moved away from its null point and then the restraint was removed. The gimbal then returned to its null. This mechanical step function clearly showed the response characteristics of the gyro.

The dampening fluid was then removed and the process was repeated. The undamped natural frequency was clearly indicated.

The gyro was then disassembled and dimensions of the various elements were recorded to further refine the mathematical model with the actual dimensions.

Carco Table Testing:

The Carco table is a three-axis flight simulation manufactured by Carco Electronics. It is a precision electrohydraulic angular positioner. (See Figure B-5).

Because of the limits of the response of the table to a given position input, a special velocity transducer (tachometer) was incorporated into the table. This device had a frequency response well above the response being investigated and therefore was suitable to compare to the response of the instrument under test.

A ramp, blast and square wave function were fed into the position input of the simulator. A sine input was also fed into the system with the function superimposed. The output of the velocity transducer was the input to the instrument being analyzed.

For the accelerometer the tangential motion of the table was used to simulate the acceleration. The output of the velocity transducer was differentiated to compare the input of the accelerometer with the output to the accelerometer on the analog computer.

Over Range Testing:

The three types of Scout instruments were subjected to inputs that were higher in magnitude than the limits of the instrument but of durations that were a fraction of a time constant for the response. To accomplish these inputs special fixtures were made. The boundaries of the systems were varied to include mounting brackets and plumbing configurations similar to the Scout vehicle.

Pressure Transducer: (See Figures B-6 and B-7)

Two types of inputs were used for the pressure transducer. A shock tube was used to generate very fast rise inputs. The input would decay, however, as the shock wave reflected up and down the tube. The applied pressure was monitored with a fast response transducer (piezo-electric) and this output was compared with the output of the Scout instrument.

To vary the input rise time a second fixture was fabricated. This fixture consisted of a large volume, a burst disc, a variable orifice, and a small chamber to which the Scout pressure transducer and the reference transducer were connected.

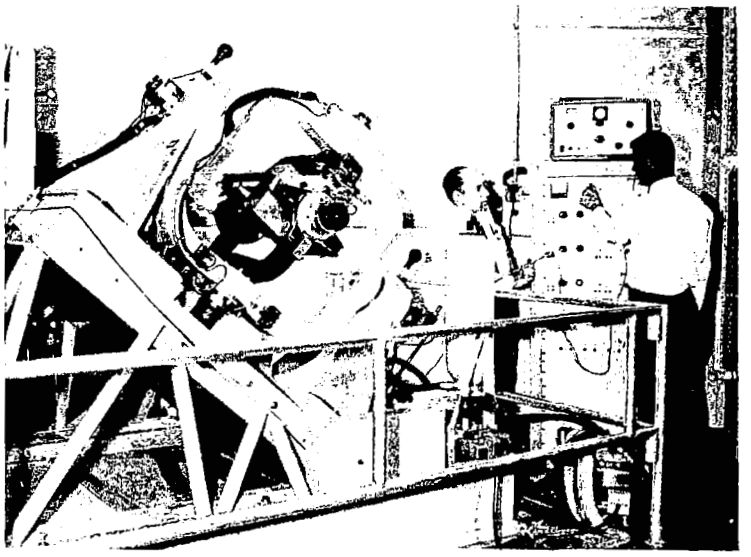

FIGURE B-5 CARCO THREE-AXES FLIGHT SIMULATOR

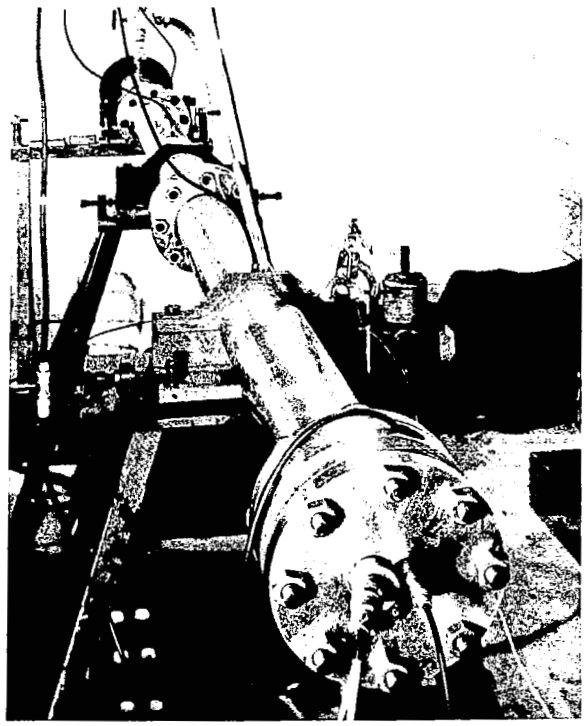

FIGURE B-6

PRESSURE SHOCK TUBE
WITH HEADCAP
SIMULATOR

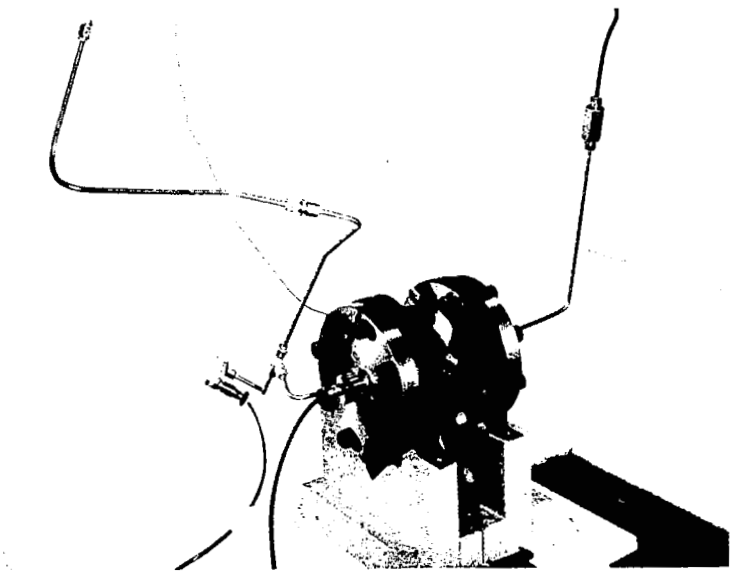

FIGURE B-7

SMALL PRESSURE
FIXTURE WITH
SIMULATED SCOUT
TUBING

The rise time was varied by initiating the burst time of the diaphragm and then later by restricting the flow into the small chamber.

When it was applicab le the plumbing was simulated and then tests were conducted on close coupled instruments. The pressure path of the motor endup was also simulated.

Gyro: (See Figure B-8)

The Scout gyro was tested on a rotating fixture that was specially constructed for the purpose. The fixture also contained the gyro mounting block and the mounting block to vehicle bracket.

Impulses were applied to the moving member with various size and material hammers. The table was also stopped with variable deceleration rates. The deceleration was accomplished by driving a shaped wedge into various materials such as bees wax, paraffin, and polyvinyl slugs.

The inputs to the system were monitored by moving through a known angle in a period of time that was monitored by a piezo-electric accelerometer.

Accelerometer: (See Figure B-9)

The Scout accelerometers were tested on the fixture that was fabricated for testing the gyros modified to accept the accelerometers and their mounting bracket. They were mounted to sense the tangential velocity of the rotating arm.

Various sizes and material hammers were used to provide an impulse of various rise times and amplitudes. Different types of stops were used to decelerate the moving element.

The input to the system was monitored by a fast response accelerometer and the output of the Scout accelerometer was compared to this input.

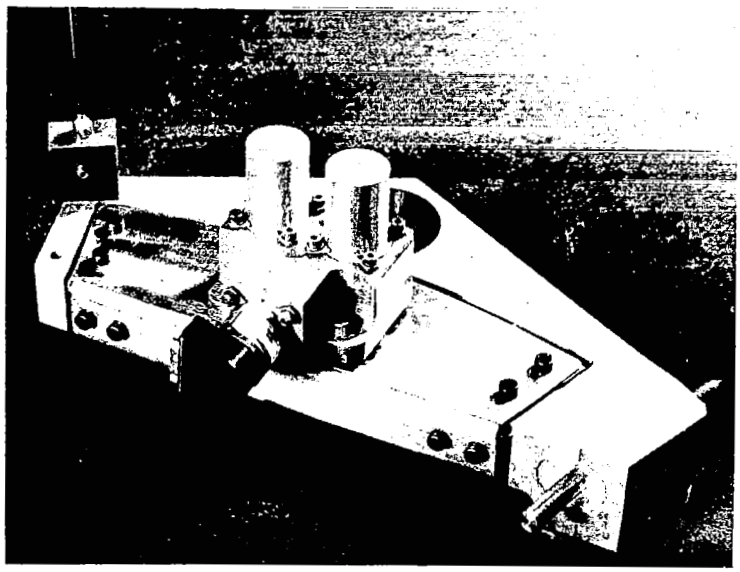

FIGURE B-8

FIXTURE FOR TESTING GYRO AND ACCELEROMETER (WITH GYRO)

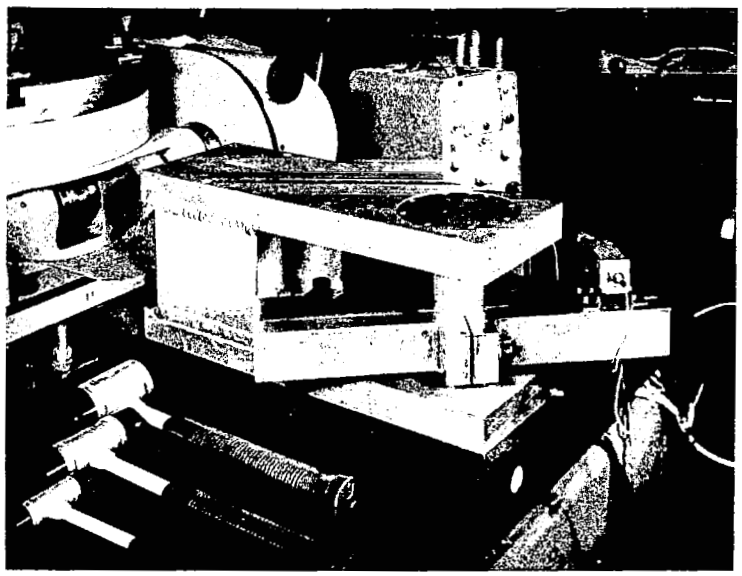

FIGURE B-9

FIXTURE FOR TESTING GYRO AND ACCELEROMETER (WITH ACCELEROMETER)

APPENDIX C

EXPERIMENTAL TEST SETUPS FOR THE SCOUT T/M INVESTIGATION

This appendix describes the various test setups used to gather the experimental information needed for the analytical descriptions of the Scout Telemetry Shelf. (Tele Dynamics Model 1799A S/N 101).

The test setups were based on the T/M shelf documentation received from NASA/Langley with the exception of the mixer input circuit. The actual shelf has a 6.981K resistor from the signal input to signal ground and this was incorporated in the test. Each test is described separately in the following pages.

Subcarrier Oscillator Steady-State Test

Each subcarrier oscillator (SCO) tested was removed from the shelf and tested individually as shown in Figure C-1. The D.C. standard supplied the input voltage which was checked with a digital voltmeter. The output frequency of the SCO was determined by a counter and monitored on an oscilloscope. The input voltage was varied between 0.0V and 5.0V except for some SCO where the voltage was varied between -15V and 30V to determine the out-of-band characteristics of the SCO. The data recorded was the d.c. input voltage with the corresponding output frequency and voltage.

Subcarrier Oscillator Transient Response Test

The transient response of an individual SCO was determined by modulating the SCO (See Figure C-2) with a square wave (OV to 5V) of a sufficiently long period to allow for the SCO settling time. The square wave was approximately changed for each SCO tested. The counter was used to verify the bandedge frequencies. The actual data was taken on a Polaroid photograph displaying the modulating frequency and the SCO output waveform. The delay trigger function of the oscilloscope was used to look at the rise and fall times of the input and output waveforms. The Plug-In was operated in its chopped mode.

Mixer Tests

The same test setup was used for all three mixer tests (See Figure C-3). The first test determined the gain of the mixer as a function of frequency. This information was obtained using a sinusoidal input and measuring the R.M.S. input and output voltages. The second test determined the gain linearity. The input level of a sinusoidal voltage was varied and the corresponding output voltage was noted. The gain of the amplifier at the various input voltages was then calculated. The last test used triangular waveforms at various repetition rates. The response of the amplifier to these waveforms was recorded on Polaroid film from an oscilloscope display.

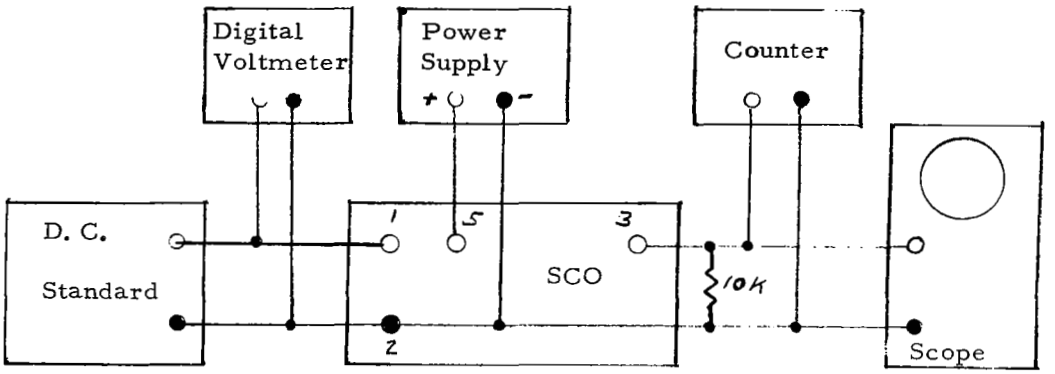

Equipment List

Item	Manufacturer and Model #
D.C. Standard	Electronic Development Corp., MV 100NR
Digital Voltmeter	Hewlett-Packard 3440A with 3443A Plug-In
Power Supply	Harrison Labs 6204A
Counter	Hewlett-Packard 522B
Oscilloscope	Tektronix 535 with Type CA Plug-In
SCO	Tele-Dynamics 5001AA-3

Figure C-4- Sub-Carrier Oscillator (SCO)
Steady-State Test

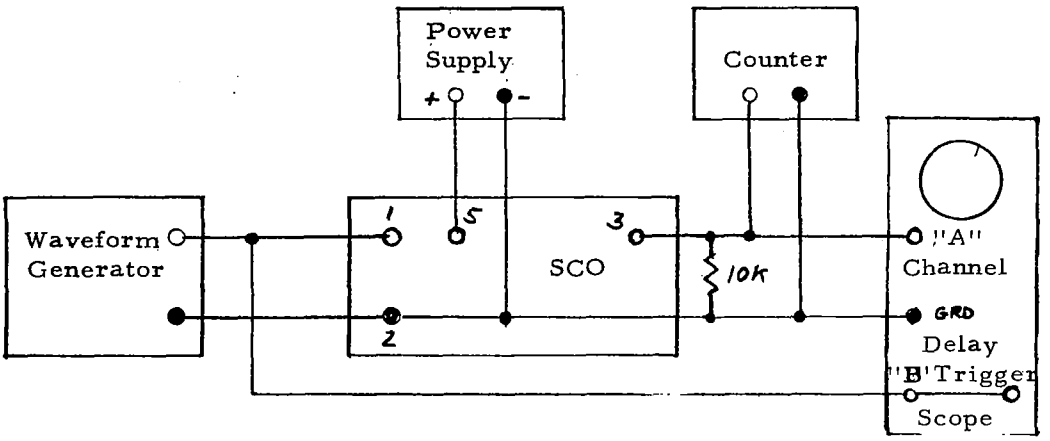

Equipment List

Item	Manufacturer and Model #
Waveform Generator	Hewlett-Packard 3300A with model 3304A Plug-In
Power Supply	Harrison Labs 6204A
Counter	Hewlett-Packard 522B
Oscilloscope	Tektronix 535 with Type CA Plug-In
SCO	Tele Dynamics 5001AA-3

Figure C-2, Sub-Carrier Oscillator
Transient Response
Test

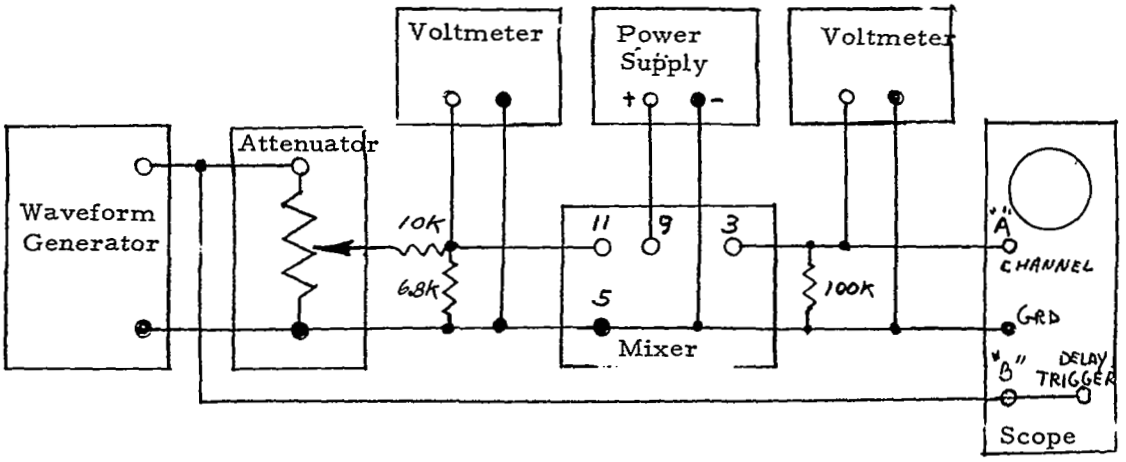

Equipment List

Item	Manufacturer and Model #
Waveform Generator	Hewlett-Packard 3300A with model 3304A Plug-In
Attenuator	Helipot T-104A
Voltmeters	Hewlett-Packard 400FL
Power Supply	Harrison Labs 6204A
Mixer	Tele-Dynamics 1197A
Oscilloscope	Tektronix 535 with Type CA Plug-In

Figure C3 - Mixer Tests

Phase-Sensitive Discriminator, Steady-State Tests

The steady-state tests on the Phase Sensitive Discriminator (P. S. D.) were performed using the test setup of Figure C-4. A test jig was made up (See Figure C-5) to facilitate the P. S. D. testing. The test jig allowed the reference voltage phase to be reversed while low-level signals were applied to the P. S. D. The power amplifier was necessary to supply the specified reference voltage level which could not be obtained from the waveform generator.

The voltmeters were used to obtain the input-output voltage relationships; the oscilloscope was used to monitor the output voltage.

Phase-Sensitive Discriminator, Transient Response Test

The transient response of the P. S. D. used the test setup of Figure C-6 which is essentially the same as Figure C-5 except for the Avco Low Frequency Generator. The L. F. Generator was used to modulate the signal voltage. A schematic of the L. F. Generator is shown in Figure C-7. The generator was originally designed to have a high power square wave capability of amplitude V_1 and V_2. The response of the P. S. D. was displayed on an oscilloscope and recorded on Polaroid film.

System Shelf Test - Configuration 1

For this test the whole shelf was powered but only one channel was modulated. The modulation waveforms were square wave, triangular and trapezoidal. The latter was supplied by using a saturating transistor amplifier, see Figure C-9, between the waveform generator and the SCO. The shelf output, see Figure C-8, was sent to discriminator for demodulation. The waveforms were observed on an oscilloscope and recorded on Polaroid film.

Saturating Transistor Amplifier

The transistor amplifier was as shown in Figure C-9. Since the waveform generator used in the tests has signal offset and signal amplitude controls, the desired waveform output was a matter of selection the proper levels of the two generator contacts. The power supply to the amplifier was set initially at +6V and then find adjusted for the proper bias operation.

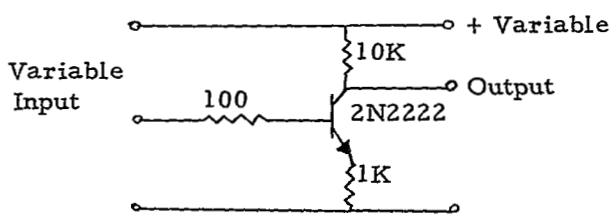

Figure C-9 - Saturating Transistor Amplifier

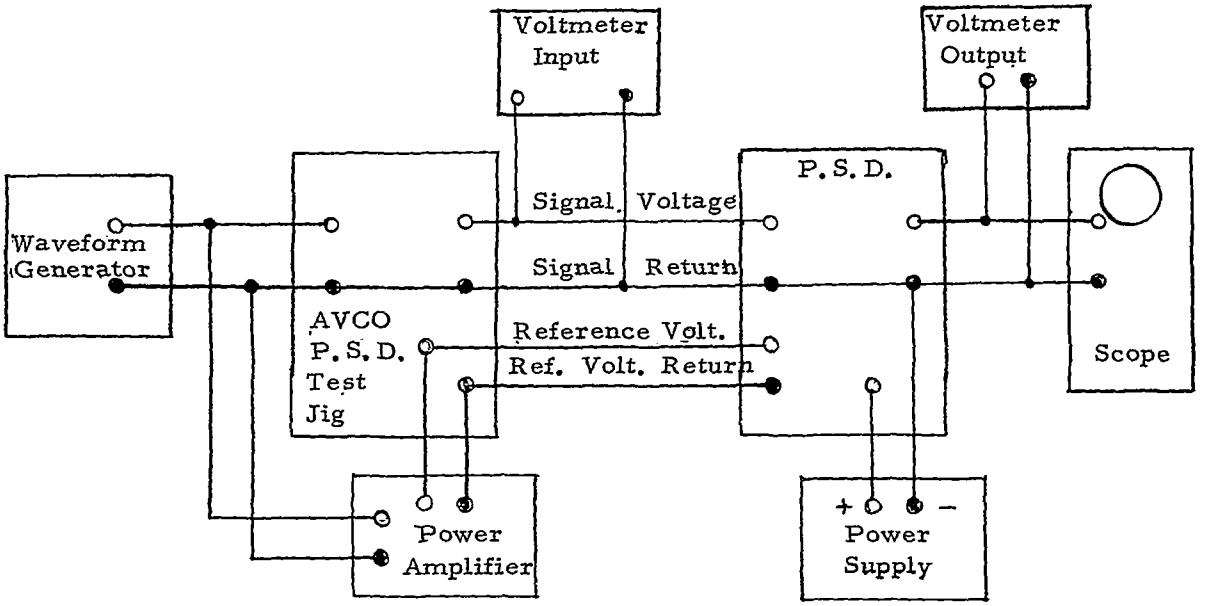

Equipment List

Item	Manufacturer and Model #
Waveform Generator	Hewlett-Packard 3300A with 3304A Plug-In
Avco P.S.D. Test Jig	Special Test Circuit
Power Amplifier	Eico HF-22
Phase Sensitive Discriminator (P.S.D.)	Tele-Dynamics 1353A
Power Supply	Harrision Labs 6204A
Voltmeter, Output	Hewlett-Packard 5245L with 5265A Plug-In
Voltmeter, Input	Hewlett-Packard 400FL
Oscilloscope	Tektronix 535 with type CA Plug-In.

Figure C4- Phase Sensitive Discriminator
Steady-State Tests

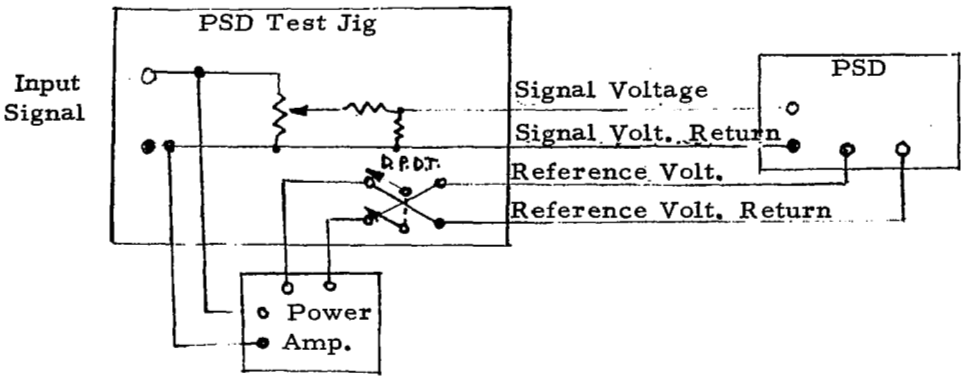

Figure C 5 - Phase Sensitive Discriminator Test Jig

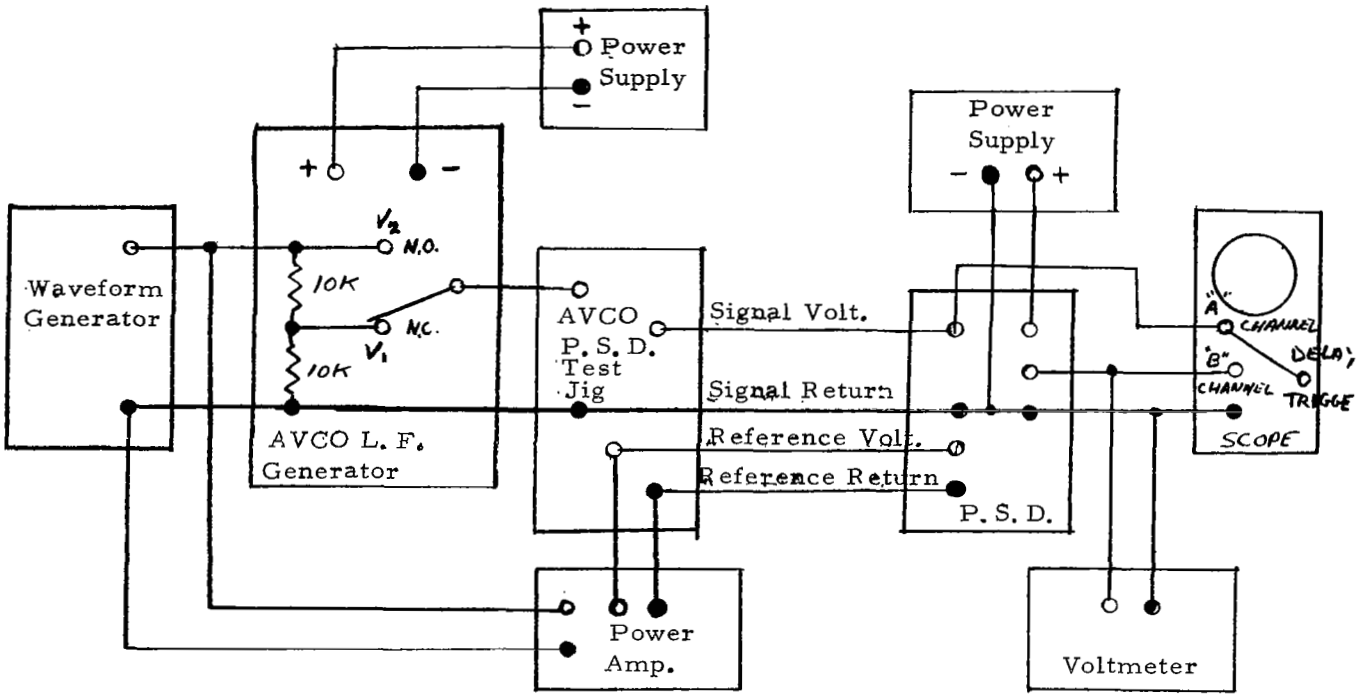

Equipment List

Item	Manufacturer and Model #
Waveform Generator	Hewlett-Packard 3300A with model 3304A Plug-In
Avco Low-Frequency Generator	Special Test Circuit
Avco P.S.D. Test Jig -	Special Test Circuit
Power Supply	Hewlett-Packard 721A
Power Amplifier	Eico HF-22
Power Supply P.S.D.	Harrison Labs 6204A
Phase Sensitive Discriminator (P.S.D.)	Tele-Dynamics 1353A
Voltmeter, Output	Hewlett-Packard 5245L with 5265A Plug-In
Voltmeter, Input	Hewlett-Packard 400FL
Oscilloscope	Tektronix 535 with Type CA Plug-In

Figure C6- Phase Sensitive Discriminator
Transient Response Test

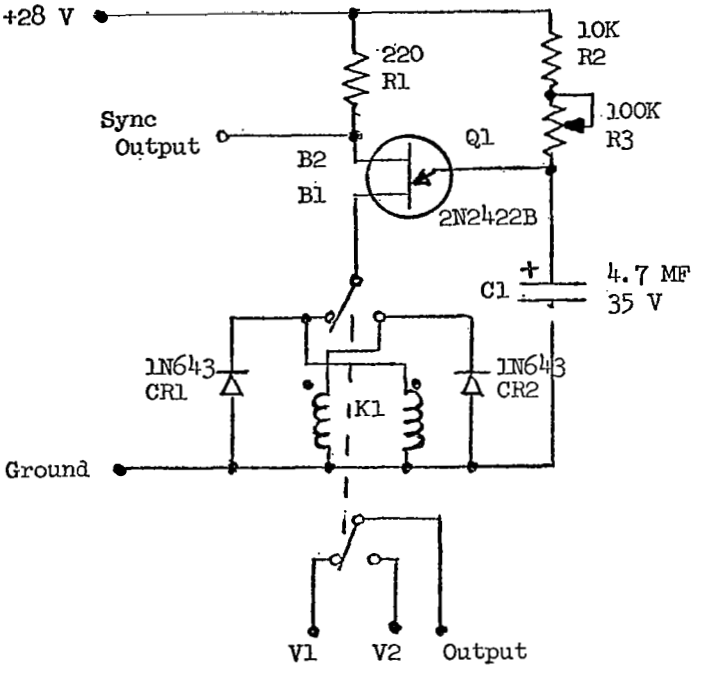

Figure C7 - Avco Low Frequency Generator

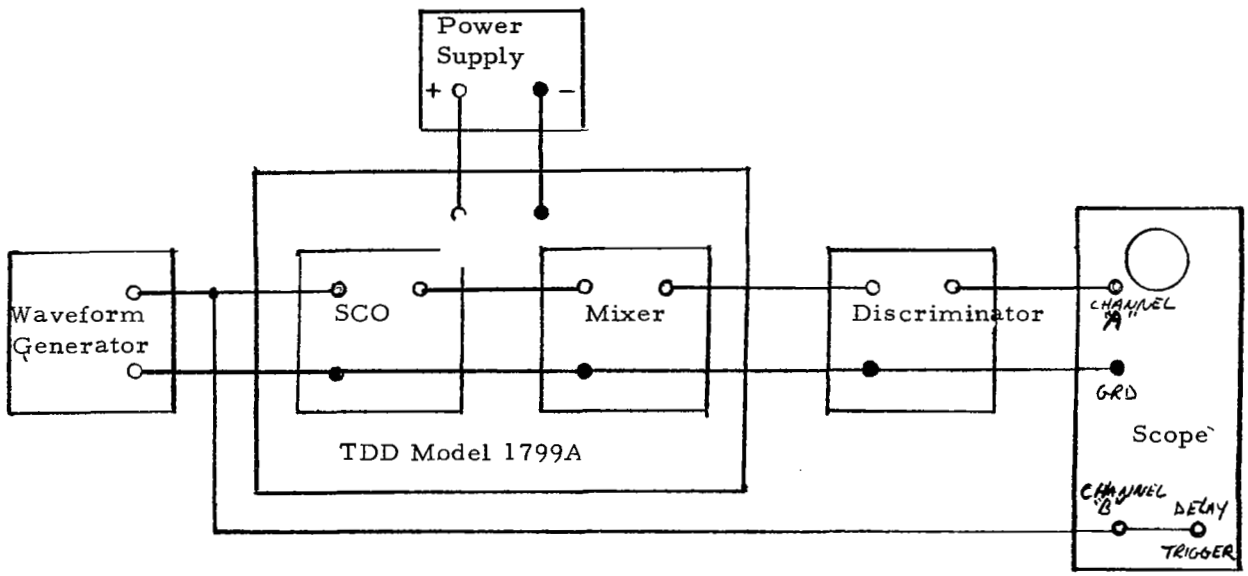

Equipment List

Item	Manufacturer and Model #
Waveform Generator	Hewlett-Packard 3300A with model 3304A Plug-In
Power Supply	Harrison Labs 6204A
Telemtery Shelf	Tele-Dynamics 1799A
Discriminator	Electro-Mechanical Research Inc. Model 229 Tunable Discriminator
Oscilloscope	Tektronix : 535 with Type CA Plug-In

Figure C8 - System Shelf Test
Configuration 1

System Shelf Test - Configuration 2

This test was connected as Configuration 1 but with the P. S. D. driving the SCO. The P. S. D. test setups of Figure C-4 and C-6 were used to drive the P. S. D. The waveforms were observed on an oscilloscope and recorded on film.

Power Interruption Test

The test setup of Figure C-8 was used with a triangular input waveform. The T/M shelf was connected to the power supply/supplies through the Avco L. F. Generator (See Figure C-10a). The rate and level of power interruption was changed with the results displayed on the oscilloscope with a Tektronix 1A4 plug-in. This displayed a high and low SCO channel, the type of power interruption and the modulating waveform.

Figure C-10b shows the method used to obtain a transient (short duration) power interruption with the same test setup.

Discriminator Filter Tests

Figure C-11 shows the test setup used to determine the response of the Discriminator Bandpass and Low pass filters. Figure C-12 shows another method that is useful in determining the transient response of the filters.

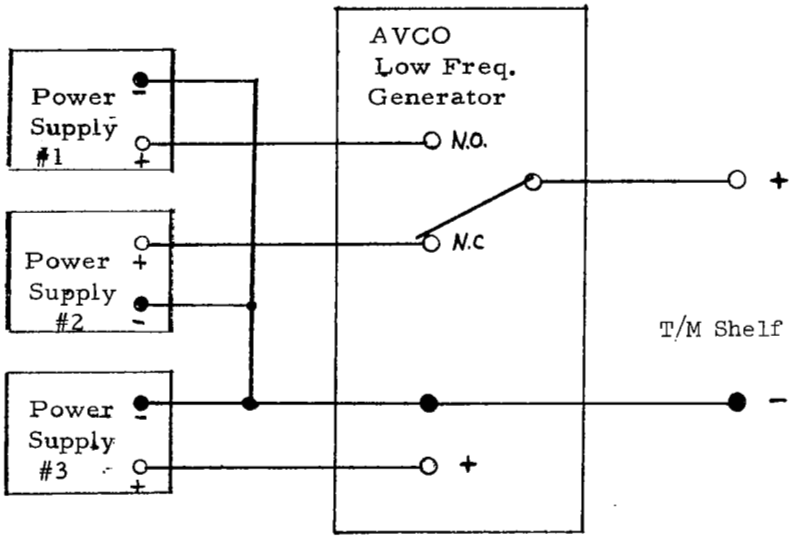

Figure 10a

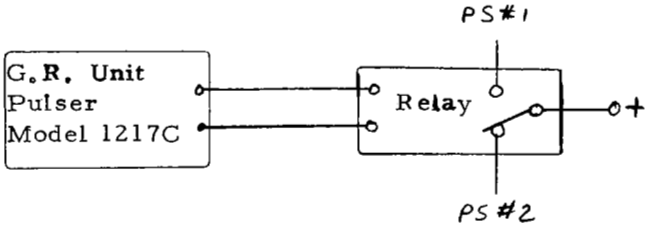

Figure 10b

Equipment List

Item	Manufacturer and Model #
Power Supply #1 and #2	Harrison Labs 6204A
Power Supply #3	Hewlett-Packard 721A

Figure C10 - Power Interruption Test

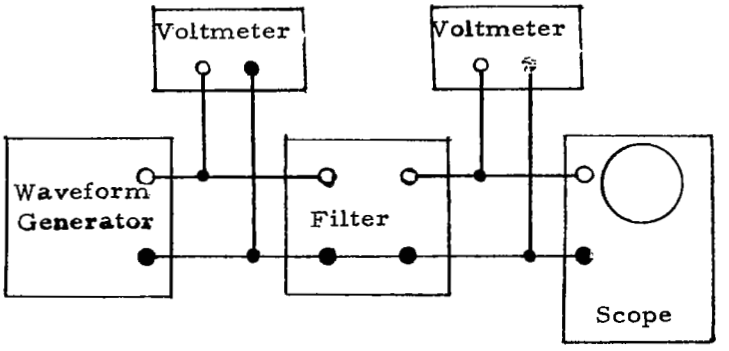

Equipment List

Item	Manufacturer and Model #
Waveform Generator	Hewlett-Packard 3300A with 3304A Plug-In
Voltmeter	Hewlett-Packard 400FL
Oscilloscope	Tektronix 535 with Type CA Plug-In
Bandpass Filter	Part of Electro-Mechanical Research Inc., Model 229 Tunable Discriminator

FigureC11 - Discriminator Filter Test

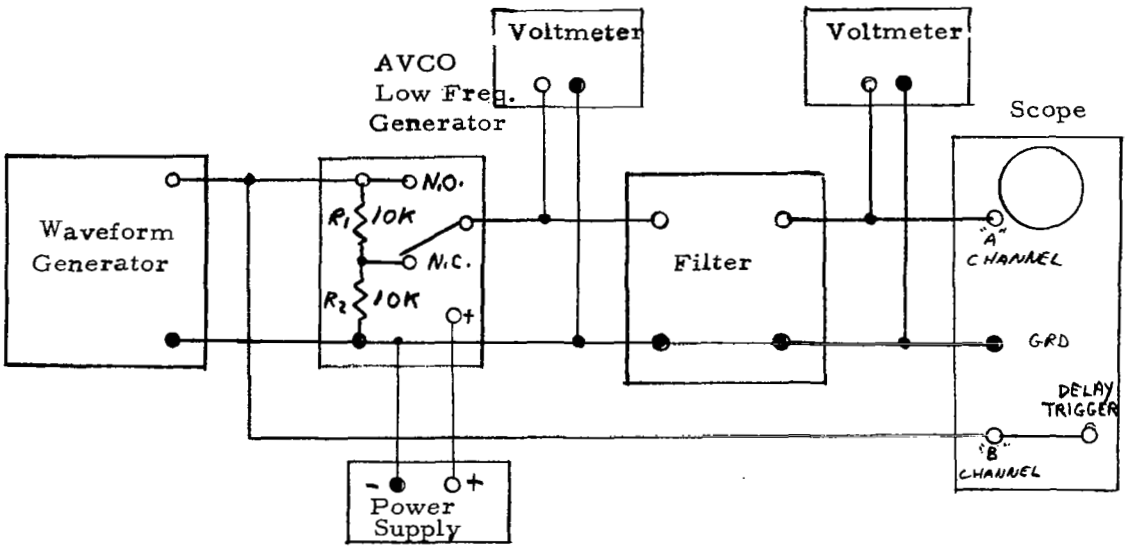

Equipment List

Item	Manufacturer and Model #
Waveform Generator	Hewlett-Packard 3300A with Model 3304A Plug-In
Avco Low-Frequency Generator	Special Test Circuit
Power Supply	Hewlett-Packard 712A
Voltmeter	Hewlett Packard 400FL
Band Pass Filter	Part of Electro-Mechanical Research Inc., Model 229 Tunable Discriminator
Oscilloscope	Tektronix 535 with Type CA Plug-In

Figure C12 - Discriminator Filter Test Transient Test

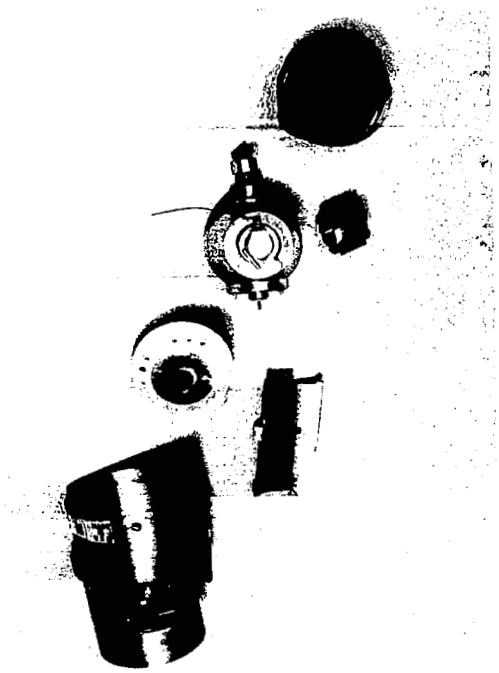

FIGURE B-1 RATE GYRO

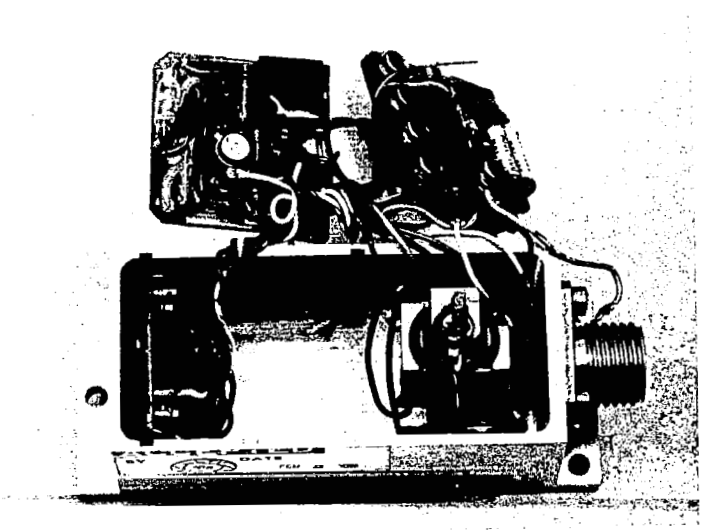

FIGURE B-2 ACCELEROMETER

FIGURE B-3

GIANNINI

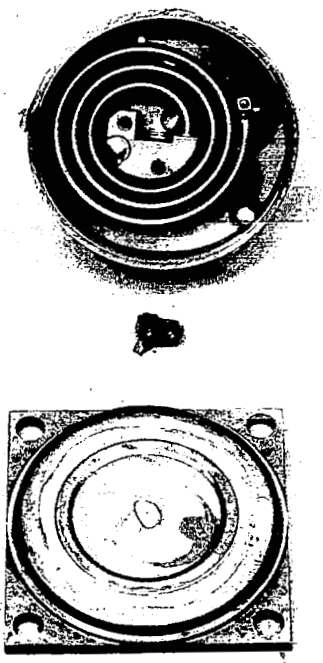

FIGURE B-4

BOURNS

REFERENCES

1. Davis, P. J.: Interpolation and Approximation, Blaisdell Publishing Company, New York, 1963.

2. Leondes, C. T. (Editor): Guidance and Control of Aerospace Vehicles, McGraw-Hill Book Company, 1963.

3. Den Hartog, J. P.: Strength of Materials, Dover Publications, Inc., 1961.

4. Timoshenko, S.: Vibration Problems in Engineering, Van Nostrand Publishers, 3rd Edition, 1955, New York.

5. Wolf, A.: An Elementary Theory of the Bourdon Gage, Journal of Applied Mechanics, September 1946, pp. A-207-A-210.

6. Streeter, V. L. (Editor): "Handbook of Fluid Mechanics" (especially, Section 20 on Transients, by H. M. Paynter), McGraw-Hill, 1961.

7. Stiltz, H. L. (Editor): Aerospace Telemetry, Prentice-Hall, 1961, Englewood Cliffs, N. J.

8. Valley, G. E. & Wallman, H. (Editors): Vacuum Tube Amplifiers, Dover Publishers (Republication), 1965, New York, N. Y.

9. Nichols, M. H., Jr. & Rauch, L. L.: Radio Telemetry, 2nd Edition, Wiley 1956, New York, N. Y.

10. Weinberg, L.: Network Analysis and Synthesis, McGraw Hill, 1962, New York, N. Y.

11. Henderson, K. W. & Kautz, W. H.: Transient Responses of Conventional Filters, I. R. E. Trans. Circuit Th., December 1958, pp. 333-347.

12. Papoulis, A.: Limits on Band Limited Signals, Proc. I. E. E. E., October 1967, pp. 1677-1686.

13. Idem: Error Analysis in Sampling Theory, Proc. I. E. E. E., July 1966, pp. 947-955.

14. Idem: The Fourier-Integral and its Applications, McGraw-Hill, New York, 1962.

15. Silverman, L. M.: Inversion of Multivariable Linear Systems, I. E. E. E., Trans. on Auto. Control, June 1969, pp. 270-276.

16. Sain, M. K. & Massey, J. L.: Invertibility of Linear Time Invariant Dynamical Systems, I. E. E. E., Trans. on Auto. Control, April 1969, pp. 141-149.

17. Dorato, P.: On the Inverse of Linear Dynamical Systems, I. E. E. E., Trans. on Systems Science & Cybernetics, January 1969, pp. 43-48 (plus correction in July issue of same journal).

NASA-Langley, 1971 —— 14